Univerza
v Ljubljani

Fakulteta za gradbeništvo in geodezijo

PODIPLOMSKI ŠTUDIJ GEODEZIJE

DOKTORSKI ŠTUDIJ

Kandidatka:

MIHAELA TRIGLAV ČEKADA, univ. dipl. inž. geod.

OPTIMIZACIJA METODOLOGIJE OBDELAVE IN ANALIZA NATANČNOSTI LETALSKEGA LASERSKEGA SKENIRANJA PRI ZAJEMU GEODETSKIH PODATKOV ZA LOKALNO PROSTORSKO PLANIRANJE

Doktorska disertacija štev.: 188

OPTIMIZATION OF THE DATA PROCESSING METHODOLOGY AND ACCURACY ANALYSIS OF AIRBORNE LASER SCANNING DATA APPLIED FOR LOCAL SPATIAL PLANNING

Doctoral thesis No.: 188

Ljubljana, 6. februar 2009

Univerza
v Ljubljani

Fakulteta za
gradbeništvo in
geodezijo

Komisijo za oceno ustreznosti teme doktorske disertacije v sestavi
doc. dr. Mojca Kosmatin Fras,
izr. prof. dr. Anton Prosen,
izr. prof. dr. Krištof Oštir,
prof. dr. Fabio Crosilla, Univerza v Vidmu, Italija,

je imenoval Senat Fakultete za gradbeništvo in geodezijo na 1. redni seji dne
25. oktobra 2006.

Komisijo za oceno doktorske disertacije v sestavi
doc. dr. Mojca Kosmatin Fras,
doc. dr. Anka Lisec,
izr. prof. dr. Krištof Oštir,
prof. dr. Fabio Crosilla, Univerza v Vidmu, Italija,

je imenoval Senat Fakultete za gradbeništvo in geodezijo na 22. redni seji dne
26. novembra 2008.

Komisijo za zagovor doktorske disertacije v sestavi
prof. dr. Bojan Majes, dekan, predsednik
doc. dr. Mojca Kosmatin Fras,
doc. dr. Anka Lisec,
izr. prof. dr. Krištof Oštir,
prof. dr. Fabio Crosilla, Univerza v Vidmu, Italija,

je imenoval Senat Fakultete za gradbeništvo in geodezijo na 24. redni seji dne
28. januarja 2009.

Univerza
v Ljubljani

*Fakulteta za
gradbeništvo in
geodezijo*

IZJAVA O AVTORSTVU

Podpisana **MIHAELA TRIGLAV ČEKADA, univ. dipl. inž. geod.**, izjavljam, da sem avtorica doktorske disertacije z naslovom: **»OPTIMIZACIJA METODOLOGIJE OBDELAVE IN ANALIZA NATANČNOSTI LETALSKEGA LASERSKEGA SKENIRANJA PRI ZAJEMU GEODETSKIH PODATKOV ZA LOKALNO PROSTORSKO PLANIRANJE«.**

Ljubljana, 6. februar 2009

……………………………..
(podpis)

ERRATA

Page	Line	Error	Correction

BIBLIOGRAFSKO - DOKUMENTACIJSKA STRAN IN IZVLEČEK

Izvleček

Zračno lasersko skeniranje (lidar) postaja čedalje bolj uporabna tehnologija daljinskega zaznavanja za pridobivanje prostorskih podatkov. Kljub temu, da različni rigorozni modeli napak zračnega laserskega skeniranja že obstajajo in so že bile izvedene terenske meritve dosežene natančnosti, še ne obstaja enostavna mera za a-priori izračun natančnosti laserskega skeniranja že pred njegovim naročilom. Preko podrobnega opisa virov napak laserskega skeniranja in poenostavitve Schenkove geolokacijske enačbe smo v tej doktorski dizertaciji zapisali enostaven a-priori model napak laserskega skeniranja. Ob tem je podan še podroben opis napak pridobljen s pregledom literature. Napake laserskega skeniranja delimo na: osnovne sistematične napake, napake pridobljene zaradi parametrov leta, napake pridobljene zaradi značilnosti odbojnika. S spreminjanjem različnih geometrijskih parametrov je bila narejena simulacija različnih virov napak in njihov vpliv na skupno velikost napak. Tako pridobljen poenostavljen model napak omogoča hiter izračun a-priori napak in poda verjetne vrednosti za povprečne in največje vrednosti skupne napake laserskega skeniranja. Poenostavljen model napak je neodvisen od kota skeniranja, kota pozibavanja nosilca laserskega skenerja ter podrobnih tehničnih specifikacij posameznega sistema za lasersko skeniranje.

Izvrednotenje prostorskih podatkov iz podatkov laserskega skeniranja je omejeno tudi s točnostjo izvrednotenja. Zahtevana točnost izvrednotenja je pogojena s geometrično ločljivostjo prostorkih podatkov (v našem primeru geometrična ločljivost prostorskih podatkov za lokalno prostorsko planiranje). Točnost izvrednotenja definira minimalno število laserskih točk na enoto površine. Minimalno število laserskih točk na enoto površine izračunamo s pomočjo Nyquistove frekvence, če uporabimo lasersko skeniranje kot samostojno tehnologijo izvrednotenja. Z izmero deleža prodiranja laserskega žarka skozi različno vegetacijo na testnem oblaku laserskih točk, smo definirali tudi končno uporabno število laserskih točk na enoto površine za različne vegetacijske razrede.

V nalogi je opisana tudi zakonska osnova ter trenutna metodologija priprave različnih geodetskih podatkov, ki se uporabljajo kot prostorske podlage za lokalno prostorsko načrtovanje v Sloveniji. A-priori natančnost laserskega skeniranja in točnost izvrednotenja prostorskih podatkov nam povesta, v katerih primerih lahko vpeljemo lasersko skeniranje kot enakovredno tehnologijo izmere trenutnim metodologijam izmere. Z uvedbo laserskega skeniranja lahko metodologijo obdelave nekaterih geodetskih podatkov optimiziramo.

BIBLIOGRAPHIC - DOCUMENTALISTIC INFORMATION AND ABSTRACT

Abstract

Aerial laser scanning (lidar) has become a widely used technique for spatial data production. Although various rigorous error models of aerial laser scanning already exist and examples of a-posteriori studies of aerial laser scanning data accuracies verified with field-work can be found in the literature, a simple measure to define a-priori error sizes is not available. In this work the aerial laser scanning error contributions are described in detail: the basic systematic error sources, the flight-mission-related error sources and the target-characteristic-related error sources. A review of the different error-source sizes is drawn from the literature in order to define the boundary conditions for each error size. Schenk's geolocation equation is used as a basis for deriving a simplified a-priori error model. By changing different geometrical parameters the simulation of error sizes is made and the influence of different error sources is studied. This simplified error model enables a quick calculation and gives a-priori plausible values for the average and maximum error size, independent of the scan and heading angles as well as being independent of any specific aerial laser scanning system's characteristics.

Spatial data production by aerial laser scanning is also limited by acquisition precision. The acquisition precision is defined by spatial data products (in our case: geodetic data for local spatial planning). The acquisition precision of spatial data products also defines the minimum point density of aerial laser scanning. The minimum point density when applying aerial laser scanning as a stand-alone-technique is defined through minimal sampling density or Nyquist frequency. Through measuring penetration rate for different vegetation classes in the test area the total usable point density is defined.

The a-priori aerial laser scanning accuracy and spatial data product precision defines when the aerial laser scanning can be applied in data extraction process in Slovenia. Through this the acquisition methodology for different geodetic data for local spatial planning production can be optimized. The review on legal acts defining the local spatial planning is given. The current and proposed data processing methodology for different geodetic data used for local spatial planning is described.

Acknowledgement

First I would like to thank my tutors Assist. Prof. Dr. Mojca Kosmatin Fras and Prof. Dr. Fabio Crosilla to introduce me in the topic of aerial laser scanning, to give me valuable directions how to proceed with my ideas, give me links to important literature and also to encourage me on my way. Especially I would like to thank Prof. Dr. Fabio Crosilla to show me how the real scientific work is performed.

Then I would like to thank Dr. Borut Jurčič Zlobec to refresh my knowledge on linear algebra and Dr. Alma Zavodnik Lamovšek for hints about the Slovenian spatial planning.

I am grateful to Geodetic institute of Slovenia for financial support of my PhD studies and also to my colleagues there for nice hours at work and moral support. To Interreg IIIA EU co-financed project HarmoGeo, in which we cooperated, I am thankful for the Nova Gorica aerial laser scanning data point cloud, used here as a test sample.

But above all I have to thank to my husband Miha who was there in bad moments, read after me all linear algebra derivations, extensively helped with English and has been there with his positive way of thinking. At the end I would also like to apologize to my sons Primož and Gregor who often had to go to bed too early, so that I could work on my PhD thesis.

TABLE OF CONTENTS

x

Triglav-Čekada, M. 2009. *Optimization of the data processing methodology and accuracy analysis of airborne laser scanning data applied for local spatial planning*, PhD thesis, Ljubljana, UL, FGG, Department for geodesy

xiv

Triglav-Čekada, M. 2009. *Optimization of the data processing methodology and accuracy analysis of airborne laser scanning data applied for local spatial planning*, PhD thesis, Ljubljana, UL, FGG, Department for geodesy

LIST OF FIGURES

xviii

Triglav-Čekada, M. 2009. *Optimization of the data processing methodology and accuracy analysis of airborne laser scanning data applied for local spatial planning*, PhD thesis, Ljubljana, UL, FGG, Department for geodesy

LIST OF TABLES

XX

Triglav-Čekada, M. 2009. *Optimization of the data processing methodology and accuracy analysis of airborne laser scanning data applied for local spatial planning*, PhD thesis, Ljubljana, UL, FGG, Department for geodesy

ABBREVIATIONS AND SYMBOLS

lidar   light detection and ranging

sonar   sound navigation and ranging

DEM   digital elevation model

DTM   digital terrain model

DSM   digital surface model

DTK5   state topographic charts in scale $1:5000$

GPS   global positioning system

DGPS   differential GPS

INS   inertial navigational system

CAS   cyclical aerial survey

CCD   charge-coupled device

SMA   Surveying and Mapping Authority of the Republic of Slovenia

h flying height

d range

t time elapsed between sending a pulse from emitter and receiving and echo to receiver

τ_p time length of emitted pulse

$\mathbf{c}(\mathrm{H})$ vegetation-height-related error vector

β_i instantaneous scan angle

γ laser beam divergence (γ_T – theoretical, γ – measured)

v_g group velocity of the travelling laser pulse in the air

FOV   field of view (IFOV – instantaneous field of view)

SW   swath width

H vegetation height

$\Delta\mathbf{p}_s$ synchronization error vector, defined by the synchronization bias Δt

$\mathbf{R}_{\text{GEO}}$ rotation matrix from the reference system defined by the local vertical to the local orthogonal reference system, $\mathbf{R}_{\text{GEO}}$ is defined by the deflection of the vertical θ

$\mathbf{R}_{\text{INS}}$ rotation matrix from the body reference system to the reference system defined by a local vertical described by the INS angles: roll ϕ, pitch θ and heading φ

$\Delta\mathbf{R}_{\text{INS}}$ error matrix of $\mathbf{R}_{\text{INS}}$: roll error $\Delta\phi$, pitch error $\Delta\theta$ and heading error $\Delta\varphi$

$\mathbf{R}_m$ mounting bias rotation matrix (its error is described by $\Delta\mathbf{R}_m$)

$\mathbf{R}_s$ rotation matrix between the laser beam and the laser system defined by scan angles (its error is described by $\Delta\mathbf{R}_s$)

$\mathbf{R}_W$ rotation matrix from the local orthogonal system to the global orthogonal coordinate system

$\mathbf{s}_0$ offset vector between the GPS/INS system and the laser system (its error vector is $\Delta\mathbf{s}_0$)

$\mathbf{x}_0$ vector of the location of the phase center of the flying platform's GPS receiver in the global geocentric coordinate system

$\Delta\mathbf{x}_0$ error vector of the GPS/INS sensor positioning

$\Delta\mathbf{x}_{ave}$ total expected average lidar error vector

$\Delta\mathbf{x}_{max}$ total expected maximum lidar error vector

$\Delta\mathbf{x}_s$ basic systematic error vector ($\Delta\mathbf{x}_{s\_ave}$ is its average value, $\Delta\mathbf{x}_{s\_max}$ is its maximum value)

1 INTRODUCTION

1.1 General considerations and motivation

Aerial laser scanning, also named LIDAR (light detection and ranging), is becoming a widely used technique for acquisition of topographic or bathymetric data. It uses an active sensor which measures the time interval between the laser pulse transmission and the pulse echo return to the receiver. This time interval defines the distance from the transmitter to the target and back to the receiver, which together with the scan angle define the location of the target in physical space. Additional information to the location is the intensity or amplitude of the returning echo. This can give us a lot of information on the material from which the echo reflected.

Aerial laser scanning technique can be used as a stand alone technique or in combination with the multi- or hyperspectral photogrammetric data. Its advantage to other remote sensed techniques is direct acquisition of 3D data points and its ability to extract data under the vegetation. The ability to acquire data under the vegetation opens ways to automate contour line generation, production of exact digital terrain models, identification of creeks and other water bodies delineations, identification of forest roads and mountain paths, etc.

The application of aerial laser scanning for different geodetic products is becoming broader every year, as new laser scanners are employed, which give more accurate measurements. Therefore the purpose of this work is to optimize data processing methodology for the production of the geodetic data in large scales (1 : 500 to 1 : 5000) with the application of aerial laser scanning. Geodetic data in large scales are mainly used for spatial planning or verification of current state of physical space on local level. Therefore the intention of this work is to find minimal terms defining which aerial laser scanning data can be applied for acquiring certain geodetic data. We focused especially in geodetic data which is used for local spatial planning.

At the Geodetic institute of Slovenia I was involved in several projects where data acquisition of different geodetic data was performed: different photogrammetric topographic data acquisition and quality control, different infrastructure objects acquisition for Cadaster of public infrastructure, etc. I was involved also in the Interreg IIIA project HarmoGeo[1] where we ordered and worked on high-resolution aerial laser scanning data. Through these practical examples, I realized that some simple measures would help a lot (e.g. a-priori accuracy assessment), when deciding which aerial laser scanning data are appropriate for certain geodetic product.

---

[1]see Appendix E on page 201

The accuracy of aerial laser scanning depends strongly on the accuracy of the laser scanner flying platform positioning. The coordinates of the laser points are calculated by direct georeferencing. Unfortunately, direct georeferencing reduces the possibilities for a-posteriori correction of the data, which is possible when applying aerophotographing. Therefore good knowledge about different error sizes of aerial laser scanning a-priori to the ordering is of great importance.

1.2   Research background

Local spatial planning and the supporting geodetic data are defined in legal acts. Spatial planning is an interdisciplinary science, which defines how the physical space on the national, regional or local level should develop. It provides guidelines and legal recommendations for directing the development of urban and rural areas (Pogačnik, 1992). For spatial planning, well prepared geodetic data for the description of the current state of physical space are of great importance as they ease the decision-making process. Different cartographic representations and geodetic databases used for spatial planning are based on different data acquisition methodologies, as they describe the physical space in different scales. When wide areas in Slovenia have to be measured, in most cases mainly photogrammetry is still applied.

The methodology of data acquisition is not defined in legal acts. Therefore the acquisition of geodetic data can be subject to acquisition methodology optimization by applying aerial laser scanning to the current acquisition methodology. This means that aerial laser scanning can replace/supplement other remotely sensed technics, field work or a combination from different sources. In order to know which geodetic data acquisition methodology can be optimized by aerial laser scanning, the a-priori accuracy assessment and the level of detail to be presented should be known.

The a-posteriori accuracy assessment of aerial laser scanning depends on different error contributors. The total achievable aerial laser scanning planimetric accuracy is in the range of 30-50 cm and in height accuracy in the range 5-15 cm (Baltsavias, 1999b; Maas, 2003). Different rigorous aerial laser scanning error models already exist (Schenk, 2001; Beinat and Crosilla, 2002; Friess, 2006; Skaloud and Lichti, 2006) and different a-posteriori studies of lidar data accuracies with field-work have already been conducted (Alharthy et al., 2004; Ahokas et al., 2005a; Burman, 2000; Crosilla and Beinat, 2005; Schenk, 2001; Schnurr et al., 2004; Maas, 2003; Thoma et al., 2005; Turton, 2006). However, a simple measure to define a-priori error sizes is not available. One of the purposes of this thesis is to develop a simple a-priori aerial laser scanning error model, applicable without the need for a thorough search through the literature and the knowledge about a specific laser scanning system, to estimate the size of different errors contributing to laser scanning measurements. The a-priori aerial laser scanning error model should not be scan-angle dependent, as the suppliers of aerial laser scanning usually deliver just the X, Y, Z coordinates of ground points and not the raw data (range and scan angle).

When describing an analytical model of aerial laser scanning errors it is common to use as a base the Schenk's geolocation equation (Schenk, 2001). Therefore we used it as a base too. All the influences on aerial laser scanning error sources can be divided in three types of error

contributions: basic systematic errors, errors resulting from the flight mission, and errors caused by the nature of the target (Ahokas et al., 2005b; McKean and Roering, 2005). A review of different error sizes and theirs behaviour have been made from the literature.

In addition to the knowledge on the a-priori error assessment, the needed precision of the geodetic data extraction is of great importance. Different purposes (e.g., detailed 3D models of urban areas, flood-risk maps, vegetation-cover analysis) dictate the desired number of points per unit area, as this value defines the level of detail that can be extracted from the aerial laser scanning data. The needed level of detail defines also the extractable precision of geodetic data.

Aerial laser scanning can be divided in three groups while evaluated by the number of points per unit area (Kraus (edt.), 2005; Crosilla and Beinat, 2005). Low-resolution aerial laser scanning data with at most 1 point per m^2 enables the production of a general DTM comparable to DTMs made by photogrammetrical stereorestitution. Medium-resolution aerial laser scanning data of 1–10 pt/m^2 enables the production of a detailed DTM for use in flood mapping. The most useful is the high-resolution aerial laser scanning data with 10 or more pt/m^2, which enables the production of detailed DTMs for use in detailed 3D city reconstruction, with a detailed representation of roads, contours and other details. High-resolution aerial laser scanning with more than 10 pt/m^2 enables the production of topographic charts in scales of $1:5000$ and even $1:1000$.

1.3   Research objectives and scope

Different geodetic data used for local spatial planning are available in Slovenia. Aerial laser scanning is a relatively new but fast-evolving remotely sensed technique which can be effectively implemented in the production of geodetic data used in local spatial planning. Traditionally, photogrammetric and geodetic methods have been applied for local spatial data acquisition, so the existing processing methodology is based upon these methods.

Considering the technical and technological features and advantages of the aerial laser scanning technology, we believe that acquisition of geodetic data with the aerial laser scanning can increase quality and up-to-date status of geodetic data used in local spatial planning. Consequently, the process of decision making in local spatial planning can be easier and faster.

To optimize the data processing methodology by applying laser scanning technology we first need to do some research. Based on our experience (e.g. Interreg IIIA project HarmoGeo, topographic data acquisition and quality control) and a thorough study of relevant literature, we defined our research hypotheses:

- A simplified a-priori analytical error model of aerial laser scanning can be developed from rigorous error models, which returns comparable values to those computed by rigorous error models. This simplified a-priori error model must give basic constraints that can be applied in aerial laser scanning ordering.

- The requested precision of geodetic data for local planning is highly dependent on the

density (spatial resolution) of laser scanning data. Studying different configurations, a minimum density of laser scanning data that allows to achieve the requested precision for different geodetic products can be found out and recommendations for general purposes can be specified.

- Knowing a-priori error assessment and required aerial laser scanning point density, a proposal for implementation of laser scanning data, specifically for each geodetic data used in local spatial planning, can be developed. This proposal should direct towards optimization of the existing data acquisition methodology.

This thesis presents the local spatial planning regulations of Slovenia. The acquisition methodology optimization of geodetic data for local spatial planning is performed on the Slovenian example. Minimal terms for aerial laser scanning ordering are defined on a theoretical example of a typical aerial laser scanner. Therefore the derived minimal terms are applicable also for other geodetic data used for other purposes, not just for local spatial planning and not just in Slovenia.

1.4   Organization and methodology of the thesis

This work is divided in four parts:

1. Legal and methodological frame of geodetic data used for local spatial planing in Slovenia: Chapters 2 and 3.

2. Detailed analysis of different aerial laser scanning error sources and the development of the simplified analytical a-priori error model:

   - Description of physical background of aerial laser scanning in Chapter 4.
   - The detailed review of literature on the topic of different aerial laser scanning error sources and their sizes, and definition of boundary conditions[2] in Chapter 5.
   - Analytical derivation of simplified a-priori error model in Chapter 6.

3. Through knowledge on requested precision of certain geodetic data and test of the penetration rate in different vegetation classes the total aerial laser scanning point density is defined in Chapter 7. This Chapter is divided in two parts:

   - Theoretical derivation of minimal aerial laser scanning point density needed for certain precision demands.
   - Definition of the optimal point density on the basis of the penetration rate testing for different vegetation classes, performed on Nova Gorica test sample. This optimal point density enables the achievement of minimal point density under canopies.

4. Proposal for acquisition methodology optimization of geodetic data used for local spatial planning in Chapter 8.

---

[2]Detailed graphical presentation of error behaviour is presented in Appendix C.

An overview of thesis is given in: Conclusions (Chapter 9), Extended summary in Slovene (Chapter 10), and also Summaries in English and Slovene on the end.

The connection between different parts of the thesis can be seen on the processing scheme of the thesis (Figure 1.1).
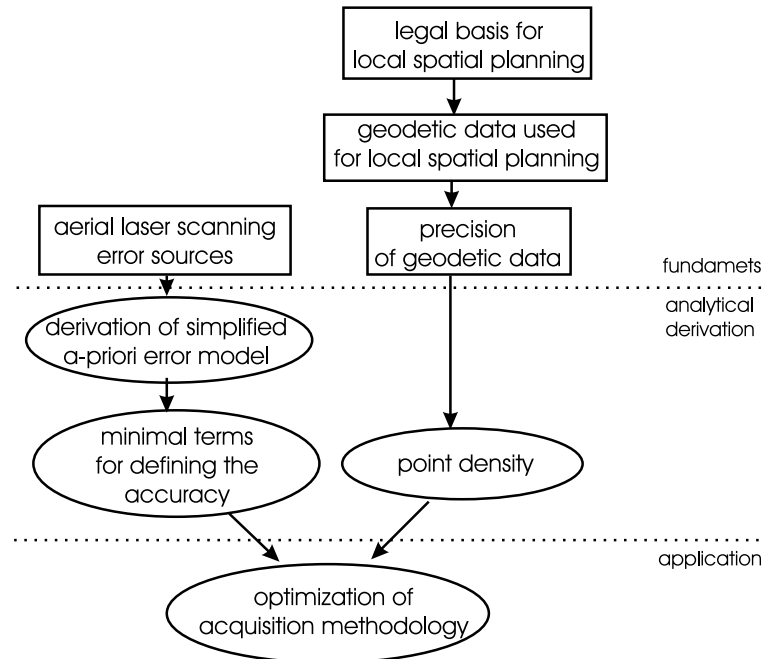
Figure 1.1: Processing scheme of the thesis.
Slika 1.1: Diagram poteka naloge.

The first two parts are mainly dedicated to the literature overview. At the end of the second part, the simplified a-priori error model is developed as an analytical derivation of the already existing Schenk's error model. Simulations of the original and the simplified error models are performed using the program Matlab. The deduction from analytical derivation and practical testing on real aerial laser scanning data is used to define the optimal point density needed for certain geodetic data. In the final part, the acquisition methodology optimization is proposed, made as a synthesis of minimal terms derived from the simplified a-priori error model, optimal point density and precision requirements of geodetic data used in local spatial planning.

Our contributions to the science are: the simplified a-priori error model of aerial laser scanning, the equations for definition of optimal point density depending on precision of geodetic data and proposal for acquisition methodology optimization for geodetic data used in local spatial planning.

2 LEGAL BASIS FOR PRODUCTION OF GEODETIC DATA USED IN LOCAL SPATIAL PLANNING IN SLOVENIA

2.1 Introduction

Spatial planning is an interdisciplinary science, which defines how the physical space on the national, regional or local level should develop. It provides guidelines and legal recommendations for directing the development of urban and rural areas (Pogačnik, 1992). Spatial planning of Slovenia is mainly regulated by the spatial planning act. This act define possible geodetic data used for spatial planning, spatial planning stakeholders, legal procedures how the spatial planning has to be conducted, and the intention of spatial planning. Spatial planning has to be a base for the sustainable development and steady urbanization, therefore a well prepared spatial plans are required. Spatial plans are based on the current physical space usage, therefore a detailed geodetic data should be used as theirs base.

In this chapter we will present the legal acts defining the spatial planning in Slovenia. Details on the history of the Slovenian spatial planning legislation can be found in Appendix A.1 on page 165.

2.2 Geodetic data used in spatial planning

For Slovenian spatial planning different state topographic maps are manufactured under the supervision of the municipalities and the Surveying and Mapping Authority of the Republic of Slovenia (SMA). These maps represent mainly 2D data, unless stated differently (Petrovič et al., 2005; Petrovič, 2007):

state-level: National general maps of different scales: National general map $1:250\,000$ (DPK 250) was completed in 2005, National general map $1:400\,000$ (DPK 400), National general map $1:750\,000$ (DPK 750) and National general map $1:1\,000\,000$ (DPK 1000). These maps are available only in raster format.

regional-level: National topographic map $1:25\,000$ (DTK 25) and National topographic map of $1:50\,000$ (DTK 50). The later represents more up-to-date spatial information as it is in a constant process of updating. Some layers of these maps are available in vector format, more for DTK 50.

local-level: National topographic map $1:5000$ (DTK 5) is maintained and available in vector format and presents a 3D product. Up to 2008 around 60% of Slovenia, mostly urban

areas, was covered with it.[1]

Geodetic surveying provides also many other topographic and real estate data for local spatial planning. Some are under the supervision of Surveying and Mapping Authority of the Republic of Slovenia (SMA) (e.g. land survey plans, Land cadastre, Building cadastre...) other are under supervision of the Ministry of the Environment and Spatial Planning, the Directorate for Spatial Planning (e.g. the instructions for spatial data system) (Petrovič et al., 2005; Petek, 2005).

Other geodetic data for presentation of the cartographic part of spatial planning documents are: land survey plans in scale 1:1000 or 1:500, ortophotographies, digital elevation model, land cadastre maps[2] and also data in other geodetic records concerning streets, railways, relief, hydrography, buildings, public infrastructure[3], geographic names, land use and spatial units (Pravilnik ...prostorski red..., 2004; Priporočila ...strokovne podlage..., 2005; Pravilnik ...občinski načrt, 2007; Pravilnik ...občinski podrobni načrt, 2007).

2.3 Current spatial planning acts
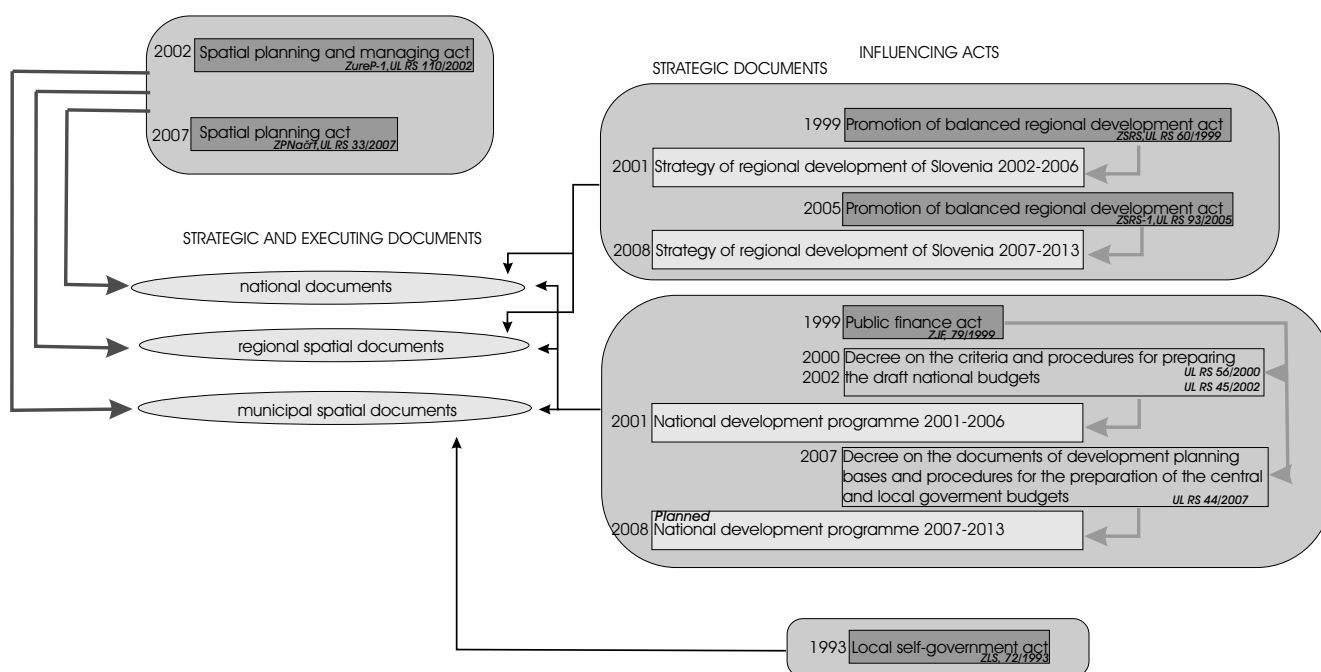
Figure 2.1: Spatial planning acts and strategies in Slovenia after 1991.
Slika 2.1: Zakoni in strategije, ki vplivajo na prostorsko načrtovanje v Sloveniji po 1991.

Spatial planning in Slovenia was enacted in the **Spatial planning and management act** – **ZureP-1** (ZureP-1, UL RS 110/2002 and 8/03) and its regulations, where the competences of the state and local spatial planning stakeholders (municipality or several municipalities together)

---

[1] for more information see the description of DTK 5 on page 22

[2] informative layer of the Land cadastre, see section 3.3.4 page 22

[3] data from the Cadastre of public infrastructure (utility system)

are described. The Spatial planning and management act was succeed by the **Spatial planning act – ZPNačrt** (ZPNačrt, UL RS 33/2007) where the spatial planning is described in detail and is in line with Directive 2001/42/ES of European parliament which regulates judgement of land use influences on the environment. Until the relevant regulations of ZPNačrt are enacted[4], some regulations of ZureP-1 stay in operation. Therefore both acts will be described.

The Spatial planning and management act (ZureP-1, UL RS 110/2002 and 8/03) and the Spatial planning act (ZPNačrt, UL RS 33/2007) define spatial planning stakeholders which prepare different spatial planning documents (see Figure 2.2[5]):

- **national** – spatial development strategy of Slovenia, spatial order of Slovenia and detailed plans of national importance

- **municipal** – spatial development strategy of the municipality with the concept of urban and landscape development and protection, spatial order of the municipality and municipal spatial plan

- **common spatial planning documents** – regional spatial development
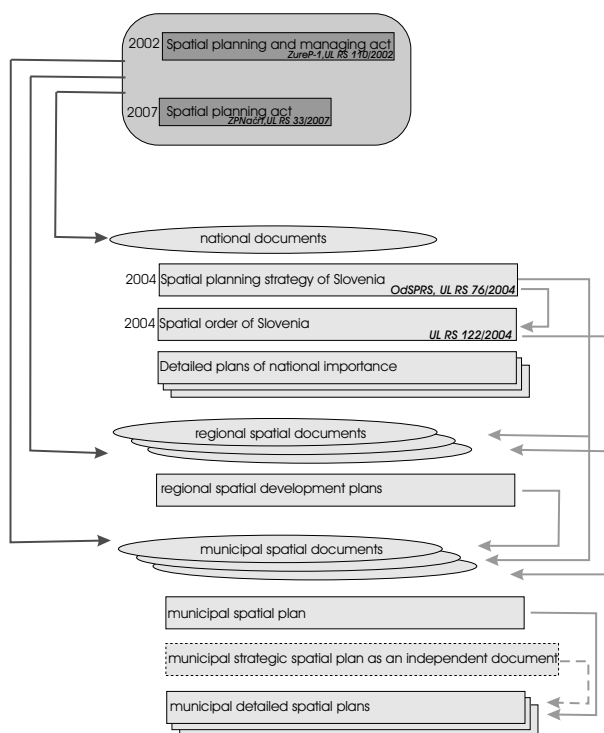
Figure 2.2: Spatial planning documents in Slovenia as proposed by current legislation.
Slika 2.2: Dokumenti, ki naj bi opredeljevali prostorsko načrtovanje po trenutni zakonodaji.

Spatial planning documents for different levels (national, regional and municipal) depend on executional subacts of ZureP-1 or ZPNačrt. Executional subacts define in detail procedures how to prepare different spatial planning documents. As spatial planning documents are legal

---

[4]some regulations can be enacted also 24 months after the ZPNačrt enaction, which was enacted on April 2007
[5]this diagram in Slovene is on Figure A.4 on page 168

documents, they come into force with subacts called decrees (e.g. Decree on spatial order of Slovenia, Decree on national location plan, Decree on the regional spatial plan). Decrees with relating spatial planning documents, become official when published in Official gazette of the Republic Slovenia[6].
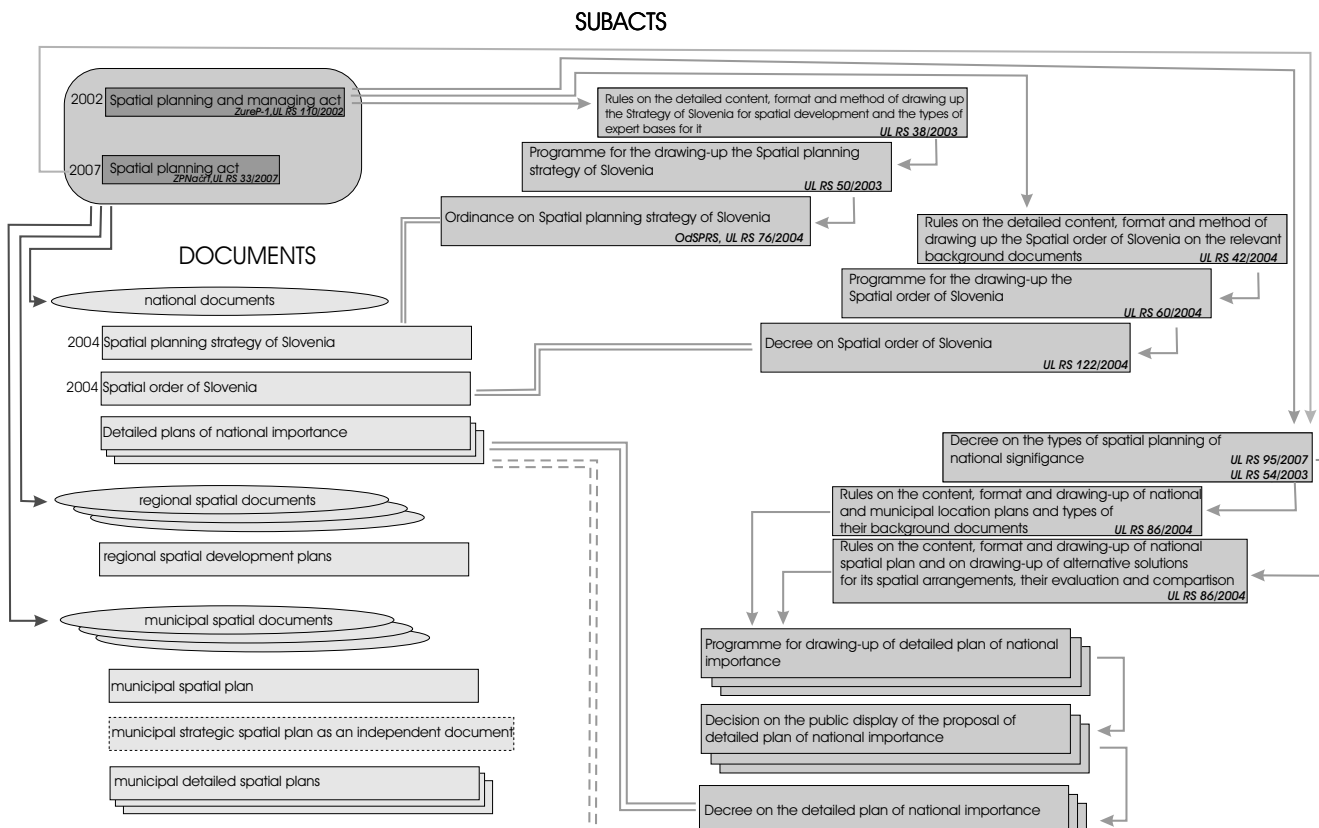
Figure 2.3: Subacts regulating national spatial planning.
Slika 2.3: Podzakonski akti, ki definirajo državno prostorsko planiranje.

Spatial planning documents are composed of:

- **obligatory part** which is the legal part of the document and

- **spatial planning maps** on which the solutions of the act are presented.

For the production of spatial planning maps different kinds of geodetic data are used. These geodetic data have to be official, confirmed by the state or municipality. Geodetic data for spatial planning can be divided in data for presentation of the cartographic part, and geodetic data for the legal part of the spatial planning document (Pravilnik ...prostorski red..., 2004; Priporočila ...strokovne podlage..., 2005).

---

[6]Uradni list Republike Slovenije — UL RS.

National spatial documents can be divided in strategic documents (Spatial development strategy of Slovenia and Spatial order of Slovenia) and spatial planning documents (different detailed plans of national importance). Detailed plans of national importance are prepared for the following purposes (Uredba ...državnega pomena, 2007):

- traffic infrastructure: road infrastructure for highways, main roads of the first and the second order, railway infrastructure on main railway lines, airport infrastructure of international/national importance, sea and river ports of international importance, traffic infrastructure on border crossings, traffic terminals of international or national importance, mixed traffic crossings of national importance

- energy infrastructure: for electrical (powerplants of 10 MW or more), gas and other energy infrastructure (pipelines which cross more than one municipality or cross the state border, refineries)

- public communication systems: GSM network

- natural environment protection: for managing the hazardeous waste

- meteorology: national network of meteorological stations

- water and sea infrastructure for preventing natural disasters

- natural and cultural heritage: for the most important monuments

- military infrastructure

- protection against natural and other disasters: objects of professional radio networks, sites for destruction of explosive bodies, spatial plans for areas affected in natural or technical disasters

As it can be seen from Figure 2.3[7], before a detailed plan of national importance comes in force, at least three decrees have to be published in Official gazette of Republic of Slovenia. This enables an active involvement of the whole interested public. Even after a decree is published, legitimate remarks and suggestions are being collected so that the spatial plan of national importance can be amended if necessary.

Strategy for regional development (Figure 2.1) demands that the planing of spatial arrangements of regional importance is done on regional level. Therefore regional spatial plans (Figure 2.4[8]) are drafted by participating municipalities in the region (ZPNačrt, UL RS 33/2007). The procedure how they come into force is the same as for Detailed plans of national importance. Therefore at least three decrees have to be published before the regional spatial plan comes into force. Unfortunately since publishing the decrees of programme for drawing-up of regional spatial plan in Official gazette of Republic of Slovenia in 2005[9], no additional decrees have been written. The

---

[7]this diagram in Slovene is on Figure A.5 on page 169

[8]this diagram in Slovene is on Figure A.6 on page 170

[9]published decrees of Programme for drawing-up of regional spatial plan: Savinjska statistična regija (SKTE3) (UL RS 10/2005), Koroška (UL RS 10/2005), Južna Primorska (87/2005) and Jugovzhodna Slovenija (UL RS 106/2005)

reason is that Slovenia still did not have defined regional borders, which is still a hot political topic.
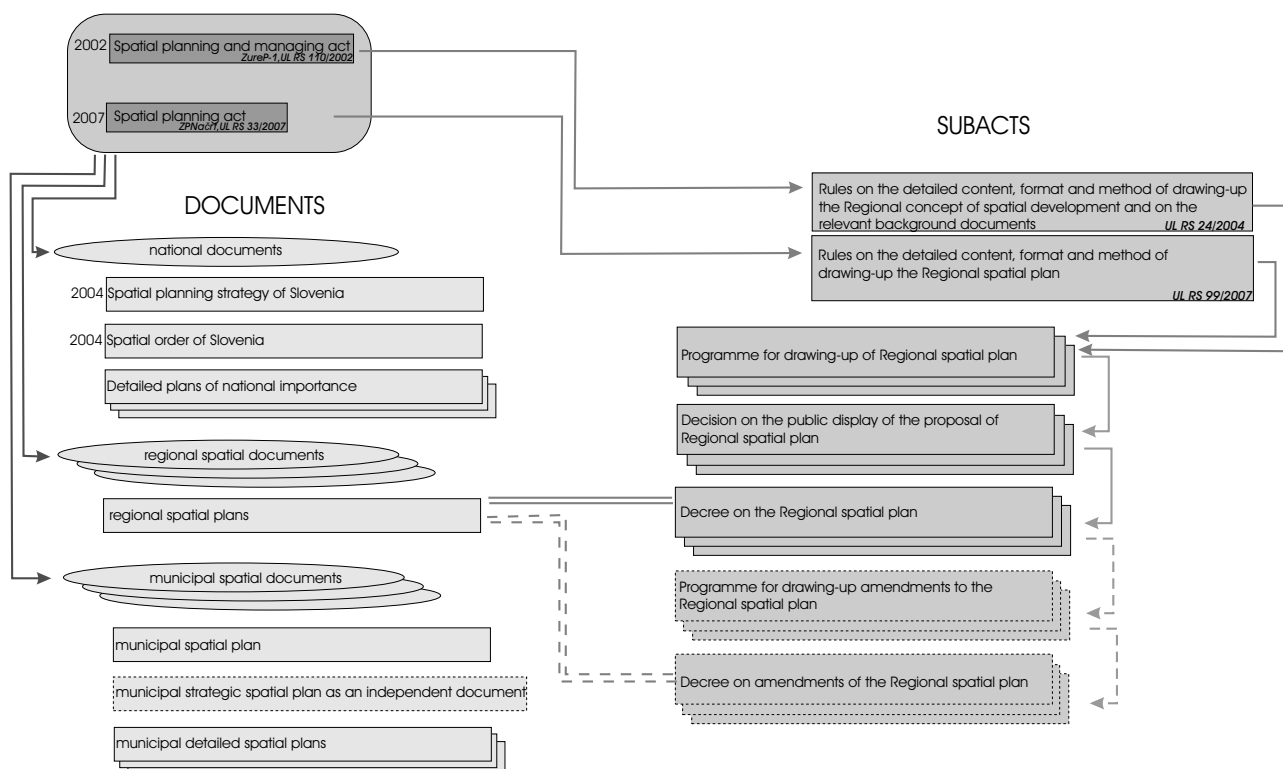
Figure 2.4: Subacts regulating regional spatial planning.
Slika 2.4: Podzakonski akti, ki definirajo regionalno prostorsko planiranje.

2.3.1 Local spatial planning

Local spatial planning under the authority of municipality must take into account national and regional (if existing) spatial planning documents. It deals with spatial arrangements of local importance and determines conditions for the alocation of buildings into space (ZPNačrt, UL RS 33/2007).

Municipal spatial planning should:

1. define the aims and guidelines for spatial evolution of the municipality physical space, especially areas of settlement

2. define current and future physical space usage

3. plan spatial arrangements in the physical space of the municipality

The subacts that influence the local spatial planning are presented in Figure 2.5[10]. They can be grouped in:

- subacts concerning planning — they define the content of local spatial planning documents

- subacts concerning managing — they define the participation of residents in municipal budget through fees

- subacts concerning spatial data — which is used for decision making and presentation of spatial planning documents

Finaly, subacts concerning spatial data influence also on the spatial planning documents, as spatial planning cannot be done without geodetic data on which the physical space is presented.
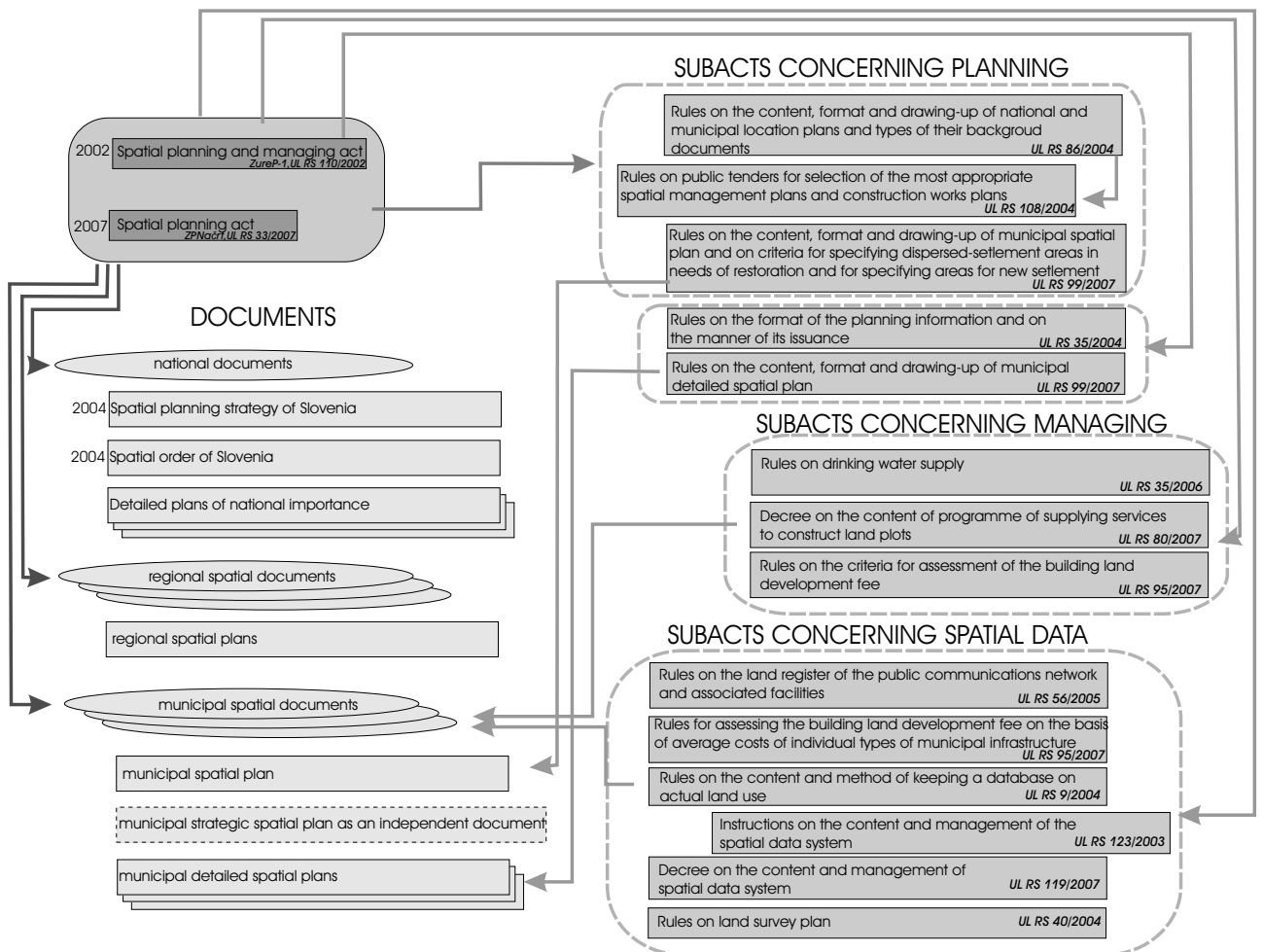
Figure 2.5: Subacts regulating local spatial planning.
Slika 2.5: Podzakonski akti, ki definirajo lokalno prostorsko planiranje.

---

[10]this diagram in Slovene is on Figure A.7 on page 171

Subacts concerning planning define in detail the strategic and operational part of the municipal spatial planning. It is divided in the following implementing documents:

1. **municipal spatial order** or **municipal spatial order plan** with the concept of urban and landscape development — it is an implementing document
2. **municipal spatial development strategy** as an autonomous document by ZureP-1, or as a part of municipal spatial order plan by ZPNačrt
3. **local detailed plans** — they are implementing documents

Similar arrangements are defined also for the physical space on the national and regional level (Figures 2.3 and 2.4).

Municipal spatial plan should not contradict the spatial planning acts defined on national level and should consider municipality direction of development and protection regulations. It should specify in detail: orientation for settlement growth and renewal (also restoration of degraded urban areas), location and development for different land use areas (landscape planning for agricultural and forested land, water and other natural resources), definition criteria for the building plots[11] and conditions for planning permissions[12], definition of areas or lines of public infrastructure and the measures for the use of public infrastructure for newly built buildings or settlements. The borders of individual planning zones should be defined in such a detail that they can be transferred in physical space and can be shown on Land cadastre.

Municipal spatial development strategy defines the basic premisses and objectives of municipal spatial development. It defines the priorities and guidelines for achieving the objectives of the municipal spatial development.

Local Detailed Plans are a basis for preparation of planning permits. The area of a local detailed plan is defined by its planning zone boundary. The planning zone should be based on plots of land. It should specify in detail: the impacts and links of the plan on the neighbouring zones, solutions and measures for environment protection and conservation of natural and cultural heritage, the sustainable use of natural resources, the solutions and measures against natural or other disasters.

2.3.2   Geodetic data used in local spatial planning

A municipal spatial plan (a plan of public infrastructure development, the plans for settlement growth and development) should be based on:

- a strategic plan should be presented on geodetic maps 1 : 50 000
- a spatial plan should be presented on land survey plan in the scale 1 : 5000 to 1 : 1000 if urban areas are dealt with; until the year 2010 the state topographic maps in scale 1 : 5000

---

[11] the plot of land on which building can be erected

[12] the legal document written by municipality, which enables the erection of a building on certain plot of a land

(Pravilnik ...občinski načrt, 2007) can be used instead of land survey plans. Also a general overview of the area in question should be presented on the national general map in scale $1:50\,000$.

- a detailed spatial plan should be presented on the land survey plan of scales from $1:5000$ to $1:500$.

- for general overview of the land use planning, defined by different detailed spatial plans, also the topographic maps or ortophotographies in scale $1:10\,000$ can be used for general overview.

The local spatial planning maps are a compilation of land survey plans, additional geodetic data and spatial planning directions. It represents the future development of physical space by the means of spatial planning doctrine.

2.3.3   Difference between the topographic map and the land survey plan

Under the ZureP-1 (ZureP-1, UL RS 110/2002 and 8/03) regulations the municipal spatial plans can be presented on the topographic maps in the scale $1:5000$ (e.g. state topographic map $1:5000$ — DTK5). The new ZPNačrt (ZPNačrt, UL RS 33/2007) and its subacts (Pravilnik ...občinski načrt, 2007, Pravilnik ...občinski podrobni načrt, 2007) enacted the land survey plan as a substitution for the topographic map.

The content of the land survey plan is defined by a subact (Pravilnik o geodetskem načrtu, 2004), while the content of the state topographic map $1:5000$ is defined by SMA technical regulations.

A land survey plan is composed of:

- a topographic map
- a certificate of the land survey plan

The topographic part of land survey plan has to obey SMA technical regulations for topographic map representation (Hašaj et. al., 2006). The technical regulations for topographic map representation define: the guidelines for production and use of topographic maps, the national coordinate system and projection[13] and the topographic symbol library. Land survey plan can represent (Pravilnik o geodetskem načrtu, 2004): relief, waters, vegetation, buildings, public infrastructure objects, land use, topographical names, geodetic points, Land cadastre, administrative units, and other morphological structures and features. The actual content of a specific land survey plan is based on its purpose. The Land cadastre data represented on land survey plans — the Land cadastre maps — has to be adjusted in planimetry to the topographic content (Petrovič et al., 2005).

The land survey plans can be acquired by: field measurements, photogrammetric stereorestitution, aerial or terrestrial laser scanning, or taken from state topographic maps $1:5000$ (DTK5)

---

[13]coordinate system D48 with Gauss-Krüger projection

and ortophotographies. (Petrovič et al., 2005). The most prevalent method for data acquisition in scales 1 : 5000 and 1 : 1000 in Slovenia is still photogrammetric stereorestitution. Although some examples of aerial laser scanning application in land survey plan production already exist in Slovenia. A differentiation census when to apply photogrammetry/aerial laser scanning or field measurements is 20 ha (Hudnik, 2008).

The second obligatory part of the land survey plan is the certificate defining the contents and the purpose of land survey plan. The certificate includes: subscriber, producer, identification number of the land survey plan, the production date and the statement of an authorized surveyor[14] where the contents and purpose of land survey plan are written.

Land survey plans in scale 1 : 5000 must be produced with graphical accuracy of at least 0.2 mm, which enables the geometrical accuracy of 1 m in physical space (Petrovič et al., 2005; Hašaj et. al., 2006).

2.4   Discussion

One of the most important roles of local spatial planning acts is to regulate settlement development. This is achieved through study of current state of the planning zone, which gives the base for guidelines of future development. Through morphology analysis of the physical space the measures and conditions for spatial development are set. Especially the detailed spatial plans should be as detailed as possible, they should give guidelines for building sizes, external structure (e.g. façade, roof slope and division, roof ridge direction), the materials used, where on the plot of land the building should stand, etc. When allowing new building erection in certain plots of land, the knowledge on the location of different public infrastructure entities is very relevant (how the house will be connected on sewage system, electricity, heating...).

The second important role of the local spatial planning is to regulate rural development, while not allowing to much fertile land to be lost for other purposes (the urbanization).

Spatial planning acts regulate the spatial planning and define which geodetic data can be used as a base for spatial planning. The most detailed local spatial planning documents are local detailed plans, which are made in scale 1 : 5000 or even 1 : 1000. In the next chapter the geodetic data which can be used for local spatial planning in Slovenia will be presented in detail. This will enable our further discussion on possible acquisition methodology optimization of this data by applying aerial laser scanning.

---

[14]To become an authorized surveyor one should pass an official state examination, where his knowledge of geodesy and public administration is verified. After the verification he is registered in official list of authorized surveyor.

3   CURRENT ACQUISITION METHODOLOGY OF GEO-DETIC DATA USED IN LOCAL SPATIAL PLANNING

3.1   Introduction

The main acquisition methodology for production and updating the spatial data in Slovenia is still photogrammetry. The majority of geodetic data used in local spatial planning is still based on it.

The main photogrammetric data sources in Slovenia are:

- Cyclic aerial survey (CAS) which is conducted by Surveying and Mapping Authority of the Republic of Slovenia (SMA) on regular basis
- special photogrammetric aerial surveys are ordered by different customers (e.g. municipalities)

For some isolated events and studies also some other remotely sensed data sources (high resolution satellite sensing, InSAR, aerial laser scanning) have been ordered in Slovenia. But mainly the costumers still use the before mentioned photogrammetric data sources, as the methodology how to order and work with these data is well established, and its accuracy and data extraction capability is already well known.

In this chapter we will present the photogrammetric data processing methodology and the basic characteristics of geodetic data used in local spatial planning in Slovenia.

3.2   Photogrammetric data processing methodology

As the photogrammetric process is already well established, just short notes on the methodology will be given in this section[1]. The main data processing parts how to derive from aerial surveys the 2D or 3D end-product are given in Figure 3.1.

---

[1]for details see Kraus (2004).

3.2.1   Aerial survey

The aerial survey results in aerophotographs acquired in stereo technique, they are named also stereophotographs. They can be recorded by analog or digital sensor. Current digital orientation procedures require photographs in digital format. The majority of aerophotographs made in Slovenia after the year 2005 are already directly recorded by a digital sensor.

The aerial survey includes also the data on location of the aeroplane in the time of the photographing: GPS and INS measurements. They are not obligatory as the orientation can be also performed without them. If these data are used, reduction of field work can be made, because less ground control points are needed in the process of orientation. In ideal cases direct georeferencing without the aerotriangulation can be made, if GPS and INS data of the platform are accurate enough. In the case of CAS photographing the aerotriangulation is still required.
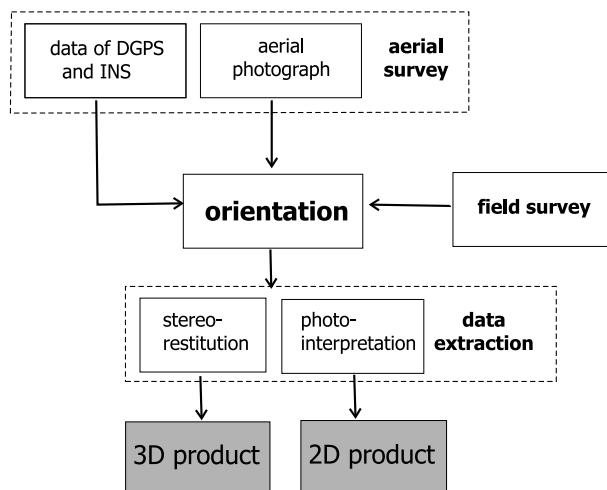
Figure 3.1: From aerial photograph to the final end-product.
Slika 3.1: Od aerofotografije do končnega izdelka.

CAS

The Cyclic aerial survey (CAS) project started in 1975, and has been conducted by SMA. The entire territory of Slovenia has been covered mainly in three to four-year cycles (Kosmatin-Fras, 2002; Oštir, 2006; Prešeren, 2007). The large scale aerophotographs of 23 cm × 23 cm format are made in scale approximately $1:17\,000$; since mid-nineties a constant scale of $1:17\,500$ has been used (Oštir, 2006). This scale is ideal for a map production in scale $1:5000$, where one map sheet represents 2250 m × 3000 m in physical space.

Before the year 2005 classical photographs of CAS were mainly recorded on black-and-white film[2], with some exceptions already recorded on color film. The whole CAS was made on color film for the first time in 2005. In 2006 the whole Slovenia was covered for the first time using digital camera[3] in color and near infrared (Prešeren, 2007). SMA plans to conduct the next CAS aerial survey of Slovenia in 2009.

---

[2]black-and-white film includes the spectral bands from 360 to 720 nm (Oštir, 2006)

[3]more information on the difference between classical and digital cameras can be found in 4.3.2 on page 33

3.2.2 Field survey

Ground control points used for orientation procedures and quality control of the aerial survey are measured by field survey. The ground control points should be measured with an accuracy 10 cm, to enable precise aerotriangulation, which is needed for end-products of scales $1 : 1000$ or $1 : 5000$. The accuracy of ground control points directly depends on the accuracy of GPS[4] measurements. Ground control points (planimetric and height) are needed to determine the scale, azimuth and attachment of photogrammetric model to the reference frame (datum) (Kosmatin-Fras, 2002). Additional control points are needed to determine the accuracy of photogrammetricaly derived end-products.

3.2.3 Orientation procedure

The orientation procedure ties the stereophotographs to the physical space. The orientation procedures can be divided in:

- interior orientation
- exterior orientation
    - relative orientation
    - absolute orientation

The purpose of **interior orientation** is to recover from the stereo-pair's project cone of rays the geometrically identical cone of rays entering the camera lens at the time of the exposure. It is done by a detailed calibration protocol of the camera, with calibration data measured by the manufacturer of the camera. It is advisable that the calibration data are checked every couple of years. The calibration data of the camera are: position of the principle point, the calibrated focal length, and image deformations defined by different errors of the optics.

The **relative orientation** reconstructs the same perspective conditions between a stereo-pair which existed when the photographs were exposed. It is conducted by removal of the y-parallaxes on six control points defined in the model space. These control points do not need to be measured in physical space, as the relative orientation is performed in the model space. The result of this procedure is the **stereoscopic model**, in which 3D relations between the objects can be seen and measured in model space.

Transformation of the stereoscopic model from the model space to the physical space defined by the local/global orthogonal reference frame is called **absolute orientation**. It is preformed by linking the model and ground coordinates of identical control points. Ground control points are measured by field survey and describe the physical space.

Complex computation of the exterior orientation of photogrammetric blocks (more than 2 photographs linked together) is done by **aerotriangulation**. Aerotriangulation reduces the number

---

[4]See description of GPS measuring techniques on page 61; for more detail see (Kozmus and Stopar, 2003). Even though the GPS presents just one of the Global Navigational Satellite Systems (GNSS), at this moment the GPS is the most commonly used systems and therefore in this thesis we will talk only about GPS.

of control points with respect to exterior orientation of each stereo-pair. Further reduction of the number of control points can be done by including DGPS and INS data of the flight.

Absolute orientation can be omitted if precise georeferencing of photographs is performed by detailed DGPS and INS data of the flight. Relative orientation should still be performed to set up the stereoscopic model from stereophotographs.

3.2.4   Data extraction

Data extraction from oriented stereophotographs is performed by stereo-restitution. Stereo-restitution gives ground coordinates of the measured objects through movement of the floating mark on object in 3D model space. It is performed using a stereo-digitizer, which can be analog or digital. Today mainly digital stereo-digitizers are used. Specific hardware is needed, which enables the presentation of 3D model space.

3.3   Current production methodology for geodetic data used in local spatial planning

3.3.1   Digital elevation models

Digital elevation models (DEM) can be divided in:

- **digital terrain models (DTM)**, describing the elevation of terrain without vegetation and buildings and

- **digital surface models (DSM)**, describing the elevation on the visible surface, e.g. tree tops and roofs of buildings.

The first project which aimed to make digital terrain model for the whole Slovenia started in year 1973 and was named DTM 100, meaning that the terrain is represented with a grid cell of 100 m × 100 m. The project was completed in 1984, but the gross error deletion continued until 1997.

In the year 1975 the first DTM which covered the whole Slovenia was produced – DTM 500, which was unfortunately never greatly acknowledged because of its poor quality.

Since 1995 the DTM 25 has been produced as a side-product of ortophotography production (Podobnikar, 2003). Its height accuracy for flat terrain is 1.5 m and for hilly terrain 6.5 m. The whole Slovenia was covered by the end of 2001 (Kosmatin-Fras, 2002).

DTMs described in previous paragraphs were all produced with photogrammertric stereo-restitution. First "non photogrammetric" DTM was InSAR DTM 25 produced by radar in-

terferometry in 2001 (Podobnikar, 2003). Its height accuracy for flat terrain is 1.9 m and for hilly terrain 13.8 m.

Parallel to DTM 25 acquisition as a side-product of ortophotography production, a new trend in DTM production is observed: DTM production as a blend of different already existing height data. In the year 2001 DTM 20 for 1/8 territory of Slovenia was produced as a blend from several different quality geodetic data sources (Podobnikar, 2003). This trend continued in the years 2003–2005, when DTM 12.5 was produced, again as a blend of several different sources which contain height information and their quality could be defined (as a metadata). In this project the whole Slovenia and its neighbourhood was covered. The following data was used: several already existing DTMs from 1973 on, digitized contour lines and other height data from topographic charts of scales 1 : 25 000 and 1 : 5000, geodetic points, cadastral points, the Slovenian border line, points and building polygons from building cadastre and other data available for just a part of Slovenian territory (e.g. DTM 10 for the City of Ljubljana). At the same time and from the same data, DTM 25 and DTM 100 were also produced (Podobnikar and Mlinar, 2006).

The latest DTM 5 was again acquired by stereo-restitution in the project of CAS 2006 aerial surveying by digital camera. In addition to stereo photographs, aerotriangulation and ortophotography production, as a side-product the DTM 5 was derived by automatic matching. Its height accuracy in unforested areas in under 1 m (Prešeren, 2007).

3.3.2   Ortophotographies 1 : 5000

Ortophotographies are produced from CAS photographs by differential rectification, which geometrically transforms the central projection of an aerial photograph into orthogonal projection. This transformation occurs piecewise, taking into consideration the inclination of the photograph and the radial deformations due to the relief (Kosmatin-Fras, 2002). Specific objects like houses or trees are in general not taken into consideration therefore the derived ortophotography is not true a ortophotography, as radial displacements of these objects (e.g. houses and high vegetation) are left on it.

The input data for ortophotography production are: scanned or digital image, parameters of exterior orientation from aerotriangulation and DTM. The resolution of the scanned/digital image must be in correct proportion to the image scale and final ground resolution. For CAS photograph of scale 1:17 500, the pixel size of scanning is 14-15 μm and the corresponding final ground pixel resolution is 0.5 m (Kosmatin-Fras, 2002).

If the existing DTM (see section 3.3.1) does not meet the accuracy specification for ortophotography production, if has to be measured by stereo-restitution from the same stereo photographs that are used for ortophotography production. For the ortophotography production of 1:5000 scale the DTM 25 was used until CAS 2006. CAS 2006 requested the use of more dense DTM, therefore DTM 5 delivered by automatic matching was used.

SMA started with production of ortophotographies in the scale 1:5000 in the year 1995 (Podob-

nikar, 2003), it was planed that the whole Slovenia will be covered by ortophotographies in a six-year cycle (Kosmatin-Fras, 2004).

The first digital CAS project of the whole Slovenia conducted in 2006 gave as a result color ortophotographies, with ground pixel resolution of 0.5 m for the whole country and also 0.25 m for urbanized areas. In addition ortophotographies in infrared color were made for the whole country with ground pixel resolution 1 m (Prešeren, 2007).

3.3.3 National topographic maps 1 : 5000 (DTK5)

The acquisition of topographic data represented on national topographic maps 1:5000 (DTK5) is under the supervision of SMA and municipalities. SMA provides the next contents: buildings, high objects, roads, railways, cable railways, land usage, water areas, axes of water bodies (rivers) and water features (Brnot, 2006). Interested municipalities can order also additional contents, e.g. the axes of electrical cables, vegetation borders, relief, characteristical lines, points, etc.

At the end of 2007 around 60% of Slovenian territory was covered with DTK5 (Petrovič, 2007).

Data acquisition for DTK5 production is made by photogrammetric stereo-restitution of CAS aerophotographs. Therefore DTK5 is not just a 2D product, but a topographical database with 3D data. It enables both the cartographic representation and 3D visualization.

DTK5 of scale 1 : 5000 must be produced with graphical accuracy of at least 0.2 mm (Hašaj et. al., 2006).

3.3.4 Land cadastre

Land cadastre is managed under regional SMA units as 46 local land cadastre offices. In these databases the following data are stored: the number of plot of land, boundary of plot of land (defined by coordinates of boundary-stones), area of the land plot, owners, the land usage and profit (for forests and agriculture areas). The Land cadastre data are stored in databases within 2700 cadastre municipalities and approximately 5 250 000 parcels (Režek, 2008). The updating of Land cadastre is performed centralized within the national SMA, on the basis of regional SMA land cadastre databases.

Land cadastre is divided on:

- formal land cadastre data, stored in land cadastre plans and land cadastre data

- informative layer called land cadastre maps

On **land cadastre maps** only the boundaries and numbers of plots of land are represented. The land cadastre maps are intended only for informative purposes, not for terrain survey (e.g.

representation in geographical information systems, for planning) because they were subject of different transformations to enable better fit of its contents on topography.

For field measurements only **original formal land cadastre data** with a legal status should be used.

New data describing parcel divisions and commassations are measured by field geodetic measurements with classical surveying measurements (theodolite, total station) or GPS. Since January 2008 all new land cadastre measurements should be delivered to regional SMA units in two coordinate systems: old D46/Gauss-Küger and new D96/ETRS89/TM[5](ZEN, UL RS 47/2006).

3.3.5   Building cadastre and Real estate register

Building cadastre

Building cadastre is a legal database of buildings and building parts. A building part (e.g. apartment) is a part of a building which can be sold separately.

For each part of a building the following data exist in the Building cadastre: number of the building part, owner of the building part and manager of the building[6], location of the building, location of the building part in a building, area of the building part, usage of the building part (residential, non-residential). Data of the Building cadastre are linked to the Land cadastre, Land register[7] and Register of spatial units.

Building cadastre was set up by photogrammetric stereo-restitution from CAS stereophotographs, where 3D outlines of independent buildings or groups of linked buildings were measured: ground height, roof top height, roof edge height. These data were a base to derive the number of floors in the building and the ground plan of each floor. New data on old buildings and building parts are delivered from the owners of building parts by their initiative. According to the law newly erected buildings should be inscribed in the Building cadastre with location measured by field measurements.

At the end of 2006 the database included more than 1 231 000 buildings and building parts (Režek, 2008), which presents around 65% of all buildings and building parts in Slovenia. Unfortunately the process of inscribing all building parts in the Building cadastre is slow, as it is based on the need of owners to define their private property. Therefore a new database which describes similar data was set up – the Real estate register.

---

[5]transformation of all spatial data of SMA into the new coordinate system is not planed before 2010.

[6]The manager of the building is in charge of dividing the bills for electricity, sewage, tap water... organizes cleaning of joint areas in the building and upon instruction of the owners organizes larger renovation works (e.g. roof renewal, renovating façade).

[7]Land cadastre describes the boundaries and area of a parcel in detail and is set by SMA. The Land register describes the same parcels, but its intention is to follow legal status of the parcel (the owner, the servitude) in detail and not its physical manifestation in nature. The Land register is set up under the Court of justice.

Real estate register

Basic difference between the Building cadastre and the Real estate register is that the cadastre data is totaly left to the initiative of the building part owners and its legal actions. On the contrary the Real estate register was set up with questioning the owners and without legal engagement of the owneres. It is managed by SMA.

Real estate register is defined in legal act ZEN (ZEN, UL RS 47/2006). First the inventory of buildings and building parts was set up by interviewing the owners or building manages on the status of buildings and building parts: the number of building parts, the owner, the building part user if it is not the same as the owner, area of the building part, building part usage and other data about the building part. The interviewing was performed on spot of the building or building part with a uniform questionnaire. The field interviewing of owners was performed in the first half of the year 2007 and when data on 1 689 941 buildings or building parts was acquired. This represents 91.4% of all buildings or building parts in Slovenia (Petek, 2007). All these data were inscribed in the Real estate register and linked with other data of SMA: Register of population, Land cadastre, Building cadastre, etc. The Real estate register was set up in the middle of 2008. Different users will be able to access its data from the end of 2008 on (Rotar, 2008).

Real estate register describes better (updated) status of buildings and building parts than Building cadastre and is therefore more suitable for spatial planning.

3.3.6 Register of spatial units

In the Register of spatial units legal data on spatial boundaries are stored: land cadastre municipalities, municipalities, settlements, local communities, election units, school units, regional SMA units and other administrative units. Also house numbers and street names are stored in the Register of spatial units. In the Register of spatial units there are: 17 272 spatial units and 514 800 house numbers (Režek, 2008).

Register of spatial units is connected to the Land cadastre spatial data.

3.3.7 Register of geographical names

Geographical names are stored in the Register of geographical names maintained by SMA. The positional accuracy of these data is 2 m (Berk and Duhovnik, 2007).

3.3.8 The cadastre of public infrastructure (Utility system cadastre)

There exist two types of cadastre of public infrastructure in Slovenia:

- municipal cadastres of public infrastructure

- national Cadastre of the public infrastructure

The Cadastre of public infrastructure on national level started with operation in the year 2006 (Mlinar et al., 2006) and is maintained by SMA. Its establishment was first defined in ZureP-1 (ZureP-1, UL RS 110/2002 and 8/03). Both municipal and national cadastres of public infrastructure are connected as municipalities are obligated to give the data from municipal cadasters to the national one. The Cadastre of public infrastructure can be used for spatial planning and even taxing (ZPNačrt, UL RS 33/2007). The Cadastre contains data contributed from different managers of public infrastructure (e.g. electricity distribution companies) and owners of public infrastructure (municipalities). By law contribution of data in this cadastre is obligatory, but there are no fines for disobeying, therefore some missing data in some areas of Slovenia still exist in 2008.

The main purpose of the establishment of the Cadastre of public infrastructure is to show the coverage of physical space with public infrastructure entities.

In the list (Pravilnik ...dejanska raba prostora..., 2004) of public infrastructure the following entities exist:

- *traffic infrastructure*: roads, railways, railway terminals, airports, harbors

- *energy infrastructure*: networks and objects of electricity, gas, oil, heating

- *communal infrastructure*: water supply, sevage, waste removal

- *river and creek infrastructure*: levees, objects needed for water monitoring

- *other infrastructure for management and protection of natural environment*

- *other objects and networks in public use*: telecommunications

Some entities of public infrastructure can be acquired using photogrammetric stereo-restitution (roads, railways) others only by fieldwork following the construction of this type of public infrastructure (e.g. water supply, sewage). Underground objects can be also acquired using of ground penetrating radar (georadar). Electricity lines can be easily identified by aerial laser scanning (the acquisition of power-lines is the prime advantage of aerial laser scanning).

3.3.9   Database on land use

Database on land use is prepared for the whole country and renewal of data is planed to be conducted every three years. It is defined by a subact (Pravilnik ...dejanska raba prostora..., 2004) and stored and maintained by SMA. In database on land use the following land uses exist: agricultural areas, forest areas, water areas, built-up areas and arid areas. The database is mainly designed for spatial planning.

Database on actual land use was mainly acquired from CAS ortophotographs, with ordinary photointerpretation without stereo-restitution. The data acquisition can be conducted also from satellite high-resolution data. Database on land use is defined only in 2D.

SMA manages also Corine land cover databases, where land uses are divided in 44 classes. It was first set up for the whole county in 1995/1996 (CLC1995) and again in 1999/2000 (CLC2000). In both cases data was acquired on the basis of satellite data. The updating of this database is intended on every 10 years.

The Ministry for agriculture established more detailed database on land use for the purpose agriculture monitoring. It is connected to SMA's database on land use. The database on land use of agricultural and forest areas defines the following entities (Pravilnik ...kmetijskih in gozdnih zemljišč, 2006): field or garden, field of hops, permanent crops on fields, greenhouse, vineyard, olive fields, permanent pasture, swamp pasture, intensive fruit garden, extensive fruit garden, other permanent plantations, neglected agriculture area, uncultivated agriculture areas, forest plantation, woods and shrubs, agriculture area grown with forest. This database uses the same incoming data for its updating as the SMA's database on land use — CAS ortophotographies or high-resolution satellite data with photointerpretation.

3.4   Discussion

In Slovenia at the moment only legal databases which describe the ownership of land and buildings should be maintained by field measurements (Land cadastre, Building cadastre). The other geodetic data used in local spatial planning are updated by the usage of photogrammetric stereo-restitution or direct photointerpretation on the basis of ortophotographies delivered from photogrammetric photographs or high-resolution satellite data. In subacts defining all these databases the methodology how to acquire data for these databases is not prescribed. In most cases only the planimetric and height accuracy are defined. This enables also the employment of other acquisition methodologies (aerial laser scanning, terrestrial laser scanning, high-resolution stereo data, etc). Therefore this work in the following chapters defines in detail which terms should aerial laser scanning fulfill to enable the substitution of photogrammetric procedures with the employment of aerial laser scanning.

4 PHYSICAL BACKGROUND OF AERIAL LASER SCANNING

4.1 Introduction

First airborne lasers were tested in 1960s; in the 1970s they were developed specifically for bathymetric and hydrographic applications. First accurate ranging measurements were possible with the use of GPS in late 1980s. In early 1990s laser profilers were gradually replaced by scanners and GPS positioning was combined with INS (inertial navigational systems) (Wehr and Lohn, 1999). Nowadays, precise kinematic positioning of the platform and referencing to external coordinate system is possible by differential GPS (DGPS) and inertial attitude determination by IMU (inertial measurement unit) (Ackermann, 1999).

As soon as lasers with high pulse repetition rates were available on the market, laser scanning systems were released. Such systems are known as laser ranging systems, which are described with two acronyms: LADAR — LAser Detection And Ranging and LIDAR — LIght Detection and Ranging. LIDAR may also be built with xenon or flash lamps which are not laser sources (Wehr and Lohn, 1999). Therefore we will call them **laser scanners**.

Laser scanners can be divided regarding the platform:

- airborne laser scanning systems (when the laser scanning unit is mounted on a helicopter or an aeroplane)

- terrestrial laser scanning systems

Terrestrial laser scanning measurements are more simple than airborne, as the terrestrial laser scanners are mounted on one usually known fixed standpoint for the whole period of the performed measurements. On the contrary, we have to calculate for each laser range measurement made by airborne laser scanner, a new position of the system.

With laser scanner measurements, predefined points on a certain object cannot be measured, as this system is not capable of any direct pointing to a predefined location. One pulse can also produce multiple returns from different objects lying on its path. This can be seen especially in the forest areas or areas covered by other vegetation. In the European type of medium dense mixed forests, 20-40% of the laser pulses penetrates to the ground in the leafed time of the

year and nearly 70% in the winter time (Ackermann, 1999). The multiple echoes derived from such types of the ground do not represent any particular surface, the ground surface has to be mathematically modelled afterwards.

4.2   Airborne laser scanners

We can divide airborne laser scanners regarding the type of range measurement into (Baltsavias, 1999b; Wehr and Lohn, 1999; Wagner, 2005a):

- **Pulse lasers** – the laser energy is emitted in pulses. There are two possibilities (Figure 4.1):
  - classical **pulse** laser, where the receiver registers only a few returns or echoes of one pulse with its intensity additional information. In first generation laser scanners, the receiver registered just the first and the last echo of one pulse. Nowadays, the last generation receivers register up to four echoes of one pulse, eg. ALTM 3100 (Wagner, 2005a);
  - the **full-waveform** laser receivers which record all returns of one pulse with amplitude and the width of returned pulse (in the test of Riegl laser LMS-Q560 at the University of Vienna up to seven returns of one pulse were recorded (Wagner, 2005b). The full-waveform lasers enable a more detailed analysis of the physical characteristics of the reflectors – the ground points. At the moment the drawback of full-waveform lasers is an enormous amount of data which has to be processed. Sometimes they are named also just **waveform** lasers (Wehr and Lohn, 1999).

- **Continuous wave lasers** – the laser energy is emitted continuously. The range is obtained by phase difference measured between emitted and received signal. They employ two frequencies: the low and the high frequency what corresponds to λ_{long} and λ_{short}. The smallest frequency – corresponding to wavelength λ_{long} – defines the longest range, the longest frequency – corresponding to λ_{short} – defines the acquisition accuracy and ranging precision.

On Figure 4.1 the y-axis represents the power in arbitrary units, the x-axis represents the time. Shaded area represents the energy of the pulse or echo, τ_p is the time length of the emitted pulse. The energy of the echo is always smaller than the energy of the pulse. On Figure 4.1A two pulses and theirs transmitted power are presented. On Figure 4.1B power of the echo received back to the receiver is shown, which triggers the counter of the receiver when a certain power threshold is exceeded. The output of this echo on the classical pulse laser system is shown on Figure 4.1C and on full-waveform system on Figure 4.1D. The former digitizes only limited number of returned echoes (max. four), the latter digitizes the whole representation of the received power signature.

Regarding the medium in which laser light is produced and multiplied, the lasers can be divided into gas (the first laser was He-Ne laser), liquid (organic pigments), solid-state (ruby, Nd:YAG[1])

---

[1]Nd:YAG is yttrium aluminium garnet, doped with a few % of Nd^{3+}

and semiconductor diodes (Ga-As diodes) (Čopič, 1995). For the remote sensing the semiconductor lasers and Nd:YAG lasers are used which cover the optical band between 0.8 and 1.6 μm (Wehr and Lohn, 1999). The solid-state Nd:YAG lasers emit pulses with duration of 10-15 ns, with wavelength of 1.06 μm and peak power of several MW (Čopič, 1995).

The detector at airborne laser scanners is InGaAs [2] avalanche photodiode (Wagner, 2005a).
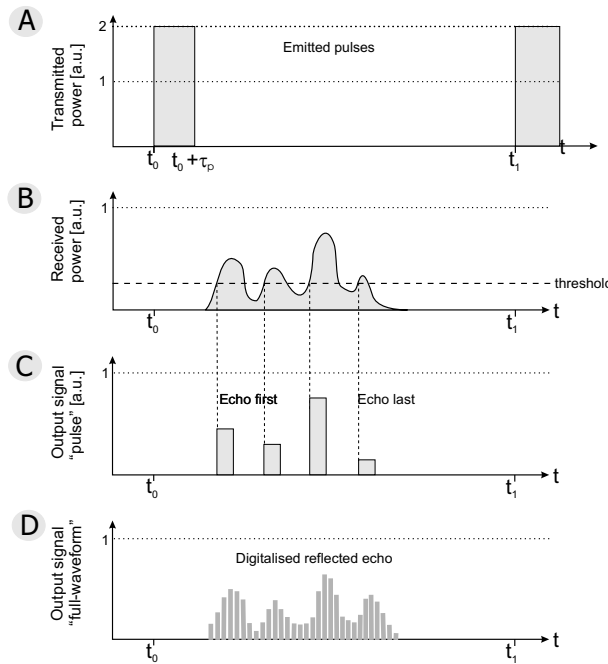
Figure 4.1: The laser pulse and its output representation in ordinary pulse and full-waveform format.
Slika 4.1: Laserski pulz in njegov odboj v navadni pulzni in obliki z opisom valovanja.

The laser scanner system can be subdivided into the following key units: laser ranging unit and positional and orientation unit. Positional and orientation unit consists out of differential GPS (DGPS) and inertial navigational system (INS).

4.3   Different types of products

As the laser scanning is a relatively new technology practically available on the market, the users are not yet well informed of the products that fulfill their needs. A short description follows about the basic possibilities among which the user of airborne laser scanners can choose.

Laser scanning data are not just numbers representing planar coordinates and height of ground points, but every point also carries information about the intensity of the returned signal from that point. If the data are presented in raster models, the intensity values are presented in pixels (Wotruba et al., 2005).

---

[2]indium gallium arsenide

Table 4.1: Typical characteristics of the ordinary and full-waveform laser scanners (Wagner, 2005a).
Tabela 4.1: Tipične značilnosti navadnega pulznega laserja in pulznega laserja z opisom oblike valovanja.

	Typical values of commercial ALS	ALTM 3100	Full-waveform example: LMS-Q560
Wavelength	1.04 or 1.54 μm	-	NIR
Pulse duration	5 – 10 ns	-	4 ns
Pulse energy	100 μm	-	-
Laser repetition rate	20 – 80 kHz	33 – 100 kHz	< 100 kHz
Scan frequency	25 – 40 Hz	max. 70 Hz	5 - 160 Hz
Max. scan angle	7 – 40°	25°	± 22.5°
Beamwidth	0.2 – 2 mrad	0.3 mrad	0.5 mrad
Flight altitude	500 – 3000 m	80 – 3500 m	< 1500 m
Laser footprint size	0.2 – 2 m	0.024 - 1 m	0.5 m at altitude 1km
Range capture / digitized bits	2 – 4 range measurements	up to 4 pulses	16 bits

Commercial tenders usually offer already filtered data: divided into the first and last pulse; but they rarely talk about the method of filtering, so it cannot be verified (McKean and Roering, 2005). As an normal end user one hardly gets real raw data. Usually the tender makes also the transformation of the data in local coordinate system (the country's legal or other coordinate system). As the tender usually does know the detailed transformational parameters between the WGS84 reference frame and the national one it is advisable that the end user of the laser scanning data performs the transformation transformation into the national coordinate system on his one.

Regarding the wavelength of airborne laser scanners they can be divided in:

- **topographic lasers** which employ only one wavelength in optical band between 800 nm and 1600 nm (Wehr and Lohn, 1999; Wagner, 2005a). The first laser scanners operated with a wavelength of 900 nm, which were still problematic for eye safety because of its high energy density. Nowadays mainly wavelengths higher than 1000 nm are used. Therefore topographic lasers typically operate at 1064 nm and 1535 nm (Wagner, 2005a). For example TopoSys laser scanner operates at 1535 nm (Wehr and Lohn, 1999). These wavelengths suffer only from water vapor and aerosols in the atmosphere, therefore aerial laser scanning becomes problematic when working in fog or smog (Wagner, 2005a)

- **bathymetric lasers** also named **green lasers**, are based on the same principles as topographic lasers, but emit pulses in two wavelengths, usually 1064 and 532 nm. The first IR wavelength reflects on the water surface, the second visible wavelength – the green light – penetrates the water and is reflected by the bottom or other objects in the water. It penetrates up to 70 m of depth (Wehr and Lohn, 1999).

Different wavelengths are employed also on other noncommercial satellite based laser systems. For example on Geoscience Laser Altimeter System (GLAS) on board of ICESat satellite uses dual-beam laser: 1064 nm wavelength is used for measuring the height of the Earth's surface and dense clouds, additional 532 nm wavelength is used for measuring vertical distribution of clouds and aerosols (Wagner, 2005a).

Additional products to laser scanning

Regarding the additional product which can be offered together with laser scanning, we can purchase:

- laser scanning data (topographic or/and bathymetric)
- laser scanning data with additional ortophotography of the same area
- laser scanning data with additional hyperspectral ortophotographs of the same area

As it was already mentioned, we can get laser scanning data with black-and-white, color or multispectral ortophotography. They can be acquired simultaneously from the same platform as laser scanning. The photographs used for production of ortophotography are made with full-frame or line digital cameras mounted on the same platform.

The number of points per unit area

The basic parameter when doing the acquisition of airborne laser scanning data is the number of points per m^2. If we summarize the experiences from Vienna and Udine universities (Kraus (edt.), 2005; Crosilla and Beinat, 2005), we can distinguish data by the number of points per m^2 required for our purposes:

- In the first group there is at most 1 point per m^2, which enables a production of a general DEM (digital elevation model) and it is comparable with the data acquired from photogrammetric stereopairs. It will be named a **low-resolution** aerial laser scanning.

- The second group with 1 to 5 points per m^2 enables the production of a detailed DEM (for example river basins for hydrological purposes). It will be named **medium-resolution** aerial laser scanning.

- The third group, where more than 5 points per m^2 are acquired, enables the production of DEMs of cities, roads and other details (10 points/m^2 is enough for the majority of such needs). In some cases this group is named **high-resolution** aerial laser scanning.

32

Triglav-Čekada, M. 2009. *Optimization of the data processing methodology and accuracy analysis of airborne laser scanning data applied for local spatial planning*, PhD thesis, Ljubljana, UL, FGG, Department for geodesy

4.3.1 Bathymetric lasers

The bathymetric lasers mounted on airborne platform can be used for shallow waters of rivers and coastal areas to acquire in same flight the river or see banks and the water bottom. They are used for acquisition of depths, which can be acquired also with SONAR[3].

The first bathymetric laser applying the full waveform digitalization was introduced in 1994 by Optech — SHOALS (Scanning Hydrographic Operational Airborne Lidar Survey) (Gutelius, 2002; Francis and Tuell, 2005). This system enables identification of fish, plankton, algae, turbid materials (floating sand and other sediments) etc., which stand in the way of laser beam propagating to the bottom (Gutelius, 2002).

The bathymetric laser SHOALS 1000T vertical accuracy in depths up to 20 m, when it is flown at 200–400 m altitude, is totaly comparable to a SONAR acoustic multi-beam system. Both systems achieve vertical accuracy of around 25 cm RMSE (Gutelius, 2002; Davis et al., 2005; Millar et al., 2005; Lockhart et al., 2005). Laser measurements do not have the same accuracy as multi-beam when searching for bigger depths on sharp objects, the reason for that is mainly the footprint size. In such cases laser-reported depths are deeper than in reality (Lockhart et al., 2005). The frequency of measurements of topographic and bathymetric lasers is not identical (e.g. SHOALS 1000T10 has 1-kHZ bathymetric and 10-kHz topographic lasers), this means that both systems cannot achieve the same number of points per unit area (Francis and Tuell, 2005).

The bathymetric lasers have been mainly used for costal maritime areas, while river measurements are still dealing with problems. Compared to costal areas, rivers have more turbid material in them and also they do not have uniform river bottom when checking its reflectance. A lot of turbid material makes bathymetric laser scanning impossible, as the green laser cannot penetrate to the bottom (Davis et al., 2005; Millar et al., 2005). The next problem when measuring rivers are large areas with very shallow water – water depths of less than 50 cm – which fall already within the limits of bathymetric laser scanning precision. To extract such small depths new algorithms for extraction have to be developed (Millar et al., 2005).

The next generation of Optech SHOALS bathymetric systems available from the year 2003 is CHARTS (Compact Hydrographic Airborne Rapid Total Survey), which consists out of bathymetric and topographic laser and a digital camera, nowdays it includes also hyperspectral sensor (Francis and Tuell, 2005). This integration of hyperspectral sensor to dual-beam laser provides the ability to conduct 3D benthic habitat mapping or coral reef mapping and 3D coastal landcover mapping or change detection at the same time from a singe platform (Francis and Tuell, 2005; Tuell et al., 2005). All sensors are integrated in one body and are post-processed together.

---

[3]Measurements of maritime areas and river depths are mainly done with SONAR (SOund Navigation And Ranging) which uses sound propagation under water. SONARs are mounted on water platforms; ships and boats. There are **single-** and **multi-beam SONARs**, which differ on the number of beams used during measurement. When using multi-beam SONAR, the area of interest can be measured quicker compared to single beam SONAR. SONAR measures the time duration between the emitted and received sound wave, out of which the distance is calculated. SONAR takes into account also the physical characteristics of the water (temperature, pressure) which influence on the speed of the sound (Karničnik, 2006).

For spectral analysis normalized full waveforms from laser and spectrometer are used together (Tuell et al., 2005).

4.3.2   Digital cameras

The first digital cameras which can compete with conventional film aerial cameras were introduced to the market around the year 2000. Digital aerial cameras can be divided in two groups as seen on Figure 4.2 (Vosselman, 2005):

- **Three-line cameras** (Figure 4.2A) which work on push broom technology. The linear-array CCD-sensors, which share the same optical system, produce forward, nadir and backward looking lines. This system requires GPS/INS system to determine the orientation of all recorded scan lines.

- **Multi-frame cameras** (Figure 4.2B) use multiple frame CCD-sensors, each having its one optical system. By combining either convergent or time-delayed recordings of these frame sensors, large digital images of up to 8000 by 14000 pixels are composed. Multi-frame sensors can be made of a different number of frames and optical systems.

Three-line cameras and multi-frame cameras are also used to construct multi- and hyerspectral cameras.

An example of tree-line camera is ADS40 by Leica Geosystems and of multi-frame camera DMC by Z/I Inc (Leberl et al., 2002).
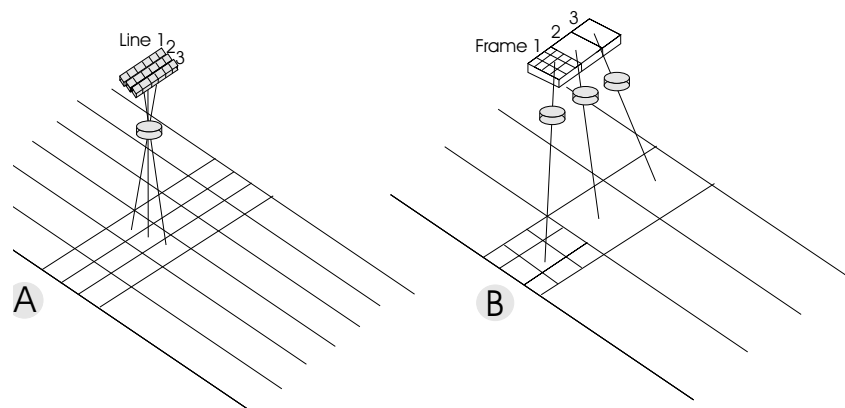
Figure 4.2: Digital aerial cameras: A) three-line sensor, B) multi-frame sensor.
Slika 4.2: Digitalni aero fotoaparati: A) trivrstični senzor, B) večslikovni senzor.

Image processing of digital camera needs different workflow and different analysis tools from convenient film areal cameras, because picture production geometry is different (Figure 4.2). Mainly the position of the platform in the time of picture exposure has to be known very precisely, this is achieved with GPS/INS measurements (Leberl et al., 2002).

For the purpose of the Cyclical Aerial Survey (CAS) the whole Slovenia was aerial surveyed for the first time with digital aerial camera ADS40 in the year 2006.

4.3.3   Multispectral and hyperspectral sensors

Sensors which register different number of spectral channels in optical spectral band can be divided in (Oštir, 2006):

- **Multispectral sensors** register several of spectral channels of visible wavelengths. For example one sensor can register channels of panchromatic, red, green, blue, infra red light. Multispectral sensors usually use different optical systems for each spectral channel.

- **Hyperspectral sensors** register a large number of narrow spectral channels, up to a few hundred (Leberl et al., 2002). Therefore every object is presented with almost continuous unique spectral signature and can be easily separated from other objects. Hyperspectral sensors usually use one optical system for all spectral channels.

On Figure 4.3 the division of optical band usually presented on the film is made on theoretical multispectral and hyperspectral sensor.
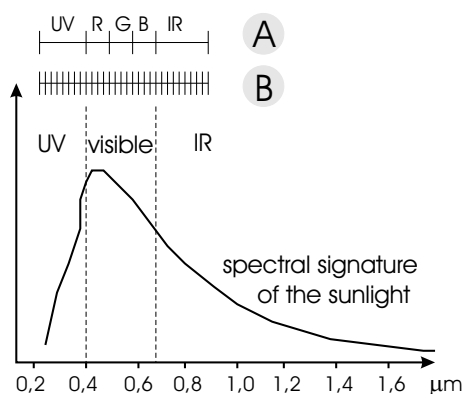
Figure 4.3: Spectral signature of the sunlight. Spectral channels of A) multispectral sensor and B) hyperspectral sensor.
Slika 4.3: Spektralni podpis sončne svetlobe. Razdelitev spektralnih pasov pri A) multispektralnih in B) hiperspektralnih senzorjih.

4.4   Basic physical characteristics of laser scanning

In this thesis only pulse lasers will be discussed, therefore the explanation of the basic physical characteristics will be limited to pulse lasers. Details about continuous wave lasers can be found in Baltsavias (1999b). The principles of range measurements are explained as well as factors which influence the magnitude of received signal. For simplification of the equations we assume only in this chapter that: the roll and pitch angle are zero, the laser scanner scans along a plane perpendicular to the flight direction, and it scans in equidistant lines. Another assumption is that the scanned terrain is flat.

4.4.1   Intensity of the received laser echo

Intensity of the received laser echo is not a physical quantity but a technical one. Intensity is the raw measurement of the laser measuring unit – the receiver. The echo of the pulse hits the surface of the receiver chip with a power of the echo. It is always smaller than the emitted power of the pulse. As this power of the echo is distributed on the surface of the receiver chip – the aperture of the chip D (Figure 4.4), the receiver measures the **power density** P/S. But as the surface of the chip remains the same, we always talk about received power (emitting and receiving apertures are usually 8–15 cm in diameter (Wehr and Lohn, 1999)). As a result of power density gained by receiver, the output of receiver is certain voltage U measured in wats (W). After a normalization of voltage measurements, usually on a voltage that is produced when measuring emitted power density, specified by industrial characteristic of certain receiver, the final output is the **intensity** of the echo.

When U_r is received voltage of pulse echo, the U_t is voltage of emitted pulse, which produced the emitted power density P/S, the intensity can be written:

$$\text{Intensity} \approx \frac{U_r}{U_t} \approx \frac{P_r}{P_t} \tag{4.1}$$

The power of the emitted pulse P_t is:

$$P_t = \frac{E_p}{\Delta \tau} \tag{4.2}$$

where τ_p is pulse duration and E_p energy of one pulse (see Figures 4.1 and 4.6). Typically airborne laser scanners employ the lasers with a pulse energy in the order of 100 μJ, a pulse duration in the order of 10 ns and consequently a pulse power in the order of 10 kW (Wagner, 2005a).

When talking about pulse lasers, one can talk about emitted and received package of energy (or energy density), as the duration of echo is known and can be taken for granted. When talking about continuous wave lasers we should strictly use the term power: emitted and received power, as the laser emitter emits the energy continuously in time (equation 4.2).
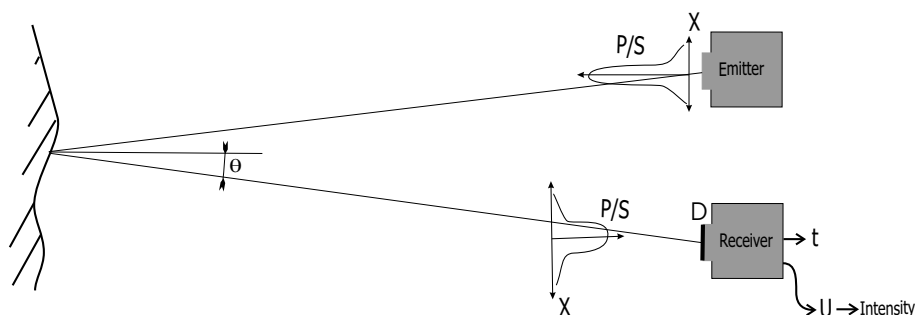
Figure 4.4: The emitter sends out a pulse which reflects back to the receiver extended because of beam divergence. θ is the angle between the normal on the terrain and laser beam – incidence angle, P/S is power density.

Slika 4.4: Oddajnik pošlje laserski pulz, ki se vrne nazaj na sprejemnik širši zaradi divergence laserskega žarka. θ je kot med normalo na teren in laserskim žarkom, P/S je gostota moči.

Since the proportion of the received power depends on numerous factors, e.g. emitted energy, reflectivity of the target, scanning angle, atmospheric conditions and also characteristics of the receiver, and all cannot be exactly modelled, we talk about the intensity. Those affecting factors will be described in detail in 4.4.3. The intensity is described in arbitrary units, usually saying the emitted power would produce the intensity 1, therefore the received power produces a proportionally smaller value.
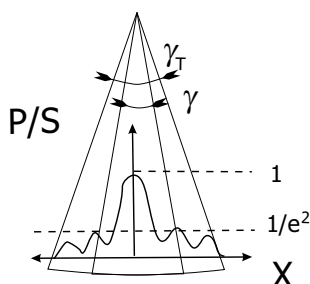
Figure 4.5: Laser beam divergence as defined with power density of returned echo. The theoretical divergence is marked with γ_T, the measured with γ.

Slika 4.5: Divergenca laserskega žarka kot jo opišemo na vrnjeni gostoti moči. Teoretična divergenca laserskega žarka je γ_T, izmerjena pa γ.

The power density of the echo is distributed approximately by Gaussian 2D function. The Gaussian function presented on Figure 4.4 is not monotonous because of the interferometric influences seen as sidelobes, what is presented in detail on Figure 4.5. There the curve is presented only in one dimension X, while in reality this is planar distribution. The echo of the pulse releases the trigger in receiver when power density exceeds a certain value. Because of the manufactural specifications (Baltsavias, 1999b) this threshold value is usually set on $1/e^2$ of the maximal power density (the power density of emitted pulse) which can be received [4]. This value presents approximately the value at 2σ of the Gaussian function.

This threshold value also defines the measured divergence of the laser beam γ, which is smaller

---

[4]Where e is the basis of the natural logarithm ~ 2.718

than the theoretical one γ_T (Figure 4.5). The strength of the diffraction sidelobes defines a measured divergence. If the sidelobes are powerful enough to exceed the threshold then γ is close to γ_T.

4.4.2   Laser measurement of the distance

The range

The **distance** or **range** (d) between the emitter, the point on the ground and the receiver is defined with the measured interval time (t), elapsing between sending pulse and receiving an echo and the group velocity v_g.

The **range** is:

$$d = v_g \frac{t}{2} \tag{4.3}$$

The time measurement of range is made when a specific point on the echo is noticed, in most cases leading edge of the rising side of the pulse (Figure 4.6), because this side is more steep (Thiel and Wehr, 2004). This specific point on the echo is defined with time when the signal voltage has reached a predetermined threshold value (Figure 4.5 on page 36). A possible error occurs if the voltage magnitudes of the transmitted and received pulses are not adjusted to the same value before they are sent to the time interval counter. If the received pulse amplitude threshold is too low, the measured time t will be too long, and vice-versa. To eliminate this time difference caused by varying pulse amplitudes, instead of constant threshold discriminators, constant fractions are generally used (e.g. $1/e^2$, as seen in Figure 4.5), which define the time point as a constant fraction of the signal (Baltsavias, 1999b; Thiel and Wehr, 2004).

The time t is measured with the time interval counter. Usually the number of cycles or counts (n) of an oscillator operating at frequency f is counted, from where the time is derived (Katzenbeisser, 2003):

$$t = \frac{n}{f} + t_e \tag{4.4}$$

Where t_e is the error of time measurement, which can be taken as constant and depends on the sensor characteristics. The nominal frequency is very high, of an order of 10 GHz, and has to be adjusted very well (Katzenbeisser, 2003; Thiel and Wehr, 2004).

The elapsed time in visual and infrared part of the wavelength depends on the **group velocity** (v_g) of the travelling laser pulse in the air, which can differ from the speed of light in the vacuum by at most 0.03% (Wagner, 2005a).

False frequency of the time interval counter or false group velocity result in scaling factor which can be seen as widening (or narrowing) the swath width and the elevation shift (Katzenbeisser, 2003).

The range resolution – vertical resolution

The **time length of the emitted pulse** τ_p has a major role in the capability of laser scanner to discriminate two neighbouring targets (Figure 4.6), as it defines the smallest **time resolution** of the system. The pulse length is 5–12 ns as defined with full width at half-maximum (see Table 4.1) (Abshire et al., 2000; Thiel and Wehr, 2004; Wagner, 2005a; Hodgson et al., 2005).

If there are two points separated by distance (range) R, the two echoes will be separated by **time difference** Δt (Wehr and Lohn, 1999; Baltsavias, 1999b; Wagner, 2005a):

$$\Delta t = \frac{2R}{v_g} \tag{4.5}$$

The receiver enables detailed measurements between two echoes when the time difference between two echoes is bigger than the time length of the emitted pulse $\Delta t > \tau_p$. It is necessary that $\Delta t > \tau_p$ in order that two echoes do not overlap (Figure 4.6A), and two ranges can be measured. If $\Delta t \leq \tau_p$ (Figure 4.6B) only one echo is measured and two targets are joint in the perception that there is only one dispersed target. In this case, the range to the first target is only measured.
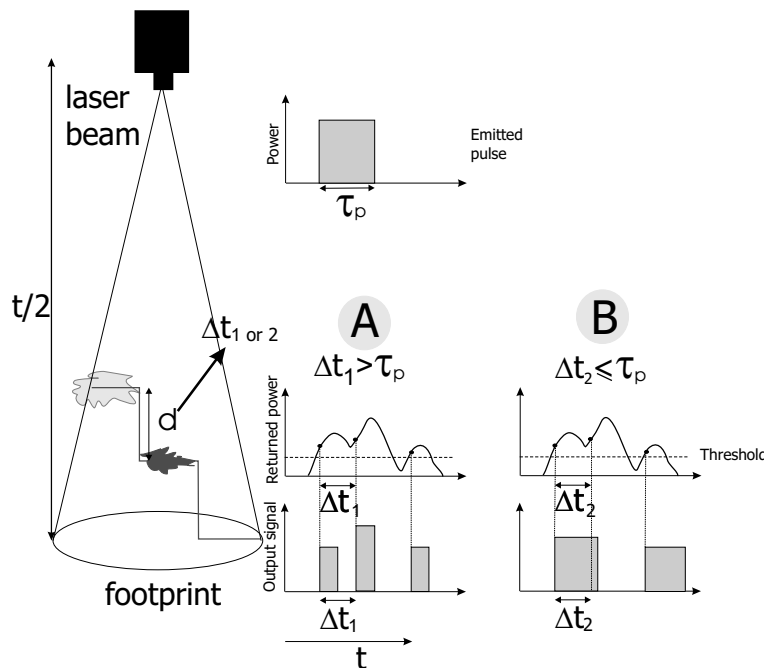
Figure 4.6: Vertical resolution. A) if $\Delta t > \tau_p$, two vertical details can be distinguished. B) if $\Delta t \leq \tau_p$, two successive vertical details cannot be distinguished.
Slika 4.6: Vertikalna ločljivost laserja. A) dva vertikalno zamaknjena detajla lahko ločimo, B) dveh vertikalno zamaknjenih detajlov ne moremo ločiti.

The shortest separation ΔR, called **range resolution**, that can be measured unambiguously, is (Baltsavias, 1999a; Wagner, 2005a):

$$\Delta d = v_g \frac{\tau_p}{2} \tag{4.6}$$

The spatial resolution – horizontal resolution

Minimal horizontal resolution between two points on the ground is defined with the footprint size.

The size and structure of laser footprint depends on the divergence and diffraction of the laser light. Therefore the laser echo is spatially distributed without uniform intensity (Figure 4.7). As the peak of the intensity is not uniform, as theoretically drawn with diffraction pattern in Figure 4.5, the definition of the center of the target – center of the laser point – is also difficult.

The transmitter and receiver are mounted on the laser system so that transmitting and receiving paths share the same optical path. This assures that objects illuminated by laser are always in the **field of view (FOV)** of the optical receiver. The narrow divergence of the laser beam defines the **instantaneous field of view (IFOV)**, which is the field of view of one laser beam. Typically IFOV ranges between 0.3 mrad and 2 mrad (Wehr and Lohn, 1999). The theoretical physical limit of the IFOV is defined by diffraction of the light. Therefore IFOV is the ratio between the laser wavelength and the laser aperture diameter (D). IFOV defines the minimum laser beam divergence (Baltsavias, 1999b):

$$\gamma \sim \text{IFOV} = 2.44 \frac{\lambda}{D} \tag{4.7}$$
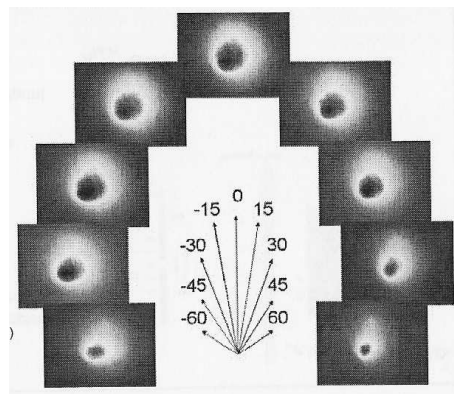
Figure 4.7: Spatial distribution of a laser beam intensity in dependence of scan angle (Wagner, 2005a).
Slika 4.7: Prostorska razporeditev intenzitete odbitega laserskega žarka v odvisnosti od kota snemanja (povzeto po Wagner, 2005a).

The laser divergence (Figure 4.5) can be given by the laser manufacturer or estimated by the IFOV. The laser divergence and the average height of the flight h define the **geometrical footprint size** a_L (Figure 4.8A) (Baltsavias, 1999b; Wehr and Lohn, 1999):

$$a_L = D + 2h \tan \frac{\gamma}{2} \tag{4.8}$$

As the laser aperture size D is usually small, it can be neglected (Figure 4.8B). Also the laser divergence γ is small ($\tan(\gamma/2) \approx \gamma/2$), therefore the equation 4.8 for flat terrain and variable

instantaneous scan angle β_i [5] can be written as (Figure 4.8C) (Baltsavias, 1999b):

$$a_L = h\frac{\gamma}{\cos^2\beta_i} \tag{4.9}$$

When looking to nadir $\beta_i = 0$ the geometrical footprint size is:

$$a_L = h\gamma \tag{4.10}$$

This simplifications hold only for large flying heights. On the contrary, D cannot be neglected for low flying heights (Wotruba et al., 2005).
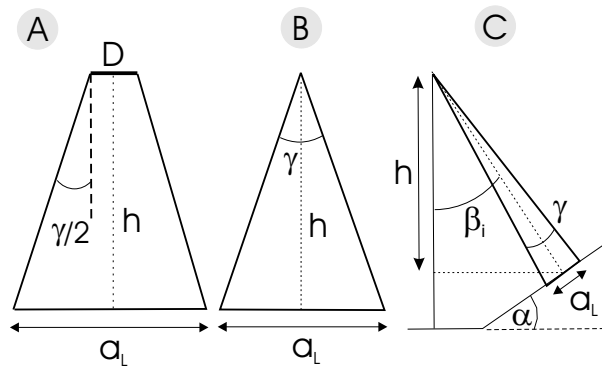
Figure 4.8: Geometrical footprint diameter a_L. A) in nadir with taking in count aperture D, B) without D, C) for inclined terrain.
Slika 4.8: Geometrični premer laserskega žarka na tleh a_L. A) v nadirju z upoštevanjem zaslonke D, B) brez upoštevanja D, C) za nagnjen teren.

The geometric footprint size depends only on the laser beam divergence and is defined by the distance between two opposite points in a beam cross section for a certain energy value. One of such geometric footprint sizes is the **laser beam diameter** where this energy value is set on $1/e^2$ of the emitted pulse energy (Baltsavias, 1999b; Wotruba et al., 2005).

The **effective footprint size** is the practical size of the footprint and depends also on the reflectivity of the target. For small flying heights (e.g. 500 m) the effective footprint size of high-reflecting targets is larger than the geometric footprint size, because of the diffraction sidelobes of the Gaussian energy distribution across the beam below the $1/e^2$ of the energy maximum which contain enough energy for triggering the echo (Wotruba et al., 2005). An example of this is presented on Figure 4.5, were also first order sidelobes are counting to the size of measured diffraction γ and consequently footprint.

---

[5] mainly it is named just as **scan angle**, but we have to separate it from **maximal scan angle** β.

Reflectivity

Target visibility – the ability to measure range and intensity of target – depends on its size, structure, the incidence angle on a terrain and reflectivity. When comparing the influence of targets size and reflectivity, the latter is more important. As an example if two objects have the same size, but have different reflectivity, they are differently measured in size, with the object having higher reflectivity, being measured larger than object with smaller reflectivity. The visibility of two objects with the same reflectivity depends also on the flying height (Wotruba et al., 2005).

Table 4.2: Albedo for different materials at the Ng:YAG wavelength 1 μm, * presents the stainless steel with black oxide coating (Wagner, 2005a; Wehr and Lohn, 1999).

Tabela 4.2: Albedo različnih materialov za Ng:YAG valovno dolžino 1 μm. * nerjavno jeklo s črno oksidno prevleko.

Material	Albedo	Material	Albedo
aluminium foil	$0.8 - 0.9$	chromium	0.6
asphalt	0.2	limestone	0.7
cement	0.4	terra cotta	0.3
copper	0.9	stainless steel	$0.2^* - 0.6$
maize leaf	0.9	maple leaf	0.4
wheat – heads	0.7	wheat – heads	0.6
sandy soil – wet	0.2	sandy soil – dry	0.3
silty soil dry	0.6	snow	$0.8 - 0.9$
water – normal incidence	< 0.01	beach sands, bare areas in dessert	0.5
water – grazing incidence	< 0.3	lava	0.1

Lambertian law of reflectivity talks about the brightness of the light source and its luminosity. The brightness is not dependent on the viewing angle. On the contrary, the luminosity of the light source depends on the angle between normal of the terrain and the light source. **Luminosity** of the body behaving by Lambertian law of reflectivity is (Strnad (edt.), 1993; Baltsavias, 1999b; Wagner, 2005a):

$$I_L = I_0 \rho \cos \theta \tag{4.11}$$

where I_0 is luminosity of the light source – laser emitter – along a perpendicular direction, ρ is the albedo of the surface, θ is the angle between normal of the terrain and the light source – the **incidence angle** (Figure 4.9).

The Lambertian law stands for rough surface, which practically means, that the roughness of the surface is verified at a given wavelength. Most surfaces are rough at laser wavelengths, the exceptions are calm water and polished metals (Wagner, 2005a). The reflectivity of the surface is called an **albedo**. An example of a well-visible target in the Ng:YAG laser wavelength of 1 μm is a rough surface with a big albedo. In Table 4.2, the albedo of different materials in the wavelength of laser are written. They are given from different practical example sources, where the values can vary up to ± 0.2. The best reflector has an albedo of 1, the reflector without
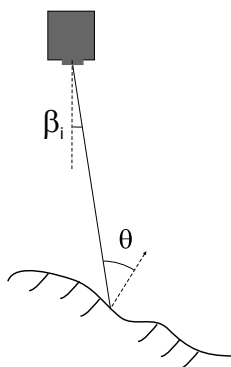
Figure 4.9: Instantaneous scan angle β_i and incidence angle θ.
Slika 4.9: Trenutni kot skeniranja β_i in vpadni kot žarka na teren θ.

reflection (a black body) has an albedo of 0.

Also the incidence angle θ has a strong influence on the target reflectivity. When θ goes to zero, there is a strong increase in brightness of two objects having the same albedo – this is called the hot-spot phenomenon, which is known also from photogrammetry. This effect is enhanced if the target is very smooth, eg. when specular reflection occurs as in the cases of mirror or calm water surface (Wagner, 2005a).
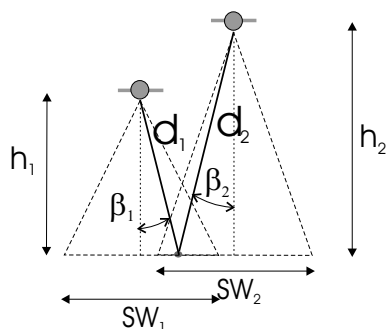
Figure 4.10: Geometry of instantaneous scan angle and range d for different flying heights h and different swath width (SW).
Slika 4.10: Geometrija kota skeniranja in razdalje za isto točko ob dveh različnih višinah leta z različno širino skeniranja (SW).

The incidence angle is connected with scan angle as seen in Figure 4.9, therefore the same point illuminated with different instantaneous scan angle as seen on Figure 4.10 has different reflectivity and consequently different intensity.

The **light current density** j at the specific small area – in our case at laser footprint size – depends on the power emitted by the light source:

$$j = \frac{dP}{dS} \tag{4.12}$$

Details on emitted power P by laser light source will be described in the next section. As this power radiates uniformly in space around the light source it depends on the square of the distance. Therefore the connection between the light current density j and the luminosity I can be written (Strnad (edt.), 1993):

$$j = \frac{I}{d^2} \tag{4.13}$$

If we compare equation (4.1), which describes intensity, and Equations (4.12), (4.13), (4.11) it can be said that, for flat terrain, intensity depends on square of range d and instantaneous scan angle:

$$\text{Intensity} \approx \frac{\cos \beta_i}{d^2} \cdot \frac{P_r}{P_t} \tag{4.14}$$

4.4.3 The laser equation

It is assumed that the laser hits a diffuse circular target and that laser footprint completely covers the entire target area, which reflects the beam back to the source. The reflected power radiates uniformly into a hemisphere. Also it is assumed that the target reflects the laser beam as black body surface. Than the Lambertian model of reflection depends only on the angle between a normal to the surface and a source (Figure 4.9). The basic relation between transmitted P_t and received P_r power is connected with the reflectivity (albedo) of the surface ρ (Wagner, 2005a):

$$P_r = \rho P_t \tag{4.15}$$

When looking more into detail, also different influences have to be included. First there is the area of the footprint A. It has to be assumed that the area of the footprint is uniform (Figure 4.8 and 4.12), therefore its cross-section can be written by equation (4.10) as $a_L = d\gamma$, where flying height h is replaced by range d. Then the power density within this area P/A is calculated. Also the atmospheric transmission μ_{at} and system transmission factor μ_{sys} of the received laser beam back to the optic have to be taken into the mind. After combining these parts a more detailed equation of power received back to the receiver can be written (Wagner, 2005a):

$$P_r = P_t \frac{D_r^2}{4\pi d^4 \gamma^2} \cdot \mu_{at} \cdot \mu_{sys} \cdot \sigma \tag{4.16}$$

where D_r is the receiver aperture, d the distance from the sensor to the target (the range) and P_T the transmitted power, γ the laser beam divergence and σ backscattering coefficient. The backscattering coefficient normalized to the laser footprint size A is σ^0.

Backscattering coefficient is defined with the reflection coefficient of the surface ρ and cone angle Ω (see Figure 4.11):

$$\sigma = \frac{4\pi}{\Omega} \cdot \rho \cdot dA \tag{4.17}$$
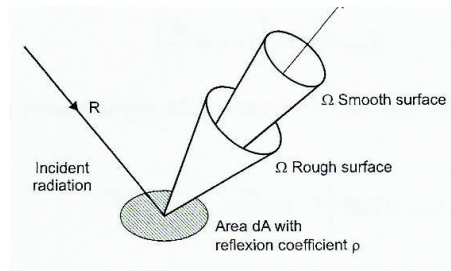
Figure 4.11: The parameters effecting on the cross section of the target (Wagner, 2005a).
Slika 4.11: Parametri, ki vplivajo na premer tarče (Wagner, 2005a).

When normalized, the backscattering coefficient to the laser footprint size is:

$$\sigma^0 = \frac{\sigma}{A} = 4 \cdot \rho \int \frac{\pi}{\Omega} \cdot \frac{dA}{A} \qquad (4.18)$$

Therefore the normalized backscattering coefficient for extended surface is $\sigma_{\text{ext}}^0 = 4\rho$.

Wagner (2005a) divides targets into (Figure 4.12):

- **small**: point-like targets smaller than a laser footprint

- **linear**: wires

- **area or extended**: uniform target as big as the whole footprint

- **volume**: the footprint is covered with different small objects at different heights; e.g. leaves, grass

When evaluating different cross sections of different types of targets, different part of power is reflected back. The extended targets reflect back all power, while line targets reflect just a part of it. This is introduced as backscattering coefficient σ which describes a backscattering of cross section per unit area. In equation (4.16) σ^0 is normalized with the laser footprint area; the reason can be seen in equation (4.18) as the ratio dA/A.
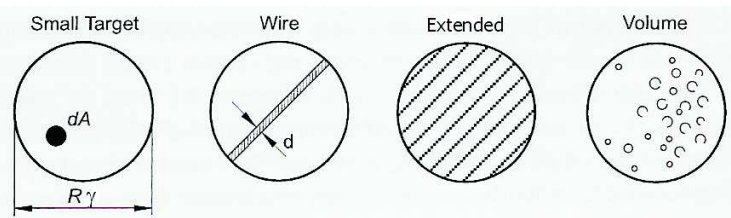
Figure 4.12: Different types of targets (Wagner, 2005a).
Slika 4.12: Različne oblike tarče (Wagner, 2005a).

The equation (4.16) written for extended targets is (Wagner, 2005a):

$$P_r = P_t \frac{D_r^2}{16d^2} \cdot \mu_{\mathrm{at}} \cdot \mu_{\mathrm{sys}} \cdot \sigma^0 \tag{4.19}$$

equation (4.16) can be written also for the energy E_p of pulse lasers, as the power of pulse lasers is by equation (4.2) the energy divided by pulse duration.

As the laser unit of a specific laser scanning system can produce in a time period just a final quantity of energy, this energy is then divided by different numbers of pulses emitted in this time period. This represents the **frequency** of laser f_p in equation (4.21). The larger is the frequency used, the lower-energy pulses are emitted in a time period and vice-versa. This means that one uses the highest frequency of a specific laser scanning system defined in technical specifications of it. The lower is the energy of a pulse, the less energy is also received back from the target with an echo. The echo with less energy is harder to be measured and its accuracy of measurement is also reduced. For optimal accuracy we need to use some medium frequency defined in technical specifications of the laser scanning system, not the maximal one.

4.4.4 Geometrical characteristics of the flight

Minimum flying height over ground

Minimum flying height over ground can be limited due to the platform specifications, legal regulations (often different for urban and other areas) and eye safety (Baltsavias, 1999b).
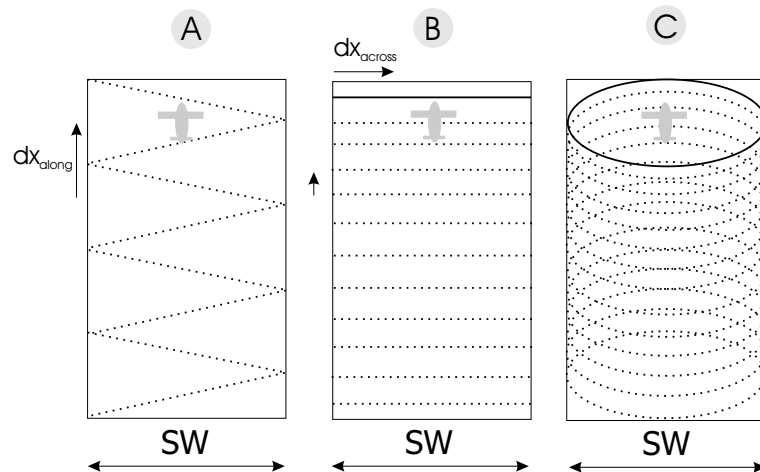
Figure 4.13: Scan pattern: A) zig-zag scan lines, B) parallel scan lines and C) Palmer elliptical scan lines.
Slika 4.13: Vzorec skeniranja: A) cik-cak linije, B) vzporedne linije in C) Palmerjev eliptični vzorec.

Swath width

The **swath width** is the length of one scan line. As the laser scanners are based on three different technical solutions for pointing laser pulses, which produce different scan patterns, the

swath width is not totaly identical for all. There are the **oscillating mirror** scanner, **rotating mirror** scanner, both produce scan lines in ordinary zig-zag pattern (Z-shaped scan) (Figure 4.13A) and **fiber scanners**, which produce parallel scan lines (Figure 4.13B). The oscillating mirror scanner named Palmer scanner does not produce zig-zag pattern but parallel ellipses (Figure 4.13C) (Oštir, 2006; Bitenc, 2007).

Swath width or length of one scan line for parallel line or elliptical scanners is:

$$SW = 2h \tan \frac{\tau}{2} \tag{4.20}$$

where τ is the laser swath angle, which is equal to double scan angle – 2β and h is flying height. The equation 4.20 (Figure 4.14) is valid also for an elliptical scan, where $\tau/2$ is being measured from the nadir direction perpendicular to the flight direction. For a Z-shaped pattern the actual scan line length between left and right swath border is a bit larger than the swath width, but the difference is very small (Baltsavias, 1999b).
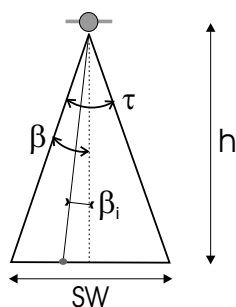
Figure 4.14: Swath width SW.
Slika 4.14: Širina pasu snemanja SW.

Number of points per scan line

Number of points per scan line is independent of flying height and swath width. It depends just on pulse repetition rate f_p [6] and scan rate f_{sc} which describes how many scan lines are performed per second (Baltsavias, 1999b; Schenk, 2001):

$$N = \frac{f_p}{f_{sc}} \tag{4.21}$$

Across track point spacing

Across track point spacing depends on swath width SW and number of points per scan line N.

$$dx_{across} = \frac{SW}{N} \tag{4.22}$$

---

[6]mainly it is named just **pulse rate**

When for Z-shaped scan the scan line is defined as seen in Figure 4.14, the above equation (4.22) is approximately valid. If the scan line is defined as full bidirectional scan from left to right the dx_across has to be multiplied by 2 (Baltsavias, 1999b).

Along track point spacing

Along track point spacing depends on flying speed over ground v and scan rate f_sc:

$$dx_\mathrm{along} = \frac{v}{f_\mathrm{sc}} \qquad (4.23)$$

For an elliptical scan, the above equation gives the largest point distance between two neighbouring scan lines, for Z-shaped scan it gives the distance along track between corresponding points of two consecutive scan lines (Baltsavias, 1999b) as seen on Figure 4.14A.

4.5   Discussion

Topographic or bathymetric aerial laser scanners apply active sensor for data acquisition, with either pulse or full-waveform receiver. Together with the distance between emitter and receiver, the intensity information of the received pulse is measured. The intensity of received pulse can give us a lot of information on the structure and reflectivity of the target from where laser pulse was reflected. The ability of receiver to distinguish between two different laser pulse echoes defines the minimal vertical resolution of range. Horizontal resolution on the other hand depends on the size of instanteneous field of view of the receiver. Minimal vertical and horizontal resolutions of receiver define the maximal possible vertical and horizontal accuracy of aerial laser scanning.

Geometrical characteristics of the flight define the density of laser points – the number of points per unit area. Different number of points per unit area enable different level of detail which can be acquired out of such data. The main groups of aerial laser scanning can be divided in: the low-resolution with less than 1 pt/m^2, medium-resolution between 1-5 pt/m^2 and high-resolution with more than 5 pt/m^2.

Aerial laser scanning can be used as a stand alone technique for measuring topography of bathymetry or together with other remotely sensed technics: multi- or hiperspectral sensors. The combination with other remotely sensed technics contributes to easier identification of different spatial phenomena.

5 THE LASER SCANNING ERROR MODEL – ERROR SOURCES

5.1 Introduction

When evaluating different data samples or products, in our case the production of geodetic data used for local spatial planning from aerial laser scanning, the quality control plays an important role. By the ISO/DIS 19113 standard the basic data quality elements are (Kosmatin-Fras, 2002):

Completeness – presence and absence of features, their attributes and relations

Logical consistency – degree of adherence to logical rules of data structure, attribution and relationship (data structure: conceptual, logical or physical)

Positional accuracy – accuracy of position of features

Temporal accuracy – accuracy of temporal attributes and temporal relationship of features

Thematic accuracy – accuracy of quantitative attributes and the correctness of non-quantitative attributes and the classifications of features and their relationships

One of the crucial quality elements of spatial data acquisition is the positional accuracy of end product. It is described with positional accuracy of aerial laser scanning, which is defined by the means of different error sources. Therefore this chapter will give a detailed overview on the laser scanning error sources: the origin of error, its behaviour, its relative size and influence to the planimetric and height accuracy. To describe the relation between errors the Schenk's geolocation equation for aerial laser scanning will be used. The described errors define the accuracy of laser scanning and therefore define also the expected accuracy of data acquired out of laser scanning.

5.2 The division of laser scanning errors

Different authors have checked the achieved airborne laser scanning accuracy by measurement of reference control points or patches (Alharthy et al., 2004; Ahokas et al., 2005a; Burman, 2000; Crosilla et al., 2005a; Schenk, 2001; Schnurr et al., 2004; McKean and Roering, 2005; Maas, 2003; Thoma et al., 2005; Turton, 2006). The results well correspond to the Baltsavias's (1999a)

accuracy in the planar range of 30–50 cm and in the height range 5–15 cm. In some cases the accuracy achieved was even better, as in the example of hydrological measurements mentioned by Thoma et al. (2005) when the achieved hight accuracy was 2 cm.

An overview of literature about the size and behaviour of different error sources will be given in this chapter. The errors will be combined in groups and different models of errors will be studied (Schenk, 2001; Filin, 2001a; Beinat and Crosilla, 2002; Skaloud and Schaer, 2003; Friess, 2006). On the basis of the simulation a simplified error model for everyday use when planing the laser scanning will be developed.

The airborne laser measuring of laser points can be divided into **three procedures** which are also separated error sources (Wehr and Lohn, 1999; Baltsavias, 1999b; Kraus (edt.), 2005):

- The basic part of the laser scanning is **the laser scanning system and its physical characteristics**. It includes the optomechanical scanner, its range resolution, maximum unambiguous range, ranging precision, laser power and energy, the relation between transmitted and received power from one pulse are counted.

- The second part is the procedure of **transformation of data from laser scanning system to local coordinate system of the platform**. Here are included: the accuracy of the determination of the shifts and drifts, the rotations of laser scanning system in the platform system and the time offsets between the laser scanning system and the platform orientation systems.

- The next important component is the **transformation of data from local coordinate system of the platform to the global coordinate system** which is defined by GPS and IMU (inertial measurement unit) measurements. Here the time drift between IMU and GPS system on the platform are included, which depends also on the accuracies of the GPS reference stations on the ground and the GPS satellite constellation at the time of measurement. At the end we usually transform points from global coordinate system to some national reference system, which can also contribute to errors.
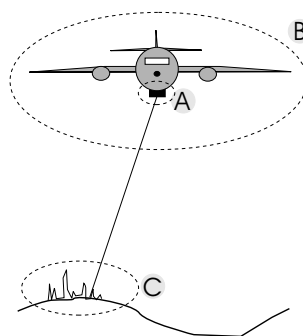
Figure 5.1: Error contributors: A) hardware/software effect errors, B) laser scanning mission, C) target.
Slika 5.1: Vzroki napak: A) strojna/programska oprema, B) misija leta, C) tarča.

On the other hand we can translate these three procedures and their influences in **three types of error contributors** (Figure 5.1) to the total accuracy assessment of the airborne laser scanning systems. In our work the errors will be divided on the basis of these three types of error contributors.

- The first are **basic systematic errors** (Schenk, 2001; Ahokas et al., 2005b) which are also called **hardware/software effect errors** (McKean and Roering, 2005). These errors behave systematically and can be modelled by the analytical model of the errors described by Schenk (2001). Hardware/software effect errors have an influence on the range, planimetric and height accuracy assessment. These errors can be removed by the calibration of the laser scanning system in the procedure of in-the-flight calibration. In this group the biggest error contributors to the total height error are the INS angular errors (INS is a part of the IMU) which present the error of measuring the rotation from body reference frame (the position of IMU in the aeroplane) to the navigational coordinate system which is defined with the local vertical. Much research has been done to resolve the correct value of INS angular errors (Burman, 2000; Schenk, 2001; Katzenbeisser, 2003; Skaloud and Lichti, 2006). The result of hardware/software effect errors is the orientation of the total planimetric errors in the direction of the flying course and they also cause bigger planimetric errors on the edges of the flying stripes (Schenk, 2001). Nevertheless these errors cause also different local shifts, drifts and distortions, which can only be found when laser scanning data is compared with an independent data set (McKean and Roering, 2005).

- The second type are **the errors of the laser scanning mission** (McKean and Roering, 2005) which behave also systematically. They have an influence on the size of the hardware/software effect errors. This group includes the error of the flying height, the speed of the platform, the influence of the wind on the flying direction, the percentage of overlapping between the flying stripes, the position and the distance to the reference GPS stations.

- The third group are **the errors caused by the nature of the target** (McKean and Roering, 2005; Ahokas et al., 2005b): the type of the terrain (flat surface, hills, mountains), the terrain slope, the influence of vegetation on the penetration of the laser beam to the ground. This type of errors usually become apparent when already working with the data. Those are usually not systematic.

The first two groups of errors can be removed in the processing phase of laser scanning data by applying different error models. In contrast, the third group of errors behaves unsystematically and is hard to model.

As laser scanning work-flow is not ended with the list of laser points, but usually only starts, the products are subject of the additional error sources. Here are included the interpolation errors, filtering errors, errors caused by improper break line detection, segmentation and smoothing of data (Ahokas et al., 2005b). Also other possible human errors which are results of improper data handling and transformation have their influence on the data (Maas, 2003).

5.3   The Schenk's analytical model for systematic errors

Schenk (2001) has developed an analytical model which describes systematic errors of laser scanning. Using the division from previous section seen on Figure 5.1 the basic systematic errors and some errors resulting from the laser scanning mission can be included in this model.

The laser geolocation equation (equation 5.1) models the incorporation of different components of the laser altimeter system by means of transformation between different reference frames (Schenk, 2001):

$$\begin{bmatrix} x_L \\ y_L \\ z_L \end{bmatrix} = \begin{bmatrix} X_0 \\ Y_0 \\ Z_0 \end{bmatrix} + \mathbf{R}_W \cdot \mathbf{R}_{GEO} \cdot \mathbf{R}_{INS} \left(\begin{bmatrix} \delta_x \\ \delta_y \\ \delta_z \end{bmatrix} + \mathbf{R}_m \cdot \mathbf{R}_s \begin{bmatrix} 0 \\ 0 \\ -d \end{bmatrix} \right) \qquad (5.1)$$

x_L, y_L, z_L	– location of the footprint in WGS84 geocentric coordinate system
X_0, Y_0, Z_0	– location of the phase center of the GPS receiver
$\mathbf{R}_W$	– rotation from the local reference frame into the global geocentric reference frame
$\mathbf{R}_{GEO}$	– rotation from reference frame defined by the local vertical, to the local reference frame
$\mathbf{R}_{INS}$	– rotation from body reference frame to reference frame defined by local vertical; this system is centered at the phase center of GPS antenna and defined by INS angles
$\delta_x, \delta_y, \delta_z$	– offset vector between the phase center of the GPS antenna and laser firing point, defined by the body frame
$\mathbf{R}_m$	– the mounting bias, which designates rotation between the altimeter and the body reference frame
$\mathbf{R}_s$	– rotation between laser beam and laser system defined by scanning angles
d	– range measurement by laser system

When the errors of these components are introduced, the geolocation equation (equation 5.1) can be written as:

$$\begin{bmatrix} x_L \\ y_L \\ z_L \end{bmatrix} = \begin{bmatrix} X_0 \\ Y_0 \\ Z_0 \end{bmatrix} + \begin{bmatrix} \Delta X_0 \\ \Delta Y_0 \\ \Delta Z_0 \end{bmatrix} + \mathbf{R}_W \cdot \mathbf{R}_{GEO} \cdot \mathbf{R}_{INS}^* \left(\begin{bmatrix} \delta_x \\ \delta_y \\ \delta_z \end{bmatrix} + \begin{bmatrix} e_x \\ e_y \\ e_z \end{bmatrix} + \mathbf{R}_m^* \cdot \mathbf{R}_s^* \begin{bmatrix} 0 \\ 0 \\ -(d+\Delta d) \end{bmatrix} \right) + \begin{bmatrix} p_x \\ p_y \\ p_z \end{bmatrix}$$
$$(5.2)$$

or written without vector components:

$$\mathbf{x}_L = \mathbf{x}_0 + \Delta\mathbf{x}_0 + \mathbf{R}_W \cdot \mathbf{R}_{GEO} \cdot \mathbf{R}_{INS}^* \left(\mathbf{s}_0 + \Delta\mathbf{s}_0 + \mathbf{R}_m^* \cdot \mathbf{R}_s^* \cdot \mathbf{h}_{-(d+\Delta d)} \right) + \Delta\mathbf{p}_s \qquad (5.3)$$

with $\Delta\mathbf{x}_0$ being the location error of the GPS phase center, $\Delta\mathbf{s}_0$ the error of translation vector between GPS/INS and laser system and $\Delta\mathbf{p}_s$ the synchronization error. Rotation matrices marked with $\mathbf{R}^*$ include errors of the specific rotation.

All written errors have considerable planimetric error components. When the tilted surface is
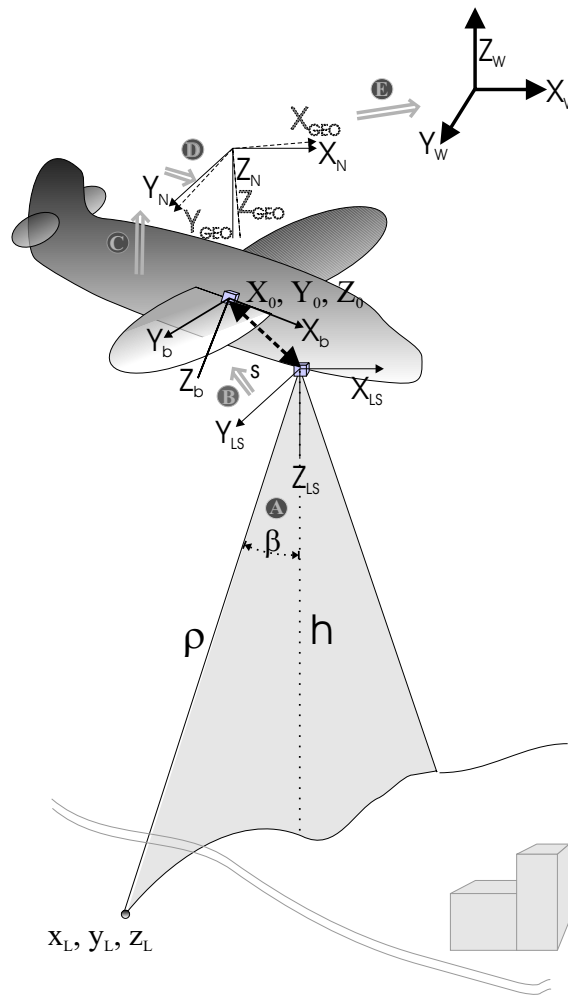
Figure 5.2: Transformation from the reference frame of the laser scanning unit to the global orthogonal reference frame – world (e.g. WGS84). Rotations: A) $\mathbf{R}_s$, B) $\mathbf{R}_m$, C) $\mathbf{R}_{\mathrm{INS}}$, D) $\mathbf{R}_{\mathrm{GEO}}$ and E) $\mathbf{R}_{\mathrm{W}}$.

Slika 5.2: Pretvoraba iz koordinatnega sistema laserske naprave v globalni ortogonalni koordinatni sistem – npr. WGS84. Rotacije: A) $\mathbf{R}_s$, B) $\mathbf{R}_m$, C) $\mathbf{R}_{\mathrm{INS}}$, D) $\mathbf{R}_{\mathrm{GEO}}$ in E) $\mathbf{R}_{\mathrm{W}}$.

measured, a special secondary elevation error can be expected. This error alters the values of vertical error with the influence of characteristics of measured surface (Schenk, 2001)[1].

5.4 Basic systematic errors – hardware/software effect errors

Basic systematic errors can be divided in the following groups (Schenk, 2001; Maas, 2003; McKean and Roering, 2005) and are described in analytical model of laser scanning:

- **laser scanner characteristics**: scan angle errors (an error of the swath angle error, scan mirror instability) and ranging error (scan rate error, pulse detection bias and noise, laser

---

[1]for details see page 77 Section 5.6.4

beam width and divergence, pulse signal to noise ratio)

- **alignment and synchronization**: alignment or mounting errors consist of errors in determining the alignment between altimeter and INS, and of an error in the determination of the offset between the phase center of the GPS antenna and the laser system; synchronization errors which can exist between INS/GPS and laser scanner instruments.

- **INS characteristics**: these errors are influenced by gyro drift, frequency of INS observations and the integration with GPS

- **GPS characteristics**: these errors are influenced by frequency of GPS observations, satellite configuration, random signal errors and quality of data post processing

- **georeferencing methods**: errors in geoid model used for data transformation from local coordinate reference frame to the global (W) coordinate reference frame (e.g. WGS84) and also errors of reference point measurements

These errors can mainly be removed by detailed calibration of the system before and between the flight.

5.4.1 Laser scanner characteristics: Rotation between laser beam and laser reference frame − $\mathbf{R}_S$

Rotation between the laser beam and the laser scanning device reference frame is defined with instantaneous scan angle β_i [2]. **Laser scanning device reference frame** (Figure 5.3) is defined by orientation of Z_{LS}-axis to the null firing point, which points to the ground. Axis X_{LS} is pointed *approximately* to the nose of the aeroplane and Y_{LS} to its right wing (Schenk, 2001; Filin, 2001a). Laser scanning device reference frame is just slightly rotated in relation to the body frame of the aeroplane. This rotations are known as mounting bias $\mathbf{R}_m$ and will be discussed later (see page 57).

Swath angle τ consists of positive and negative scan angle. The positive scan angle $+\beta$ is positive in counter clockwise direction as seen on Figure 5.3. Therefore the mathematical type of rotation matrices will be used (see equation B.3 on page 173).

In the ideal case the scanning plane lies in $Z_{\mathrm{LS}}Y_{\mathrm{LS}}$-plane of the laser system and the laser beam rotates just around axis X_{LS} in the counter clockwise direction, therefore the $\mathbf{R}_S$ can be written as:

$$\mathbf{R}_s = \mathbf{R}_x(\beta) = \begin{bmatrix} 1 & 0 & 0 \\ 0 & \cos\beta & -\sin\beta \\ 0 & \sin\beta & \cos\beta \end{bmatrix} \tag{5.4}$$

If the laser scanning device has a possibility to aim the laser in the direction towards the nose of the aeroplane (e.g. Palmer scanner), also the rotation around the Y_{LS} has to be taken into account. In this case an additional angle α is introduced which points in counter clockwise

---

[2]for more details on β_i see page 40

direction. This rotation can be written with equation B.3 (on page 173) as $\mathbf{R}_y(\beta)$ where the angle is replaced by α.
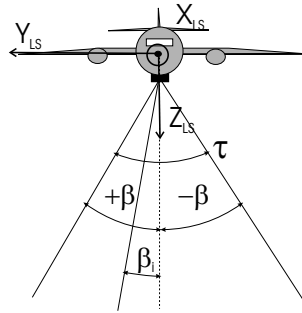
Figure 5.3: The definition of the instantaneous scan angle β_i in the laser scanning device reference frame.
Slika 5.3: Definicija trenutnega kota skeniranja β_i v koordinatnem sistemu laserskega skenerja.

For our ideal theoretical case just rotation β around X-axis will be used. Therefore the rotation between laser beam and laser system $\mathbf{R}_s^*$ with included errors $\Delta\mathbf{R}_s(\beta_i)$ can be written as:

$$\mathbf{R}_s^* = \Delta\mathbf{R}_s(\beta_i) \cdot \mathbf{R}_s(\beta_i) \tag{5.5}$$

Scan angle errors

Instantaneous scan angle can be affected by three errors (Schenk, 2001):

- **Index error** is the angle ϵ between the instantaneous scan angle zero and the direction of the Z_{LS} axis. It is constant for all scan angles (Figure 5.4A).

- **Swath angle error** $\Delta\tau$ increases linearly as it depends on the equation 5.6 (Figure 5.4A)

- **Misalignment of the scanning plane** means that the scanning plane and the X_{LS}-axis are not perpendicular. This offset is represented by two small angular errors: vertical beam misalignment $\Delta\varphi$ and horizontal beam misalignment $\Delta\kappa$ (Figure 5.4B and 5.4C). Vertical and horizontal beam misalignments are caused by the tolerance of the laser beam alignment with respect to the scanning mirror (Latypov, 2005).

Scan angle errors have their origin in the construction of the laser scanners (see page 45). Especially the misalignment errors strongly depend on the type of the laser system. A detailed reconstruction of misalignment errors for rotating polygon mirror type laser scanners can be found in Latypov (2005).

The instantaneous scan angle β_i of a linear scanner is not directly measured, but is derived from the pulse number i of the studied angle and the number of pulses per scan line N (equation 4.21) and the swath angle τ (equation 4.20 on page 46) (Schenk, 2001):

$$\beta_i = \frac{\tau}{2} - i \cdot \frac{\tau}{N-1} \tag{5.6}$$

If the index and swath angle errors (Figure 5.4A) are taken into the account, the instantaneous scan angle is β_i^*:

$$\beta_i^* = \frac{\tau + \Delta\tau}{2} - i \cdot \frac{\tau + \Delta\tau}{N - 1} + \epsilon \tag{5.7}$$

Therefore the scan angle error $\Delta\beta_i$ in the scanning plane is:

$$\Delta\beta_i = \beta_i^* - \beta_i = \epsilon + \frac{\Delta\tau}{2} - \frac{\Delta\tau}{N - 1} \cdot i \tag{5.8}$$
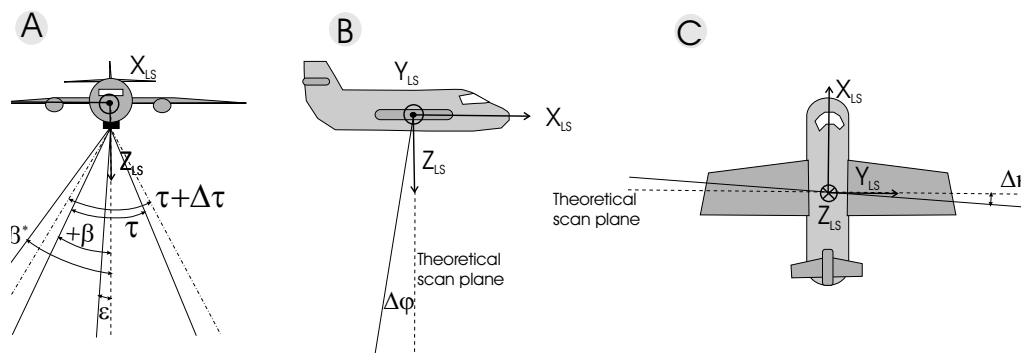
Figure 5.4: The errors which influence the scan angle: A) index error and swath angle error, B) vertical beam misalignment and C) horizontal beam misalignment.
Slika 5.4: Napake, ki vplivajo na kot skeniranja: A) indeksna napaka in napaka širine pasu skeniranja, B) vertikalno neujemanje laserskega žarka in C) horizontalno neujemanje laserskega žarka.

As only theoretically the scanning plane corresponds with the $Y_{LS}Z_{LS}$-plane (equation 5.5), when calculating the $\mathbf{R}_s$ also other two misalignments of the scanning plane have to be considered: the vertical beam $\Delta\varphi$ and horizontal beam $\Delta\kappa$ misalignments (Figures 5.4B and 5.4C). All three angles are small ($\Delta\varphi$, $\Delta\kappa$ and $\Delta\beta_i$), therefore the rotation matrix for small angles can be written (see equation B.4 on page 173 Appendix B.1):

$$\mathbf{R}_s^* = \Delta\mathbf{R}_s \cdot \mathbf{R}_s = \begin{bmatrix} 1 & -\Delta\kappa & \Delta\varphi \\ \Delta\kappa & 1 & -\Delta\beta_i \\ -\Delta\varphi & \Delta\beta_i & 1 \end{bmatrix} \cdot \mathbf{R}_s \tag{5.9}$$

THE SIZE

Index error measured at a laboratory calibration yields an ϵ of $0.006°$, when the position of a laser point at a distance of 1 meter is tested and 0.1 mm offset from the zero angle is measured. Jutzi and Stilla (2003) mention even smaller ϵ of $0.001°$. **Maximum index error** can be expected to be three times greater, therefore $\epsilon \approx 0.01°$-$0.02°$ is good estimate for it. Similar consideration leads to a **swath angle error** of $\Delta\tau = 0.03°$. The misalignment of the scanning plane $\Delta\varphi = \Delta\kappa = 0.03°$ can be expected (Schenk, 2001). In order to keep the misalignment effect within 10 cm over the entire scan line, at flight altitude of 1000 m, the error tolerance for the vertical beam misalignment should not exceed $0.057°$ (Latypov, 2005).

5.4.2   Alignment between INS/GPS and laser scanner: Transformation to the body reference frame − $\mathbf{R}_m$

The **body reference frame** is defined with the direction of X_b-axis *directly* to the nose of the aeroplane and Y_b to its right wing, the Z_b is pointed towards earth (Schenk, 2001; Filin, 2001a; Bäumker and Heimes, 2002). While the **laser scanning reference frame** X_{LS}-axis is pointed *approximately* to the nose of the aeroplane (Figure 5.5). The transformation from the laser scanning device reference frame to the body reference frame is described with the translation $\mathbf{s}_0$ and rotations $\mathbf{R}_m$ named **mounting bias** (Schenk, 2001) or **bore-sight alignment** (Katzenbeisser, 2003; Skaloud and Lichti, 2006).
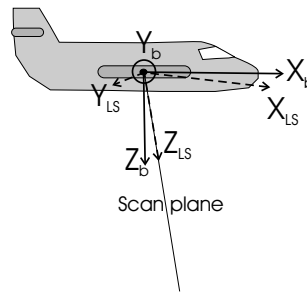
Figure 5.5: The body reference frame (b) and laser reference frame (LS).
Slika 5.5: Referenčni sistem nosilca (b) in referenčni sistem laserskega skenerja (LS).

The translation vector $\mathbf{s}_0$ consists out of two components, which are measured on the ground after the installation of systems in the flying platform (Schenk, 2001):

- **laser system alignment**: $\mathbf{s}_{\text{LS}}$ presents the distance between the laser system origin and INS origin, sometimes it is called also **lever arm** (Katzenbeisser, 2003)

- **GPS alignment**: $\mathbf{s}_{\text{GPS}}$ is a distance between the center of GPS antenna and the INS origin

Therefore the translation vector $\mathbf{s}_0$ can be written as:

$$\mathbf{s}_0 = \mathbf{s}_{\text{LS}} + \mathbf{s}_{\text{GPS}} \tag{5.10}$$

Mounting bias can be considered as a misalignment between INS and laser scanning device reference frames. This is an industrial error of fixation of the laser ranging device in the same direction as INS is oriented. The same orientation can in practice never be accomplished. Therefore the value of mounting bias rotations $\mathbf{R}_m$ and its error $\Delta\mathbf{R}_m$ are derived from the in-the-flight calibration (Schenk, 2001).

The mounting bias is described with rotation from body reference frame to laser ranging device reference frame $\mathbf{R}_b^{\text{LS}}$ (Cramer, 1997):

$$\mathbf{R}_m = (\mathbf{R}_b^{\text{LS}})^{-1} \quad \Delta\mathbf{R}_m = (\Delta\mathbf{R}_b^{\text{LS}})^{-1} \tag{5.11}$$

The mounting bias with included errors $\mathbf{R}_m^*$ is:

$$\mathbf{R}_m^* = \Delta\mathbf{R}_m \cdot \mathbf{R}_m \tag{5.12}$$

The mounting bias angles (m_x, m_y, m_z) are small – ordinary less than $3°$ (Bäumker and Heimes, 2002; Morin and El-Sheimy, 2002; Skaloud and Lichti, 2006) – so the rotation matrices for small angles can be written. Both coordinate systems are righthanded and the rotation from body reference frame to laser coordinate system is clockwise so the geodetical coordinate system can be used (page 173 Appendix B.1 equation B.2):

$$\mathbf{R}_b^{\text{LS}} = \begin{bmatrix} 1 & m_z & -m_y \\ -m_z & 1 & m_x \\ m_y & -m_x & 1 \end{bmatrix} \tag{5.13}$$

The influence of alignment vectors $\mathbf{s}_0$ and mounting bias $\mathbf{R}_m$ on the final range depends also from the error of the definition of INS angles $\Delta\mathbf{R}_{\text{INS}}$ as seen in equation 5.2. The error of INS angles will be described in detail on page 63.

Error of the mounting bias — $\Delta\mathbf{R}_m$

As the errors of mountain bias are small, the error matrix $(\Delta\mathbf{R}_m)^{-1} = \Delta\mathbf{R}_b^{\text{LS}}$ for small angles can be written (Schenk, 2001; Toth, 2002):

$$\Delta\mathbf{R}_b^{\text{LS}} = \begin{bmatrix} 1 & \Delta m_z & -\Delta m_y \\ -\Delta m_z & 1 & \Delta m_x \\ \Delta m_y & -\Delta m_x & 1 \end{bmatrix} \tag{5.14}$$

THE SIZE

As already noted before, the mounting bias angles are usually smaller than $3°$. They are measured by in-the-flight calibration. The procedure of calibration is not standardized, so the methods how the mounting bias is derived, can differ (Schenk, 2001; Katzenbeisser, 2003).

Information about the accuracy achieved is also linked to the procedure of the calibration and is difficult to interpret. The values of errors depend on the procedure of calibration and from other system errors. After in-the-flight calibration the error of $0.01° = 36''$ in all three angles can be assumed. After the installation and before the in-the-flight calibration, the errors are much larger, e.g. $0.3°$ (Schenk, 2001). Katzenbeisser (2003) states that the size of this error before the calibration can easily be $0.2°$. When the behavior of mountain bias in longer period of operation is investigated – the stability of mountain bias – the maximal differences of $0.003–0.005°$ can be expected, if the mounting of INS/GPS system with photogrammetrical camera and INS/GPS system with laser scanner can be compared (Cramer and Stallmann, 2002).

Error of the translation vector — $\Delta\mathbf{s}_0$

The error of translation vector between laser system and GPS is:

$$\Delta\mathbf{s}_0 = \Delta\mathbf{s}_{LS} + \Delta\mathbf{s}_{GPS} \tag{5.15}$$

The distances between the INS, GPS and laser system are measured on the ground. This values are hardly ever calibrated through the procedure of the in-the-flight calibration, therefore larger errors must be expected (Schenk, 2001).

The error of translation vector depends on the size of mounting bias angles. If the maximal size of $0.3°$ for one component is checked at the distance 5 m between the laser system and GPS, the component error of 3 cm can be expected (Schenk, 2001).

5.4.3   INS and GPS characteristics

The position of platform is measured by global positioning system – GPS, the attitude by inertial navigational system – INS. The errors gained by both systems influence several terms of equation 5.3:

- Error of position of the phase center of GPS receiver $\Delta\mathbf{x}$

- INS angle errors $\Delta\mathbf{R}_{\text{INS}}$

- synchronization error $\Delta\mathbf{p}_s$

Also some non-systematic errors are found in laser strips which can originate in inaccuracies of GPS and INS. Typically, these errors cause some wave-like patterns in laser scanning data (Ahokas et al., 2005b).

To understand better the errors which can be gained, a short description of both systems and their integration will be made.

Inertial navigational system INS

Inertial navigational system (INS) is a totaly independent system which main part is **inertial measuring unit (IMU)**. IMU calculates location and attitude of the flying platform based on angle and acceleration measurements performed in time. The location of the platform depends only on the location of the departure point and time which passed from the departure. The location and attitude are derived by integration of angle and acceleration measurements in time, using the Newton's law of motion. The angles are measured by three gyroscopes and
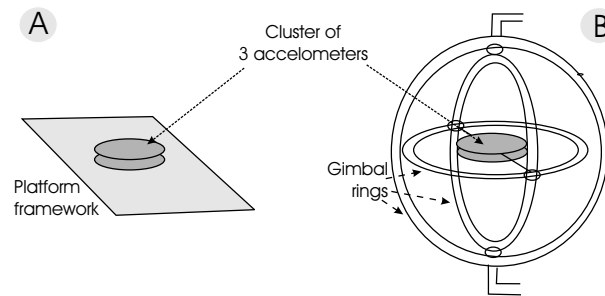
Figure 5.6: Inertial navigational systems: A) strap-down and B) gimbal.
Slika 5.6: Inercialni navigacijski sistem: A) pritrjen, B) kardanski.

acceleration with three accelerometers (Cramer, 1997; Burman, 2000; Bäumker and Heimes, 2002; Coren and Sterzai, 2006).

As seen on Figure 5.6 there are two INS configurations (Cramer, 1997; Burman, 2000):

- **gimballed system**: keeps axes oriented in a global reference frame, as the accelerometer triad is rigidly mounted on the inner gimbal of three gyroscopes. This inner gimbal is isolated from the platform rotations and stays in a desired orientation in space during the motion of the platform.

- **strap-down system**: uses orthogonal accelerometers and gyroscope triads rigidly fixed to the axes of the moving platform.

Mainly strap-down INS are used for flying platforms performing laser scanning, because of their easier manufacture and lower price (Cramer, 1997; Burman, 2000; Bäumker and Heimes, 2002). When using strap-down INS the angle and acceleration measurements are performed in body reference frame (Burman, 2000). The INS sensor axes are the same as the body reference frame axes, therefore the body reference frame is *approximately* the same as the **inertial navigational system reference frame** (Cramer, 1997).

The angles measured by IMU are inertial **navigational system angles or INS angles** (see Figure 5.9 on page 63). It is important that the frequency of attitude measurements is large, as the aircraft can change its altitude and angle very quickly. Today's IMU fitted to laser scanning systems update on average the angle and attitude measurements with frequency of 100 Hz, better systems also with 200 Hz (Baltsavias, 1999a; Turton, 2006) or even 400 Hz (Legat et al., 2006; Skaloud and Lichti, 2006). The errors caused by quick jumps and turns of the platform do not behave systematically, therefore it is important that the flight planning minimizes the appearance of such cases.

IMU measurements provide very high relative accuracy, but if the system is running in stand-alone mode when it depends only on the departure point, the absolute accuracy deteriorates with time. When adding GPS measurements these errors can mainly be eliminated (Cramer, 1997).

The INS systematic errors are (Grejner-Brzezinska and Wang, 1998; Schenk, 2001):

- initialization errors – the errors of initial position and velocity

- alignment errors – difference between body and inertial navigational reference frame, which should be the same when using strap-down INS system[3]

- sensor compensation errors – accelerometer and gyroscope biases and drifts

- gravity model errors – the influence of the unknown local gravity model to the platform movement

It is hard to model these quantities as some are time and flight direction related (Schenk, 2001).

Global positioning system (GPS)

The final accuracy of the laser scanning is directly related to the quality of the geodetic reference points used and cannot be improved beyond the quality of these points (Schnurr et al., 2004). Therefore it is very important how the measurements of the platform trajectory are performed. To get submeter precision necessary for laser scanning missions the dual frequency **differential GPS** (DGPS) positioning is necessary. Even better precision in the centimeter range can be achieved if dual frequency **post-processed kinematic GPS** is used (Schnurr et al., 2004; Kozmus and Stopar, 2003). DGPS and post-processed kinematic GPS both need reference station on the ground (Figure 5.7). The measurements from reference station are used to calculate reference coordinates needed for the correction of the mobile GPS station location (the platform) in real time or in the proces of post-processing. For the connection between the mobile and the reference station in real time the RTCM[4] protocol is used. Methods differ in the way how they handle GPS signal and in precision achieved: DGPS uses just code information of the signal, the post-processed kinematic GPS uses code and phase information of the signal and is therefore more accurate (Kozmus and Stopar, 2003; Katzenbeisser, 2003).

With DGPS detailed post-processing or post-processed kinematic GPS the following errors can be eliminated or decreased: ionospheric and tropospheric disturbance, satellite and receiver clock error (Cramer, 1997; Burman, 2000; Kozmus and Stopar, 2003).

To achieve the precision needed for detailed positioning of laser scanning measurements some additional practical rules should be implied:

- the distance between mobile and reference GPS station should not exceed 10 km (Cramer, 1997; Behan et al., 2000; Kozmus and Stopar, 2003; Turton, 2006), in very stable atmospheric conditions and with good satellite geometry this distance can be maximized even on 25 km (Katzenbeisser, 2003)

---

[3]this is not the mounting bias error $\Delta\mathbf{R}_m$, which describes the diference between body and laser reference frame

[4]Radio Technical Commission For Maritime Service
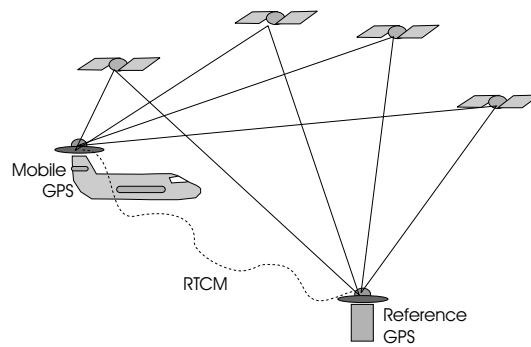
Figure 5.7: The principle of DGPS and kinematic post-processed GPS methods. The receivers can be connected by RTCM protocol.
Slika 5.7: Princip delovanja DGPS- in kinematične relativne GPS-izmere. Premični in statični sprejemnik sta lahko povezana z RTCM-protokolom.

- when working on larger area (where 10 km distance to reference station would be exceeded), the ground control framework with more reference stations should be used, which should include at least 8 known points (Schnurr et al., 2004)

- good satellite constellation and geometry should be achieved, meaning PDOP[5] < 2.5 (Katzenbeisser, 2003), with at least 6 well positioned satellites used (Turton, 2006)

- at the start and at the end of the mission it is recommended to measure some static GPS data with mobile GPS station parked near the reference station (Behan et al., 2000; Burman, 2000)

- if permanent reference receivers are available, they should be used (Burman, 2000); in Slovenia this is the SIGNAL network

The frequency of GPS measurements of position is much lower than the frequency of IMU. On the average the 1–2 Hz frequency of GPS is used, although 10 Hz would be possible (Baltsavias, 1999a; Grejner-Brzezinska and Wang, 1998; Maas, 2002; Schnurr et al., 2004; Legat et al., 2006).

Integration of GPS and INS

Integration of GPS and INS data reduces the size of errors of both systems, by removing errors of one system by tracking these errors with the other system. Mainly GPS and INS data are integrated in the office after the flight mission in the procedure of post-processing. Some tests also have been made to integrate these data already in-the-flight, which would ease planning of the flying mission (Legat et al., 2006).

---

[5]Position Dilution of Precision — measure of the geometrical strength of the GPS satellite configuration (Teunissen and Kleusberg, 1998). It shows the amount of error in position. PDOP less than 4 presents the positional accuracy better than 1 meter.
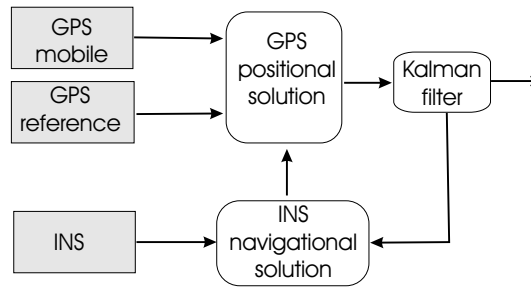
Figure 5.8: Tightly coupled Kalman filter.
Slika 5.8: Trdno sklopljeni Kalmanov filter.

The common method of integrating GPS and INS observations is **Kalman filtering** (Cramer, 1997; Burman, 2000; Schnurr et al., 2004; Ding et al., 2005). Tightly coupled Kalman filtering (Figure 5.8) is widely accepted for GPS/INS integration of flying platforms. It treats errors of position, velocity, acceleration and parameter error of INS modelling as variables, which can be feed forward and backward to compensate sensor errors and to correct the navigational output (Ding et al., 2005). Kalman filter can help also with gross-error detection mechanism which monitors the quality of GPS data before using them to update the filter strategies, which can be very important especially in mountainous environments (Legat et al., 2006). More information about Kalman filter can be found in Welch and Bishop (2006).

5.4.4   Rotation from body reference frame to navigational reference frame $\mathbf{R}_{INS}$
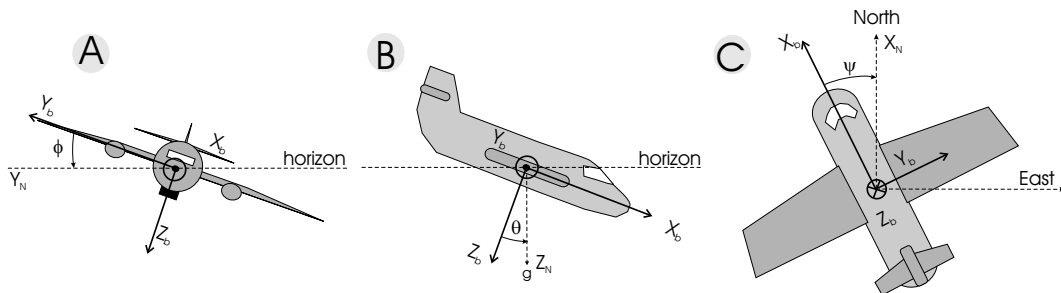
Figure 5.9: From body to navigational coordinate system: A) roll ϕ, B) pitch θ, C) heading ψ.
Slika 5.9: Iz koordinatnega sistema nosilca v navigacijski koordinatni sistem: A) zibanje ϕ, B) guganje θ in C) pozibavanje ψ.

The position of the platform in the local level reference frame is described in the **navigational reference frame**. The navigational reference frame is defined by the physical characteristics of the geoid: the vertical point towards the center of the Earth's mass. Therefore the navigational reference frame is defined by local vertical and the direction to the north (astronomical meridian), while X_N axis is pointed northward, Y_N axis is pointed eastward and Z_N axis is pointed vertical in the direction of the plumb line – direction of local gravity (Figure 5.9). The rotation between the body reference frame and the navigational reference frame is described with INS angles $\mathbf{R}_{INS}$ (Figure 5.2C). INS angles measured in strap-down INS are defined in body reference frame (inertial navigational system reference frame). They are defined by the Euler angles: heading ψ, roll ϕ and pitch θ (Schenk, 2001; Bäumker and Heimes, 2002).

The rotation from body to navigational reference frame is $\mathbf{R}_{\mathrm{INS}}$:

$$\mathbf{R}_{\mathrm{INS}} = \mathbf{R}_b^N \tag{5.16}$$

The INS angles between the body and navigational coordinate systems are defined in body coordinate system and have counter clockwise direction. Therefore the rotation matrices for mathematical coordinate system can be used (see equation B.3 on page 173).

$$\mathbf{R}_{\mathrm{INS}} = \mathbf{R}_z(\psi) \cdot \mathbf{R}_y(\theta) \cdot \mathbf{R}_x(\phi) = \begin{bmatrix} \cos\psi & -\sin\psi & 0 \\ \sin\psi & \cos\psi & 0 \\ 0 & 0 & 1 \end{bmatrix} \cdot \begin{bmatrix} \cos\theta & 0 & \sin\theta \\ 0 & 1 & 0 \\ -\sin\theta & 0 & \cos\theta \end{bmatrix} \cdot \begin{bmatrix} 1 & 0 & 0 \\ 0 & \cos\phi & -\sin\phi \\ 0 & \sin\phi & \cos\phi \end{bmatrix} \tag{5.17}$$

$$\mathbf{R}_{\mathrm{INS}} = \begin{bmatrix} \cos\psi \cdot \cos\theta & \cos\psi \cdot \sin\theta \cdot \sin\phi - \sin\psi \cdot \cos\phi & \cos\psi \cdot \sin\theta \cdot \cos\phi + \sin\psi \cdot \sin\phi \\ \sin\psi \cdot \cos\theta & \sin\psi \cdot \sin\theta \cdot \sin\phi + \cos\psi \cdot \cos\phi & \sin\psi \cdot \sin\theta \cdot \cos\phi - \cos\psi \cdot \sin\phi \\ -\sin\theta & \cos\theta \cdot \sin\phi & \cos\theta \cdot \cos\phi \end{bmatrix} \tag{5.18}$$

When taking into account also the errors of INS angles, the rotation matrix from body to navigational reference frame $\mathbf{R}_{\mathrm{INS}}^*$ is written:

$$\mathbf{R}_{\mathrm{INS}}^* = \Delta\mathbf{R}_{\mathrm{INS}} \cdot \mathbf{R}_{\mathrm{INS}} \tag{5.19}$$

Error of INS angles

Systematic errors of the INS listed on page 60 can be modelled as constant errors of INS angles (Schenk, 2001).

The INS error rotation matrix $\Delta\mathbf{R}_{\mathrm{INS}}$ can be written by replacing the angles (ψ, θ and ϕ) in equation 5.18 with errors of these angles ($\Delta\psi$, $\Delta\theta$ and $\Delta\phi$). As these errors are small the rotation matrix for small angles can be written (see equation B.4 on page 174):

$$\Delta\mathbf{R}_{\mathrm{INS}} = \begin{bmatrix} 1 & -\Delta\psi & \Delta\theta \\ \Delta\psi & 1 & -\Delta\phi \\ -\Delta\theta & \Delta\phi & 1 \end{bmatrix} \tag{5.20}$$

THE SIZE

Depending on the price of the INS (the precision of the manufacturing) the errors from $0.004°$ to $0.02°$ can be expected after calibration (Katzenbeisser, 2003). Similar accuracies of 0.005–$0.01°$ are given by Skaloud and Lichti (2006). Cramer (1997) divides the INS systems based on their price, where those more expensive ($\sim$\$750.000) achieve accuracy better than $0.0003°$, medium priced ($\sim$\$100.000) from 0.003 to $0.005°$ and low priced ($\sim$\$10.000) from 0.01–$0.02°$. These error components are given for roll and pitch angles. The heading has the biggest error, which is two times larger as the one of roll and pitch (Katzenbeisser, 2003). Sometimes is even three to five times larger (Cramer, 1997).

5.4.5 Rotation from navigational reference frame to local ellipsoid reference frame – $\mathbf{R}_{\mathrm{GEO}}$

Local ellipsoid reference frame is defined by the normal to the local ellipsoid. The origin of local ellipsoid reference frame is at the origin of navigational reference frame. The difference between the navigational reference frame (geoid) and local ellipsoid reference frame (local ellipsoid) is described by the deflection of the vertical. As the local ellipsoid represents the approximation of the local geoid, the difference between the gravity model based on geoid and the one based on local ellipsoid is therefore the deflection of the vertical and gravity anomaly. The **deflection of the vertical** θ (Figure 5.10) is defined as the angle between the normal on the local ellipsoid and the local vertical. It contains two components presented on Figure 5.11) (Pribičević, 2000; Kuhar, 2006):

- ξ in the direction of astronomical meridian (direction north-south) and

- η in the direction of first vertical (direction East-West), also called longitudinal component
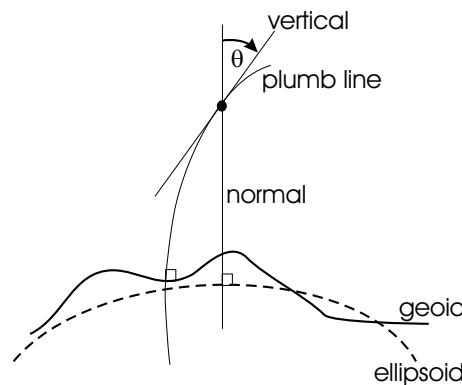
Figure 5.10: Deflection of the vertical θ.
Slika 5.10: Odklon navpičnice θ.

The value of deflection of the vertical can be given just for points measured in astronomical – navigational (Φ and Λ) – and geodetical – local ellipsoid (φ and λ) – reference frame. The difference defines the components of the deflection of the vertical:

$$\xi = \Phi - \varphi \quad \text{and} \quad \eta = (\Lambda - \lambda) \cdot \cos \varphi \qquad (5.21)$$

The deflection of vertical ε in the direction of azimut α is[6]:

$$\varepsilon = \xi \cdot \cos \alpha + \eta \cdot \sin \alpha \qquad (5.22)$$

Both reference frames are right-handed and their Z-axis points down, one in the direction of the gravitation, the other in the direction of the normal to the ellipsoid.

---

[6]mainly the deflection of the vertical is described by ε
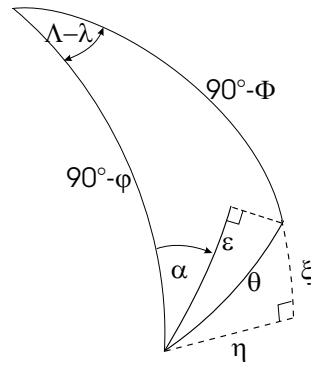
Figure 5.11: The components of deflection of the vertical θ: ε in the direction of azimuth (α), ξ in the astronomical meridian plane and η in first vertical plane.

Slika 5.11: Komponenti odklona navpičnice θ: ε komponenta v smeri azimuta (α), ξ v smeri meridiana in η v smeri prvega vertikala.

The rotation $\mathbf{R}_{\mathrm{GEO}}$ between navigational and local ellipsoid reference frame can be written by the components of the deflection of the vertical and difference between azimuts $\Delta A = \xi \cdot \tan\varphi$.

$$\mathbf{R}_{\mathrm{GEO}} = \mathbf{R}_N^{\mathrm{GEO}} = \mathbf{R}_z(\Delta A) \cdot \mathbf{R}_y(\xi) \cdot \mathbf{R}_x(\eta) \tag{5.23}$$

Average maximal values of the deflection of the vertical ε are not higher than 20"(Vaniček and Krakiwski, 1996), so the rotation matrix for small-angle rotation matrix can be written. The maximal differences in the deflection of the vertical, when the mass arrangements in the Earth crust differ significantly, do not exceed $\Delta\varepsilon = 0.017° \approx 1'$ (Schenk, 2001) or 40" (Pribičević, 2000).

As both navigational and the local reference frame are right-handed and the deflection of the vertical is measured in the clockwise direction from navigational to local orthogonal reference frame, the rotation matrix $\mathbf{R}_{\mathrm{GEO}}$ can be written:

$$\mathbf{R}_{\mathrm{GEO}} = \begin{bmatrix} 1 & \Delta A & -\xi \\ -\Delta A & 1 & \eta \\ \xi & -\eta & 1 \end{bmatrix} \tag{5.24}$$

Due to historical reasons, the reference frame which describes the local ellipsoid in Slovenia is the Bessel ellipsoid[7]. The second possibility is the local European ellipsoid ETRS98[8] which is Earth-centered (Pribičević, 2000).

---

[7]**Bessel ellipsoid** with denotation **D48** describes the official coordinate system in Slovenia, this ellipsoid is not Earth-centered

[8]**ETRS98** – European Terrestrial Reference System 89, which coincided with International Terrestrial Reference Frame ITRF on the beginning of 1989 (Stopar and Kuhar, 2001); it is defined on GRS80 ellipsoid which is used for gravimetric measurements (Kuhar, 2006) and does not differ much from the ellipsoid WGS84 (Pribičević, 2000).

THE SIZE

In Slovenia and surroundings Pribičević (2000) calculated the components of the deflection of the vertical on 98 measured astrogeodetic points (Figure 5.12). When using Bessel ellipsoid as the local ellipsoid, the ξ component does not exceed 17" and the η does not exceed 20". When using ETRS89 for local ellipsoid the highest ξ does not exceed 18" and η 10". Here the mean values are smaller, they are around 5". Bessel shows greater values as the whole ellipsoid is not correctly tied to the geoid, because of the historical errors. This can be seen on Figure 5.12B as greater values of component η.
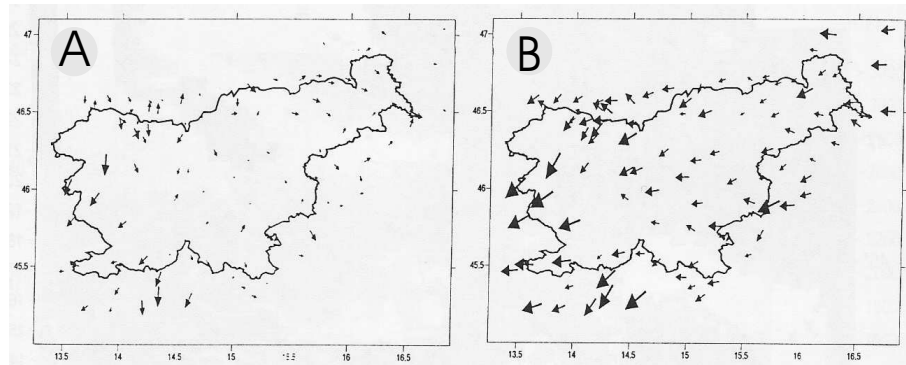
Figure 5.12: Measured deflection of the vertical in Slovenia and surrounding: A) on ETRS89, B) on Bessel ellipsoid (Pribičević, 2000).
Slika 5.12: Merjeni odkloni navpičnice v Sloveniji in okolici: A) na ETRS89, B) na Besslovem elipsoidu (Pribičević, 2000).

5.4.6   Rotation from the local reference frame to the global reference frame – $\mathbf{R}_W$

Local reference frame is defined with the orientation of local vertical and has its origin in GPS phase center on the flying platform. To come from local reference frame (L) to the global reference frame (W), the origin of reference frame has to be moved from the GPS phase center on the flying platform to the center of the Earth and the coordinate axes have to be rotated by $\mathbf{R}_W$ (Figure 5.13). Local reference frame in our example is *GEO* reference frame. The origin is moved from local reference to global reference frame by knowing the location of the flying platform in the global reference frame ($\mathbf{x}_0$).

When the platform is located on the Northern hemisphere and East of Greenwich (Figure 5.14) rotation from local to global reference frame can be written as:

$$\mathbf{r}^L = \mathbf{R}_z(\lambda) \cdot \mathbf{R}_y(\varphi + 90°) \cdot \mathbf{r}^W = \mathbf{R}_W^L \cdot \mathbf{r}^W \tag{5.25}$$

$\mathbf{R}_z(\lambda)$ is taken from equation B.3 (on page 173) as λ rotates in the counter clockwise direction around z axis. In contrast, the $\mathbf{R}_y(\varphi + 90°)$ rotates in clockwise direction around y axis and is taken from equation B.2.
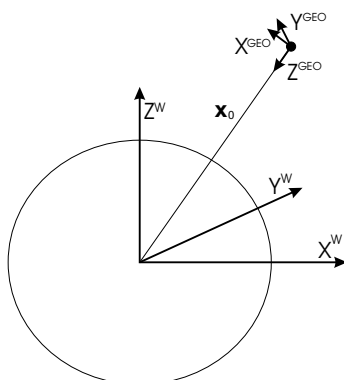
Figure 5.13: Transformation from local ellipsoid based reference frame, with the origin in GPS on flaying platform (GEO), to the global ellipsoid reference frame (W).

Slika 5.13: Transformacija iz lokalnega koordinatnega sistema z izhodiščem v centru GPS antene na nosilcu snemanja (GEO) ter globalnim referenčnim sistemom z izhodiščem v središču Zemlje (W).

$$\mathbf{R}_W^L = R_z(\lambda) \cdot R_y(\varphi + 90°) = \begin{bmatrix} \cos\lambda & -\sin\lambda & 0 \\ \sin\lambda & \cos\lambda & 0 \\ 0 & 0 & 1 \end{bmatrix} \cdot \begin{bmatrix} \cos(\varphi + 90°) & 0 & -\sin(\varphi + 90°) \\ 0 & 1 & 0 \\ \sin(\varphi + 90°) & 0 & \cos(\varphi + 90°) \end{bmatrix} \quad (5.26)$$

$$\mathbf{R}_W^L = \begin{bmatrix} \cos\lambda & -\sin\lambda & 0 \\ \sin\lambda & \cos\lambda & 0 \\ 0 & 0 & 1 \end{bmatrix} \cdot \begin{bmatrix} -\sin\varphi & 0 & -\cos\varphi \\ 0 & 1 & 0 \\ \cos\varphi & 0 & -\sin\varphi \end{bmatrix} = \begin{bmatrix} -\sin\varphi \cdot \cos\lambda & -\sin\lambda & -\cos\varphi \cdot \cos\lambda \\ -\sin\varphi \cdot \sin\lambda & \cos\lambda & -\cos\varphi \cdot \sin\lambda \\ \cos\varphi & 0 & -\sin\varphi \end{bmatrix} \quad (5.27)$$

Rotation from the local to the global reference frame $\mathbf{R}_W$ is inverse matrix of rotation from global to local ellipsoidal reference frame L:

$$\mathbf{R}_W = (\mathbf{R}_W^L)^{-1} \quad (5.28)$$
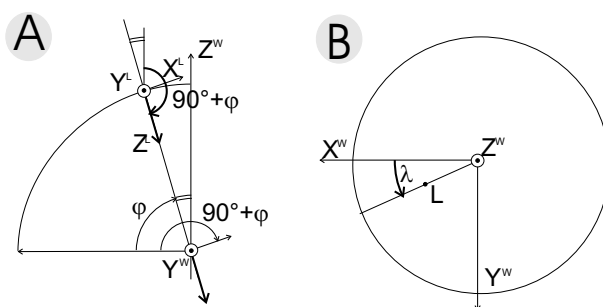
Figure 5.14: Transformation from global earth-centered and earth-fixed ellipsoid (W) to the local ellipsoid reference frame (L = GEO). Figure A) shows rotation around y axis, B) rotation around z axis.

Slika 5.14: Transformacija iz globalnega koordinatnega sistema s centrom v središču Zemlje (W) v lokalni koordinatni sistem (L = GEO). A) rotacija okoli osi y in B) rotacija okoli osi z.

How to change change the ellipsoidal (ϕ, λ, h) and cartesian coordinates (X, Y, Z) is described in Appendix B.2 on page 174.

5.5   Errors resulting from the laser scanning mission

The laser scanning mission influences on the accuracy of the data through the effects of (McKean and Roering, 2005):

- flying altitude above ground level
- percentage of overlap between flight lines
- flying speed
- location of the GPS base station and its distance to the flying platform
- air turbulence during the flight
- air characteristics

These effects influence on several errors also described in the equation 5.3 (on page 52):

- the error of the position of the phase center – $\Delta\mathbf{x}_0$
- the influence on the range measurements Δd
- synchronization errors

Weather conditions (air pressure, humidity and temperature), which are not the same as defined in laser scanning unit calibration protocols, influence the error assessment of the laser scanning, as they change the group velocity[9] of laser pulse travelling (Alharthy et al., 2004). They influence also on the accuracy of GPS measurements (McKean and Roering, 2005). These errors can be reduced using in-the-flight calibration of the laser system during the laser scanning mission.

5.5.1   Synchronization errors – $\Delta\mathbf{p}_s$

Laser scanning system, INS and GPS all use their own time and their own frequency of measurement. The highest frequency is the laser scanning system frequency with typical values between 20–40 kHz (Baltsavias, 1999a; Friess, 2006), nowadays also 200 kHz are used (TopoSys, 2008). When looking at the positioning system, the highest frequency is the INS frequency, with typical value of 100 Hz, better systems also with 200 Hz (Baltsavias, 1999a; Turton, 2006) or even 400 Hz (Legat et al., 2006; Skaloud and Lichti, 2006). GPS works on much lower frequency, typically of 1-2 Hz (see chapter 5.4.3 on page 59). Although GPS has the smallest frequency it has the most accurate clock, which can differ from the **standard GPS time** at most for 1 μs – this difference is called **GPS synchronization error** Δt_{GPS}. The GPS time is used as the time reference for the other two systems (Ding et al., 2005; Ding et al., 2008).

There may be a time shift between INS measurements and GPS clock Δt_{INS}, called **INS synchronization error** and also a time shift between the laser system clock and the GPS clock Δt_{LS}, called **laser system synchronization error**. Both combined present the **synchronization error** Δt.

---

[9]for details on group velocity see p. 37
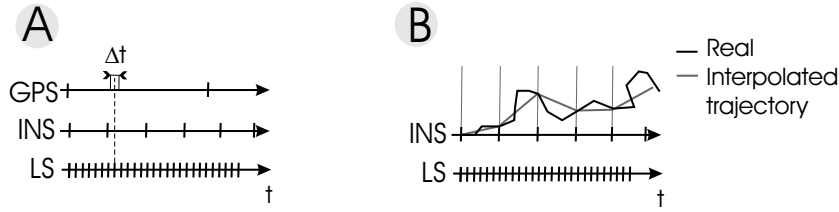
Figure 5.15: Time biases: A) synchronization error, B) interpolation error (Schenk, 2001).
Slika 5.15: Razlike v času: A) napaka sinhronizacije, B) napaka interpolacije (Schenk, 2001).

After the integration of GPS and INS measurements, the observational vector $\mathbf{r}_{LS}(t)$ of laser scanning point can be written as (Ding et al., 2008):

$$\mathbf{r}_{\mathrm{LS}}(t) = \mathbf{r}_{\mathrm{GPS}}(t) - \mathbf{r}_{\mathrm{INS}}(t) \tag{5.29}$$

As $\mathbf{r}_{\mathrm{INS}}(t)$ depends on the trajectory movement described with acceleration and on the departure point location $\mathbf{r}_{\mathrm{INS}}(0)$ and velocity $v_{\mathrm{INS}}(0)$, the observation vector is:

$$\mathbf{r}_{\mathrm{LS}}(t) = \mathbf{r}_{\mathrm{GPS}}(t) - \left(\mathbf{r}_{\mathrm{INS}}(0) + \int v_{\mathrm{INS}}(0)dt + \int\int a(t)dtdt \right) \tag{5.30}$$

When adding the synchronization error Δt, the equation 5.30 is written as:

$$\mathbf{r}_{\mathrm{LS}}^{*}(t) = \mathbf{r}_{\mathrm{GPS}}(t) - \left(\mathbf{r}_{\mathrm{INS}}(0) + \int v_{\mathrm{INS}}(0)dt + \int\int a(t+\Delta t)dtdt \right) \tag{5.31}$$

After applying Taylor expansion to the INS measurements, the equation 5.31 becomes:

$$\mathbf{r}_{LS}^{*}(t) = \mathbf{r}_{\mathrm{LS}}(t) - \int\int a'(t)\Delta t dtdt \tag{5.32}$$

The position error $\Delta\mathbf{p}_s$ caused by the synchronization error Δt can be seen in equation 5.32 as:

$$\Delta\mathbf{p}_s = \mathbf{r}_{\mathrm{LS}}(t) - \mathbf{r}_{\mathrm{LS}}^{*}(t) = \int\int a'(t)\Delta t dtdt \tag{5.33}$$

From equation 5.33 one can see that the magnitude of positional error gained by synchronization error depends on the change of the platform velocity $a'(t)$. Platform velocity represents the dynamics of the platform movement.

When using Kalman filter for INS using 100 Hz and GPS using 1 Hz a smooth flight trajectory of 20 Hz can be interpolated (Ding et al., 2008). This means that the position and the attitude (location) of the platform for the laser measurements in-between 0.05 s intervals are calculated on the basis of the interpolation. Therefore also the **interpolation error** can be expected, as the location at the time of laser scanning pulse has to be interpolated from discrete samples – e.g. 20 Hz sample of trajectory obtained from Kalman filter. The interpolated location of the

platform differs from the real location of the platform as seen on Figure 5.15B. The exact location of the platform at the time of laser pulse cannot be measured and is unknown, therefore the size and behaviour of the interpolation error is not known and can not be treated as systematic (Schenk, 2001). The behaviour of interpolation error strongly depends on the air turbulence during the flight.

THE SIZE

Suppose that the integrated INS/GPS system can catch sudden changes from static mode to a free fall, and the GPS updating rate is 1 Hz. When the RMS error of expected $\Delta\mathbf{p}_s$ is 5 cm, the time synchronization accuracy between INS and GPS should be set to 1 ms (Ding et al., 2008). As the $\mathbf{v}_a$ brings just one part of positional accuracy, it should be kept to minimum. Therefore Schenk (2001) mentions $\Delta\mathbf{p}_s$ of approximately 1 cm which allows $1 \cdot 10^{-4}$ s of synchronization error between laser system and GPS. Katzenbeisser (2003) even states that the synchronization error Δt can be smaller than 10 μs, what would bring $\Delta\mathbf{p}_s$ of 0.005 cm.

5.5.2   Gravity model errors

When conducting laser scanning, there are usually no gravity anomaly measurements included. The uncertainties in knowledge of gravity field produce errors that can not be eliminated just by INS measurements. When connecting INS and GPS measurements, these errors are bounded to other GPS errors, which cannot be eliminated in whole (Grejner-Brzezinska and Wang, 1998). They are included in $\Delta\mathbf{X}$ error – the error of the GPS phase center.

The difference between the geoid and the local ellipsoid defines also the **gravity anomaly** $\Delta\mathbf{g}_m$. This is the difference between real gravity and gravity model in a certain point. The acceleration vector of the platform $\mathbf{a}^*$ measured by INS is (Grejner-Brzezinska and Wang, 1998; Kuhar, 2006):

$$\mathbf{a}^* = \mathbf{a} + \mathbf{g}_m + \Delta\mathbf{g}_m \tag{5.34}$$

where $\mathbf{a}$ is the measured acceleration vector, $\mathbf{g}_m$ the gravity vector of the gravity model used and $\Delta\mathbf{g}_m$ the difference between the gravity model (ellipsoid) and real gravity (geoid). One needs to know the nominal value of gravity g_0, the gravity anomaly Δg, and the components of the deflection of the vertical (ξ and η)[10]. The difference between model and real gravity can be written as:

$$\Delta\mathbf{g}_m = \begin{bmatrix} -g_0\xi \\ -g_0\eta \\ \Delta g \end{bmatrix} \tag{5.35}$$

If the local values of gravity gradient depending on the height are not measured, the value of -0.3086 mGal/m can be used[11] (Lisec, 2002).

---

[10]on deflection of the vertical see p. 65
[11]1 μm/s^2 = 0.1 mGal (Kuhar, 2006)

5.5.3 Influence of INS and GPS errors on the position of the phase center – $\Delta\mathbf{x}_0$

Although INS and GPS data are integrated, the introduced errors (see page 5.4.3) can never be entirely removed. Therefore the error of position of the GPS phase center $\Delta\mathbf{x}_0$ is considered. Here unremoved influences of the ionosphere, troposphere, satellite constellation, multipath and flight dynamics can be counted. If all these influences are optimal, $\Delta\mathbf{x}_0$ behaves almost systematically and its value can be estimated. On the other hand, if previously mentioned conditions are not optimal, these residuals behave unsystematically.

THE SIZE

In optimal conditions the GPS/INS trajectory residuals are lower than 0.05–0.1 m (Skaloud and Lichti, 2006). As an example, the company Applanix, which is a major manufactor of GPS/INS positioning systems, states that the accuracy of sensor positioning is 0.05–0.10 m after postprocessing (Maas, 2003). If all conditions listed on page 61 are fulfilled, the positional accuracy of 0.05 m can be achieved (Katzenbeisser, 2003). Others (Schenk, 2001; Lee et al., 2003) also mention that the trajectory residuals are in the order of 0.1 m.

5.5.4 Flying altitude – influence on the range measurements Δd

The main factors, through which flying altitude influences the accuracy of range measurements, are already described in section 4.4 (from page 35 on), therefore only short summary will be given here. Range measurement depends on group velocity v_g and time which is measured with time interval counter. The error of time measurement t_e can be taken as constant and is given by sensor manufacturer. This error can change as the sensor is liable to temperature changes and aging effects, therefore regular calibration of the sensor is needed. Normally the resolution of time measurement or **round trip time** (t_e) is 1 ns (Baltsavias, 1999b). Round trip time is a result of improper adjustment of the time interval counter oscillator frequency. To achieve range resolution of 3 cm, the nominal frequency has to be 10 GHz (Katzenbeisser, 2003). Typically this frequency is used for lasers with pulse length of 10 ns (Thiel and Wehr, 2004).

The error of group velocity dv_g is derived from the difference between reference and real air temperature, pressure and air humidity (Katzenbeisser, 2003; Thiel and Wehr, 2004). Therefore the equation 4.3 on page 37 for range with included errors can be written:

$$d + \Delta d = \frac{1}{2}(v_g + dv_g)(t + t_e) \tag{5.36}$$

After the simplification $(dv_g \cdot t_e)/(v_g \cdot t) = 0$ the relative range error is:

$$\frac{\Delta d}{d} = \frac{1}{2}\left(1 + \frac{dv_g}{v_g} + \frac{t_e}{t}\right) \tag{5.37}$$

THE SIZE

For the infrared wavelengths the group velocity v_g is 299.710.484 m/s at the temperature of 12 °C, the pressure of 1000 mbar and 60% humidity (Rees, 2001, cit. by Wagner, 2005a). When neglecting the pressure difference for acquisation area on shore (0 m over see level) and at 2000 m over see level, in both examples flying 1000 m over ground, a range difference of 6 cm will be increased (Katzenbeisser, 2003). If the velocity of light is used instead of group velocity, the errors of range of cca. 10 cm can be expected (Wagner, 2005a).

The before mentioned time resolution of 1 ns, can add to the whole range measurement an error of 15 cm. The laser scanner manufacturers specify range accuracies which are by a factor 10 better than this value, but such specifications normally apply for simple targets (Baltsavias, 1999b).

5.6   Errors resulting from the characteristic of the target

Errors which are related to the target characteristics are (McKean and Roering, 2005):

- target's reflectivity

- target's structure and roughness

- vegetation canopy type and density

- terrain slope and aspect at point reflections

These factors are not described in equation 5.3 on page 52, therefore an additional error matrix $\mathbf{c}(H)$ will be introduced. It is composed of errors of reflectivity, structure of the target, and thickness of vegetation or snow.

5.6.1   Reflectivity and structure of the target

Which target will be seen by laser light is defined by the target reflectivity, that also depends on the target structure. In Section 4.4.3 (page 43) the relation between transmitted and received power is described by the laser equation. After simplification, the laser equation for extended targets is written as equation 4.19 and will be repeated here (Wagner, 2005a):

$$\frac{P_r}{P_t} = \frac{D_r^2}{16d^2} \cdot \mu_{\text{at}} \cdot \mu_{\text{sys}} \cdot \sigma^0 \tag{5.38}$$

To see how this equation depends on albedo (reflectivity) of the target, the normalized backscattering coefficient of the laser footprint σ^0 will be replaced with the normalized backscattering coefficient for extended targets $\sigma^0_{\text{ext}} = 4\rho$, where ρ is the albedo of the surface. We are also

74

Triglav-Čekada, M. 2009. *Optimization of the data processing methodology and accuracy analysis of airborne laser scanning data applied for local spatial planning*, PhD thesis, Ljubljana, UL, FGG, Department for geodesy

interested in the main error sources in range measurements so the system transmission factor μ_{sys} will be taken as constant, which does not influence the measurement, therefore $\mu_{\text{sys}} = 1$. After rearranging equation 5.38 the range is:

$$d = \frac{D_r}{2}\sqrt{\rho\mu_{\text{at}}\frac{P_t}{P_r}} \tag{5.39}$$

To get a reflection of the target back to the receiver, a certain value of P_r has to be exceeded. Therefore P_t/P_r can be taken as constant and only the influence of albedo and atmospheric transmission on the range can be evaluated. Also the aperture of the system D_r is not liable to changes during one flight. Therefore equation 5.39 can be rearranged with included changes or errors:

$$d + \Delta d = \frac{D_r}{2}\sqrt{\frac{P_t}{P_r}} \cdot \sqrt{(\rho + \Delta\rho)(\mu_{\text{at}} + \Delta\mu_{\text{at}})} \tag{5.40}$$

To simplify our equation even further, we will suppose that during one flight μ_{at} also does not change significantly, therefore the article $\Delta\mu_{\text{at}}$ will be eliminated. This way the difference in the range, depends only on the albedo change:

$$d + \Delta d = \frac{D_r}{2}\sqrt{\mu_{\text{at}}\frac{P_t}{P_r}} \cdot \sqrt{(\rho + \Delta\rho)} \tag{5.41}$$

By Taylor expansion and treating the constant article of the equation as $k = \frac{D_r}{2}\sqrt{\mu_{\text{at}}\frac{P_t}{P_r}}$, the equation 5.41 can be written:

$$d + \Delta d = \frac{k}{\sqrt{\rho}} \cdot \left(1 + \frac{\Delta\rho}{\rho}\right)^{\frac{1}{2}} = \frac{k}{\sqrt{\rho}}\left(1 + \frac{1}{2}\frac{\Delta\rho}{\rho} - \frac{1}{8}\left(\frac{\Delta\rho}{\rho}\right)^2 + \frac{1}{48}\left(\frac{\Delta\rho}{\rho}\right)^3 - ...\right) \tag{5.42}$$

The values of albedo are always lees than 1, the differences between two different types of material are in the order of 0.2–0.3 as seen in Table 4.2 on page 41. Therefore the third article of Taylor expansion can be neglected. The final version of equation which links the changes/errors of range and changes/errors of albedo is:

$$d + \Delta d = \frac{k}{\sqrt{\rho}}\left(1 + \frac{1}{2}\frac{\Delta\rho}{\rho} - \frac{1}{8}\left(\frac{\Delta\rho}{\rho}\right)^2\right) \tag{5.43}$$

equation 5.43 defines how the flying altitude, described with range, influences the visibility of the weakly visible target. To exceed the limit when certain target is seen, albedo of the target should be changed or the flying height reduced.

For two different targets with the same albedo also microstructure of the target is important when checking the visibility of target (Jutzi and Stilla, 2003; Wagner, 2005a), for more details see page 44.

5.6.2   Height error resulting from the thickness of vegetation

As in photogrammetry, the results of aerial laser scanning depend on the season, when the laser scanning is conducted. Although more echoes are received from one pulse it is not certain that the last echo did reach the bare ground. This influence is bigger in summer months when the vegetation thickness under the trees is bigger and also the foliage is denser. This effect is the most pronounced in deciduous tree areas. With other words the penetration rate for the same type of vegetation changes with the season. Nevertheless, when using high density data (2-10 pt/m^2) the overall differences in DTM derived from leaf-on and leaf-off season differ for less than 5 cm (Hyyppä et al., 2005; Ahokas et al., 2005b).

The vegetation influences the accuracy of digital terrain model values derived from laser scanning in two factors (Kraus and Pfeifer, 1998; Ahokas et al., 2003; Pfeifer et al., 2004; Gorte et al., 2005; Brzank et al., 2005; Hodgson et al., 2005; McKean and Roering, 2005; Hopkinson et al., 2005; Hyyppä et al., 2005; Hopkinson et al., 2006; Göpfert and Heipke, 2006; Raber et at., 2007):

- systematic drift of terrain heights

- bigger variation in heights compared to bare ground measurements – mainly this influence can be described by standard deviation of measurements (Pfeifer et al., 2004)

The reason for systematic drift of the identified terrain point heights in vegetation is algorithm-based, as more last returns in vegetation are measured somewhere in the middle of the vegetation height than on bare ground. Therefore the bare ground measurements are scarce and identified by DTM algorithms as outliers. Systematic drift can sometimes be negative as small hills are wrongly identified as vegetation (Brzank et al., 2005).

The variation in DTM heights or standard deviation of measurements is vegetation type dependent.

From extended research on 13 datasets collected by different models of airborne laser scanners in Canada (Hopkinson et al., 2006), the connection between standard deviation SD and vegetation height H was found to be linear at least for certain groups of vegetation types:

- for **short vegetation** (aquatic, grass-herb, low shrub) when $H < 2$ m: $H = 2.7 \cdot SD$

- for **forest vegetation** when 2 m $< H < 4$ m: SD and H are not correlated

- for **tall vegetation** when $H > 4$ m: $H = 2.5 \cdot SD$

The multiplier of 2.5 for all vegetation heights (short grass to tall trees) does not statistically significantly differ from the before mentioned multipliers of 2.7 for short vegetation and 2.5 for tall vegetation (Hopkinson et al., 2006). When checking **very short vegetation** (e.g. short grass) when $H \leq 20$ cm, the influence of vegetation is stohastic and the connection between standard deviation and vegetation hight cannot be given (Gorte et al., 2005). Gorte et al. (2005)

also derived a similar linear relation between point height SD and shift of the DTM for very short vegetation: $H = 2.2 \cdot \mathrm{SD} - 0.03$.

When comparing laser data and measured ground control points, which are taken as true earth without errors, the standard deviation (SD) becomes the height accuracy of laser data for certain vegetation type (Pfeifer et al., 2004). Therefore the first approximate for vegetation height related error vector $\mathbf{c}(H)$ can be introduced from Hopkinson et al. (2006) connection between the SD and vegetation height (H), which was introduced for short and tall vegetation:

$$\mathbf{c}(H) = \begin{bmatrix} 0 \\ 0 \\ H/2.5 \end{bmatrix} \tag{5.44}$$

Another trend is seen that higher vegetation produces higher variability in the data, therefore the errors become higher. Ahokas et al. (2003) and Hyyppä et al. (2005) state that in forested areas the increase in flying altitude from 400 to 1500 m rises the random error of DTM derivation by 50% and gives a different value of systematic error.

The higher density laser data is used, the deeper penetration into the vegetation is possible also for conifer forests. Therefore higher laser frequencies have to be used to reach to the bare ground – it is recommended to use high density laser scanning with 8-10 pt/m^2 (Chasmer et al., 2006; Reutebuch et al., 2003). When using such high density laser scanning the sub-canopy elevation mapping gives comparable accuracy to that in open areas (Deems and Painter, 2006). Raber et al. (2007) found only weak relationship between different vegetation type and number of points per unit area, with a general upward trend of errors when applying smaller number of points per unit area. Therefore the equation 5.44 should be amended with flying height and density of points per unit area relation in the future.

To evaluate the accuracies of the laser scanning data cloud correctly, it is necessary to divide the point cloud into segments including just one type of vegetation. Therefore, the procedures of introducing the height texture (Pfeifer et al., 2004; Brzank et al., 2005) or vegetation roughness (McKean and Roering, 2005) in point cloud to automatically distinguish between different vegetation types are investigated. The variability of intensity and different proportion of different pulse returns (a combination of first and other returns) in different vegetation types is studied too (Moffiet et al., 2005; Brzank et al., 2005; Morsdorf et al., 2005). Also data fusion of laser scanning with imaging spectrometer can be used to classify vegetation land cover (Koetz, et al., 2007).

5.6.3 Height error resulting from the thickness of snow

When acquiring laser scanning data on terrain covered by snow, the snow can be treated as a certain vegetation type which induces additional upward drift of the terrain. On the other hand also the vegetation type under the snow should not be forgotten as it adds a certain variability in data which is vegetation type related, as already mentioned in previous section (Hopkinson et al., 2001).

The laser beam penetrates a few cm into the snow or glacier, which depends on the structure of snow or glacier (the size of ice grains...). Therefore additional vertical errors in the order of 1 cm can be expected (Deems and Painter, 2006). When using laser scanning for glacier and avalanches monitoring in mountainous terrain a careful flight planning should be done to minimize the additional vertical errors (see next chapter). When monitoring glaciers, higher flying altitudes are used. For flying altitude of 2000 m above ground the vertical error of 20 cm can be expected and usefulness of data set for glacier surface elevation change in the range of 0.5 to 0.7 m is expected (Geist et al., 2003). On the other hand snow depth from 25 to 40 cm in the areas covered by forest already present a problem (flying altitudes around 700 m) (Hopkinson et al., 2001).

5.6.4   Additional vertical error in steeper terrain

The majority of tests of laser scanning error assessment is done in flat or just slightly hilly terrain (McKean and Roering, 2005). Larger errors can be expected when working in steeper terrain. There are two types of additional vertical error (Baltsavias, 1999b; Schenk, 2001; Hodgson and Bresnahan, 2004; McKean and Roering, 2005; Deems and Painter, 2006):

- the influence of planimetric basic systematic errors (hardware/software effect errors) on the height error

- the influence of laser footprint spread over the inclined terrain – time-walk error

The **influence of planimetric systematic errors** (Figure 5.16A) can be described by the angle of slope α. The maximal additional hight error is (Baltsavias, 1999b):

$$|\Delta z_{\mathrm{add1}}| = |\Delta x \Delta y| \cdot \tan \alpha \tag{5.45}$$

The maximum error will only occur if the displacement is perpendicular to the contour line. The error will be zero for displacement parallel with contour line. Unfortunately, in practice the direction of planimetric error is not known. Planimetric error is often reported to be approximately 1/1000 of the flying altitude on most airborne laser scanners (Hodgson and Bresnahan, 2004). When knowing the behaviour of planimetric errors and the shape of terrain, the additional hight error can be minimized with correct flight planing.

For example 100 cm horizontal error on a 10° slope can induce an additional vertical error of 18 cm.

The **time walk error** (Figure 5.16B) depends only on the principle of laser scanning – the spread of laser footprint because of the laser divergence. Because of the divergence the laser footprint is not just a point but a circular area of certain diameter. At the first contact with the ground the echo is returned to the laser system. On flat terrain this point is in the center of the laser footprint, from where planimetric coordinates are given also. On steep terrain the first point from which range (vertical distance) is measured is on the upper part of the footprint. On
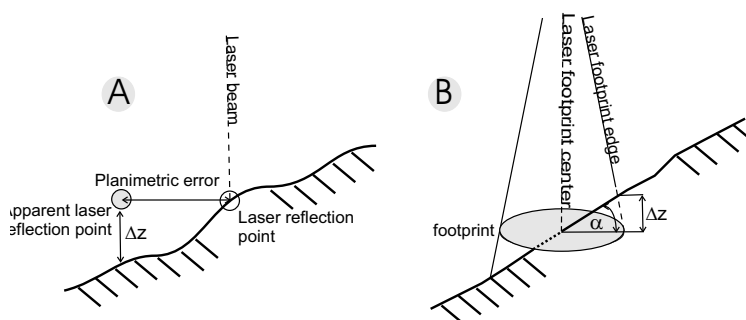
Figure 5.16: A) vertical error induced by horizontal errors, B) vertical error induced by laser footprint spread.

Slika 5.16: A) napaka zaradi planimetrične napake skeniranja, B) napaka zaradi velikosti odtisa laserske točke na tleh.

the other hand the planimetric position is given for the center of the laser footprint, which lies downhill. This error does not exist on flat terrain where both points coincide. The time walk error can be written as (Baltsavias, 1999b; McKean and Roering, 2005):

$$|\Delta z_{\mathrm{add2}}| = \frac{h\gamma|\tan\alpha|}{2} \tag{5.46}$$

where h is the flying altitude, γ angle of laser beam divergence, α the slope of the terrain. Typical commercial laser scanners have a divergence of a laser beam in the order of 0.2 to 1 mrad (Baltsavias, 1999a). This error grows rapidly even for laser scanners with a small divergence. At a terrain slope of 60% and flying altitude of 600 m this error is approximately 20 cm.

When slope angle and aspect are changing significantly over small spatial scales, the probability increases that individual laser scanner reflections will record inaccurate elevations because of the additional vertical errors (McKean and Roering, 2005).

The **influence of different number of points per unit area in sloped terrain** on height error component can be described with a simple empirically gained equation defined by Kraus (2004):

$$\Delta Z[\mathrm{cm}] = \pm(\frac{6}{\sqrt{n}} + 120\tan\alpha) \tag{5.47}$$

where ΔZ is height error component, n number of points per unit area and α terrain slope.

THE SIZE

When checking the behaviour of DTM accuracy for different vegetation types, Hodgson et al. (2005) found no influence of slope bellow 8° on the vertical error behaviour. The observed vertical errors for different vegetation types on slopes of 25° are twice as big as those on relatively low slopes (α less than 4°) (Hodgson and Bresnahan, 2004).

5.7   Discussion

As the laser scanning points are calculated with direct georeferencing the knowledge about the behaviour of different errors contributing to inaccuracy of laser scanning points is of great importance.

In this chapter the details on positional and height error sources were described in detail. The error sizes and its behaviour was discussed. The errors were connected together with Schenk's geolocation equation. Three major error sources were discussed:

- the basic systematic errors

- the errors of laser scanning mission

- the errors caused by nature of the target

Only the basic systematic errors behave systematically and can mainly be removed by correct in-the-flight calibration. As person placing order cannot know if the in-the-flight calibration was performed correctly, we should not neglect them. On the other hand the errors resulting from the laser scanning mission and the errors resulting from the characteristic of the target can never be totaly removed. The errors resulting from laser scanning mission do not behave systematically. The errors resulting from the characteristic of the target behave systematically if the laser scanning data is segmented by the vegetation type or/and slope of the terrain. As the laser data is usually acquired for new detailed presentation of the terrain, no segmentation of data by this two factors is done in advance. Therefore the removal of vegetation height or/and slope related errors can be done only when already working with laser data.

For the purpose of ordering the Schenk's error model has to be simplified, as ordinary engineer who is in-charge of data ordering for municipality will not have time to search for sizes of errors and calculate them with Schenk's error model. Therefore we will simplify this model in the next chapter.

6 SIMPLIFIED LASER SCANNING ERROR MODEL – A-PRIORI ERROR ESTIMATION

6.1 Introduction

Our purpose in this chapter is to get an equation, which will be simple and useful for planning the laser scanning mission, meaning that a person with basic technical knowledge can use it, without deep search of literature for the size of errors. Also the equation will not be scan angle dependent, as providers usually do not deliver scan angle components for each point. Therefore our derivation do not have an intention to give an exact error model. Examples of exact models can be found in literature (Schenk, 2001; Beinat and Crosilla, 2002; Friess, 2006; Skaloud and Lichti, 2006). The result of our error model will give an estimation of average and total error of laser points in one laser scanning mission.

The simulations of Schenk's and simplified error models were performed in the Matlab.

6.2 Simplification

Basic systematic errors presented in Schenk's error model (equation 5.3 on page 52) will be expanded by vegetation type related errors $\mathbf{c}(H)$ (equation 5.44 on page 76), and by synchronization error Δp_s described in Section 5.5.1 on page 69. The rotation from local to global ortogonal reference system $\mathbf{R}_W$ will be neglected, as we will treat GPS measurements as related to local reference system, the same as in Schenk's computations (2001). In our simplification the local and the global reference systems from Figure 5.13 coincide and the GPS phase center of the flying platform is situated in the center of the Earth.

When adding errors of individual components, which are treated as uncorrelated, the basic geolocation equation with included errors can be written as:

$$\mathbf{x}_L = \mathbf{x}_0 + \Delta\mathbf{x}_0 + \mathbf{R}_{\text{GEO}} \cdot \Delta\mathbf{R}_{\text{INS}} \cdot \mathbf{R}_{\text{INS}} \left(\mathbf{s}_0 + \Delta\mathbf{s}_0 + \Delta\mathbf{R}_m \cdot \mathbf{R}_m \cdot \Delta\mathbf{R}_s \cdot \mathbf{R}_s \cdot \mathbf{h}_{-(d+\Delta d)} \right) + \Delta\mathbf{p}_s + \mathbf{c}(H)$$

$$(6.1)$$

By testing Schenk's error model, it can be seen that is mainly scan angle and heading angle dependent, if roll and pitch angles are small (e.g. we allow maximal roll or pitch angles of $\pm 6°$, as the flying platform has to be nearly horizontal regarding the terrain during the flight).

The variability of Schenk's and in our thesis developed average error model can be seen already on Figures 6.1 and 6.2, where the influence on flying height and $\Delta\mathbf{R}_{\text{INS}}$ is presented. Other variabilities can be seen in Appendix C, where the next influences are graphically presented:

- changing $\Delta\mathbf{R}_s$ and $\Delta\mathbf{R}_m$ is presented on Figure C.1 and C.2 on pages 181 and 182

- changing $\mathbf{R}_m$ is presented on Figure C.3 on page 183

- changing $\mathbf{R}_{\text{INS}}$ values (roll and pitch) is presented on Figure C.6 and C.7 on page 186 and 187

- changing $\mathbf{R}_{\text{GEO}}$ is presented on C.4 and C.5 on pages 184 and 185

There Schenk's error model describes sine curve with non-negligible amplitude. With simplification we would like to derive an error model, which is not scan angle and heading dependent, as the users of simplified error model will not use it for different scan angles and different headings. To predict a-priori error size from Schenk's error model for different scan angles and/or flying heights, we have to know which heading angles will be used during the flight. Unfortunately the heading angle cannot be planned. Therefore the purpose of our simplified error model is to give an average and maximal expected error values, without numerous calculations of equation 6.1 as were needed to draw Figures in Appendix C. Simplified error model should give an average value of errors, when used for different scan angle or different heading. Therefore we are searching for average value of Schenk's error model. Secondary the simplified error model should represent maximal error value, used to foresee the maximal errors, which can be expected, if basic systematic errors were not totally removed in the post-processing.

The simplification of equation 6.1 will start with basic systematic errors term. First the behaviour of the inner term $\Delta\mathbf{R}_m \cdot \mathbf{R}_m \cdot \Delta\mathbf{R}_s \cdot \mathbf{R}_s \cdot h_{-(d+\Delta d)}$ will be studied and treated as the only error source. Other components of plain systematic errors will be added afterwards. When ordering lidar survey mission, the sizes of $\Delta\mathbf{R}_m$, $\mathbf{R}_m$ and $\Delta\mathbf{R}_s$ components are not known, as these are connected to the specific lidar system, which will be used in survey mission. Therefore one should apply some general numerical values representing the majority of lidar systems available on the market, and treat these components as fixed. As $\mathbf{R}_m$ is also not known in the process of lidar ordering, it will be treated as constant value too. Therefore the vector $\mathbf{x}_1$ of the inner term can be written as:

$$\mathbf{x}_1 = \Delta\mathbf{R}_m \cdot \mathbf{R}_m \cdot \Delta\mathbf{R}_s \cdot \mathbf{R}_s \cdot \mathbf{h}_{-(d+\Delta d)} \tag{6.2}$$

Three general types of $\Delta\mathbf{R}_m$ and $\Delta\mathbf{R}_s$ errors with variations were taken into account when doing simulations (Table 6.1). These values can be found in literature:

- maximal errors (for details see Section 5.4.1 and 5.4.2)

- errors approximately half size of maximal errors and

- minimal possible errors
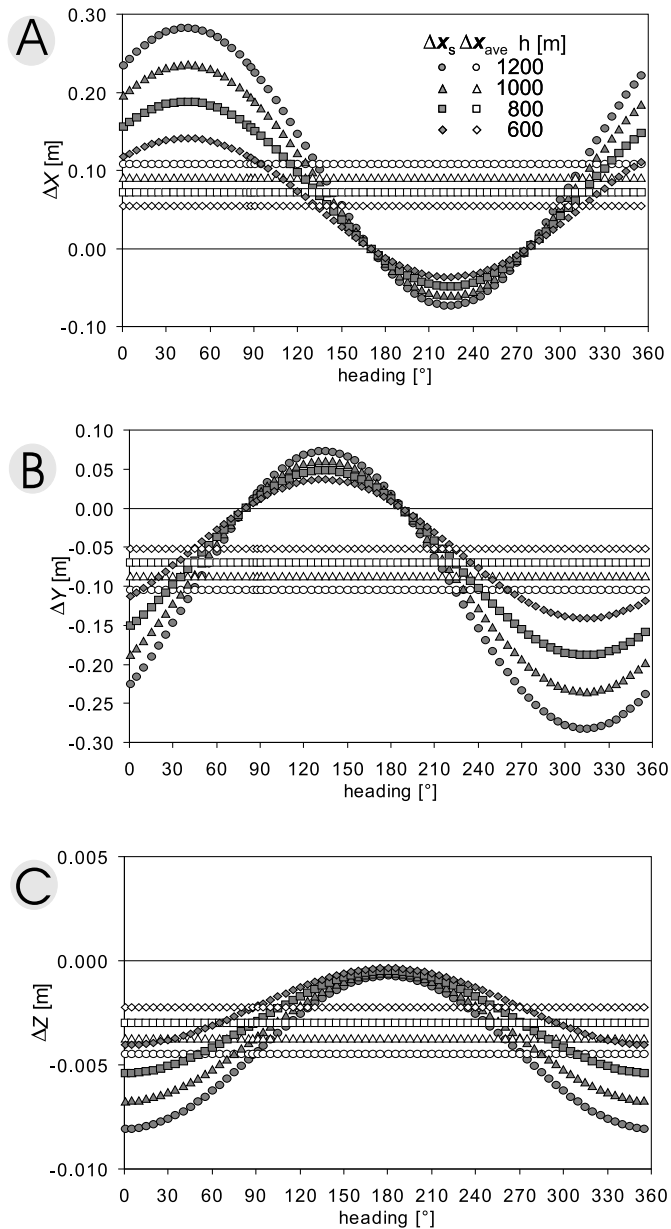
Figure 6.1: Basic systematic errors by Schenk's $\Delta \mathbf{x}_s$ and simplified average $\Delta \mathbf{x}_{ave}$ error model for **different flying height** h, scan angle $0°$, with variable heading angle. The simulation is done for $\Delta \mathbf{R}_{INS}$ values of $\Delta\phi = \Delta\theta = 0.005°$ and $\Delta\psi = 0.007°$, and average magnitude of roll and pitch angles of $1°$. Error components A) ΔX , B) ΔY and C) ΔZ.

Slika 6.1: Osnovne sistematične napake po Schenkovem $\Delta \mathbf{x}_s$ in poenostavljenem povprečnemu modelu napak $\Delta \mathbf{x}_{ave}$ pri različni višini leta h in kotu skeniranja $0°$.
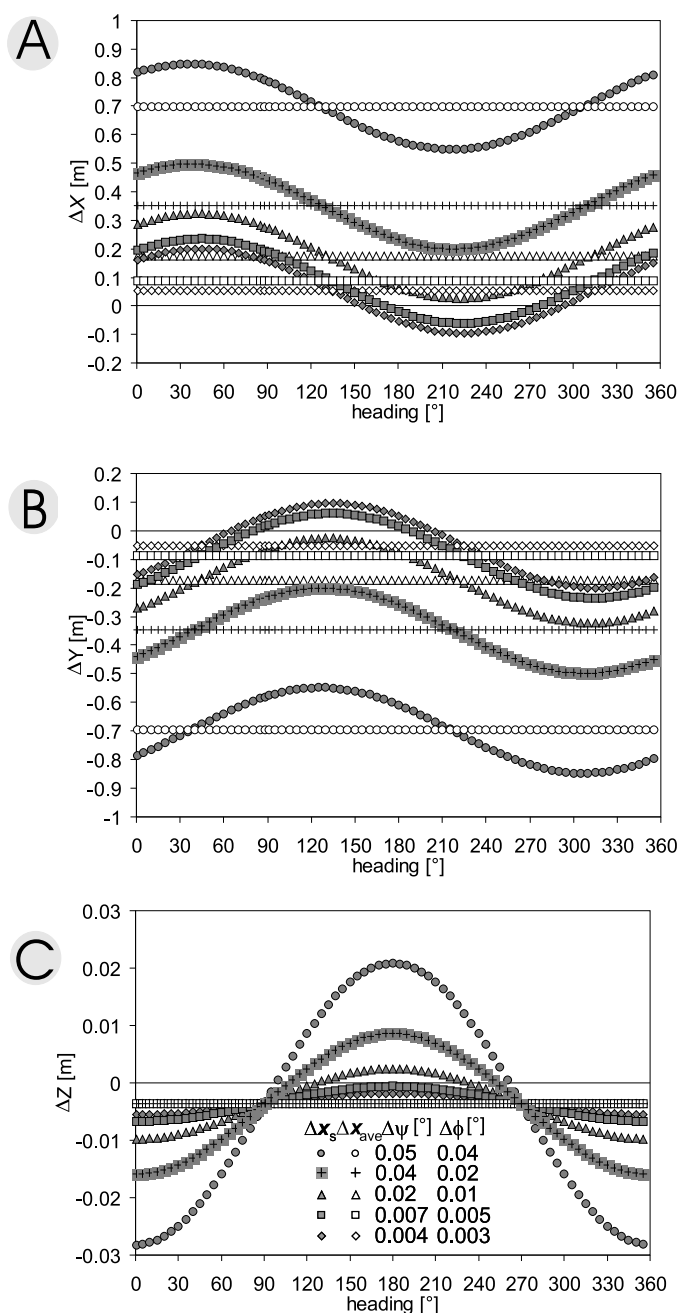
Figure 6.2: Basic systematic errors by Schenk's $\Delta\mathbf{x}_s$ and simplified average $\Delta\mathbf{x}_{ave}$ error model for **different $\Delta\mathbf{R}_{\mathrm{INS}}$ values** and variable heading angle. The simulation is done for flying height of 1000 m and scan angle $0°$ and average magnitude of roll and pitch angles of $1°$. Error components: A) ΔX, B) ΔY and C) ΔZ.

Slika 6.2: Osnovne sistematične napake po Schenkovem $\Delta\mathbf{x}_s$ in poenostavljenem povprečnemu modelu napak $\Delta\mathbf{x}_{ave}$ pri različni vrednostih kotov $\Delta\mathbf{R}_{\mathrm{INS}}$ in spremenljivem kotu pozibavanja. Za višino leta 1000 m in kot skeniranja $0°$.

Table 6.1: Different combinations of $\Delta\mathbf{R}_m$ and $\Delta\mathbf{R}_s$ errors, all are expressed in degrees [°].

Tabela 6.1: Največja, srednja in najmanjša kombinacija napak $\Delta\mathbf{R}_m$ in $\Delta\mathbf{R}_s$, vse napake so izražene v stopinjah [°].

	ε	$\Delta\tau$	$\Delta\beta_i$	$\Delta\kappa$	$\Delta\varphi$	dm_x	dm_y	dm_z
maximum	0.020	0.030	0.0350	0.030	0.030	0.010	0.010	0.010
medium	0.010	0.015	0.0175	0.015	0.015	0.005	0.005	0.005
minimum	0.001	0.005	0.0035	0.003	0.003	0.003	0.003	0.003

The maximal possible mounting bias angles, which are represented in $\mathbf{R}_m$, were below 3° (3°, 1°, 0.01° and 0.001° were tested (see Appendix C Figure C.3 on page 183). Such $\mathbf{R}_m$ values can be expected, if precise fixation of INS/GPS system and laser scanner can be performed. The laser point planimetric and height difference of just few centimeters between highest and smallest mentioned mounting bias value was calculated. Therefore a very small mounting bias angles $\mathbf{R}_m$ – all components equal to 0.001° – were used for our simulation.

For clarity, we will define the product of mounting bias and rotation between the laser beam and the laser system, as $\mathbf{K}_1$:

$$\mathbf{K}_1 \equiv \Delta\mathbf{R}_m \cdot \mathbf{R}_m \cdot \Delta\mathbf{R}_s = \begin{bmatrix} k_{11} & k_{12} & k_{13} \\ k_{21} & k_{22} & k_{23} \\ k_{31} & k_{32} & k_{33} \end{bmatrix} \qquad (6.3)$$

From Table 6.1 the values of $\mathbf{K}_1$ matrix, with diagonal values of approximately 1, can be calculated. Now $\mathbf{x}(h)_1$ can be written as:

$$\mathbf{x}(h)_1 = \mathbf{K}_1 \cdot \mathbf{R}_s \cdot \mathbf{h}_h = \mathbf{K}_1 \cdot \begin{bmatrix} 1 & 0 & 0 \\ 0 & \cos\beta & -\sin\beta \\ 0 & \sin\beta & \cos\beta \end{bmatrix} \cdot \begin{bmatrix} 0 \\ 0 \\ h \end{bmatrix} \qquad (6.4)$$

where the range $d + \Delta d$ is replaced by flying height h and scan angle rotation matrix $\mathbf{R}_s$ from equation 5.4 (on page 54) is written out.

The error vector $\mathbf{x}_1$ will be expanded with other error sources that represent the basic systematic errors. First the translation vector $\mathbf{s}_0$ between laser and GPS system and its error $\Delta\mathbf{s}_0$ should be added. If we postulate that INS/GPS and laser systems are unique for one aeroplane (helicopter), than the translation vector $\mathbf{s}_0$ is measured only once at the installation of both systems – its value is constant for every laser scanning mission carried out with this aeroplane. In order of simplicity, we postulate that both systems are fixed at an identical point. Therefore the $\mathbf{s}_0$ is 0 and also the translation vector error $\Delta\mathbf{s}_0$ is neglected.

The terms representing just errors will be treated as variables, therefore they will be grouped and put in brackets on the right side of equation 6.5:

$$\mathbf{x}_L = \mathbf{x}_0 + \mathbf{R}_{\mathrm{GEO}} \cdot \Delta\mathbf{R}_{\mathrm{INS}} \cdot \mathbf{R}_{\mathrm{INS}} \cdot \mathbf{x}(h)_1 + (\Delta\mathbf{p}_s + \Delta\mathbf{x}_0 + \mathbf{c}(H)) \qquad (6.5)$$

The first two terms of equation 6.5 represent the basic Schenk's geolocation equation with included errors. The terms in brackets represent the errors of synchronization, sensor positioning and vegetation height. To transform this expanded Schenk's geolocation equation into equation describing just errors, the first two terms of equation 6.5 are replaced with term representing just Schenk's basic systematic errors (without $\mathbf{s}_0 + \Delta\mathbf{s}_0$ term which was already neglected and $\mathbf{X}_0$ which is self-dependent term in equation 6.8):

$$\Delta\mathbf{x}_s = \mathbf{R}_{\mathrm{GEO}} \cdot \Delta\mathbf{R}_{\mathrm{INS}} \cdot \mathbf{R}_{\mathrm{INS}} \cdot \mathbf{x}(h)_1 - \mathbf{R}_{\mathrm{GEO}} \cdot \mathbf{R}_{\mathrm{INS}} \cdot \mathbf{x}(h)_1^* \tag{6.6}$$

where $\mathbf{x}(h)_1$ includes fixed errors and is described in equation 6.4 and $\mathbf{x}(h)_1^*$ which does not include errors is:

$$\mathbf{x}(h)_1^* = \mathbf{R}_m \cdot \mathbf{R}_s \cdot \mathbf{h}_h \tag{6.7}$$

Now the total error of lidar point is:

$$\Delta\mathbf{x} = \Delta\mathbf{x}_s + \Delta\mathbf{p}_s + \Delta\mathbf{x}_0 + \mathbf{c}(H) \tag{6.8}$$

6.3   The simulation

6.3.1   Neglecting $\mathbf{R}_{\mathrm{GEO}}$

First the influence of $\mathbf{R}_{\mathrm{GEO}}$ was evaluated for scan angle of $0°$ and flying height of 1000 m. Following the discussion in Section 5.4.5 on $\mathbf{R}_{\mathrm{GEO}}$ the middle values of deflection of the vertical $\eta = 0.0028°$ and $\xi = 0.0028°$ for Bessel ellipsoid in Slovenia were used for geographical latitude of $\varphi = 45°$. In simplified and Schenk error models only the differences of 10^{-5} m can be noted when changing the deflection of the vertical components from $0°$-$0.0055°$. In Appendix C the behaviour of Schenk's model when changing $\mathbf{R}_{\mathrm{GEO}}$ is presented: on Figure C.4 on page 184 for scan angle $0°$ and on Figure C.5 on page 185 for scan angle $20°$ is presented. Therefore its influence on simplified error model can be neglected and basic systematic error can be written without $\mathbf{R}_{\mathrm{GEO}}$:

$$\Delta\mathbf{x}_s = \Delta\mathbf{R}_{\mathrm{INS}} \cdot \mathbf{R}_{\mathrm{INS}} \cdot \mathbf{x}(h)_1 - \mathbf{R}_{\mathrm{INS}} \cdot \mathbf{x}(h)_1^* \tag{6.9}$$

Therefore, also **simplified total error of laser scanning points** (equation 6.8) is written without $\mathbf{R}_{\mathrm{GEO}}$:

$$\Delta\mathbf{x} = (\Delta\mathbf{R}_{\mathrm{INS}} \cdot \mathbf{R}_{\mathrm{INS}} \cdot \mathbf{x}(h)_1 - \mathbf{R}_{\mathrm{INS}} \cdot \mathbf{x}(h)_1^*) + \Delta\mathbf{p}_s + \Delta\mathbf{x}_0 + \mathbf{c}(H) \tag{6.10}$$

6.3.2   Basic systematic errors

In next sections the behaviour of **basic systematic errors** written with equation 6.9 will be studied. The simplified model $\mathbf{x}_s$ was tested using simulation of laser points by changing the $\mathbf{R}_{\mathrm{INS}}$, $\Delta\mathbf{R}_{\mathrm{INS}}$ and flying height.

As already mentioned in Chapter 5, $\mathbf{R}_{\text{INS}}$ and $\Delta\mathbf{R}_{\text{INS}}$ have major influence on the size of basic systematic error of laser point. The flying platform has to be nearly horizontal regarding the terrain during the flight, therefore roll and pitch angles with maximal values of $\pm 6°$ can be expected. As these angles are small, the average value of angles for whole flight mission is $0°$, the average magnitude of angle on the other hand is a half of maximal value $3°$ (Figure 6.3). If we are even more strict, the maximal values of $\pm 2°$ can be used, with the average magnitude of angle $1°$. For the simulations just the average magnitudes of these angles will be used. The heading of aeroplane changes with time and direction of aeroplane, therefore the heading varies from $0°$ to $360°$ and therefore it cannot be replaced by an average magnitude. In reality, all angles of $360°$ are not covered in one flight mission.
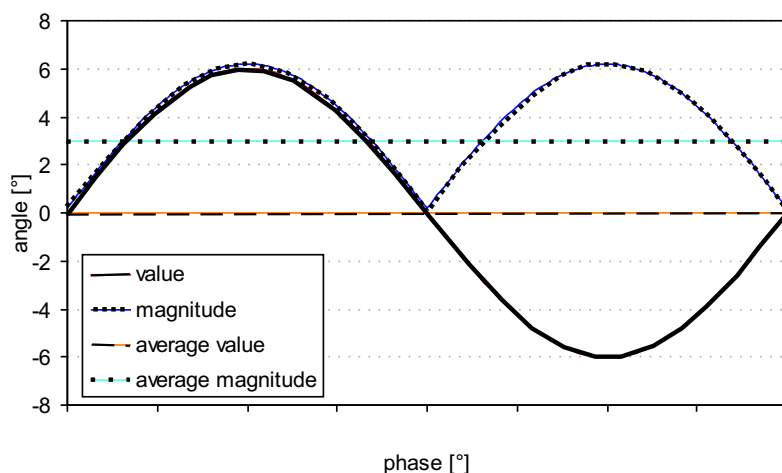
Figure 6.3: Evenly changing angle can be represented by its average value or average magnitude.
Slika 6.3: Zvezno spreminjajoči se kot po enoti časa lahko opišemo z njegovo povprečno velikostjo in povprečno magnitudo.

First the influence of $\Delta\mathbf{R}_{\text{INS}}$ was tested. Different values of $\Delta\mathbf{R}_{\text{INS}}$ combinations already described in Section 5.4.4 were tested. The majority of laser scanning providers nowadays aim for better accuracy, therefore a trend is seen to employ medium-priced INS as defined by Cramer (1997) (see page 64). Hereafter our simulations are therefore based on $\Delta\mathbf{R}_{\text{INS}}$ values of roll and pitch errors of $\Delta\phi = \Delta\theta = 0.005°$, and heading error $\Delta\psi = 0.007°$ were used unless stated differently.

As can be seen in Appendix C on Figure 6.2 (page 84) the difference between applying the worst INS combination of low priced INS ($\Delta\phi = \Delta\theta = 0.04°$, $\Delta\psi = 0.05°$) and middle value of medium-priced INS ($\Delta\phi = \Delta\theta = 0.005°$, $\Delta\psi = 0.007°$) brings more than 60 cm difference in planimetric components (ΔX and ΔY) and 2 cm difference in height component (ΔZ).

In Appendix C on Figure 6.1 (page 83) the behaviour of simplified and Schenk's error model for different flying heights and different headings for scan angle $0°$ is presented. All three components of Schenk's error model $\Delta\mathbf{x}_s$ describe the sine curve, while $\mathbf{R}_{\text{INS}}$ values of roll and pitch errors of $\Delta\phi = \Delta\theta = 0.005°$, and heading error $\Delta\psi = 0.007°$ were used. The amplitude of sine curve of Schenk's error model describes the variability in error components and is only

flying height dependent.

In Appendix C on Figures C.8 (page 188), C.9 (page 189), C.10 (page 190) and C.11 (page 191) the behaviour of basic systematic errors for different scan angles, roll, pitch and different headings in shown.

6.4   The average value of basic systematic errors

Basic systematic errors depend mainly on scan angle, heading angle and flying height as seen in Appendix C. To predict the error size for different scan angles and flying height, we have to know which heading will be used during the flight for each laser point. Unfortunately the heading angle cannot be planned. Therefore we would like to get average and maximal values of basic systematic errors, without the numerous calculations of equation 6.9. If the heading is changing evenly during the flight, different values from $0° - 360°$ can be expected. Therefore the average size of plain systematic errors can be calculated as an integral of heading in range of $0° - 360°$ for individual error vector component (ΔX_s, ΔY_s, ΔZ_s):

$$\Delta \mathbf{x}_s = \begin{bmatrix} \Delta X_s \\ \Delta Y_s \\ \Delta Z_s \end{bmatrix} \tag{6.11}$$

The error components of vector $\Delta \mathbf{x}_s$ are written out in Appendix C on page 177.

Therefore **the average size of basic systematic errors for different scan angles** $\Delta \mathbf{x}_{s\_ave}(\beta)$ can be calculated as an integral over heading for individual error vector components $< \Delta \mathbf{x}_s >$:

$$\Delta \mathbf{x}_{s\_ave}(\beta) = < \Delta \mathbf{x}_s > = \begin{bmatrix} < \Delta X_s > \\ < \Delta Y_s > \\ < \Delta Z_s > \end{bmatrix} = \begin{bmatrix} \frac{1}{2\pi} \int_0^{2\pi} \Delta X_s d\psi \\ \frac{1}{2\pi} \int_0^{2\pi} \Delta Y_s d\psi \\ \frac{1}{2\pi} \int_0^{2\pi} \Delta Z_s d\psi \end{bmatrix} = \tag{6.12}$$

$$= \begin{bmatrix} -\Delta\theta \sin\theta x_1(1,1) + \Delta\theta \cos\theta \sin\phi x_1(2,1) + \Delta\theta \cos\theta \cos\phi x_1(3,1) \\ \Delta\phi \sin\theta x_1(1,1) - \Delta\phi \cos\theta \sin\phi x_1(2,1) - \Delta\phi \cos\theta \cos\phi x_1(3,1) \\ -\sin\theta x_1(1,1) + \cos\theta \sin\phi x_1(2,1) + \cos\theta \cos\phi x_1(3,1) + \sin\theta x_1^*(1,1) - \cos\theta \sin\phi x_1^*(2,1) - \cos\theta \cos\phi x_1^*(3,1) \end{bmatrix}$$

If the error components of $\Delta \mathbf{R}_m$ and $\Delta \mathbf{R}_s$ are small, we can say that $\mathbf{x}_1(h) \approx \mathbf{x}_1^*(h)$, therefore the average value of height error component is 0 m.

The final derivation of **average value error value independent from heading and independent from scan angle** can be calculated as an integral over heading and over scan angle:

$$\Delta \mathbf{x}_{s\_ave} = << \Delta \mathbf{x}_s >> = \begin{bmatrix} << \Delta X_s >> \\ << \Delta Y_s >> \\ << \Delta Z_s >> \end{bmatrix} = \begin{bmatrix} \frac{1}{2\pi} \int_0^{2\pi} d\psi \int_{-\beta_0}^{\beta_0} d\beta \Delta X_s \\ \frac{1}{2\pi} \int_0^{2\pi} d\psi \int_{-\beta_0}^{\beta_0} d\beta \Delta Y_s \\ \frac{1}{2\pi} \int_0^{2\pi} d\psi \int_{-\beta_0}^{\beta_0} d\beta \Delta Z_s \end{bmatrix} = \tag{6.13}$$

$$
= \begin{bmatrix}
\frac{h \cdot \sin \beta_0}{\beta_0}(-\Delta\theta \sin\theta k_{13} + \Delta\theta \cos\theta \sin\phi k_{23} + \Delta\theta \cos\theta \cos\phi k_{33}) \\
\frac{h \cdot \sin \beta_0}{\beta_0}(\Delta\phi \sin\theta k_{13} - \Delta\phi \cos\theta \sin\phi k_{23} - \Delta\phi \cos\theta \cos\phi k_{33}) \\
\frac{h \cdot \sin \beta_0}{\beta_0}(-\sin\theta k_{13} + \cos\theta \sin\phi k_{23} + \cos\theta \cos\phi k_{33} + \sin\theta R_m(1,3) - \cos\theta \sin\phi R_m(2,3) - \cos\theta \cos\phi R_m(3,3))
\end{bmatrix}
$$

where β_0 is maximal possible scan angle and k_{13}, k_{23}, k_{33} are components of $\mathbf{K}_1$ matrix (equation 6.3) and $R_m(1,3)$, $R_m(2,3)$, $R_m(3,3)$ are components of $\mathbf{R}_m$ matrix (equation 5.11).

If $\mathbf{x}_1(h) \approx \mathbf{x}_1^*(h)$ the average error value of height component is 0 m. For the selected values of $\Delta\mathbf{R}_m$, $\mathbf{R}_m$ and $\Delta\mathbf{R}_s$ explained on the page 85, the upper coefficients have the next values:

$$
\begin{aligned}
k_{13} &= 1.22 \cdot 10^{-4} \\
k_{23} &= -1.22 \cdot 10^{-4} \\
k_{33} &= 1 \\
R_m(1,3) &= 1.74 \cdot 10^{-5} \\
R_m(2,3) &= -1.74 \cdot 10^{-5} \\
R_m(3,3) &= 1
\end{aligned}
\tag{6.14}
$$

Now the $\Delta\mathbf{x}_{s\_ave}$ value can quickly be calculated, with deciding only on roll, pitch angles and their errors and inserting these values in equation 6.13. Also total scan angle and heading angle independent error can now quickly be calculated, without the multiplication of matrices, while replacing in equation 6.8 $\Delta\mathbf{x}_s$ with $\Delta\mathbf{x}_{s\_ave}$:

$$
\Delta\mathbf{x} = \Delta\mathbf{x}_{s\_ave} + \Delta\mathbf{p}_s + \Delta\mathbf{x}_0 + \mathbf{c}(H) \tag{6.15}
$$

On Figure 6.4 the average values for different scan angles, $\Delta\mathbf{R}_{INS}$ and constant flying height of 1000 m are presented. First, we consider planimetric components. When applying higher values of $\Delta\mathbf{R}_{INS}$ the average value of basic systematic errors increases. The averages between different scan angles for $\Delta\phi = \Delta\theta = 0.02°$, $\Delta\psi = 0.03°$ and average magnitude of roll or pitch angles of $3°$ differ for altogether 3 cm. The averages between different scan angles for $\Delta\phi = \Delta\theta = 0.005°$ and $\Delta\psi = 0.007°$, differ for 0.7 cm.

On Figure 6.4C the average height component values are drawn. These values are $\Delta\mathbf{R}_{INS}$ independent. They depend mainly on average magnitude of roll and pitch. If using average height error value for different scan angles of 0 m (derived for $\mathbf{x}_1(h) \approx \mathbf{x}_1^*(h)$), a difference of at most 5 cm from real average value can be gained, when unfavorable scan angles are used. When checking the average height error value independent from scan angle at most a few cm difference from 0 m can be expected. Therefore when applying in a laser scanning mission small $\Delta\mathbf{R}_{INS}$ values the average height value of 0 m is a good approximation for average basic systematic height error.
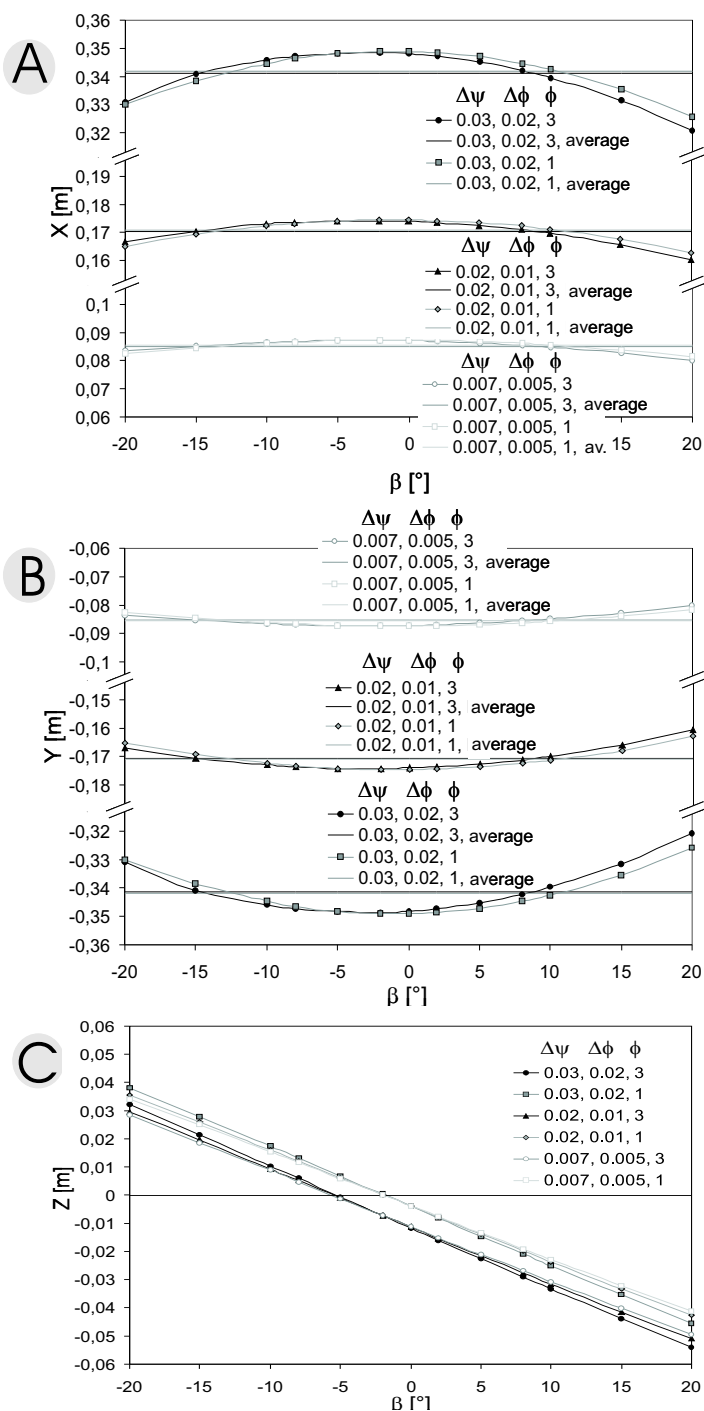
Figure 6.4: The average error values for different scan angles calculated by equation 6.12 and average error value independent from scan and heading angle (marked with average) calculated by equation 6.13. The simulation is done for roll-pitch errors $\Delta\phi$ and heading error $\Delta\psi$ combinations and average magnitude of roll and pitch angles ϕ written in legend. Error components: A) ΔX, B) ΔY, C) ΔZ.

Slika 6.4: Povprečne vrednosti napak odvisna of kota skeniranja (enačba 6.12) in neodvisna od kota skeniranja (enačba 6.13) označene z average. V legendah so podane INS napake zibanja in guganja $\Delta\phi$, napake pozibavanja $\Delta\psi$ ter srednjo velikost kotov zibanja in guganja ϕ

6.5   The maximal value of basic systematic errors

The average value can now be conveniently calculated with equation 6.13. When planning laser scanning measurements, also the largest expected errors are of our great interest. In Appendix C on Figure C.8, C.9, C.10 and C.11 (pages 188–191) the sizes of errors for different headings and different scan angles are drawn for Schenk's and average basic systematic error.

For basic systematic error model the maximum errors are not fixed on constant heading angles and therefore cannot be known in advance. The headings on which maximum errors appear are varying according to scan angle, $\Delta \mathbf{R}_{\text{INS}}$ and average magnitude of roll or pitch angles (Figure 6.5). The greatest maximum errors can be expected for scan angle of $20°$.

The headings of maxima were calculated as first derivatives $\partial \Delta \mathbf{x}_s / \partial \psi$ for each of the $\Delta \mathbf{x}_s$ components. The differentiation between maxima and minima was done by inspection of the second derivatives $\Delta^2 \mathbf{x}_s / \partial \psi^2$ (see Appendix C on page 180). Some maxima for different flying heights and $\Delta \mathbf{R}_{\text{INS}}$ with scan angle $20°$ are drawn on Figure 6.6.

To calculate a maximum of one component with equation 6.15 at least three equations have to be calculated and analyzed ($\partial \Delta \mathbf{x}_s / \partial \psi$, $\Delta \mathbf{x}_s (\partial \Delta \mathbf{x}_s / \partial \psi)$ and $\Delta^2 \mathbf{x}_s / \partial \psi^2$). In order to quickly derive a-priori maximum error size a faster method has to be proposed.

It would be the most convenient, if average value of basic systematic error would be somehow connected to maximal value, as it would reduce the computational effort. Therefore, the maximal values for scan angle $20°$ and average values independent from scan angle $\Delta \mathbf{x}_{s\_ave}$ (equation 6.13) were plotted on Figure 6.7. With first and second derivatives calculated maximum values were derived for different flying heights and different $\Delta \mathbf{R}_{\text{INS}}$ combinations. Planimetric and height component shows linear correlation between maximum and average value. With the adjustment of indirect observations the least squares fitting of the following linear regression for 32 values of $\Delta \mathbf{x}_{s\_max}$ and $\Delta \mathbf{x}_{s\_ave}$ was performed [1]:

$$\Delta \mathbf{x}_{s\_max} = \begin{bmatrix} \Delta X_{s\_max} \\ \Delta Y_{s\_max} \\ \Delta Z_{s\_max} \end{bmatrix} = \begin{bmatrix} \Delta X_{s\_ave} \cdot k_{x\_ave} + \Delta\psi \cdot k_{x\_\Delta\psi} + \Delta\phi \cdot k_{x\_\Delta\phi} + h \cdot k_{x\_h} + k_{x\_0} \\ \Delta Y_{s\_ave} \cdot k_{z\_ave} + \Delta\psi \cdot k_{y\_\Delta\psi} + \Delta\phi \cdot k_{y\_\Delta\phi} + h \cdot k_{y\_h} + k_{y\_0} \\ \Delta Z_{s\_ave} \cdot k_{z\_ave} + \Delta\psi \cdot k_{z\_\Delta\psi} + \Delta\phi \cdot k_{z\_\Delta\phi} + h \cdot k_{z\_h} + k_{z\_0} \end{bmatrix}$$

$$(6.16)$$

The maximum value components depend on average error value $\Delta \mathbf{x}_{s\_max}$ components, heading error $\Delta\psi$, roll and pitch errors $\Delta\phi$ (as $\Delta\phi = \Delta\theta$) and flying height h. Statistical analysis on the significance of the estimated unknown parameters ($r=5$) was carried out by t-Student test – for component X the unknown parameters are k_{x_ave}, $k_{x\_\Delta\psi}$, $k_{x\_\Delta\phi}$, k_{x_h}, k_{x_0}. For a significance level α equal to 95%, the statistically not significant parameters were picked out by testing the null hypothesis of the t-test (Mikhail and Ackerman, 1976; Crosilla et al., 2005b):

$$\frac{\hat{k}}{\hat{\sigma}_k} \leq t(n-r)_{1-\alpha} \tag{6.17}$$

---

[1] details how the least square fitting and statistical analysis on the significance of estimated unknowns was performed are in Appendix D from page 193 on
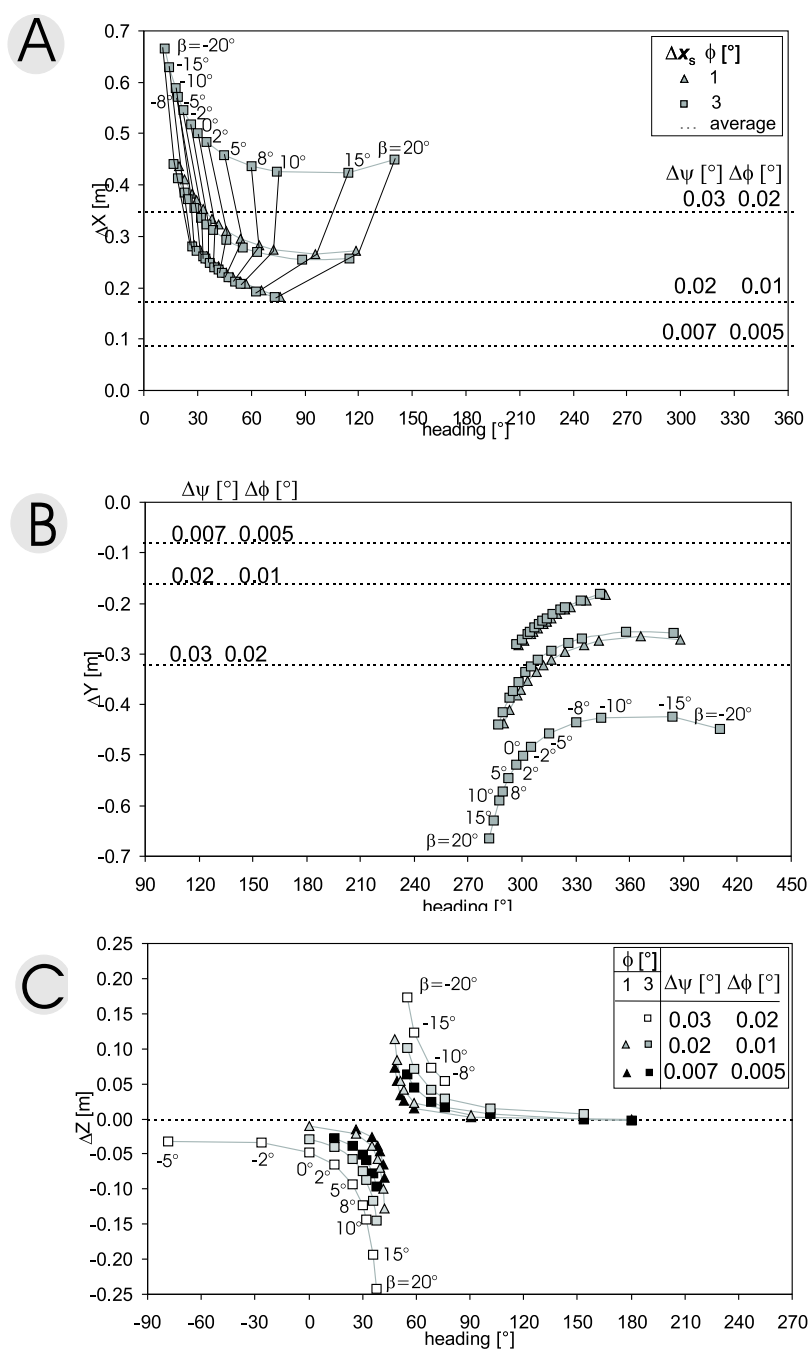
Figure 6.5: The heading values for maxima at different scan angles: 20°, 15°, 10°, 8°, 5°, 2°, 0°, -2°, -5°, -8°, -10°, -15°, -20° and $\Delta\mathbf{R}_{\text{INS}}$ values: $\Delta\phi = \Delta\theta = 0.005°$, $\Delta\psi = 0.007°$, $\Delta\phi = \Delta\theta = 0.01°$, $\Delta\psi = 0.02°$, $\Delta\phi = \Delta\theta = 0.02°$, $\Delta\psi = 0.03°$ and average magnitude of roll and pitch angles of 1° and 3°. Error components: A) ΔX, B) ΔY, C) ΔZ.

Slika 6.5: Koti pozibavanja za maksimume ob različnih kotih skeniranja: 20°, 15°, 10°, 8°, 5°, 2°, 0°, -2°, -5°, -8°, -10°, -15°, -20°; in različnih kombinacijah $\Delta\mathbf{R}_{\text{INS}}$ kotov: $\Delta\phi = \Delta\theta = 0.005°$, $\Delta\psi = 0.007°$, $\Delta\phi = \Delta\theta = 0.01°$, $\Delta\psi = 0.02°$, $\Delta\phi = \Delta\theta = 0.02°$, $\Delta\psi = 0.03°$; ter srednji velikosti kotov zibanja in guganja 1° in 3°.
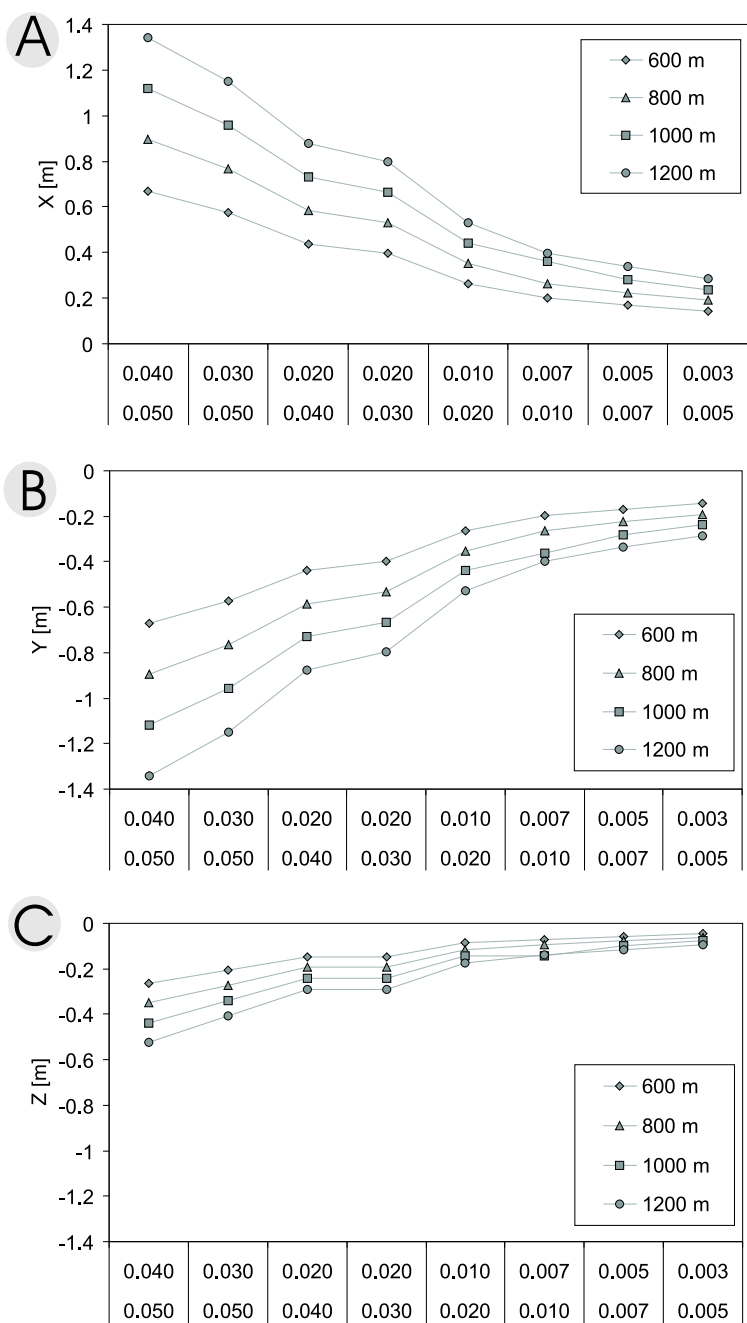
Figure 6.6: The maxima of simplified basic systematic error model for scan angle of 20°, for different $\Delta\mathbf{R}_{\mathrm{INS}}$ combinations and for different flying heights. The average magnitude or roll and pitch angles 3° is used. Error components: A) ΔX, B) ΔY, C) ΔZ.

Slika 6.6: Velikosti maksimumov v poenostavljenem Schenkovem modelu napak za kot skeniranja 20°, različne kombinacije $\Delta\mathbf{R}_{\mathrm{INS}}$ kotov in različne višine leta. Povprečna velikost kotov zibanja in guganja je 3°.
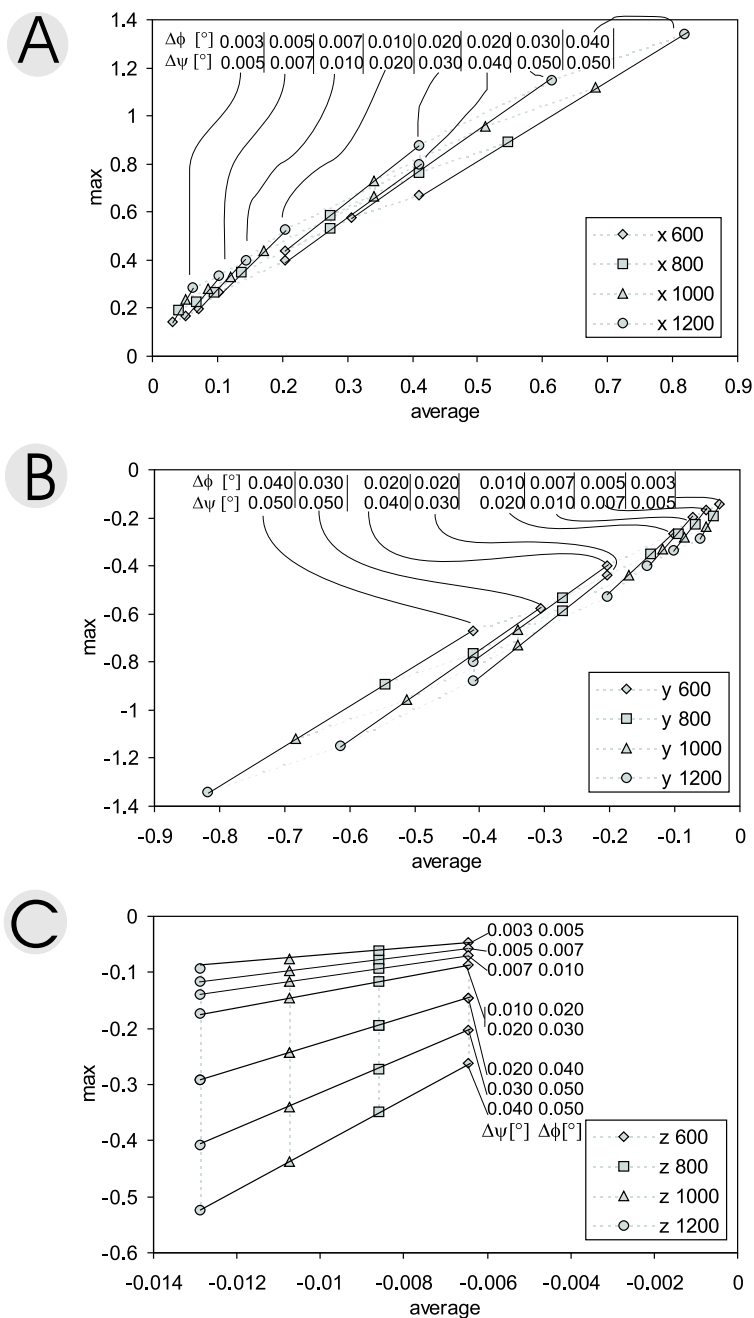
Figure 6.7: The correlation between maxima for scan angle of 20° and average value independent from scan angle, for different $\Delta \mathbf{R}_{INS}$ and flying heights combinations. The average magnitude or roll and pitch angles 3° is used. Error components: A) ΔX, B) ΔY, C) ΔZ.

Slika 6.7: Korelacija med vrednostmi maksimumov za kot skeniranja 20° in povprečno vrednostjo neodvisno od kota skeniramnja pri različnih kombinacijah $\Delta \mathbf{R}_{INS}$ kotov in različno višino leta. Povprečna velikost kotov ϕ in θ je 3°.

After neglecting the parameter satisfying the null hypothesis, the least squares fitting was performed once again with reduced number of parameters. The rejection of parameter can be accepted when a-posteriori variance factors of both least square fittings are statistically the same. This is performed applying a F-test with significance level $\alpha = 95\%$ and converges to the satisfaction of the null hypothesis (Albertella et al., 1997; Crosilla et al., 2005b):

$$\frac{(n-r)\hat{\sigma}^2_{0(r-1)} - (n-r-1)\hat{\sigma}^2_{0(r)}}{r \cdot \hat{\sigma}^2_{0(r)}} \leq F(1, n-r-1)_{1-\alpha} \tag{6.18}$$

Figure 6.4 shows, that if absolute values of average planimeric components are used, the ΔX and ΔY average components are the same, because the roll and pitch errors are the same. The same can be said for maxima. Therefore final derivation of maximal error can be written only for planimetric $|\Delta X_{s\_max}| = |\Delta Y_{s\_max}|$ and height component ΔZ_{s_max}. With reduction of factors by equation 6.17 and 6.18 the final version of simplified maximum value of basic systematic errors can be written as:

$$\Delta \mathbf{x}_{s\_max} = \begin{bmatrix} |\Delta X_{s\_max}| = |\Delta Y_{s\_max}| \\ \\ \Delta Z_{s\_max} \end{bmatrix} = \tag{6.19}$$

$$= \begin{bmatrix} \Delta X_{s\_ave} \cdot 1.44 + \Delta\psi \cdot 5.60 + \Delta\phi \cdot (-7.59) + h \cdot 1.79 \cdot 10^{-4} \\ \Delta\phi \cdot (-8.74) + h \cdot 2.11 \cdot 10^{-4} + 0.15 \end{bmatrix}$$

The average error components and flying height are written in meters, the errors of heading and pitch ($\Delta\phi = \Delta\theta$) are written in degrees.

6.6 Adding errors of synchronization, sensor positioning and vegetation height

To get overall a-priori error estimation the basic systematic errors (average and maximum value) should be expanded with the errors of synchronization, sensor positioning and vegetation height. After the process of post-processing the synchronization error vector $\Delta\mathbf{p}_s$ of 5×10^{-5} m can be expected (see Section 5.5.1 on page 69). As its size is very small it can be neglected.

In optimal conditions for GPS measurements sensor positioning error has a value of $|\Delta\mathbf{x}_0| = 0.05 - 0.10$ m (Section 5.5.3 on page 72) and therefore cannot be neglected. Looking at the planimetric error components, the additional $\Delta\mathbf{x}_0$ does not bring a big change. On the contrary, $\Delta\mathbf{x}_0$ has a major influence on the height error component, with its average value of 0 m gained by basic systematic errors.

The vegetation height related error (Section 5.6.2), which acts only on the height error component should not be overlooked. This error (equation 5.44) is vegetation height dependent. In the process of laser scanning planning it is therefore important to define the major vegetation types in the area of interest, and for each vegetation type to calculate the vegetation related error. For example, if not considering that the area of interest is covered with conifer forest an

additional height error of at least 0.2 m for laser scanning points representing the ground can be expected when flying at 1000 m compared to the area covered by asphalt.

When neglecting the $\Delta \mathbf{p}_s$ and $\Delta \mathbf{s}_0$ the final version of our simplified laser scanning error model presenting **whole a-priori expected errors** can be written for average and maximal expected basic systematic errors:

$$\Delta \mathbf{x}_{ave} = \Delta \mathbf{x}_{s\_ave} + \Delta \mathbf{x}_0 + \mathbf{c}(H) = \tag{6.20}$$

$$= \begin{bmatrix} \frac{h \cdot \sin \beta_0}{\beta_0} (-\Delta \theta \sin \theta k_{13} + \Delta \theta \cos \theta \sin \phi k_{23} + \Delta \theta \cos \theta \cos \phi k_{33}) \\ \frac{h \cdot \sin \beta_0}{\beta_0} (\Delta \phi \sin \theta k_{13} - \Delta \phi \cos \theta \sin \phi k_{23} - \Delta \phi \cos \theta \cos \phi k_{33}) \\ \frac{h \cdot \sin \beta_0}{\beta_0} (-\sin \theta k_{13} + \cos \theta \sin \phi k_{23} + \cos \theta \cos \phi k_{33} + \sin \theta R_m(1,3) - \cos \theta \sin \phi R_m(2,3) - \cos \theta \cos \phi R_m(3,3)) \end{bmatrix}$$

$$+ \Delta \mathbf{x}_0 + \mathbf{c}(H)$$

$$\Delta \mathbf{x}_{max} = \Delta \mathbf{x}_{s\_max} + \Delta \mathbf{x}_0 + \mathbf{c}(H) = \tag{6.21}$$

$$= \begin{bmatrix} \Delta X_{s\_ave} \cdot 1.44 + \Delta \psi \cdot 5.60 + \Delta \phi \cdot (-7.59) + h \cdot 1.79 \cdot 10^{-4} \\ \Delta \phi \cdot (-8.74) + h \cdot 2.11 \cdot 10^{-4} + 0.15 \end{bmatrix} + \Delta \mathbf{x}_0 + \mathbf{c}(H)$$

6.7 Discussion

There are many cases when customer needs to order laser scanning data, but does not posses any knowledge on error contributors sizes (described in Chapter 5). To decide which laser scanning data are useful, he has to specify the purpose of laser scanning acquisition, as the purpose defines the level of detail presented in laser scanning point cloud and the overall accuracy of laser scanning points.

Different purposes (e.g. detailed 3D models of urban areas, flood risk maps, vegetation cover analysis) dictate the desired number of points per unit area, as this value defines the level of detail which can be extracted from laser scanning data (see Section 4.3 on page 31).

Overall allowed laser scanning accuracy also defines the level of detail, which can be extracted from laser scanning data (see Chapter 7 on page 99). The simplified error model defined in this study gives us a tool to define in advance the average and maximal expected error sizes. It can also be used as a first approximation when a-posteriori error quality control field-work is planned, for example to decide on the GPS measurement protocol (real time kinematic – RTK or differential GPS method – DGPS).

Through the description of different laser scanning error groups (basic systematic errors, flight mission related and target's characteristics related errors) and evaluation of its sizes derived from literature, the Schenk's error model describing basic systematic errors was simplified and amended with flight mission and target characteristics related errors. Simplification of error model is based on the simulation of different error sources in laser scanning point cloud. Based on the comparison of influences of different error source values on total error size, the following error sources were neglected: the rotation from global to local orthogonal coordinate system $\mathbf{R}_W$,

the rotation from reference system defined by local vertical to local orthogonal reference system $\mathbf{R}_{\mathrm{GEO}}$, the offset vector $\mathbf{s}_0$ between GPS/INS and laser scanning system, the error of offset vector $\Delta\mathbf{s}_0$ and the error of synchronization between GPS/INS/lidar system $\Delta\mathbf{p}_s$. The simplified error model treats mounting bias $\mathbf{R}_m$, its error $\Delta\mathbf{R}_m$ and the error of scan angle measurements $\Delta\mathbf{R}_s$ as constant. The most important appendix to Schenk's error model is vegetation height related error $\mathbf{c}(H)$ from the group of target characteristic errors, which has the greatest influence on total error size of laser scanning points in areas covered with vegetation.

Simplified error model gives us an average and maximal error size of laser scanning points for the whole laser scanning point cloud independent from scan and heading angle. On the contrary the maximum error size in original Schenk's error model is heading angle dependent. To calculate the average and maximal error size with this simplification, we have to decide only on the permitted size of roll, pitch and heading error components $\Delta\mathbf{R}_{\mathrm{INS}}$, GPS sensor positioning errors $\Delta\mathbf{x}_0$, vegetation height related error $\mathbf{c}(H)$ and flying height h. Therefore our simplified error model gives us an easy tool to define possible error sizes in laser scanning point cloud a-priori to laser scanning mission, as the average and maximal possible error sizes can be calculated with using just two simple equations.

Now we will insert in the simplified error model the realistic values. In Table 6.2 few values of basic systematic (equations 6.13 and 6.19) and whole a-priori expected errors (equations 6.20 and 6.21) divided on planimetric and height components are presented.

Table 6.2: The absolute values of planimetric ($|\Delta X|$) and height components ($|\Delta Z|$) expressed in meters for basic ($_b$) and whole expected errors for different $\Delta\mathbf{R}_{\mathrm{INS}}$ values, average magnitude of roll and pitch ($\phi = \theta$) and flying height (h).
Tabela 6.2: Absolutne vrednosti po planimetriji ($|\Delta X|$) in višini ($|\Delta Z|$) zapisane v metrih za sistematične napake ($_b$) in skupno končno napako.

$\Delta\phi = \Delta\theta[°]$	$\Delta\psi[°]$	$\phi = \theta[°]$	h [m]	average				maximum			
				$|\Delta X|_b$	$|\Delta Z|_b$	$|\Delta X|$	$|\Delta Z|$	$|\Delta X|_b$	$|\Delta Z|_b$	$|\Delta X|$	$|\Delta Z|$
0.005	0.007	3	1000	0.08	0	0.15	0.05	0.28	0.10	0.35	0.15
0.005	0.007	3	800	0.06	0	0.13	0.05	0.23	0.07	0.30	0.14
0.005	0.007	3	600	0.05	0	0.12	0.05	0.17	0.06	0.21	0.13
0.02	0.04	3	1000	0.34	0	0.41	0.05	0.73	0.23	0.80	0.28
0.02	0.04	3	800	0.26	0	0.31	0.05	0.58	0.19	0.65	0.26

The difference between applying $\Delta\mathbf{R}_{\mathrm{INS}}$ values of $\Delta\phi = \Delta\theta = 0.005°$, $\Delta\psi = 0.007°$ and $\Delta\phi = \Delta\theta = 0.02°$, $\Delta\psi = 0.04°$ is evident. If we employ laser scanning mission with the $\Delta\mathbf{R}_{\mathrm{INS}}$ values of $\Delta\phi = \Delta\theta = 0.02°$, $\Delta\psi = 0.04°$, and do not correctly eliminate basic systematic errors, this data will not meet the accuracy specifications of laser scanning mentioned already by Baltsavias (1999a) and Maas (2003). But in the process of ordering, we do not know if the post-processing will be done correctly. Therefore it is better to define in advance smaller allowed errors of INS angles and smaller flying height if the accuracy requirements are strict.

GPS sensor positioning error $\Delta\mathbf{x}_0$ and vegetation height related error $\mathbf{c}(H)$ have a greater impact on height error component (discussed in Section 6.6). If the laser scanning mission is not carried out in ideal conditions regarding GPS measurements, an overall 0.1 m error vector can be gained

through GPS sensor positioning error. Therefore the customer should give detailed boundary values for GPS measurements through definition of allowed PDOP values and maximal distance to reference GPS station during the flight (it should not exceed 10 km). It is recommended that PDOP does not exceed 2.5 (Katzenbeisser, 2003), with at least 6 well-positioned satellites used (Turton, 2006). After the acquisition the customer should also have an insight in detailed GPS measurement protocol, to see if these conditions were fulfilled.

The vegetation-height-related error should be considered carefully as it adds a large share to the total vertical accuracy of the aerial laser scanning. It is recommended that a-priori to the aerial laser scanning ordering a segmentation of the area by vegetation types is conducted, to define the regions where special care should be taken regarding the vertical accuracy. This includes a definition of the penetration rate and a definition of the optimal laser scanning point density for a certain product and vegetation type (e.g., undercanopy extraction of the DTM, roads, buildings). The accuracy and the precision of the data acquired in forested areas increases when laser scanning is conducted in the leaf-off season, when the point density is increased and when the flying height is reduced. Unfortunately, this does not help much when working in a dense conifer forest. Secondary vertical errors should also be considered and evaluated carefully when aerial laser scanning is conducted in mountainous terrain through the a-priori flight direction planning, depending on the type and direction of the relief.

In addition to data describing GPS positioning accuracy and different characteristics of laser scanning system applied, the customer should not be satisfied with laser scanning data without the strip overlap. Suppliers of laser scanning data often tend to deliver data without the strip overlap, as this minimizes the data storage size. But the strip overlap is an ideal place where the customer should make a first a-posteriori control, to check if the laser scanning data fulfills the accuracy specifications given when ordering laser scanning data.

In our derivation we did not deal with transformations between different global and national coordinate systems, but in practice the definition of coordinate system in which laser scanning data are presented (WGS84, ETRS89...) is very important. Not knowing which transformational parameters were used when transforming data from one coordinate system to another (e.g. from the global to the national one), it can cause different shifts and drifts of laser scanning point cloud expressed in several tens of meters.

7   THE DENSITY OF AERIAL LASER SCANNING POINTS PER UNIT AREA

7.1   Introduction

The positional accuracy of a point on a map depends in part on the accuracy of survey and in part on the accuracy the points have been located on printed map (Maling, 1989).

The total positional accuracy of a map can be written with positional root mean square error of a map **s** (Maling, 1989):

$$\mathbf{s} = \sqrt{s_1^2 + s_2^2} \tag{7.1}$$

where s_1 is the accuracy of a survey, s_2 is the **geometrical accuracy** of a map. The geometrical accuracy of a map can be named also the **precision** of the map. The accuracy of an aerial laser scanning survey can be defined a-priori with simplified error model, described in Chapter 6. The smaller is the scale of the map, the smaller is the importance of survey errors. With the scale 1 : 25 000 (1 : 50 000 and on) the influence of s_1 disappears, and the positional accuracy depends only on geometrical accuracy of a map (Maling, 1989).

Which laser scanning data sample enables a production of a map with a certain geometrical accuracy depends also on the density of laser scanning points per unit area. The minimum point density per unit area defines the ability to reconstruct the shape of the object, the accuracy of its shape delineation and the ability to distinguish two small objects from each other. These parameters define also the completeness of the end product, which is also one of the most important data quality elements described on page 49. The minimum point density influences also the thematic accuracy, as the shape of the object tells a lot about its class (e.g. the separation between houses and pavements). Unlike the completeness quality element, the thematic accuracy element cannot be defined just out of minimum point density. To better define it, also intensity information and classification information should be used together with the minimum point density.

Therefore it is very important to know which point density has to be ordered a-priori to the aerial laser scanning mission, to enable the best completeness of the end product and its positional accuracy. As higher point density means longer acquisition of data which is more expensive, the minimum satisfactory point density for certain geodetic product intended for local spatial planning should be defined.

The theoretical minimum satisfactory points per unit area has to be increased in practice, as the data one wishes to extract are in a lot of cases obstructed by different types of vegetation. The theoretical minimum satisfactory point density will be defined through the geometrical accuracy of a map. Through testing different vegetation classes the penetration rate will be defined in test samples. The theoretical minimum satisfactory point density and a penetration rate will give usable point density for practical data extraction.

7.2   Geometric accuracy of geodetic data used in local spatial planning

The following geodetic data used in local spatial planning, which can be liable to acquisition methodology change from photogrammetry to aerial laser scanning (described in chapter 8 on page 118) will be discussed here:

- land survey plans or national topographic maps in scale $1:5000$

- land survey plans or topographic maps in scale $1:1000$

- Real estate register

- some layers of the Cadastre of public infrastructure: the layers which are not hidden under-ground (traffic infrastructure, river and creek infrastructure, other infrastructure for management and protection of natural wealth).

The common entities of the majority of these databases are line objects and surface objects. In the group of line objects the same entity described on national topographic maps and in the Cadastre of public infrastructure are roads and railways. Common surface objects in all four databases are buildings, described also in the Cadastre of public infrastructure as some objects of river and creek infrastructure (e.g. buildings needed for water monitoring). As surface objects are composed out of line objects (e.g. building in 2D is described with four lines) the minimal number of points per unit area needed for good definition of different lines and surface elements can be developed solely from line objects.

We will treat all four databases as cartographic representations. While the first two already are cartographic representations, the last two are not. The last two are compositions of location data (a location where certain object is and its dimension) and attribute data (attribute tables connected to location). If all these databases are treated as cartographic representations, the minimal length and width of line object represented on it and the accuracy of its shape delineation can be defined through **geometrical accuracy**, which is restricted by the **drawing accuracy** and the **scale** of the map. The geometrical accuracy limits also the **level of detail** presented on a map. If level of detail is used for image processing, we would talk about a **resolution** of an image.

The drawing accuracy was defined in history of cartography as minimal line thickness which can be drawn by a pen to a sheet of paper. For Slovenian topographic map representations it was

defined as 0.13 mm in "Pravilnik o znakih za temeljne topografske načrte" (1982). For the scale of 1 : 1000 it defines the minimal object 0.13 m in physical space. In the scale of 1 : 5000 this minimal line thickness represents 0.65 m in nature. For different cartographic scales in general the drawing accuracy is better than 0.25 mm (Maling, 1989).

"Pravilnik o znakih za temeljne topografske načrte" (1982) also defines minimal surface square represented on a map, it is limited with 0.5 mm long line.

Location data of Real estate register was taken from the Building cadastre, where the acquisition of spatial data was made on the basis of the CAS. The CAS enables an acquisition of details mainly for scale 1 : 5000 (e.g. ortophotographies produced out of CAS are in scale of 1 : 5000, the national topographic maps are in scale 1 : 5000). With photogrammetrical stereorestitution 3D data for approximately 1 400 000 buildings were acquired for the Building cadastre on the basis of CAS (Triglav et al., 2003). The Building cadastre location data was acquired with the same CAS as national topographic maps of 1 : 5000 and also the same methodology, therefore we can say their positional accuracy is the same as those of the national topographic map 1 : 5000. The accuracy of the photogrammetric stereo-restitution for Building cadastre was 0.5 m.

The geometrical accuracy of the Cadastre of public infrastructure is divided in 5 classes (Pravilnik ...dejanska raba prostora..., 2004):

1. the data on accuracy does not exist
2. accuracy better than 0.1 m
3. 0.1–1 m
4. 1–5 m
5. accuracy worse than 5 m

The majority of data is stored in the accuracy class better than 1 m. If we presented this data in scale of 1 : 5000, this accuracy class would present 0.2 mm in the scale of the map. This fits well in drawing accuracy defined by Maling (1989).

Table 7.1: Geometrical accuracy defined with drawing accuracy and minimal dimensions of square object (e.g. building) still represented on maps of different scales. *geometrical accuracy defined by drawing accuracy written in "Pravilnik o znakih za temeljne topografske načrte" (1982).
Tabela 7.1: Geometrična ločljivost in minimalna dimenzija kvadratnega objekta (npr. stavbe) predstavljena v različnem merilu. *Geometrična ločljivost definirana z grafično natančnostjo opredeljeno v "Pravilnik o znakih za temeljne topografske načrte" (1982).

Scale 1:	geometrical accuracy*	common geometrical accuracy	minimal dimension
	0.13 mm	0.2 mm	0.5 mm
5000	0.65 m	1.0 m	2.5 m
1000	0.13 m	0.2 m	0.5 m

To define a common drawing accuracy for national topographic maps of 1 : 5000 and 1 : 1000, the Real estate register and the Cadastre of public infrastructure the lowest drawing accuracy of all these databases should be used. This is the accuracy of the Cadastre of public infrastructure,

which is 0.2 mm. This common drawing accuracy still fits well with acceptable drawing accuracy defined by Maling (0.25 mm).

From upper deduction and prescribed scales of land survey plans (national topographic maps) for local spatial planning[1], we can say that $1:5000$ and $1:1000$ scales are the scales of our interest. Therefore the geometrical accuracy and minimal dimensions corresponding to these scales are written in Table 7.1.

7.3 Theoretical minimal point density defined by Nyquist frequency

In previous section we defined a common drawing accuracy of 0.2 mm for all data of our interest, through translation of certain database positional accuracy to common drawing accuracy for maps in different scales. Now we will define the minimal density of laser scanning points per unit area which satisfies this common drawing accuracy.
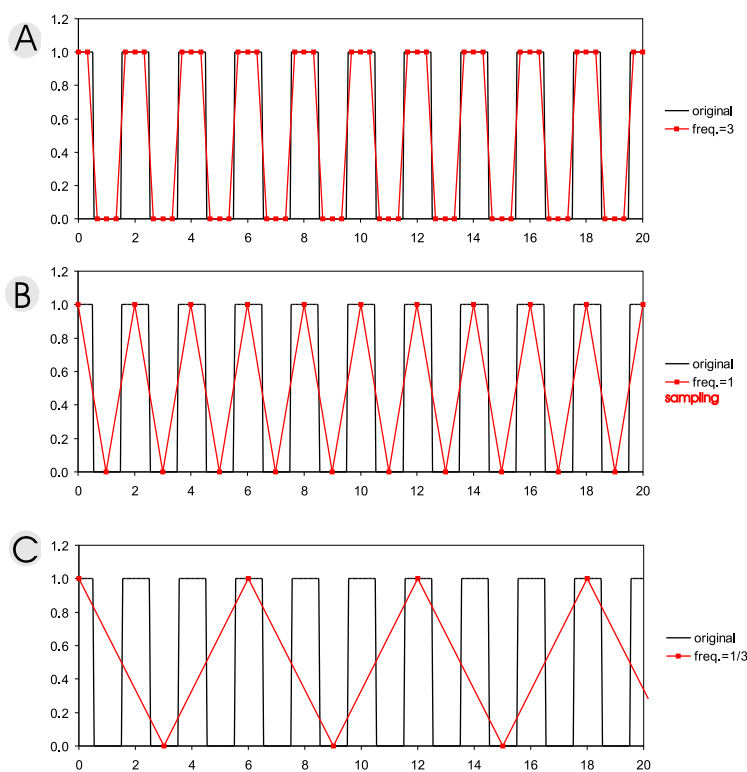
Figure 7.1: Black are the physical representations with frequency 2 units, red are sampling frequencies: A) 3-times bigger than Nyquist frequency B) Nyquist frequency, C) 3-times smaller than Nyquist frequency.

Slika 7.1: Črne barve je pojav v naravi s frekvenco pojavljanja 2 enoti. Rdeča je frekvenca vzorčenja. Frekvence vzorčenja: A) 3-krat večja frekvenca kot Nyquistova frekvenca, B) Nyqistova frekvenca, C) 3-krat manjša kot Nyquistova frekvenca.

---

[1]see section 2.3.2 on page 14

The fundamental theorem which describes the frequency of signals which well enough describe the physical representation of some frequency is the **sampling theorem**, called also **Nyquist-Shannon theorem**[2] (Göpfert, 1987; Kraus, 2004). Originally, the theorem describes sampling of time-depended signals, therefore the term frequency is applied. In our case we study spatial phenomena and a more appropriate term would be density of objects. Nevertheless, we will keep using the original term "frequency".

When the frequency of objects equally separated by each other in physical space is known, we can compute by sampling theorem a minimal frequency of sampling:

$$f_s = f_r/2 \tag{7.2}$$

where f_r is real frequency of objects in physical space and f_s is sampling frequency, which still enables the correct representation of physical space; it is called the Nyquist frequency.

On Figure 7.1 the objects representing physical space are colored black. For easier understanding we can say that the signal represents houses which are equally separated between each other, and width of the houses equals the width of the separation between them. The frequency of objects (houses) is 2 units. At example Figure 7.1A the frequency of sampling — red — is three times bigger than the Nyquist frequency, therefore the houses are well represented in detail. The minimum frequency which still enables trustworthy representation of houses is the Nyquist frequency presented in Figure 7.1B. If the frequency of sampling is smaller than the Nayquist frequency (Figure 7.1C), part of the information is lost.
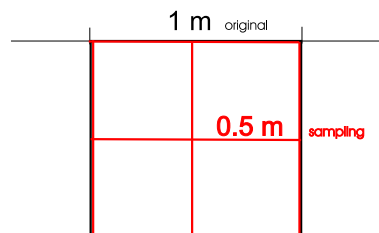
Figure 7.2: 2D principle of Nyquist frequency — how to define a resolution.
Slika 7.2: Odražanje Nyquistove frekvence v 2D – primer prostorska ločljivost senzorja.

How this principle of sampling manifests can be shown with raster photographs (ground truth pixel size — resolution). If the minimal object size in physical space which we would like to represent on an end-product is 1 m long by one side, than an aerophotograph with a ground truth pixel size of 0.5 m should be used (Figure 7.2). The minimal object size still represented on map is defined by geometrical accuracy which defines the minimal distance represented in physical space. Meaning that if we wish to satisfy drawing accuracy of 0.2 mm in the scale 1 : 5000, which gives graphical accuracy of 1 m, we have to use for production of such map an aerophotograph with a resolution of 0.5 m.

The same can be applied for laser scanning data. Therefore if we wish to satisfy graphical accuracy of 1 m, the Nyquist frequency tells us that we should use the separation distance

---

[2]in German is called **Abtasttheorem**

between two laser points of 0.5 m, which results in density of laser points of 4 pt/m^2 (Figure 7.3A). As it can be seen on this figure, the points in four corners have to be divided between four areas of 1 m^2, and the points on the middle of edges have to be divided between two areas of 1 m^2. On Figure 7.3B the drawing accuracy of 0.13 mm in scale of $1:5000$ gives us the required density of laser scanning points of 10 pt/m^2. This density already falls in the class of high resolution laser scanning.
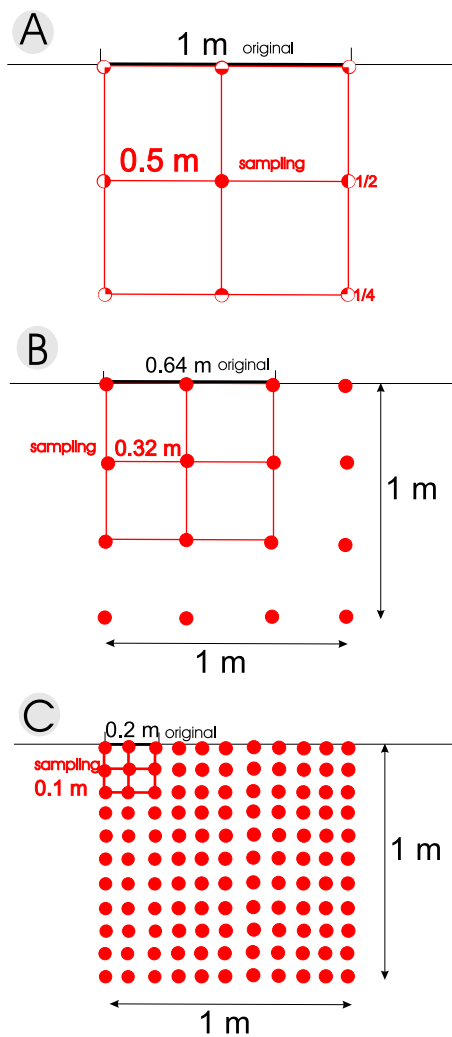
Figure 7.3: The density of laser scanning points defined by Nyquist frequency.
Slika 7.3: Gostota laserskih točk definirana z Nyqustovo frekvenco.

The simple equation of theoretical minimum laser point density ρ_t in pt/m^2 depending on requested geometrical accuracy of a map GA defined in [m] is:

$$\rho_t = \frac{1}{(GA/2)^2} \tag{7.3}$$

If we go even further with requested accuracy for accurate representation on the scale of $1:1000$ with drawing accuracy of 0.2 m (Figure 7.3C), we come to enormous density of laser points per unit area – 100 pt/m^2. For such a density an aerial laser scanning becomes uneconomic, therefore I would propose to replace it with terrestrial laser scanning.

On the other hand, we can also define the minimum number of points which enables representation of an object with minimal dimension on different scales. In the third column of Table 7.1 we find minimal dimensions of one square side, which should be represented in certain scale. In the scale 1 : 5000 the minimal represented dimension fits to 2.5 m in physical space, therefore a Nyquist separation between two laser points should be 1.25 m. This gives us laser point density of 0.64 pt/m².

7.4 Optimal point density in vegetation obstructed areas

In the case we wish to extract details of objects that are hidden under vegetation (e.g. houses under trees, roads in forest), the before mentioned theoretical minimal number of points per unit area should be larger. One possibility is to define point density under the vegetation when ordering laser scanning data, but still we would like to have an approximation of total laser scanning point density, to check in advance if the tender will be able to satisfy our needs.

We will name this total point density, which enables the desired point density under the vegetation, the **optimal point density**.

7.4.1 Test area – the penetration rate

The test was performed on aerial laser scanning point cloud of Nova Gorica acquired in early April of 2006 with the average total point density 15-20 pt/m², covering 200 ha of Nova Gorica. The acquisition was made in early leaf-on season[3].

The tested laser scanning point cloud was automatically classified with TerraScan to the next classes, distinguished by different heights:

- ground (last echo)

- low vegetation (before-last echo near the class ground)

- medium vegetation (vegetation lower than 2 m)

- high vegetation (vegetation between 2 m and 30 m)

- buildings

- errors

---

[3]for more details on test area and project in which it was acquired see Appendix E on page 201

We studied the penetration rate in four different vegetation areas (Figure 7.4):

1. scarce mediteranean forest

2. dense forest

3. mixed vegetation: grassland, orchard and forest

4. built-up area with houses
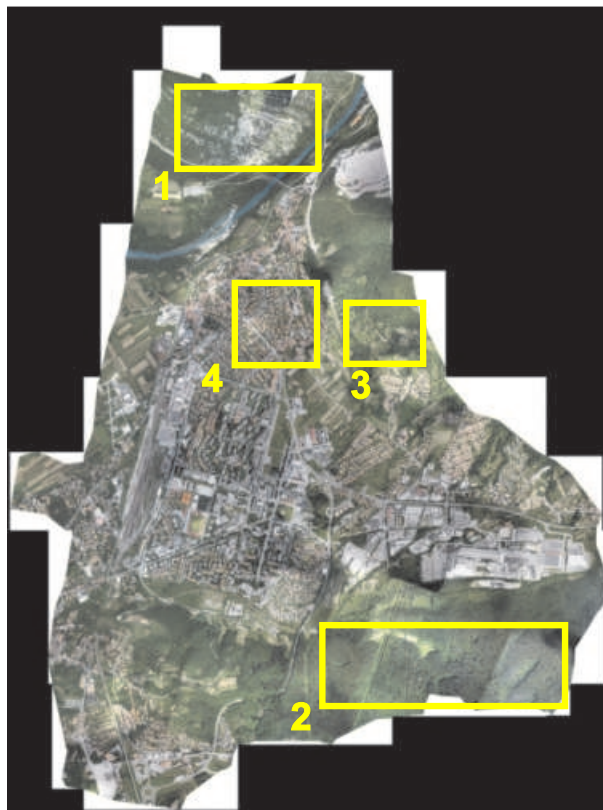
Figure 7.4: The locations of four different vegetation areas in the laser scanning data sample of Nova Gorica.
Slika 7.4: Lokacije štirih različnih vegetacijskih tipov v laserskem oblaku točk Nove Gorice.

For each vegetation area an average total point density and point densities in each classification class were measured at 10 locations. The size of each test area was 100 m × 100 m. Typical examples of four vegetation areas are presented in Figure 7.5. For the first two classes also cross profiles of laser point cloud are given, so one can easy see the difference between these two forest types.

In Table 7.2 we can see the density of points in each class. For the first three vegetation areas we merged classes of houses and errors in one class named *other*. This class gives us an approximation how many points cannot be used in other classes. In the forth vegetation area a class of *houses* becomes significant therefore it is excluded from the *other* class. In column *any class* all laser points are gathered. From this class it can be seen that the point density of Nova Gorica laser point cloud is not uniform. This has several reasons:

- we used point cloud with strip overlap, to enable checking of direct orientation accuracy, therefore on some areas double point density can be seen

- to enable better penetration rate in leaf-on season when laser scanning was conducted, on some areas more narrow strip widths were used – mainly the areas with heavy vegetation (first and second vegetation area)

- to reduce a secondary height error in steeper terrain also more narrow strips were used (first vegetation area)

To better see a share of points which fall in each class, a penetration rate was calculated from Table 7.2. A total point density represented in *any class* is treated as 100% of points. A Table 7.3 enables a comparison between different vegetation areas.

Table 7.2: Average point density with standard deviation for all four vegetation areas written in pt/m^2.

Tabela 7.2: Povprečna gostota točk s standardno deviacijo za vse štiri vegetacijske tipe, zapisano s številom točk na m^2.

	any class	ground	low veg.	medium veg.	high veg.	houses	other
1	21.66±8.40	1.91±0.89	2.67±1.82	5.56±2.85	8.15±3.16		*3.37±2.51*
2	20.02±5.59	0.79±0.22	0.38±0.14	1.75±0.42	14.56±4.37		*2.55±1.91*
3	15.82±3.54	2.96±0.93	2.14±0.84	2.60±0.86	4.99±2.35		*3.13±1.91*
4	16.44±2.39	2.99±0.41	2.44±0.55	3.10±0.69	3.04±0.78	2.60±0.72	*2.27±1.00*

Table 7.3: The penetration rate with standard deviation for all four vegetation areas expressed in %.

Tabela 7.3: Delež točk v posameznem razredu, za vse štiri vegetacijske tipe, s standardno deviacijo zapisano v %.

	ground	low veg.	medium veg.	high veg.	houses	other
1	**9±3**	**11±4**	25±4	40±12		*15±9*
2	**4±2**	**2±1**	9±4	73±9		*12±9*
3	**20±9**	**13±5**	16±4	31±14		*19±10*
4	**19±5**	**15±4**	19±3	18±3	16±4	*13±5*

Mainly our interest for topographic mapping is in the classes *ground* and *low vegetation*, as these two classes show points on the ground and near ground. It can be said that all details which should be presented on 2D topographic map can be extracted out of these two classes: roads, paths, railways, water borders, building foundations, contour lines, relief break lines. Therefore the first two classes are written in bold.

Vegetation areas 3 — mixed vegetation and 4 — built-up areas give us a penetration rate to summed *ground* and *low vegetation* classes of 33% and 34%, respectively. In vegetation area 1 — scarce mediteranian forest the penetration rate to summed class is 20%. The lowest penetration rate to summed class is 6% in vegetation area 2 – dense forests. These values enable us the calculation of total point density – the usable point density – which enables a production of topographic charts in scales of 1 : 5000 and 1 : 1000.
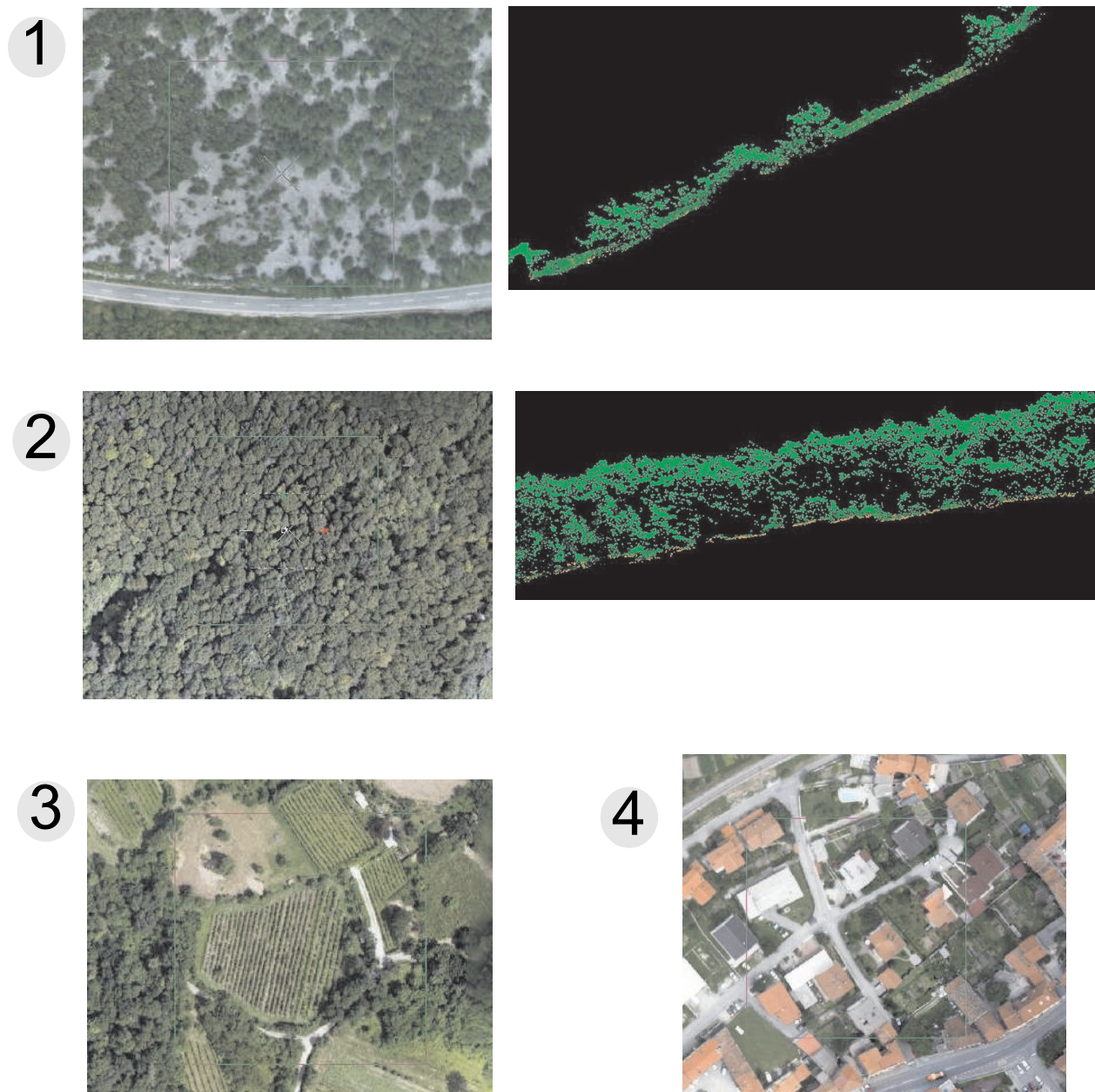
Figure 7.5: Typical examples of four different vegetation areas.
Slika 7.5: Tipični primeri štirih različnih vegetacijskih tipov.

The optimal point density $\rho_o[\mathrm{pt/m^2}]$ can be calculated out of theoretical minimum laser point density $\rho_t[\mathrm{pt/m^2}]$ and a penetration rate for summed *ground* and *low vegetation* classes:

$$\rho_o[\mathrm{pt/m^2}] = \frac{\rho_t[\mathrm{pt/m^2}] \cdot 100}{\text{penetration rate}} \tag{7.4}$$

The optimal point density for the four tested vegetation areas are written in Table 7.4 where in the second column summed penetration rates for *ground* and *low vegetation* classes are written. The optimal point densities for scale 1 : 5000 are calculated for drawing accuracy of 0.2 mm, which gives the minimum point density of 4 pt/m^2.

The optimal point density for scale $1:1000$ would grow from 100 pt/m^2 up to enormous numbers, which could be acquired just with terrestrial laser scanning. E.g. for 3rd and 4th class the usable point density would be 300 pt/m^2.

Table 7.4: Optimal point density for different vegetation areas. The optimal point densities are calculated for drawing accuracy of 0.2 mm and scale $1:5000$.

Tabela 7.4: Uporabna skupna gostota točk za štiri testirane vegetacijske razrede. Izračunane so za grafično natančnost 0.2 mm in merilo $1:5000$.

	penetration rate	$1:5000$
1	20%	20 pt/m^2
2	6%	67 pt/m^2
3	33%	12 pt/m^2
4	34%	12 pt/m^2

From the numbers presented in Table 7.4 we can conclude that the laser scanning point cloud of Nova Gorica with mean density of 15-20 pt/m^2 can be used for acquisition of topographic data for scale $1:5000$ for all other vegetational areas except dense vegetation. In the areas covered with dense vegetation the mean point density would not satisfy the requirement of optimal point density.

7.5 Discussion

First we defined the minimal point density for ideal laser scanning point cloud (all points on the ground) with Nyquist frequency. With the study of penetration rate in laser scanning point cloud of Nova Gorica, which was conducted in leaf-on season, we calculated optimal point density which enables us acquisition of data under canopies. We proved that our laser scanning point cloud of Nova Gorica enables an acquisition of data for scale $1:5000$. The only exception which could not be covered with this scale are areas under dense vegetation.

If we know the penetration rate for a certain vegetation class, which was not covered in our test, we can now calculate optimal point density, which enables the acquisition of data for maps or other geodetic data in certain scale. The penetration rate for certain vegetation area changes with leaf-on and leaf-off season. Therefore a proposal for further studies would be to map different vegetation classes from the Database on land use and define their penetration rate in leaf-on and leaf-off season. This will enable a potential aerial laser scanning orderer to check, which vegetation classes are represented in his area of interest and decide which optimal point density he has to order.

8 PROPOSED ACQUISITION METHODOLOGY OPTIMIZATION OF GEODETIC DATA USED IN LOCAL SPATIAL PLANNING BY APPLYING AERIAL LASER SCANNING

8.1 Introduction

In the previous Chapters (6 and 7) defined a-priori aerial laser scanning error assessment and required point density set up the minimal terms defining the aerial laser scanning point cloud needed for geodetic data production (Figure 8.1). Knowing these terms, a proposal for data acquisition methodology change or optimization can be given. In geodetic data production, used in local spatial planning, the current data acquisition methodology is the photogrammetric stereo-restitution. Here we will discuss possible optimization of current data acquisition methodology by applying aerial laser scanning.
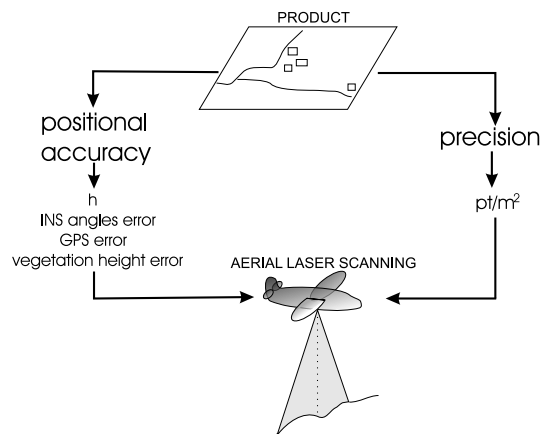
Figure 8.1: The end-product defines what needs to be ordered.
Slika 8.1: Končni produkt določa kakšne podatke laserskega skeniranja moramo naročiti.

First we will describe the proposed data processing methodology, if aerial laser scanning is applied. Then we will discuss which geodetic data used in local spatial planning can be prone to data acquisition methodology change (Chapter 3). At the end a proposal is given, how to perform the data acquisition methodology change.

8.2 Aerial laser scanning data processing methodology

8.2.1 Ordering aerial laser scanning data

When ordering laser scanning data one should be aware of the type of the terrain to be acquired (e.g. flat, hilly, vegetation obstructed) and above all of the purpose of data acquisition (e.g. DTM generation, detailed 3D data acquisition for land survey plan or topographic map production, etc). As the terrain type and the purpose of data acquisition influence on the requested accuracy and the needed number of points per unit area (see Chapters 6 and 7).

In general the customer cannot order **true raw data** from the laser scanning system, as this means we would have to get also the GPS and INS data from the platform and make the a-posteriori calibration of the system on our own. Usually the supplier does not deliver these calibration data acquired in-the-flight. This is connected to the laser scanning unit uniform software and its licence.

When **raw data** are ordered, the delivered data present the coordinates of the measured points written in the global reference frame (e.g. WGS84). They should not be mistaken for true raw data, where range and scan angle data for each point are delivered.

8.2.2 From raw to georeferenced data

From raw to calibrated data

True raw data are written in a standard binary format (e.g. LAS), which is processed by the software included with the laser scanning unit. In true raw format the range length (d) and the instantaneous scan angle β_i are written in polar coordinate system for every echo of the returned pulse (Figure 8.2). For every echo also the information on intensity of the reflectance is given. In separate files we have data of GPS – the data describing the trajectory of the laser scanning platform, and INS measurements (inertial navigational system) – the data on velocity and acceleration. Ordinary GPS and INS measurements are not directly connected to the flight but are processed together afterwards (Burman, 2000).

All these data have to be synchronized in time and the rotations and translations between all the three systems must be known. This is called **calibration**. It is used to connect the trajectory of the laser scanning platform with the measured laser scanning data (Kraus (edt.), 2005). Best results are achieved when calibration is performed in-the-flight, covering the measured area.

The calibrations intention is to recover systematic errors, therefore just random errors should be left after it. Calibration proceeds in several steps; the first is laboratory individual system (GPS, INS, laser unit) calibration, second the whole system calibration on the platform and the third is in situ calibration in the time of laser scanning acquisition of data – in-the-flight calibration (Schenk, 2001; Skaloud and Lichti, 2006).
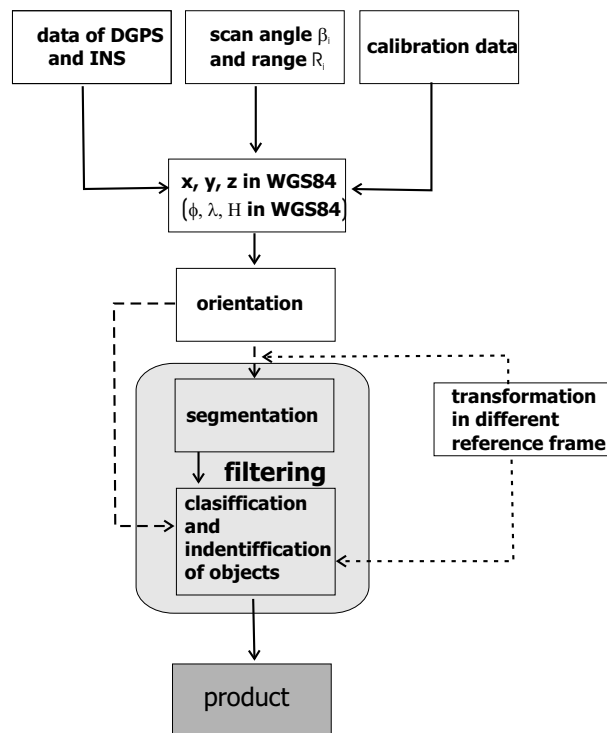
Figure 8.2: From true raw data to final product with segment based filtering.
Slika 8.2: Od surovih podatkov do končnega izdelka s filtriranjem na osnovi segmentov.

The orientation of data

This includes the orientation of data in the global coordinate system. It is performed with in-the-flight calibration.

The **relative orientation** ties the lasers scanning strips together in one laser scanning point cloud. It is performed by laser scanning strip adjustment with applying tie points/patches from two adjoining strips (Kager, 2005). Tie patches can be determined by hand (Kraus (edt.), 2005) or by the automatic segmentation of the strip overlap (Pfeifer et al., 2005) or by automatic edge determination of tie patches (Jutzi et al., 2005).

The **absolute orientation** ties the laser scanning point cloud to the ground and its coordinate system (global coordinate system). For high accuracy aerial laser scanning (2 cm planimetric accuracy) at least six known ground points in ground control framework have to be used: three fixed in order to control the scale, orientation and position and three to ensure that the requirements of the network accuracy can be meet (Schnurr et al., 2004).

In laser scanning **tie or control patches** are used instead of points, as we cannot find the representation of exact measured point on two adjoining strips and also on the ground. Instead planar surfaces, e.g. roofs (Figure 8.3), which can be seen in the laser cloud and defined out of ground measurements are used. The control patch is defined with at least 4 points measured on it planar surface of the patch. The equivalent to one ground control point used in aerial

photographing are three control patches with differently oriented planar surfaces (Kager, 2005). For the purpose of control, also edges seen in laser scanning point cloud and measured on the ground can be used. Edges can be found on boundaries between two or three different reflection types (eg. grass and concrete) or on the edges between two different slopes (eg. roofs)(Wotruba et al., 2005, Jutzi et al., 2005). The third possibility for ground control are artificial high reflecting targets. They should differ in size, in dependance to laser scanning point density (Schnurr et al., 2004).
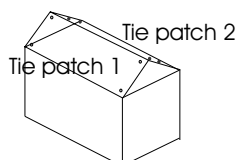
Figure 8.3: Two tie patches.
Slika 8.3: Vezni ploskvi.

Transformation in national reference frame

After postprocessing the ground coordinates of laser scanning points in global reference frame (e.g. WGS84) are derived. To transform them in national reference frame the transformation parameters from WGS84 to national reference frame have to be known.

If no transformation parameters are known, they are calculated with the help of identical points with known coordinates in both reference frames.

8.2.3   Filtering the data

With the so-called **filtering methods**, a classification of the points into terrain and object points is performed (Tóvári and Pfeifer, 2005). The filtering in laser scanning terminology has to be distinguished from the basic meaning of the term filtering – the data thinning.

Filtering can be performed on raw data or on interpolated regular grid. If interpolated regular grid is used, it has a disadvantage that it is influenced by interpolation errors. On the other hand, interpolated regular grid has an advantage, that there can be applied already existing filtering methods which are used for image processing (Wehr and Lohn, 1999; Vosselman04b).

Filtering algorithms can be divided into (Tóvári and Pfeifer, 2005):

- **point based filtering**: points or raster units are the smallest units of the process. All of points are separately investigated and labelled as terrain or object points
- **segment based filtering**: first the segmentation of the point cloud on the basis of some homogeneity criterion is made, afterwards these segments are classified as terrain or object segments
- **combination of point and segment based filtering**

The results of filtering are mainly disjunction of digital terrain models and buildings.

Point based filtering

The basic idea of point based filtering is that large height difference between two nearby points is unlikely to be caused by a steep slope in the terrain. More likely the higher point is not a ground point.

Mathematical morphological approach is based on structure elements describing admissible height differences depending on horizontal distance between two points. The smaller is the distance between the ground point and the point in question, the less height difference can be expected between them (Vosselman and Mass, 2001; Tóvári and Pfeifer, 2005).

Progressive approach starts with identifying out some ground points in a first step, afterwards more and more points are classified as ground points in some geometrical shape around these first ground points. Mostly the procedure works with triangles (Tóvári and Pfeifer, 2005).

Surface model approach draws through the entire point cloud, or point set in question, a surface model. A first surface model is used to calculate residuals from this surface model to the points. If the measured points lie above it, they have less influence on a shape of the surface in the next iteration and vice-versa (Kraus and Pfeifer, 1998; Pfeifer et al., 2001; Tóvári and Pfeifer, 2005). At first the iterative robust interpolation was developed (Kraus and Pfeifer, 1998), to reduce computational time than a hierarchical approach was added (Pfeifer et al., 2001).

Segmentation based filtering

In the contrast to the point based filtering, the segment based filtering works with larger units called segments, compounded out of more points. The segmentation of data is an automated method in which the point cloud is divided in smaller parts – segments – which are geometrically or physically defined. It is often the first step in the extraction of information from the point cloud. This procedure is usually run before classification procedures.
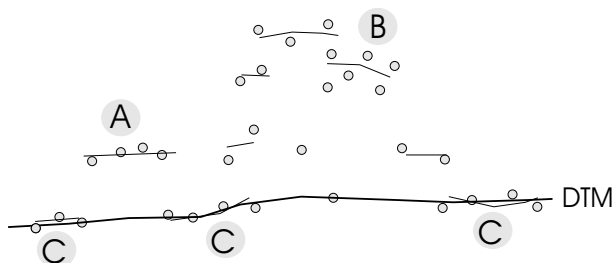
Figure 8.4: Laser points divided in segments, which present: A) a house, B) trees, C) ground.
Slika 8.4: Laserske točke razdeljene na segmente, ki predstavljajo: A) streho hiše, B) drevje, C) tla.

The segmentation of data is more important than point based filtering for close-range laser scanning applications, where modelling of surface is its main goal (Tóvári and Pfeifer, 2005).

Methods of segmentation can roughly be divided in two categories (Vosselman et al., 2004b):

- the ones which segment a point cloud based on criteria like proximity of points or similarity of locally estimated surface normals and

- the ones which directly estimate surface parameters by clustering and locating maxima in parameter space – this category is more robust, but can be used only for shapes like planes and cylinders which can be described with a few parameters

Algorithms for segmentation can be divided as (Vosselman et al., 2004b):

- **Extraction of smooth surface from a point cloud:** because in early research the laser data was transformed into regular grid resembling a raster image, these algorithms have their roots in image processing:

  - *scan line segmentation*: at first it splits each scan line into segments and than merges scan line segments of adjacent scan lines based on the same similarity criterion
  - *surface growing* into a point cloud is the equivalent of region growing in images. A method has to identify seed surfaces (e.g. a plane) to start surface growing.
  - *connecting components in 3D grid domain*: the procedures act in 3D space of uniform volume elements in which the laser data are transformed. Similar operations as in 2D image processing can be applied to 3D volume element space.

- **Iterative extraction of planar surfaces:** the surface growing algorithm is transformed into plane growing algorithm if the criterion to enforce local planarity is modified to global planarity. Planar surfaces are extracted by merging two smooth surfaces if their equations are similar.

- **Direct extraction of parameterized shapes** is used mainly to extract man-made objects which can be described by planes, cylinders and spheres, described with only few parameters. These methods use robust non-iterative methods that detect clusters in parameter space (e.g. 3D Hough transform).

The majority of segmentation algorithms described in literature (e.g. Akel et al., 2005; Tóvári and Pfeifer, 2005; Crosilla and Beinat, 2005; Filin and Pfeifer, 2006) are based on scan line or surface growing (Sithole and Vosselman, 2005).

A problem in segmentation algorithms is still forested sloped terrain, where easily described surfaces can not be found. Therefore with segmentation a vast number of small segments is found (Figure 8.4 area B), which do not describe any specific surface (Tóvári and Pfeifer, 2005).

8.2.4 Classification and final identification of objects

The basic purpose of classification is recognition of objects in the data sample or other remotely sensed scene. It can be divided in visual, which is performed by the operator, and digital clas-

sification which is performed automatically. Digital classification can be divided in supervised and unsupervised classification (Oštir, 2006).

Classification of objects in laser point cloud can be done on raw point cloud, segmented raw data or on interpolated laser point cloud presented as gridded digital elevation model. While classification just on raw laser point cloud is not a very effective method, mainly segmentation of data is used. In segmented data each segment is annotated to a specific object (street, roof, etc.). If gridded digital elevation model is used, classification can be made on vector data or on digital elevation model presented with a raster, where methods for other remotely sensed raster scene classification can be used.

Laser scanning data classification can be done on just range measurements filtered by height or with the help of intensity information. Mainly classification is based just on range measurements. The methods of classification on the basis of range measurements were described in Section 8.2.3 on page 115.

Intensity information can be presented in a form of a scene, usually transformed and interpolated into a regular grid on a digital elevation model — digital ortophotography of intensity (Pfeifer et al., 2001). Digital ortophotography of intensity presents a great help when performing visual classification and identification of objects. As laser pulse can produce few echoes (at least first and last echo), digital ortophotographies of different height levels of terrain can be produced and used for classification.

Intensity depends on range and scan angle, what is written in equation 4.14 and on other factors (atmospheric and systematic) influencing the received power from an echo P_r (see Section 4.4.3 on page 43). With radiometric calibration of intensity data, when the influence of scan angle and range are eliminated, the pseudo-reflectance maps can be made. They enable classification of bare ground, grass, sparse vegetation and dense vegetation (Coren and Sterzai, 2006). Just pseudo-reflectance maps are not enough for precise automated classification (Coren and Sterzai, 2006; Hasegawa, 2006; Bitenc, 2007) therefore other classification methods based on range measurements have to be used for good classification. When just raw intensity information of raw data is used, old asphalt and grass can be separated (Hasegawa, 2006).

8.3 Possible implementation of aerial laser scanning

The acquisition methodology for geodetic data production should not be hard to change. This is proven by the examples from abroad, where the acquisition methodology was changed in countrywide DTM production. In the past DTMs were produced mainly by photogrammetric stereo-restitution, nowadays the method of choice is becoming the aerial laser scanning. Already some countrywide DTMs exist (or DTMs covering a part of a country comparable in size to Slovenia) acquired by aerial laser scanning:

- the Netherlands: DTM with grid size 4 m × 4 m (Artuso et al., 2003; Ahokas et al., 2005a)

- Switzerland: DTM with grid of approximately 2 m × 2 m (Artuso et al., 2003; Luethy and Stengele, 2005),

- province Bolzano in Italy, for urbanized areas a DTM with grid of 2.5 m ×2.5 m and non-urbanized area DTM with grid 5 m × 5 m (Wack and Stelzl, 2005),

- various states of Germany (Artuso et al., 2003; Ahokas et al., 2005a)

Based on analytical derivations given in Chapter 6 and 7 we prepared Table 8.1, where minimum terms for aerial scanning data ordering are given. The values are given for aerial laser scanning as a stand-alone acquisition technique. If other remotely sensed acquisition methods are used in addition to aerial laser scanning, the numbers in the last two columns can be reduced. In the last two columns the required optimal density of points is given: first for build-up areas and areas with mixed vegetation; second for medium density forest, for which the scarce meditetanean forest was taken as a base.

At the moment aerial laser scanning cannot be applied in Slovenia for the **Land cadastre** and the **Building cadastre** as these two are legal evidences, where acquisition methodology is defined by law. In both cases the new planimetric and height data can be acquired only by field measurements with theodolite or detailed GPS-measurements. Nevertheless, if extensive studies prove the capability of aerial laser scanning in Land and Building cadastre measurements, the ways would be open to amend the law, which defines the acquisition methodology. Therefore we left them in Table 8.1 just as a proposal. For the Land cadastre and the Building cadastre data updating, stand-alone aerial lasers scanning can be applied. Additionally, the usage of aerial laser scanning in the Building cadastre would open ways for different automatic procedures for new building search. The locations of new buildings are a special problem of the Building cadastre and Real Estate Register, as new buildings are written in the Building cadastre at a slow pace.

8.3.1 Databases where stand-alone aerial laser scanning can be applied

Digital terrain model gains the most, if aerial laser scanning is applied for its production. For DTM production already low-resolution aerial laser scanning (1 pt/m^2 or less) would satisfy. More than 50% of Slovenia is covered by forest, therefore conventional photogrammetric

Table 8.1: Applicability of aerial laser scanning data for geodetic data acquisition. The minimal terms are: geometrical accuracy of the geodetic data GA, accuracy of INS-angles, roll and pitch $\Delta\phi = \Delta\theta$ and heading $\Delta\psi$, flying height $h[m]$, density of points [pt/m^2].

Tabela 8.1: Minimalni pogoji, ki definirajo kakšne laserske podatke moramo uporabiti za izdelavo določenega končnega izdelka. Minimalni pogoji: geometrična ločljivost geodetskih podatkov GA, natančnost INS-kotov $\Delta\phi = \Delta\theta$ in $\Delta\psi$, višina leta $h[m]$ ter gostota laserskih točk [pt/m^2].

geodetic data	GA	$\Delta\mathbf{R}_{INS}$ [°]		h	density [pt/m^2]	
	[m]	$\Delta\phi = \Delta\theta$	$\Delta\psi$	[m]	urban areas	medium forest
Land cadastre	0.1	0.005	0.007	600	12	20
Building cadastre	0.5	0.005	0.007	800	12	20
DTM 5	1.5/6.5*	0.020	0.040	1000	1	1
Cadaster of public infrastructure**	1	0.005	0.007	800	12	20
DTK 5	0.65	0.005	0.007	800	12	20
Land survey plans $1:5000$	0.65	0.005	0.007	800	12	20

* height accuracy for flat and mountainous terrain

**layers which are not underground

automatic matching, which was used for DTM 5 production, does not give sufficient accuracy, especially in forest areas. For DTM 25 and DTM 5 the following height accuracies were specified (GU RS, 2008): for mountainous terrain 6.5 m, for hilly terrain 3 m and for flat terrain 1.5 m. Using aerial laser scanning, the accuracy in hilly and mountainous terrain, could be increased, especially if laser scanning is conducted in leaf-off seasons. The greatest advantage of DTM production by aerial laser scanning would be its uniform accuracy.

Some layers of the **Cadaster of public infrastructure** (utility system cadastre) could be acquired by aerial laser scanning. This addresses only layers which are not buried underground: traffic infrastructure, energy infrastructure, river and creek infrastructure and other infrastructure for management and protection of natural environment. If high-resolution aerial laser scanning (10 pt/m^2) was applied, no additional ortophographies would be needed to acquire location of the infrastructure. Nevertheless, aerial laser scanning has the same limitations as photogrammetry, therefore no underground acquisition is possible.

National topographic maps ($1:5000$) or **land survey plans** ($1:5000$ or even $1:1000$) could easily be produced, if high-resolution aerial laser scanning was applied. The classification of different land use classes could also be made, based on the object height differences and intensity variations. The application of aerial laser scanning could even automate some processes (e.g. automatization of the contour line production). It would also present an elegant way how to acquire objects under trees (e.g. creeks, forest roads), especially if aerial laser scanning was conducted in leaf-off season. Again the interpretation of data would be easier if additional photographic data of the same area existed.

8.3.2   Databases where aerial laser scanning would yield additional data

If the **database on land use** is understood in spatial planning manner (five classes of land use in SMA database) also classification based on the aerial laser scanning could be applied for it. For more detailed database, e.g. for forestry and agriculture, an additional color, multispectral or even hyperspectral photographs would be needed. When multispectral or hyperspectral photographs are applied, classification based on these photographs only could be performed and a need for aerial laser scanning becomes obsolete.

Ortophotographies production cannot be performed if no additional photographic data is acquired. But when applying aerial laser scanning, we can manufacture more accurate ortophotographies. Production of true ortophotographies becomes easier and more accurate already if low-resolution aerial laser scanning (1 pt/m^2 or less) is applied.

8.4   Proposed acquisition methodology optimization

Data acquisition of aerial laser scanning is becoming less expensive every year. If aerial laser scanning is ordered together with remotely sensed data acquired from the same platform, the additional data can often be ordered at a reduced price. This enables, not only the change from photogrammetric stereo-restitution to stand-alone aerial laser scanning, but also the data acquisition optimization based on the combination of different remotely sensed techniques.

In this section we will describe the proposed optimization of data acquisition methodology by applying aerial laser scanning. The proposal is based on our analytical derivation of a-priori aerial laser scanning error assessment and knowledge on characteristics of geodetic data used in local spatial planning.

The proposed optimization of data acquisition methodology by applying aerial laser scanning unfortunately requires also a change of the processing methodology. We propose a change from classical photogrammetric stereo-restitution or photointerpretation (Figure 3.1 on page 18), to the aerial laser scanning data processing methodology (Figure 8.2 on page 113). Introducing such data processing methodology change in geodetic practice means that a new data processing software has to be applied and staff training needs to be conducted.

8.4.1   Land survey plans 1 : 5000 and DTK5

The land survey plans 1 : 5000 represent the same topographic content as DTK5. The land survey plans can have also other layers which are not presented on DTK5 (see Section 2.3.3 on page 15). Let us take for example that we need to prepare a land survey plan 1 : 5000 with an additional layer of land cadastre map. Currently, the land survey plan presenting such topics would be acquired by two acquisition technics: the topographic layers would be acquired by photogrammetric stereo-restitution, the land cadastre changes would be acquired by field measurements (Figure 8.5A).

If we apply aerial laser scanning as a stand-alone acquisition technology, we have to apply high-resolution aerial laser scanning as proposed in Table 8.1. For easier identification and delineation of lines it is advisable to apply photographic material as an additional data. The ortophotographies in scale 1 : 5000 would be the most appropriate data. As these ortophotographies present just data for easier photointerpretation, it is not urgent that they are new (recorded on the date of aerial laser scanning). We can use available old ortophotographies. The changes in the physical space made from the date of old ortophotographies to the date of aerial laser scanning, will be easily found in laser scanning point cloud. Therefore the arrow connecting ortophotographies to aerial laser scanning on Figure 8.5B is optional.

The proposed acquisition methodology change for renovation of the Land cadastre data is currently just a scientific forecast. We can propose a change from field work to aerial laser scanning, based on a-priori laser scanning error assessment defined in our work. But at this moment such a change is not allowed, because the acquisition methodology for Land cadastre is defined in a legal act.
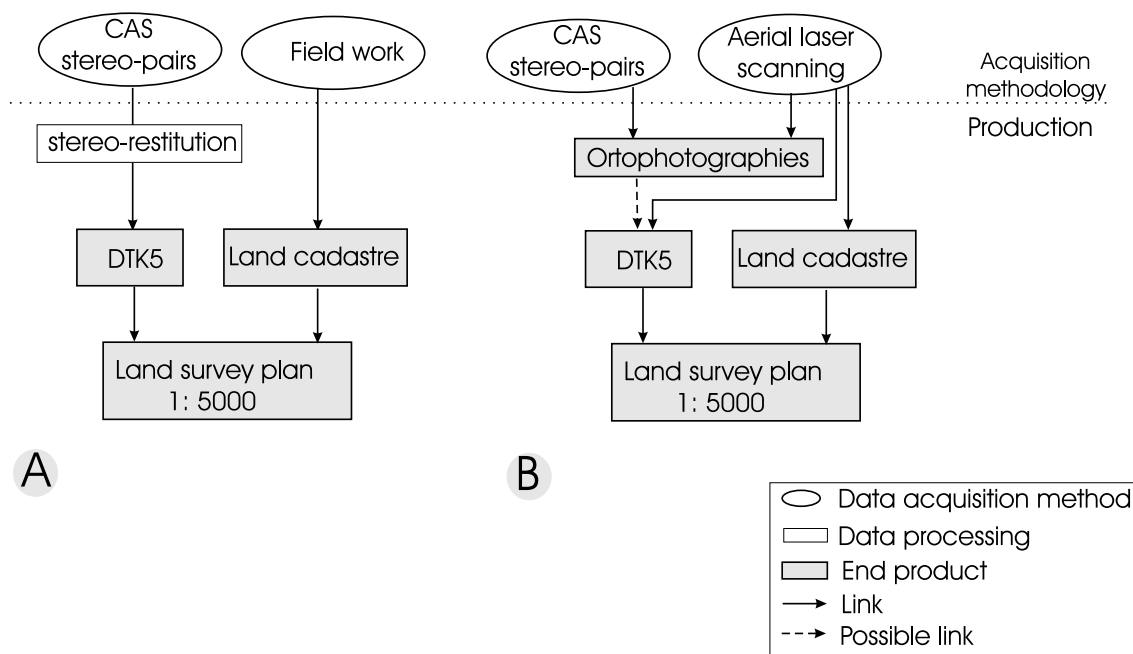
Figure 8.5: Data acquisition methodology for DTK5 and land survey plan 1 : 5000: A) current, B) proposed.
Slika 8.5 Metodologija zajema podatkov pri izdelavi DTK5 in geodetskega načrta 1 : 5000: A) obstoječa, B) predlagana.

As the Land cadastre is the most accurate geodetic data discussed in this work, we have to propose an additional term that has to be fulfilled if aerial laser scanning was applied in the Land cadastre measurements. For measuring the Land cadastre changes the most important additional term is the visibility of boundary-stones in the laser scanning point cloud. This can be achieved by marking the boundary-stones by highly reflective colors which are easily distinguished in laser scanning point cloud. Alternatively, we can apply an even greater point density as proposed in Table 8.1. To introduce aerial laser scanning of Land cadastre measurement in geodetic practice

more practical research should be done.

When aerial laser scanning is applied in the Land cadastre acquisition, this will also mean a reduction in necessary field work. It will be minimized to reference points measurements and coloring the boundary-stones.

8.4.2   DTM 5 for more accurate ortophotographies and Database on land use

Geodetic data used in local spatial planning in Slovenia currently depend mainly on photogrammetric stereo-restitution on the basis of the CAS. If aerial laser scanning is implemented as a stand-alone or additional source of data, the final geodetic data would gain in accuracy assessment. This can be seen on Figure 8.6 where the proposed optimization of the acquisition methodology for production of ortophotographies and database on land use is presented. If aerial laser scanning is introduced to DTM 5 production (the proposal from Table 8.1), the manufactured DTM 5 would achieve vertical accuracy of 0.3 m or better. This vertical accuracy would be uniform for open areas and areas obstructed by vegetation.
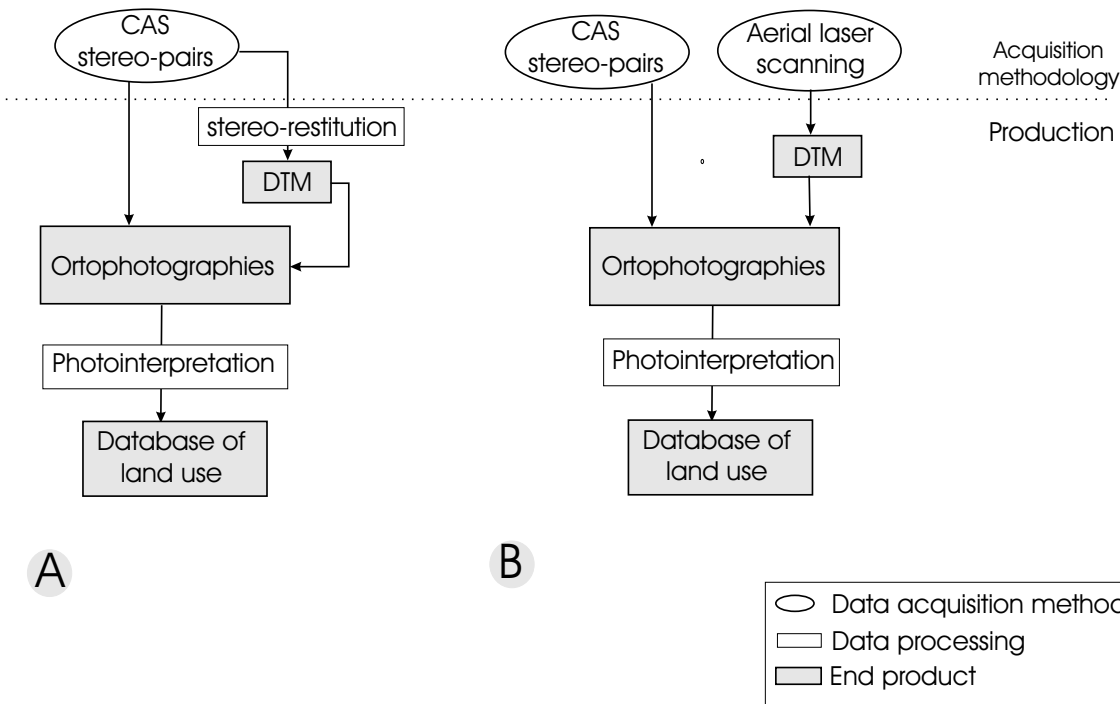
Figure 8.6: Data acquisition methodology for ortophotographies and database on actual land use production: A) current, B) proposed.
Slika 8.6 Metodologija zajema podatkov pri izdelavi ortofotografij in dejanski rabi prostora: A) obstoječa, B) predlagana.

As DTM 5 is the source for ortophotography production, by better accuracy of DTM 5, the ortophotographies also gain on their positional accuracy. More accurate ortophotographies would enable more accurate positional accuracy in the process of photointerpretation for different purposes — production of different databases on land use. Therefore the acquisition methodology

optimization for DTM 5 production would enable better positional accuracy for different products based on DTM 5.

As the acquisition of buildings in the scale 1 : 5000 for DTK5 production is possible by applying aerial laser scanning, the Building cadastre could also apply aerial laser scanning for new building recognition. This acquisition change is hindered by legal definition of Building cadastre, as for our proposed acquisition methodology change in Land cadastre.

8.4.3   Cadastre of public infrastructure

Cadastre of public infrastructure includes different types of data on infrastructure objects, which can be acquired by different data acquisition methodologies. As already mentioned in Section 3.3.8 (on page 24) for underground data, only field work and ground penetration measurements can be applied. For data above ground several acquisition methodologies can be applied: from field work to photogrammetric stereo-restitution and already applied aerial laser scanning. If aerial laser scanning is already performed for energy infrastructure, than it economic that the same data sample is also used for acquisition of other types of infrastructures on this area (e.g. roads). In Table 8.1 we defined the minimal terms that have to be fulfilled so that aerial laser scanning can be applied for infrastructure objects above ground. Unfortunately, aerial laser scanning cannot be applied for all types of infrastructure described in the Cadastre of public infrastructure.

8.5   Discussion

The acquisition methodology of the majority of geodetic data used in local spatial planing can be changed from photogrammetric stereo-restitution or photointerpretation, which is used today, to aerial laser scanning, if high-resolution laser scanning is applied. Stand-alone aerial laser scanning without additional photographic data can already be applied. Exceptions where we have to use photographic data and its derivations include: the detailed databases in land use and ortophotographs. We proved in our work that also databases on land use and ortophotographies can gain, if aerial laser scanning is applied in DTM 5 production. DTM 5 and photographs form basic incoming data for ortophotography production.

The main difference between both methodologies is the way how data are georeferenced, which also influences the accuracy of end-product. For aerial laser scanning direct georefenencing is used, for photogrammetry aerotriangulation. Even though direct georeferencing is already possible in photogrammetric practice, aerotriangulation is mainly used with additional GPS/INS data from flying platform, which enables a-posteriori georeferencing. In the contrast the aerial laser scanning has to define the position of each echo of the laser pulse already directly in space, therefore no other possibility than direct georeferencing is possible. If unfavorable conditions in the time of filming/scanning occurs, we have more control over a-posteriori aerotriangulation than over the on-the-spot direct georeferencing of the laser scanning data. Therefore the accu-

racy specifications for aerial laser scanning GPS/INS accuracies should be more strict that for photogrammetric aerotriangulation usage.

If aerial laser scanning is applied for the production of geodetic data used in local spatial planning, the person placing an order should know in advance what has to be ordered, to enable a product acquisition accurate and detailed enough, comparable to the one acquired by classical photogrammetric procedure. We applied in this thesis developed simplified a-priori error model and analytical derivation of optimal point density to set up the minimal terms which define aerial laser scanning data, which can be applied for certain geodetic product used in local spatial planning (Table 8.1). We also proposed the acquisition methodology optimization for these geodetic products. The application of the methodology change in Slovenian geodetic practice is the work for future studies.

9   CONCLUSIONS

Local spatial planning is based upon geodetic data which represents the current state of physical space: land survey plans in scale $1:5000$ (or topographic maps), ortophotographs, Land cadastre, Building register, Cadastre of public infrastructure, Database on land use, etc. These data are used as a foundation for planning physical space development in the view of natural and cultural heritage preservation, steady settlement development and sustainable development. Spatial planning in Slovenia is enacted by the spatial planning act. The development of local physical space is regulated by the local spatial planning documents, which must be adjusted to regional and national spatial planning documents. As the local spatial planning documents are legal documents, they should be based on high quality and up-to-date geodetic data. The purpose of this thesis was to find minimal terms defining which aerial laser scanning data can be applied for certain geodetic data used for local spatial planning. In this way the optimization of acquisition methodology of such geodetic data can be done by the application of aerial laser scanning.

Aerial laser scanning can be used as a stand alone technique or with additional remotely sensed data (multi- or hyperspectral data). Aerial laser scanning system measures locations of points in the physical space by instantaneous scan angle and range. DGPS and INS systems give the location and orientation of flying platform. After the integration of aerial laser scanning data, DGPS and INS data each point is described with X, Y, Z coordinates and the intensity value of the echo. Additionally used remotely sensed data contributes to easier identification of details for aerial laser scanning. To set up a foundation when aerial laser scanning can be applied for geodetic data production, we decided to investigate the derivation of minimal terms when aerial laser scanning is used as a stand-alone technique. This opens ways for future research in the minimal term optimization when aerial laser scanning is used in combination with other remotely sensed techniques.

Different rigorous error models of aerial laser scanning are available, but they are too complicated for typical person who orders aerial laser scanning. In the process of local spatial planning, different professional profiles (geodesists, cartographers, architects, rural and urban planners, landscape planners) come in contact with the ordering or the supervision of the data acquisition from aerial laser scanning. The most appropriate error model usable for such a broad professional society should be simple and must give reliable error values a-priori to the ordering. Therefore a simplified a-priori error model was developed in this work.

A thorough research on different errors sources has been made on the basis of literature re-

view. Different error sources have been identified and evaluated according to error sizes and importance. As a base for error model development and simplification, the Schenk's geolocation equation was used. The error sources were divided in three groups: basic systematic errors, flight mission related errors and errors caused by the target characteristics (the object from which the laser echo reflects). The most important scientific improvement of Schenk's error model in our work is the introduction of vegetation height related error (from a group of target characteristic errors). The vegetation height related error has the greatest influence on the total error size of laser scanning points in areas covered by vegetation. If we take for example Slovenia, which territory is over 50% covered with forests, this error plays an important role when deciding on permitted error sizes.

Analytically we developed a simplified a-priori error model, which returns an average and maximal error size for the whole aerial laser scanning point cloud. This simplified error model is independent from scan and heading angle. To calculate the average and maximal error sizes, we have to decide only on the permitted size of roll, pitch and heading error components, GPS sensor positioning errors, vegetation height related error and flying height. Therefore our simplified error model provides an easy tool to define possible error sizes in aerial laser scanning a-priori to laser scanning ordering. Just two simple equations define the average and maximal possible error sizes.

The study of the error model provided also some practical hints, how to check the delivered laser scanning point cloud, to be certain that it satisfies our needs. The contractor should deliver data with strip overlap to enable checking of vertical accuracy. To enable checking of GPS sensor positioning error after flight, it is sensible to retrieve GPS measurement protocol with PDOP values.

Although secondary height related errors are not included in the simplified a-priori error model, they should be considered if aerial laser scanning in mountainous terrain is to be conducted. In addition the errors resulting from unknowing local transformational parameters of local coordinate system in which laser scanning point cloud was transformed are not included. They can be avoided if transformational parameters are well known or one of the global coordinate systems is used (WGS84 or ETRS89).

With a-priori known accuracy of laser scanning, we have to decide in advance also on the level of detail which we would like to present in the final product – the geodetic data for local spatial planning. The level of detail, which can be acquired from a aerial laser scanning, defines the precision of the final product. The precision which can be acquired from the laser scanning data is connected with laser scanning point density by Nyquist frequency (minimal sampling density).

When producing a cartographic product at a certain scale (e.g. national topographic map in scale $1:5000$) the accuracy of a map and its precision are defined in advance. The precision is defined by geometrical accuracy of the map. Geometrical accuracy is defined through drawing accuracy and scale of the map. The minimal point density of laser scanning points is defined by Nyquist frequency. This is a theoretical value, in order to satisfy it, all points should lie on the ground. In a typical laser scanning point cloud this is not the case, as the laser points are scattered

by height. Therefore the total needed point density which satisfies the specified geometrical accuracy was calculated for four vegetation classes in leaf-off season: scarce mediteranean forest, dense forest, mixed vegetation (grassland, orchard and forest) and built-up area with houses. Prior to that, the penetration rate of laser points in these vegetation classes was measured on the test sample of the city of Nova Gorica, Slovenia. The total needed point density was calculated with the knowledge on the penetration rate and theoretical derivation of point density by Nyquist frequency.

If we use areal laser scanning as a supplementary technique to multi- or hyperspectral data, the point density can be reduced, because the laser scanning is used just to enable height representation. The multi- or hyperspectral data are used in this case as fundamental data for identification and reconstruction of the objects. In this case the precision of the end-product is defined through the resolution of the photograph.

By first defining a-priori accuracy and point density of the laser scanning point cloud, we proposed a methodology change from photogrammetric stereo-restitution to stand-alone laser scanning for the following geodetic data: land survey plans in scale $1:5000$ (topographic maps), Real estate register and for above ground layers of the Cadastre of public infrastructure. For all these products the aerial laser scanning conduced in leaf-off season with the total needed point density around 15 pt/m^2 would satisfy. The only exception are objects under dense vegetation, which would require larger total needed point density. To achieve the prescribed vertical accuracy of 10 cm for all these products, laser scanning on 600–800 m over ground should be used, with INS accuracies $0.005°$ of roll and pitch, and $0.007°$ of heading.

With a-priori known laser scanning accuracy and total needed point density we can decide on appropriate laser scanning data which satisfy our needs. This knowledge defines the optimal laser scanning data for a certain geodetic product used in local spatial planning.

The scientific value of this work is that the a-priori error estimation and total needed point density are analytical derivations and therefore give unique values. All the boundary conditions for error sizes are collected at one place, and the user of our equations does not need to search through additional literature and laser scanner specifications to calculate the a-priori error estimation or needed total point density. The developed equations are easy to use and therefore can be applied by different professional profiles which are in contact with spatial planning. This way the knowledge about the aerial laser scanning technology becomes accessible to a broader professional society. As a consequence, also the acquisition methodologies of different geodetic data can be optimized with aerial laser scanning. The proposal for acquisition methodology optimization for geodetic data used in local spatial planning in Slovenia was given in this work.

In this way we confirmed all three hypotheses of our work:

- The simplified a-priori error model was developed analytically from the Schenk's rigorous error model. It defines the minimal terms for aerial laser scanning ordering.
- The Nyquist frequency connects the laser scanning point density and the requested preci-

sion of certain geodetic data. Together with the knowledge on penetration rate for certain vegetation class the total needed point density was defined.

- The acquisition methodology optimized with adding aerial laser scanning opens ways for better precision of data acquisition. The majority of geodetic data for local spatial planning can gain if aerial laser scanning is applied as an additional source of spatial information. For land survey plans in scale $1:5000$ (topographic maps), Real Estate Register and above-ground layers of the Cadastre of public infrastructure, the aerial laser scanning as stand-alone technique presents an equivalent data acquisition methodology to the existing ones.

Our acquisition methodology optimization proposal opens ways to data processing methodology studies and cost-benefit studies of aerial laser scanning applied in geodetic data production.

10   RAZŠIRJENI POVZETEK V SLOVENŠČINI

10.1   Uvod

Zračno lasersko skeniranje, imenovano tudi lidar (LIDAR – Light Detection and Ranging), je metoda daljinskega zaznavanja, ki se čedalje več uporablja za zajem topografskih in batimetričnih podatkov. Zračno lasersko skeniranje se lahko uporablja kot samostojna tehnika snemanja, v kombinaciji s klasičnim fotogrametričnim snemanjem (multispektralno snemanje) ali v kombinaciji z ostalimi tehnikami daljinskega zaznavanja (npr. hiperspektralno snemanje). Poglavitni prednosti zračnega laserskega skeniranja pred fotogrametričnimi metodami snemanja sta v tem, da podatke o višinski razporeditvi točk na reliefu pridobimo direktno z izmero in da lahko izmerimo tudi točke pod vegetacijo. Z direktno izmero reliefa pod vegetacijo se nam odprejo možnosti za samodejno izdelavo plastnic, zajem potokov, zajem gozdnih cest in natančnejšo izdelavo digitalnega modela reliefa (DMR). Če metodo uporabimo v kombinaciji s fotogrametričnim snemanjem, se poenostavi identifikacija objektov ter poda možnost za izdelavo natančnejših pravih ortofotografij.

Namen doktorske disertacije je opredelitev minimalnih pogojev, ki opredeljujejo, kakšne podatke zračnega laserskega skeniranja lahko uporabimo za izdelavo ali posodobljanje geodetskih podatkov, ki se uporabljajo kot prostorske podlage v lokalnem prostorskem načrtovanju v Sloveniji. Ti minimalni pogoji morajo biti zadostni pogoji za opredelitev naročila, ki ga posredujemo ponudnikom zračnega laserskega skeniranja. Omogočiti nam morajo, da se o obstoječem oblaku točk odločimo, ali je primeren za našo uporabo. V tej nalogi smo se osredotočili na dva zelo pomembna vidika, ki določata, katere podatke zračnega laserskega skeniranja moramo izbrati za določen namen:

- poznavanje natančnosti zračnega laserskega skeniranja pred snemanjem: preko a-priori modela napak zračnega laserskega skeniranja določimo optimalne parametre snemanja glede na potrebe

- preko znane geometrične ločljivosti geodetskih podatkov, uporabnih za izdelavo prostorskih podlag, določimo gostoto točk zračnega laserskega skeniranja na enoto površine (št. točk/m^2)

Ob dobrem poznavanju, katere podatke naročamo za posamezni namen, se nam odprejo možnosti tudi za optimizacijo metodologije zajemanja podatkov.

Na osnovi prej opisanega namena naloge smo postavili naslednje hipoteze naloge:

- Iz obstoječih rigoroznih modelov napak lahko analitično izpeljemo poenostavljen model napak, ki bo uporaben za a-priori izračun natančnosti laserskega skeniranja. Poenostavljen model napak nam bo podal osnovne omejitve, ki jih moramo upoštevati pri naročanju zračnega laserskega skeniranja.

- Zahtevana geometrična ločljivost geodetskih podatkov, ki jih bomo izdelali na osnovi zračnega laserskega skeniranja, opredeli gostoto laserskih točk na enoto površine.

- Ob poznavanju velikosti napak in gostote točk na enoto površine pred izvedbo samega zračnega laserskega skeniranja podamo tudi okvirje za lažje odločanje o vpeljavi zračnega laserskega skeniranja v geodetsko prakso. To nam omogoči tudi optimizacijo metodologije zajemanja podatkov za različne geodete podatke, ki se uporabljajo kot prostorske podlage pri lokalnem prostorskem načrtovanju.

V nalogi je najprej opisana zakonodaja, ki ureja lokalno prostorsko načrtovanje v Sloveniji. Na osnovi te zakonodaje so opredeljeni prostorski podatki, ki se lahko uporabljajo za prostorsko planiranje ter njihova trenutna metodologija zajema.

Ob temeljitem pregledu obravnave napak zračnega laserskega skeniranja smo ugotovili, da so posamezni viri napak sicer podrobno raziskani (Alharthy et al., 2004; Ahokas et al., 2005a; Burman, 2000; Crosilla and Beinat, 2005; Schenk, 2001; Schnurr et al., 2004; Maas, 2003; Thoma et al., 2005; Turton, 2006), manjka pa splošen in predvsem uporaben model, ki bi lahko služil pri načrtovanju oz. naročanju snemanja. Z možnostjo a-priori izračuna napak zračnega laserskega skeniranja in znano predvideno geometrično ločljivost geodetskih podatkov se lahko že pred naročilom zračnega laserskega skeniranja odločimo o izbiri parametrov snemanja, ki bodo dali najbolj optimalne rezultate.

Položajna natančnost zračnega laserskega skerniranja je 30-50 cm, višinska natančnost pa 5-15 cm, vendar so lahko te vrednosti večje, če snemanje izvedemo v slabših pogojih od idealnih (Baltsavias, 1999a; Maas, 2003). Napake niso enake na celotnem območju snemanja, temveč so odvisne od več dejavnikov. V nalogi zato želimo raziskati vpliv posameznih dejavnikov in te vplive upoštevati v analitičnem modelu skupne ocene natančnosti zračnega laserskega skeniranja. S takim modelom lahko predhodno izračunamo natančnost zajetih podatkov brez uporabe programske opreme, ki jo bo za obdelavo podatkov uporabil ponudnik laserskega skeniranja.

Izvedbo zračnega laserskega skeniranja lahko opredelimo še po gostoti izmerjenih točk na enoto površine (število točk na m^2). Če povzamemo izkušnje z Univerze na Dunaju in v Vidmu (Kraus, 2005; Crosilla, 2005), lahko podatke ločimo glede na gostoto posnetih točk, ki ustrezajo določeni potrebi po predstavitvi terena. V prvi skupini so podatki z največ 1 točko/m^2, ki omogočajo izdelavo splošnih DMR-jev in so primerljivi s trirazsežnimi podatki, pridobljenimi na osnovi fotogrametrične stereorestitucije. Druga skupina z 1 do 5 točkami/m^2 omogoča izdelavo podrobnejših DMR-jev (npr. za izdelavo reliefa poplavnih območij za potrebe hidrografije). V tretjo skupino sodijo podatki z več kot 5 točkami/m^2, ki omogočajo izdelavo najbolj podrobnih DMR-jev za potrebe prikazov urbanih območij, cest in drugih detajlov (10 točk/m^2 izpolni večino takšnih potreb). Gostoto laserskih točk na enoto površine pa lahko vnaprej predvidimo z

Triglav-Čekada, M. 2009. *Optimization of the data processing methodology and accuracy analysis of airborne laser scanning data applied for local spatial planning*, PhD thesis, Ljubljana, UL, FGG, Department for geodesy

131

upoštevanjem geometrične ločljivosti izdelka, ki ga želimo izdelati ob uporabi določenega oblaka točk zračnega laserskega skeniranja. S pomočjo Nyquistove frekvence smo v doktorskem delu opredelili teoretično potrebno gostoto točk na enoto površine za izbrane geodetske podatke. Preko izmere deleža prodiranja laserskih žarkov skozi različne tipe vegetacije na testnem setu laserskih podatkov iz Nove Gorice pa smo določili še optimalno uporabno gostoto točk na enoto površine.

A-priori ocena napak in optimalna gostota laserskih točk na enoto površine podata osnovne parametre zračnega laserskega skeniranja, ki jih moramo poznati že pred naročilom snemanja. S tem smo odprli možnost še za optimizacijo metodologije zajema podatkov pri izdelavi in ažuriranju geodetskih podatkov, ki jih uporabljamo pri lokalnem prostorskem načrtovanju.

10.2 Zakonske osnove in trenutna metodologija izdelave geodetskih podatkov za potrebe lokalnega prostorskega načrtovanja

Prostorsko planiranje oz. načrtovanje se ukvarja s celostnim urejanjem prostora držav, regij in občin. Med lokalno prostorsko načrtovanje uvrščamo planiranje za potrebe regij in občin. Prostorski planer oz. nosilec urejanja prostora potrebuje za izdelavo kvalitetnih prostorskih načrtov kakovostnih kartografske in druge podatkovne osnove, ki prikazujejo trenutno stanje preučevanega prostora (Pogačnik, 1992). Ker v času izdelave doktorske disertacije regije v Sloveniji še niso bile določene, smo se v nalogi osredotočili na občinsko prostorsko načrtovanje.

10.2.1 Zakonske osnove

Podrobno je prostorsko načrtovanje v Sloveniji zakonsko opredeljeno v Zakonu o prostorskem načrtovanju (ZPNačrt, UL RS 33/2007) ter njegovem predhodniku, to je bil Zakonu o urejanju prostora (ZureP-1, UL RS 110/02 in 8/03). V zakonih in njunih podzakonskih aktih so opredeljene pristojnosti države in lokalnih skupnosti (občin ali več občin skupaj) pri pripravi prostorskih aktov za potrebe urejanja prostora. Prostorske ureditve se načrtujejo s prostorskimi akti, ki opredeljujejo usmeritve v zvezi s posegi v prostor, vrste možnih posegov v prostor ter pogoje in merila za njihovo izvedbo. Prostorski akt vsebuje grafični in tekstualni del. Grafični del temelji na različnih geodetkih podatkih, ki prikazujejo trenutno stanje prostora, govorimo o prostorskih podlagah, na katerih temelji prostorsko načrtovanje. Prostorske akte pripravljajo nosilci urejanja prostora (državni organi oz. organi lokalnih skupnosti ter nosilci javnih pooblastil) in jih delimo na državne, občinske in medobčinske prostorske akte. Na sliki A.3 (stran 167) so zapisani akti, ki opredeljujejo prostorsko načrtovanje na vseh treh ravneh.

Zaradi racionalnosti in uporabnosti strokovnih podlag za različne strateške in izvedbene prostorske akte se za pripravo strokovnih podlag uporabijo različni geodetski podatki in drugi podatki iz uradnih evidenc, katerih vodenje je v državni oz. lokalni pristojnosti (ZureP-1, UL RS 110/02 in 8/03). Geodetske podatke in izdelke za pripravo strokovnih podlag prostorskih aktov občine delimo na prostorske podlage oz. izdelke za prikazovanje kartografskega dela pros-

torskega akta in geodetske podatke, ki jih uporabimo tudi pri izdelavi formalnopravnih prilog prostorskega akta. Med geodetske podatke, ki jih v Sloveniji lahko uporabimo za lokalno prostorsko načrtovanje, štejemo: državno topografsko karto v merilu 1 : 50 000 (DTK 50), geodetski načrt v merilu 1 : 5000 (ali državno topografsko karto 1 : 5000 – DTK5), ortofoto načrte v merilu 1 : 5000, DMR, podatke Zemljiškega katastra, Katastra stavb ali Registra nepremičnin, Registra prostorskih enot, Zbirnega katastra gospodarske javne infrastrukture (podatki o prometni, komunalni, električni infrastrukturi, infrastruktura za zaščito naravne dediščine, telekomunikacijska omrežja), uradne podatke o vrsti rabe prostora in Register zemljepisnih imen.

10.2.2   Današnja metodologija izdelave geodetskih podatkov za občinsko prostorsko načrtovanje

Formalnopravni lokacijski podatki, kot so podatki Zemljiškega katastra in Katastra stavb, se vzdržujejo le na osnovi terenskih meritev s klasično ali GPS-izmero. Register nepremičnin povzema lokacijske podatke iz Katastra stavb, njegovi atributni podatki pa so se določili tudi na osnovi terenskega popisa. Register prostorskih enot se obnavlja na osnovi formalnopravnih aktov, ki definirajo nove meje prostorsih enot, ki pa ne potekajo po mejah Zemljiškega katastra.

Geodetski načrti v merilu 1 : 5000 so izdelani na osnovi topografskih podatkov, ki prikazujejo stanje prostora v merilu 1 : 5000. Poleg topografskih podatkov so na geodetskih načrtih lahko prikazani tudi drugi podatki (npr. zemljiški kataster). Geodetskim načrtom enakovreden podatkovni sloj so državne topografske karte v merilu 1 : 5000 (DTK5). DTK5 se izdelujejo s pomočjo fotogrametrične stereorestitucije stereoparov cikličnega aerosnemanja (CAS). Enako so bili izmerjeni tudi podatki o reliefu (DTM 100, 25, 12,5 in 5). InSAR-posnetki so bili osnova za še eno verzijo DMR 25. Na osnovi kombinacije različnih višinskih podatkov, ki so vsebovali še podatek o višinski natančnosti, je bil izdelan DMR 12,5 (Podobnikar, 2003). Kot vhodni podatek za izdelavo ortofotografij v merilu 1 : 5000 so bili uporabljeni podatki DMR 25 in CAS-stereopari.

Večina nadzemnih vodov v Zbirnem katastru gospodarske javne infrastrukture (prometna, energetska infrastruktura, rečna infrastruktura ter infrastruktura za upravljanje in zaščito naravne dediščine) se lahko zajemajo s fotogrametričnimi postopki ali daljinskim zaznavanjem ter klasično ali GPS-izmero na terenu. Podzemne vode lahko izmerimo le ob nameščanju teh vodov v zemljo, kar se večinoma izvaja s klasično ali GPS-izmero.

Za prostorsko načrtovanje so pomembni tudi podatki o dejanski rabi prostora. Le-ta se na državni ravni vodi v dveh stopnjah detajla. Geodetska uprava Republike Slovenije ciklično vzdržuje podatke o dejanski rabi prostora, ki je razdeljena na pet razredov rabe (Pravilnik ...dejanska raba prostora..., 2004), in se vzdržuje na osnovi fotointerpretacije posnetkov CAS. Ministrstvo za kmetijstvo vodi podrobnejšo bazo o dejanski rabi kmetijskih in gozdnih zemljišč, kjer je opredeljenih 16 razredov rabe (Pravilnik ...kmetijskih in gozdnih zemljišč, 2006). Tudi ta raba je določena na osnovi fotointerpretacije ortofotografij CAS ali satelitskih posnetkov.

10.3 Pregled napak zračnega laserskega skeniranja

Različni avtorji so preverjali doseženo natančnost zračnega laserskega skeniranja z a-posteriori izmero terenskih kontrolnih točk oz. kontrolnih področij (Alharthy et al., 2004; Ahokas et al., 2005b; Burman, 2000; Crosilla et al., 2005; Schenk, 2001; Schnurr et al., 2004; McKean in Roering, 2005; Thoma et al., 2005). Rezultati se ujemajo z že prej omenjenimi odstopanji 30-50 cm po planimetriji in 5-15 cm po višini, ki jih je prvi podal Baltsavias (1999a) in potrdil Maas (2003).

Obstoječi rigorozni modeli napak zračnega laserskega skeniranja (Schenk, 2001; Beinat in Crosilla, 2002; Friess, 2006; Skaloud in Lichti, 2006) so prezapleteni za vsakodnevno uporabo pri načrtovanju zračnega laserskega skeniranja, zato smo se odločili, da enega izmed njih poenostavimo. Kot osnovo za izdelavo poenostavljenega modela napak smo uporabili Schenkov model napak (Schenk, 2001). S pomočjo podrobnega pregleda literature smo opredelili tipe napak, njihove velikosti in obnašanje ter njihov vpliv na skupno napako zračnega laserskega skeniranja.

Osnovno geolokacijsko enačbo zračnega laserskega skeniranja lahko opišemo z naslednjimi procesnimi sklopi (Wehr in Lohn, 1999; Baltsavias, 1999b; Kraus, 2005): opredelitev laserskega snemalnega sistema z njegovimi fizikalnimi karakteristikami, postopek transformacije podatkov iz snemalnega sistema v lokalni koordinatni sistem nosilca laserskega sistema (helikopter ali letalo), transformacija podatkov iz lokalnega koordinatnega sistema nosilca v globalni koordinatni sistem ter transformacija iz globalnega v nacionalni koordinatni sistem. Vsak procesni sklop je obremenjen tudi z napakami.

Neodvisno od delitve procesnih sklopov, lahko napake zračnega laserskega skeniranja delimo glede na izvor napak (Slika 5.1 na strani 50). Prvo skupino napak predstavljajo osnovne sistematične napake oz. napake vpliva programske in strojne opreme (McKean in Roering, 2005), ki jih lahko modeliramo z analitičnim modelom napak (Schenk, 2001). Drugo skupino napak imenujemo napake misije snemanja in so po naravi tudi sistematične napake (McKean in Roering, 2005). V tretji skupini so napake, ki nastanejo zaradi lastnosti terena oz. tarče, od katere se laserski žarek odbije. Zadnje navadno odkrijemo ob končni uporabi laserskih podatkov in se ne obnašajo sistematično.

10.3.1 Opis osnovnih sistematičnih napak s Schenkovim modelom

Osnovne sistematične napake lahko modeliramo s Schenkovo geolokacijsko enačbo, ki jo opišemo z rotacijami med različnimi sistemi (Slika 5.2 na strani 53):

$$\mathbf{x}_L = \mathbf{x}_0 + \Delta\mathbf{x}_0 + \mathbf{R}_W \cdot \mathbf{R}_{GEO} \cdot \Delta\mathbf{R}_{INS} \cdot \mathbf{R}_{INS} \left(\mathbf{s}_0 + \Delta\mathbf{s}_0 + \Delta\mathbf{R}_m \cdot \mathbf{R}_m \cdot \Delta\mathbf{R}_s \mathbf{R}_s \cdot \mathbf{h}_{-(d+\Delta d)} \right) \qquad (10.1)$$

kjer imajo spremenljivke naslednje pomene:

$\mathbf{x}_L$ je vektor laserske točke na tleh v globalnem ortogonalnem koordinatnem sistemu (KS) (npr. WGS84)

$\mathbf{x}_0$ je vektor lokacije GPS-sprejemnika na nosilcu snemanja (helikopter ali letalo), določen v globalnem ortogonalnem koordinatnem sistemu, $\Delta\mathbf{x}_0$ natančnost določitve $\mathbf{x}_0$

$\mathbf{R}_{\mathrm{W}}$ je rotacijska matrika za prehod iz lokalnega ortogonalnega KS v globalni ortogonalni KS

$\mathbf{R}_{\mathrm{GEO}}$ je rotacijska matrika za prehod meritve iz geoida na elipsoid (lokalni ortogonalni KS)

$\mathbf{R}_{\mathrm{INS}}$ je rotacijska matrika za prehod iz lokalnega KS nosilca snemanja v KS, ki ga opisuje geoid (je definiran z lokalno navpičnico), $\Delta\mathbf{R}_{\mathrm{INS}}$ je napaka $\mathbf{R}_{\mathrm{INS}}$

$\mathbf{s}_0$ je vektor zamika med centrom GPS/INS-sistema in laserskega sistema, $\Delta\mathbf{s}_0$ je napaka $\Delta\mathbf{s}_0$

$\mathbf{R}_m$ je matrika nepravilne namestitve laserskega sistema v ničto lego, $\Delta\mathbf{R}_m$ je napaka $\mathbf{R}_m$

$\mathbf{R}_s$ je rotacijska matrika zasuka med ničto in trenutno lego laserskega žarka, definirana je s koti skeniranja, $\Delta\mathbf{R}_s$ so napake kotov skeniranja $\mathbf{R}_s$

$\mathbf{h}_{-(d+\Delta d)}$ vektor razdalje do laserske točke na tleh, $\Delta\mathbf{p}_s$ napaka sinhronizacije med INS, GPS in laserskim sistemom

Rotacija med trenutnim kotom ter ničtim kotom laserskega žarka – $\mathbf{R}_s$

Rotacija med trenutnim kotom in ničtim kotom laserskega žarka je definirana s trenutnim kotom skeniranja β_i[1]. Rotacijo $\mathbf{R}_s$ zapišemo z enačbo 5.4 (stran 54). Osi koordinatega sistema laserske naprave so definirane na naslednji način: Z_{LS} z ničto lego laserskega žarka, X_{LS} približno v smeri nosu letala, Y_{LS} skozi desno krilo (Schenk, 2001; Filin, 2001a). Na izmero trenutnega kota skeniranja vplivajo naslednje napake: indeksna napaka ε, napaka določitve širine pasu snemanja $\Delta\tau$ ter vertikalno in horizontalno neujemanje ravnine skeniranja s teoretično ravnino skeniranja (Slika 5.4 na strani 56). Indeksna napaka je lahko med 0,001° in 0,02° (Jutzi and Stilla, 2003; Schenk, 2001). Podobne vrednosti imajo tudi napake določitve širine pasu snemanja in napake neujemanja ravnine skeniranja s teoretično ravnino skeniranja, ki lahko dosežejo do 0.03° (Schenk, 2001; Latypov, 2005). Zato lahko matriko $\Delta\mathbf{R}_s$ zapišemo kot matriko z majhnimi koti (enačba 5.9 na strani 56).

Ujemanje INS/GPS in laserskega sistema – $\mathbf{R}_m$ in $\mathbf{s}_0$

Ujemanje INS/GPS in laserskega sistema predstavlja transformacijo laserskih meritev v koordinatni sistem nosilca laserskega skeniranja. Laserski sistem nosilca je definiran z: Z_b je pravokotna na trup letala in kaže poti tlom, X_b kaže točno proti nosu letala, Y_b pa je usmerjena skozi desno krilo (Slika 5.5 na strani 57). Transformacija laserskih meritev v koordinatni sistem nosilca je sestavljena iz translacije $\mathbf{s}_0$ in rotacije $\mathbf{R}_m$. Rotacijo $\mathbf{R}_m$ izmerimo v postopku kalibracije med letom. Vsebuje kote, ki so po navadi manjši od 3° (Bäumker in Heimes, 2002; Morin in El-Sheimy, 2002; Katzenbeisser, 2003; Skaloud in Lichti, 2006), zato jo lahko zapišemo z rotacijsko matriko za majhne kote (enačba 5.13 na strani 58). Napake določitve teh kotov $\Delta\mathbf{R}_m$ so odvisne od postopka kalibracije med letom (enačba 5.14 na strani 58). Po sami kalibraciji med letom lahko pričakujemo največje napake kotov do 0,01° (Schenk, 2001; Katzenbeisser, 2003). Napaka translacije $\Delta\mathbf{s}_0$ pa je odvisna od velikosti $\mathbf{R}_m$ in $\mathbf{s}_0$.

---

[1]V primeru skenerjev, ki tvorijo Z-obliko ali elipsasto obliko pasu snemanja (glej stran 45) moramo upoštevati še dodatna dva kota skeniranja v ostalih dveh ravninah. V teoretičnih izpeljavah po navadi predpostavimo, da obravnavamo skener z vzporednimi linijami skeniranja.

Rotacija med koordinatnim sistemom nosilca in navigacijskim koordinatnim sistemom − $\mathbf{R}_{INS}$

Rotacija iz koordinatnega sistema nosilca v navigacijski koordinatni sistem, ki je definiran z geoidom, je opredeljena z Z_N-osjo, usmerjeno v smeri navpičnice (proti centru geoida), X_N proti severu, Y_N proti vzhodu (Slika 5.9 na strani 63). Rotacijo iz koordinatnega sistema nosilca v navigacijski koordinatni sistem $\mathbf{R}_{INS}$ izmerimo z INS in opišemo z Eulerjevimi koti: pozibavanje ψ, zibanje ϕ in guganje θ. Tem kotom pravimo tudi INS-koti. Kota zibanja in guganja sta večinoma v velikostnem redu do $10°$, pozibavanje pa ima lahko vrednosti $0°$-$360°$. Rotacija $\mathbf{R}_{INS}$ je zapisana z enačbo 5.18 (stran 64).

Med napake $\mathbf{R}_{INS}$ oz. napake INS-kotov štejemo (Grejner-Brzezinska in Wang, 1998; Schenk, 2001): inicializacijske napake določitve začetne lege in hitrosti nosilca, napake ujemanj med sistemi (razlika med izhodiščem navigacijskega sistema in sistema nosilca), kompenzacijske napake INS-sistema ter napake gravitacijskega modela. Vse te napake je težko modelirati, saj so nekatere odvisne od časa, druge pa od smeri leta. Odvisno od cene INS-sistema, ki določa natančnost izdelave INS-sistema, lahko pričakujemo napake zibanja ϕ in guganja θ v okviru $0,004°$-$0,02°$ po kalibraciji med letom (Katzenbeisser, 2003; Skaloud in Lichti, 2006; Friess, 2006). Napaka pozibavanja ψ je dvakrat večja od napak zibanja in guganja (Katzenbeisser, 2003). Za razliko of INS-kotov so napake INS-kotov majhne in za njih lahko zapišemo rotacijsko matriko majhnih kotov (enačba 5.20 na strani 64).

Rotacija iz navigacijskega sistema v lokalni koordinatni sistem − $\mathbf{R}_{GEO}$

Lokalni koordinatni sistem GPS-sprejemnika na nosilcu snemanja je opredeljen z normalo na lokalni elipsoid. Razlika med navigacijskim in lokalnim sistemom je opisana z odklonom navpičnice, ki opisuje kot med normalo na lokalni elipsoid in navpičnico na geoidu. Največji odkloni navpičnice ne presegajo $0,0175°$ (Vaniček in Krakiwski, 1996; Pribičević, 2000). Rotacija $\mathbf{R}_{GEO}$ je zapisana z rotacijsko matriko za majhne kote (enačba 5.24 na strani 66). Ker so že odkloni navpičnice opisani z zelo majhnimi koti, predstavljajo napake izmere odklona navpičnice zanemarljive vrednosti.

Rotacija iz lokalnega v globalni koordinatni sistem − $\mathbf{R}_W$

Rotacija iz lokalnega v globalni koordinatni sistem predstavlja uskladitev med lokalnim koordinatnim sistemom GPS-sprejemnika na nosilcu snemanja, z izhodiščem v faznem centru GPS-sprejemnika in z osjo Z_{GEO} usmerjeno po normali globalnega elipsoida, in globalnim koordinatnim sistemom z izhodiščem v središču Zemlje (npr. WGS84).

10.3.2   Napake zaradi misije snemanja

Na natančnost zračnega laserskega skeniranja vplivajo tudi lastnosti postopka snemanja: višina leta, hitrost leta, odstotek preklopa med snemalnimi pasovi, oddaljenost referenčne GPS-postaje, zračna turbulenca in ostali vremenski pogoji, ki vplivajo na stabilnost leta in natančnost GPS-izmere.

Napaka sinhronizacije – $\Delta \mathbf{p}_s$

Laserski skener, INS in GPS uporabljajo vsak svoj lokalni čas in svojo frekvenco meritev. Največjo frekvenco meritev ima laserski skener s povprečnimi vrednostmi 20-40 kHz (Baltsavias, 1999a; Friess, 2006) in največjo 200 kHz (TopoSys, 2008). Sledi INS s povprečno frekvenco 100 Hz in največjo 200-400 Hz (Baltsavias, 1999a; Turton, 2006; Legat et al., 2006; Skaloud in Lichti, 2006). GPS meri položaj nosilca z mnogo manjšo frekvenco, povprečno 1-2 Hz in največjo 10 Hz (Baltsavias, 1999a; Maas, 2002; Schnurr et al., 2004; Legat et al., 2006). Vendar ima med vsemi sistemi GPS najnatančnejšo uro, katere neujemanje s standardnim GPS-časom lahko znaša največ 1 μs. Temu neujemanju pravimo napaka GPS-sinhronizacije. GPS-čas je referenca tudi za ostala dva merinika (laserski skener in INS) (Ding et al., 2005).

Neujemanje med INS-časom meritve in GPS-časom je napaka INS-sinhronizacije. Neujemanje med časom pulza laserskega skenerja in GPS-časom je napaka sinhronizacije laserskega skenerja. Vsota zgornjih napak sinhronizacije poda skupno napako sinhronizacije Δt, ki definira položajni vektor napake sinhronizacije $\Delta \mathbf{p}_s$. Po izvedeni povezavi GPS- in INS-meritev s Kalmanovim filtrom, velikost skupne napake sinhronizacije raste s povečevanjem oddaljenosti od ničte lege nosilca in s povečevanjem razlike v hitrosti med ničto in trenutno lego nosilca. Če uporabimo nosilec z 100 Hz INS in 1 Hz GPS, lahko določimo gladko trajektorijo nosilca s frekvenco 20 Hz (Ding et al., 2005). Vmesne meritve lege nosilca izračunamo na osnovi interpolacije. Tako lokacija nosilca ob vsaki laserski meritvi ni določena, ampak jo večinoma določimo na osnovi interpolacije. Zato v teh interpoliranih legah tudi velikost in obnašanje napake sinhronizacije ni znana in je ne moremo obravnavati kot sistematično (Schenk, 2001). Napaka sinhronizacije je v veliki meri odvisna od zračnih turbulenc, ki onemogočajo stabilen let nosilca v času snemanja. Katzenbeisser (2003) trdi, da Δt lahko obdržimo pod 10 μs, kar omeji vektor napake sinhronizacije na $5 \cdot 10^{-5}$ m. Vektor napake sinhronizacije lahko izračunamo z enačbo 5.33 (stran 70).

Napaka izmere lege faznega centra GPS – $\Delta \mathbf{x}_0$

Kljub temu, da so meritve INS in GPS integrirane v skupno meritev lege nosilca, vseh napak INS in GPS ne moremo v celoti odpraviti. To so neodstranjeni vplivi ionosfere, troposfere, razporeditve GPS-satelitov, večkratnih odbojev, dinamike leta in gravitacijskih anomalij. Zato je vpeljana napaka izmere lokacije z GPS, imenovana tudi napaka izmere lege faznega centra GPS – $\Delta \mathbf{x}_0$. Če so zgornji vplivi optimalni, se ta napaka obnaša skoraj sistematično in jo lahko določimo. V obratnem primeru pa je ne moremo določiti. V optimalnih pogojih je napaka lege faznega centra GPS-merilnika med 0,05 in 0,1 m (Schenk, 2001; Maas, 2003; Katzenbeisser, 2003; Lee et al., 2003; Skaloud in Lichti, 2006).

Vpliv višine leta na natančnost izmere razdalje

Razdalja med laserskim oddajnikom in tarčo na tleh, od katere se laserski žarek odbije, je odvisna od grupne hitrosti v_g potovanja laserskega žarka v zraku in izmerjenega časa med oddajo in sprejemom laserskega žarka. Natančnost izmerjenega časa je odvisna od natančnosti merilnika časa t_e, ki jo definira izdelovalec merilnikov in jo lahko obravnavamo kot konstanto. V realnosti ta napaka ni konstantna, saj na njeno velikost vplivajo spremembe v temperaturi in staranje merilnika. Po navadi je natančnost merilnika časa 1 μs (Baltsavias, 1999b). Da dosežemo natančnost meritve razdalje 3 cm, moramo uporabiti merilnik časa s frekvenco meritve časovnih intervalov 10 GHz (Katzenbeisser, 2003). Take merilnike časa uporabljajo za izmero laserskih žarkov z dolžino pulza 10 μs.

Zanemarimo spremembo grupne hitrosti med meritvami na morski obali ali pa v gorah na nadmorski višini 2000 m in v obeh primerih vzemimo enako višino leta 1000 m. Tedaj lahko pričakujemo napako v izmerjeni razdalji 6 cm zaradi neupoštevanja razlik v zračnem pritisku (Katzenbeisser, 2003).

10.3.3   Napake zaradi lastnosti tarče, od katere se odbije laserski žarek

Napake zaradi lastnosti tarče niso vključene v Schenkov model napak. Mi smo jih uvedli z vektorjem $\mathbf{c}(H)$, kjer je H višina vegetacije. V to skupino štejemo: napaka zaradi različne odbojnosti tarče, napake odvisne od višine vegetacije, dodatna vertikalna napaka v hribovitem svetu in napake zaradi motnosti vode, če uporabljamo batimetrični laser.

Napaka zaradi različne odbojnosti tarče

Odbojnost je odvisna od fizikalnih značilnosti površja tarče, od katerega se odbije laserski žarek (gladkost v valovni dolžini laserskega žarka). Mikrostrukturo tarč, od katerih se odbije laserski žarek, lahko delimo po Wagnerju (2005a) (Slika 4.12 na strani 44): točkovni objekti, manjši od obsega laserskega žarka na tleh; linearni objekti, kot so žice; ploskovni elementi, ki zajamejo celoten obseg laserskega žarka; volumenski objekti, kjer se v obsegu laserskega žarka nahaja veliko majhnih objektov na različnih višinah (npr. listje, trava). Različna mikrostruktura in odbojnost tarče vplivata na to, kolikšen del gostote moči laserskega žarka se bo od tarče odbil, in ali bo ta presegla prag laserskega sprejemnika. Če primerjamo dva objekta z enako odbojnostjo in različno mikrostrukturo, zadnja določa, kateri objekt bo laserski sprejemnik zaznal. Velja tudi obratno (Jutzi in Stilla, 2003; Wagner, 2005a).

Napaka zaradi višine vegetacije, snega ali motnosti vode pri batimetričnih laserjih

Enako kot pri fotogrametričnih postopkih izmere je zračno lasersko skeniranje odvisno od letnega časa, v katerem se izvaja. Kljub temu, da laserski sprejemnik lahko prepozna več odbojev istega laserskega pulza, ne vemo, ali je zadnji odboj res dosegel tla pod vegetacijo ali pa se je odbil že kje vmes. Če obravnavamo zadnji odboj, kot da se je odbil od tal, v resnici pa se je odbil na vmesni vegetaciji, s tem pridelamo višinsko napako zaradi vegetacije. Kakšen delež laserskih

odbojev se v resnici odbije od tal, določamo na osnovi deleža prodiranja. Določiti moramo dva deleža prodiranja: enega za zimsko obdobje brez listja in enega za poletno obdobje, ko je vegetacija gosta in s tem onemogoča prodiranje. Za bolj natančen prikaz tal pod vegetacijo je smiselna uporaba zračnega laserskega skeniranja v zimskem obdobju, saj s tem zmanjšamo napako, ki bi jo dobili zaradi vegetacije. Žal to ne velja za območja, poraščena večinoma z iglavci. Če uporabimo lasersko skeniranje s srednjo gostoto laserskih točk na enoto površine (2-10 točk/m^2) je razlika med digitalnima modeloma terena, izmerjenima pozimi ali poleti, manj kot 5 cm (Hyyppä et al., 2005; Ahokas et al., 2005b).

Vegetacija vpliva na natančnost digitalnega modela terena na dva načina: sistematični višinski zamik točk terena glede na prava tla in večja variabilnost v višinah za enako razgiban teren, kot če bi snemali tla brez vegetacije (Kraus in Pfeifer, 1998; Ahokas et al., 2003; Pfeifer et al., 2004; Gorte et al., 2005; Brzank et al., 2005; Hodgson et al., 2005; Hopkinson et al., 2005; Hyyppä et al., 2005; Hopkinson et al., 2006; Göpfert in Heipke, 2006; Barilotti et al., 2006; Raber et at., 2007). Sistematični višinski zamik večinoma opazimo v zelo gosti vegetaciji, kjer je večina zadnjih odbojev izmerjena nekje na sredi vegetacije, le redki zadnji odboji pa prodrejo prav do tal in so zato obravnavani kot grobe napake. Podobno je pri snemanju z batimetričnim laserjem v motni oz. kalni vodi, saj se količina delcev v vodi obnaša enako kot količina listja na drevju. Bolj je voda motna, manj lahko vanjo prodremo z laserjem. Pri snemanju zasneženih območij se debelina snežne oddeje obnaša podobno kot zelo gosta vegetacija. Laserski žarek prodre v sneg le kakšen centimeter (Deems in Painter, 2006), ostali sneg pa nam doda sistematično višinsko razliko glede na prava tla, ki se nahajajo pod snegom.

Različni avtorji (Hodgson in Bresnahan, 2004; Hodgson et al., 2005; Hopkinson et al., 2005; Reutebuch et al., 2003; Pfeifer et al., 2004; Ahokas et al., 2003; Raber et at., 2007) so preučevali povezavo med standardno deviacijo (SD) ali srednjim kvadratnim pogreškom (RMSE) in tipom vegetacije. Hopkinson et al. (2006) je ugotovil linearno povezavo $H = 2,5 \cdot SD$ med SD in višino vegetacije predvsem za nizke ($H < 2$ m) in visoke ($H > 4$ m) vegetacijske tipe, medtem ko pri gozdnem podrastju (2 m $< H <$ 4 m) ni ugotovil korelacije. Gorte et al. (2005) je ugotovil podobno povezavo $H = 2,2 \cdot SD$ - 0,03 za zelo nizko vegetacijo ($H < 20$ cm). Če primerjamo laserske podatke in terensko izmerjene kontrolne točke, ki jih obravnavamo kot točke brez napak, postane standardna deviacija višinska natančnost laserskih podatkov za določen vegetacijski tip (Pfeifer et al., 2004). Zato lahko kot prvi približek višinske napake, ki jo povzroči vegetacija, vzamemo kar izvedbo po Hopkinson et al. (2006) za nizko in visoko vegetacijo $\mathbf{c}(H)_z = H/2,5$ (v vektorski obliki je zapisana v enačbi 5.44 na strani 76).

Višina leta in gostota laserskih točk na enoto površine tudi vplivata na natančnost izmere digitalnega modela terena za posamezne vegetacijske tipe. Ahokas et al. (2003) in Hyyppä et al. (2005) pravita, da če povečamo višino leta s 400 m na 1500 m, povečamo variablinost izračunanega digitalnega modela reliefa za 50 % in seveda povečamo tudi sistematično napako višine, pridobljeno zaradi vegetacije. Večjo gostoto laserskih točk uporabljamo, globlje v vegetacijo uspemo prodreti, to velja tudi za iglaste gozdove. Za določitev terena pod vegetacijo s primerljivo natančnostjo, kot je določen teren na območjih brez vegetacije, moramo uporabiti zračno lasersko skeniranje z veliko gostoto točk 8-10 točk/m^2(Reutebuch et al., 2003; Chasmer et al., 2006; Deems and Painter, 2006). Raber et al. (2007) je našel le šibko povezavo med

tipom vegetacije in gostoto laserskih točk, z generalnim trenom povečanja napak, ko se zmanjša gostota točk.

Dodatna višinska napaka zaradi snemanja v hribovitem svetu

Večina testov dosežene točnosti zračnega laserskega skeniranja se je izvajala na ravnem ali rahlo hribovitem terenu, kjer so tudi določili mejne vrednosti posameznih prej omenjenih napak. Če snemamo v hribovitem svetu, moramo upoštevati še dva dodatna tipa napak (Baltsavias, 1999b; Schenk, 2001; Hodgson in Bresnahan, 2004; Deems in Painter, 2006): vpliv osnovnih planimetričnih sistematičnih napak na višinsko napako in vpliv velikosti odtisa laserskega žarka na tleh na višinsko napako (Slika 5.16 na strani 78).

Hodgson et al (2005) ni odkril dodatne višinske napake pri preučevanju natančnosti digitalnega modela terena za naklone terena, manjše od 8°. Skupne vertikalne napake za naklone terena 25° so dvakrat večje od osnovne vertikalne napake, ki jo dosežemo ob izmeri relativno ravnega terena (naklon manj kot 4°) (Hodgson in Bresnahan, 2004).

10.4   Izpeljava poenostavljenega modela napak zračnega laserskega skeniranja

Na osnovi podrobnega pregleda literature iz prejšnjega poglavlja, ki opisuje različne tipe napak, smo postavili robne pogoje za velikost posameznih napak, ki vplivajo na skupno oceno natančnosti laserskega skeniranja. Za opis vseh izvorov napak Schenkov model sistematičnih napak ne zadošča. Zato smo se odločili, da Schenkovemu modelu dodamo elemente, ki bodo opisali še ostale pomembne nesistematične vplive na skupno oceno natančnosti laserskega skeniranja. Tako smo mu dodali napako sinhronizacije $\Delta\mathbf{p}_s$ in napako vpliva vegetacije $\mathbf{c}(H)$.

Ker je Schenkov model odvisen od kota skeniranja, smo se odločili, da ga poenostavimo. Tipičen naročnik laserskega skeniranja, ki potrebuje podatke za potrebe lokalnega prostorskega načrtovanja, ne prejme podatkov o razdalji do točke in o kotu skeniranja, ampak že izračunane koordinate točke na tleh v formatu X,Y,Z. Ker tipičen naročnik tudi ni vešč uporabe linearne algebre, smo se odločili, da z analitično izpeljavo zapišemo enačbo, ki bo čim bolj enostavna.

Najprej smo s pomočjo simulacije v Matlabu preučili vpliv napak na originalni Schenkov model napak. Ugotovili smo, da je Schenkov model odvisen predvsem od kota skeniranja β_i in kota pozibavanja ψ, če sta kota zibanja ϕ in guganja θ majhna. Schenkov model ob spreminjajočem kotu pozibavanja opišemo s sinusuido, ki pa ima nezanemerljivo amplitudo (glej grafe v prilogi C na straneh 181-191). To nam ne omogoča hitrega izračuna srednje in največje napake.

Potem smo se lotili poenostavitve sistematičnih napak, ki so opisane z osnovnim Schenkovim modelom. Vpeljali smo naslednje poenostavitve:

- Ker pred samim snemanjem ne vemo, kakšen laserski skener bo izvajalec uporabil, smo členu $\mathbf{K}_1 \equiv \Delta\mathbf{R}_m\mathbf{R}_m\Delta\mathbf{R}_s$ priredili vrednosti, pridobljene iz literature. Po testiranju različnih vrednosti smo zaradi njihovega majhnega vpliva na celotno napako privzeli za kote v matriki $\mathbf{R}_m$ vrednosti 0,001°. Za $\Delta\mathbf{R}_m$ in $\Delta\mathbf{R}_s$ smo privzeli minimalne vrednosti

iz tabele 6.1 na strani 85.

- Predpostavili smo, da se izhodišča INS/GPS-sistemov in laserskega skenerja nahajajo na istem mestu, zato lahko $\mathbf{s}_0$ in njena napako $\Delta\mathbf{s}_0$ zanemarimo.

- Pri izpeljavi poenostavljenega modela natančnosti dovoljujemo kote zibanja in guganja do $\pm 6°$, saj s tem omejimo nosilec v čim bolj horizontalno lego glede na teren v času snemanja.

- Razdaljo $d + \Delta d$ izmerjeno z laserskim žarkom, smo nadomestili z njenim približkom v obliki višine leta h.

- V poenostavitvi nismo obravnavali rotacije iz lokalnega v globalni koordinatni sistem (Schenk, 2001). Predposavili smo, da je izhodišče lokalnega sistema kar v izhodišču globalnega, torej da se fazni center GPS na nosilcu nahaja kar v središču Zemlje in da koordinatne osi lokalnega in globalnega koordinatnega sistema sovpadajo.

- Definirali smo vektor z napakami $\mathbf{x}(h)_1 \equiv \mathbf{K}_1 \cdot \mathbf{R}_s \cdot \mathbf{h}_{-h} = \Delta\mathbf{R}_m \mathbf{R}_m \Delta\mathbf{R}_s \cdot \mathbf{R}_s \cdot \mathbf{h}_{-h}$ in vektor brez napak $\mathbf{x}(h)_1^* \equiv \mathbf{R}_m \cdot \mathbf{R}_s \cdot \mathbf{h}_{-h}$

Na osnovi zgornjih poenostavitev sedaj zapišemo enačbo skupne napake laserskega skeniranja:

$$\Delta\mathbf{x} = (\mathbf{R}_{\text{GEO}} \cdot \Delta\mathbf{R}_{\text{INS}} \cdot \mathbf{R}_{\text{INS}} \cdot \mathbf{x}(h)_1 - \mathbf{R}_{\text{GEO}} \cdot \mathbf{R}_{\text{INS}} \cdot \mathbf{x}(h)_1^*) + (\Delta\mathbf{p}_s + \Delta\mathbf{x}_0 + \mathbf{c}(H)) \quad (10.2)$$

V prvem oklepaju enačbe 10.2 se nahajajo osnovne sistematične napake $\Delta\mathbf{x}_s$, v drugem oklepaju pa si sledijo še napaka sinhronizacije $\Delta\mathbf{p}_s$, napaka določitve faznega centra GPS $\Delta\mathbf{x}_0$ in napaka, pridobljena zaradi vegetacije $\mathbf{c}(H)$.

10.4.1   Osnovne sistematične napake — $\Delta\mathbf{x}_s$

Da bi lahko poenostavili enačbo 10.2, smo najprej preučili vpliv $\mathbf{R}_{\text{GEO}}$. V Sloveniji lahko na Besselovem elipsoidu izmerimo srednjo vrednost odklona navpičnice 0,0028°, največjo pa 0,0055° (Pribičević, 2000). Razlika med tema dvema vrednostima, nam prinese razliko v posamezni koordinatni komponenti osnovne sistematične napake samo 10^{-5} m. Zato lahko matriko $\mathbf{R}_{\text{GEO}}$ v enačbi 10.2 zanemarimo.

INS-koti in napake INS-kotov imajo največji vpliv na celotno vrednost sistematične napake. Na osnovi splošne predpostavke, da dovoljujemo kote zibanja in guganja do $\pm 6°$, dobimo povprečno vrednost kotov zibanja ϕ in guganja θ 0°, povprečno velikost kotov pa 3° (glej sliko 6.3 na strani 87). Če smo še bolj strogi in dovoljujemo kote zibanja in guganja samo do $\pm 2°$, dobimo povprečno vrednost kotov ponovno 0° in povprečno velikost kotov 1°. V simulaciji oz. našem analitičnem izvajanju poenostavitve bomo uporabili samo povprečno velikost kotov. Pozibavanje ψ nosilca laserskega skenerja se spreminja s časom in smerjo, v katero je nosilec obrnjen, zato je lahko kot pozibavanja predstavljen z vrednostmi 0-360°.

Pri testiranju obnašanja osnovne sistematične napake s spreminjajočo matriko $\Delta\mathbf{R}_{\text{INS}}$ smo uporabili realne vrednosti napak INS-kotov, ki se dandanes uporabljajo pri zračnem laserskem

skeniranju. V večini naših primerov smo uporabili vrednosti napake zibanja in guganja $\Delta\phi = \Delta\theta = 0.005°$ in napako pozibavanja $\Delta\psi = 0.007°$.

Povprečna vrednost osnovne sistematične napake

S simulacijo smo ugotovili, da so osnovne sistematične napake najbolj odvisne od kota skeniranja β_i, kota pozibavanja ψ in višine snemanja. Ob predostavki, da se kot pozibavanja med letom spreminja enakomerno, lahko izračunamo **povprečno vrednost osnovnih sistematičnih napak za različne kote skeniranja** $\Delta\mathbf{x}_{s\_ave}(\beta)$ kot integral po kotu pozibavanja 0°-360° za vsako koordinatno komponento $\Delta\mathbf{x}_s$ posebej:

$$\Delta\mathbf{x}_{s\_ave}(\beta) = < \Delta\mathbf{x}_s > = \left[\begin{array}{c} \frac{1}{2\pi} \int_0^{2\pi} \Delta X_s d\psi \\ \frac{1}{2\pi} \int_0^{2\pi} \Delta Y_s d\psi \\ \frac{1}{2\pi} \int_0^{2\pi} \Delta Z_s d\psi \end{array} \right] \tag{10.3}$$

Povprečno vrednost $\Delta\mathbf{x}_{s\_ave}$ **neodvisno od kota skeniranja** pa izračunamo kot dvojni intergral po kotu pozibavanja in kotu skeniranja, od najmanjše do največje vrednosti kota skeniranja:

$$\Delta\mathbf{x}_{s\_ave} = << \Delta\mathbf{x}_s >> = \left[\begin{array}{c} \frac{1}{2\pi} \int_0^{2\pi} d\psi \int_{-\beta_0}^{\beta_0} d\beta \Delta X_s \\ \frac{1}{2\pi} \int_0^{2\pi} d\psi \int_{-\beta_0}^{\beta_0} d\beta \Delta Y_s \\ \frac{1}{2\pi} \int_0^{2\pi} d\psi \int_{-\beta_0}^{\beta_0} d\beta \Delta Z_s \end{array} \right] \tag{10.4}$$

Izračunani integrali po posamezni komponenti so izpisani na strani 88:

- povprečna vrednost odvisna od kota skeniranja v enačbi 6.12

- povprečna vrednost neodvisna od kota skeniranja v enačbi 6.13

Vrednosti naših poenostavljenih modelov povprečnih vrednosti $\Delta\mathbf{x}_s$ lahko izračunamo, če poznamo vrednosti napake INS-kotov in višino leta. Če primerjamo velikosti povprečnih planimetričnih komponent in višinske komponente osnovne sistematične napake, ugotovimo, da so povprečne vrednosti višinske komponente zelo majhne (velikostni razred 1 cm).

Največja vrednost osnovne sistematične napake

Če planiramo naročilo zračnega laserskega skeniranja, nas poleg povprečne vrednosti napake zanima tudi največja napaka, ki se nahaja v celotnem oblaku laserskih točk. Ta napaka nam pove mejno natančnost naših podatkov. Največje napake se nahajajo pri največjih kotih skeniranja. Žal pa je največja napaka, če uporabimo konstanten kot skeniranja, odvisna od kota pozibavanja in je zato ne moremo preprosto izračunati.

Najprej moramo izračunati kot pozibavanja, pri katerem se pojavlja največja napaka. Za vsako koordinatno komponento osnovne sistematične napake $(\Delta X_s, \Delta X_s, \Delta X_s)$ izračunamo odvod po kotu pozibavanja. Odvod $\partial\Delta\mathbf{x}_s / \partial\psi$ nam poda kote pozibavanja, pri katerih se pojavijo največje ali najmanjše vrednosti $\Delta\mathbf{x}_s$. Katera vrednost je največja, ugotovimo z izračunom drugega

odvoda $\Delta^2 \mathbf{x}_s / \partial \psi^2$ (glej prilogo C na strani 180). Kot pozibavanja, pri katerem je drugi odvod manjši od nič, predstavlja največjo vrednost funkcije $\Delta \mathbf{x}_s$. Torej če želimo izračunati največjo vrednost osnovne sistematične napake, moramo izračunati vsaj tri vrednosti (prvi odvod, drugi odvod in izračun same vrednosti napake).

Da bi dobili enostavnejši postopek, kako izračunati največjo napako, smo se odločili preveriti korelacijo med največjo napako in povprečno napako, ki je neodvisna od kota skeniranja in smo jo izračunali v prejšnjem razdelku. Na sliki 6.7 (stran 94) so predstavljene največje vrednosti osnovne sistematične napake pri kotu skeniranja $20°$ in povprečna osnovna sistematična napaka, ki je neodvisna od kota skeniranja. Izračunali smo jih za različne višine leta in različne kombinacije napak INS-kotov. Ugotovili smo, da so napake med seboj linearno korelirane. Z izravnavo na osnovi indirektnih opazovanj po metodi najmanjših kvadratov (glej prilogo D na strani 193) smo izračunali linearno regresijo za 32 vrednosti $\Delta \mathbf{x}_{s\_ave}$ in $\Delta \mathbf{x}_{s\_max}$. Med sabo smo povezali naslednje parametre: $\Delta \mathbf{x}_{s\_ave}$, $\Delta \mathbf{x}_{s\_max}$, napako pozibavanja $\Delta \psi$, napako zibanja in guganja $\Delta \phi$ ($\Delta \phi = \Delta \theta$) ter višino leta h. S pomočjo t-Studentove testne statistike in ob stopnji značilnosti testa $\alpha = 95 \%$ smo izločili parametre z neznačilnim vplivom. Končno linearno povezavo med največjo in povprečno osnovno sistematično napako zapišemo kot:

$$\Delta \mathbf{x}_{s\_max} = \begin{bmatrix} |\Delta X_{s\_max}| = |\Delta Y_{s\_max}| \\ \\ \Delta Z_{s\_max} \end{bmatrix} = \tag{10.5}$$

$$= \begin{bmatrix} \Delta X_{s\_ave} \cdot 1.44 + \Delta \psi \cdot 5.60 + \Delta \phi \cdot (-7.59) + h \cdot 1.79 \cdot 10^{-4} \\ \Delta \phi \cdot (-8.74) + h \cdot 2.11 \cdot 10^{-4} + 0.15 \end{bmatrix}$$

V enačbi 10.5 je višina leta zapisana v metrih, napake, povezane z INS-koti, pa v stopinjah.

10.4.2 Napake sinhronizacije, lege faznega centra GPS in napake, povezane z višino vegetacije

Sedaj moramo k povprečni in največji vrednosti osnovne sistematične napake prišteti še napako sinhronizacije $\Delta \mathbf{p}_s$, napako lege faznega centra GPS $\Delta \mathbf{x}_0$ in napako, povezano z višino vegetacije, $\mathbf{c}(H)$.

Ker lahko ob idealnih pogojih pričakujemo vektor napake sinhronizacije, ki ni večji od $5 \cdot 10^{-5}$ m, lahko njegove posamezne komponente zanemarimo. Obratno je z napako lege faznega centra GPS, ki ob idealnih pogojih znaša $|\Delta \mathbf{x}_0| = 0{,}05$–$0{,}10$ m in je zato ne moremo zanemariti.

Napake, odvisne od višine vegetacije, vplivajo samo na višinsko komponento skupne napake in so odvisne od posameznega tipa vegetacije. Zato je pomembno, da že med samim procesom naročanja podatkov zračnega laserskega skeniranja razmejimo območje po glavnih vegetacijskih tipih. Na primer, če obravnavamo iglast gozd kot tla brez vegetacije, bomo pridelali 0,2-metrsko višinsko napako zaradi vegetacije ob snemanju na višini 1000 m.

Dokončno poenostavljeno obliko enačbe za izračun povprečnih in največjih napak laserskega skeniranja zapišemo:

$$\Delta\mathbf{x}_{ave} = \Delta\mathbf{x}_{s\_ave} + \Delta\mathbf{x}_0 + \mathbf{c}(H) \tag{10.6}$$

$$\Delta\mathbf{x}_{max} = \Delta\mathbf{x}_{s\_max} + \Delta\mathbf{x}_0 + \mathbf{c}(H) \tag{10.7}$$

Naš poenostavljen model napak ni odvisen od kota skeniranja in kota pozibavanja nosilca laserskega skeniranja ter podrobnih tehničnih specifikacij posameznega sistema za lasersko skeniranje. Vnaprej moramo predvidevati samo višino leta, velikosti napak INS-kotov in tip vegetacije, ki ga bomo posneli.

10.5   Optimalna gostota točk zračnega laserskega skeniranja

Z geometrično ločljivostjo karte opredelimo preciznost izdelave karte. Geometrično ločljivost izračunamo s pomočjo grafične natančnosti in merila karte. Grafična natančnost je definirana kot najožja debelina črte na izrisani karti. Pravilnik o znakih za temeljne topografske načrte (1982) je opredelil najožjo debelino črte na 0,13 mm, minimalno dimenzijo entitete, predstavljene na karti, pa 0,5 mm za različne kartografske prikaze Slovenije. Če to grafično natančnost uporabimo pri izrisu karte merila 1 : 1000, dobimo geometrično ločljivost karte 0,13 m v naravi. Maling (1989) definira 0,25 mm kot grafično natančnost karte. Grafična natančnost omejuje tudi velikost minimalnih entitet, ki so na karti prikazane.

Ker se v tem doktorskem delu ukvarjamo z geodetskimi podatki, ki jih potrebujemo pri lokalnem prostorskem načrtovanju, smo princip prenosa grafične natančnosti v geometrično ločljivost izvedli tudi za nekaj drugih podatkovnih baz, kjer bi lahko uporabili zračno lasersko skeniranje.

Kot prostorske podlage za lokalno prostorsko načrtovanje večinoma uporabljamo DTK5 ali pa geodetske načrte v merilu 1 : 5000, njihova geometrična ločljivost je 0,65 m. Na njih lahko prikažemo še podatke Katastra stavb in zemljiškokatastrskega prikaza. Osnovni lokacijski podatki Katastra stavb so bili izvrednoteni na osnovi fotogrametrične stereorestitucije s posnetkov CAS. Ker pa so posnetki CAS namenjeni večinoma za merila 1 : 5000, lahko opredelimo geometrično ločljivost Katastra stavb preko vira zajema na 0,65 m. V postopku zajema stavb je bila geometrična natančnost zajema definirana na 0,5 m, kar se dobro ujema z našim zgornjim izvajanjem. Register nepremičnin povzema lokacijske podatke iz Katastra stavb, torej je njegova lokacijska natančnost enaka.

Geometrična ločljivost Zbirnega katastra gospodarske javne infrastrukture je razdeljena v 5 razredov (natančnost boljša od 0,1 m, 0,1–1 m, 1–5 m, natančnost slabša od 5 m, neznana natančnost). Večina podatkov se nahaja v prvih dveh razredih, zato lahko rečemo, da je povprečna geometrična ločljivost v Zbirnem katastru gospodarke javne infrastrukture boljša od 1 m. Če bi te podatke predstavili na karti merila 1 : 5000, bi s tem zadostili pogojem za grafično natančnost 0,2 mm, ki ustrezajo grafični natančnosti kot jo je opredelil Maling (1989).

Z uporabo Nyquistove frekvence oz.   teorema vzorčenja pa preko poznavanja minimalne

geometrične ločljivosti določimo potrebno gostoto laserskih točk na enoto površine, ki bo zadostila zahtevi po določeni geometrični ločljivosti. Najmanjša frekvenca vzorčenja, ki nam omogoči zajem določenih objektov, je enaka polovici frekvence pojavljanja teh objektov v naravi. Geometrično ločljivost obravnavamo kot frekvenco objektov v naravi. Na sliki 7.3 (stran 104) vidimo, kako določimo minimalno gostoto laserskih točk, ki nam omogoči zajem z določeno geometrično ločljivostjo. Z znano geometrično ločljivostjo karte GA lahko izračunamo najmanjšo potrebno gostoto točk $\rho_t = 1/(GA/2)^2$. Grafična natančnost 0,2 mm karte merila 1 : 5000, ki da geometrično ločljivost 1 m, zahteva gostoto laserskih točk 4 točke/m^2.

Laserske točke pa niso razporejene samo v eni ravnini, ampak so prostorsko razpršene. Zato teoretična minimalna gostota točk na enoto površine ni dovolj za izdelavo izdelkov z zahtevano geometrično ločljivostjo. Na primeru oblaka laserskih točk iz Nove Gorice z gostoto 15–20 točk/m^2 (podrobnosti o testnem setu podatkov so v prilogi E na strani 201) smo preučili vpliv različnih vegetacijskih tipov na delež prodiranja laserskega žarka do tal. Deleže prodiranja do tal smo izmerili za: mediteransko vegetacijo, gost gozd, mešano rastje (travniki, vinogradi in gozd) in za poseljeno območje (hiše, mešana vegetacija ob hišah). Če do tal prodre zelo majhen delež vseh točk, moramo minimalno gostoto točk, zahtevano z geometrično ločljivostjo, povečati. Z upoštevanjem deleža prodiranja izračunamo optimalno gostoto laserskih točk, ki nam v resnici omogoča zajem podatkov z določeno geometrijsko ločljivostjo. Optimalno gostoto točk izračunamo z enačbo, kjer je GA zahtevana geometrična ločljivost:

$$\rho_o[\text{točk/m}^2] = \frac{1}{(GA/2)^2} \cdot \frac{100}{\text{delež prodiranja}} \tag{10.8}$$

Za štiri vegetacijske tipe, v katerih smo testirali delež prodiranja in predvideno grafično natančnost 0,2 mm v merilu 1 : 5000, smo dobili naslednjo optimalno gostoto točk: za mediteransko vegetacijo 20 točk/m^2, za gost gozd 67 točk/m^2, za mešano rastje in poseljena območja 12 točk/m^2.

10.6   Predlagana metodologija izdelave geodetskih podatkov z upoštevanjem zračnega laserskega skeniranja

Z znano a-priori točnostjo zračnega laserskega skeniranja in znano optimalno gostoto laserskih točk pred snemanjem lahko opredelimo, kakšne podatke zračnega laserskega skeniranja potrebujemo za izdelavo oz. posodabljanje določene geodetske podatkovne baze.

Zračnega laserskega skeniranja zaenkrat še ne moremo vpeljati v uradne evidence Zemljiškega katastra in Katastra stavb, saj se ti dve evidenci vzdržujeta le na podlagi detajlnih terenskih meritev. Metoda vzrževanja teh dveh evidenc je predpisana s podzakonskimi akti. Če bi želeli spremeniti zakonski akt, bi morali predhodno izvesti detajlno študijo primernosti nove metode zajema. Na osnovi rezultatov doktorske naloge trdimo, da lahko vnaprej opredelimo zahtevano natančnost in gostoto točk, ki nam bi omogočila vzdrževanje obeh evidenc tudi s pomočjo zračnega laserskega skeniranja.

Zračno lasersko skeniranje bi lahko vpeljali tudi v izmero nadzemnih vodov Zbirnega katastra gospodarske javne infrastrukture.

Zračno lasersko skeniranje z gostoto točk 20 točk/m^2, natančnostjo INS-kotov zibanja in guganja 0,005° in pozibavanja 0,007° ter z višino leta 800 m nad tlemi pa zadosti potrebam po geometrični ločljivosti in položajni natančnosti kart merila 1 : 5000 (slika 8.5 na strani 121). Zračno lasersko skeniranje s takimi karakteristikami je zadosten vhodni podatek za samostojen zajem in posodabljanje geodetskih načrtov 1 : 5000 in DTK5. Če pa poleg zračnega laserskega skeniranja uporabimo še aerofotografije, se sama identifikacija objektov poenostavi, s čimer lahko postopek zajema podatkov pospešimo. Takšna kombinirana metodologija zajema bi omogočila tudi natančnejši zajem podatkov, saj ne bi bili omejeni z višinsko natančnostjo stereorestitucije. Natančnost zajema višin je v primeru fotogrametričnega postopka v veliki meri odvisna od natančnosti operaterja. Natančnost višin je v primeru kombinirane metodologije zajema odvisna samo od natančnosti zračnega laserskega skeniranja.

Največ pa bi z vpeljavo zračnega laserskega skeniranja pridobil državni digitalni model reliefa (DMR). Tu nismo omejeni z visoko natančnostjo laserskega skeniranja in veliko gostoto točk, saj bi že zračno lasersko skeniranje s slabo natančnostjo INS-kotov in majhno gostoto točk (1 točka/m^2), občutno izboljšalo natančnost trenutnih DMR-jev. Tako izdelan DMR bi imel enovito natančnost v nezaraščenih in zaraščenih območjih, s čimer bi odpadla dvojna definicija natančnosti trenutnih DMR-jev. Iz višinske natančnosti 1,5 m v nezaraščenem in 6,5 m v zaraščenem delu, ki je bila predpisana za DMR 25, bi prišli na višinsko natančnost obeh tipov območij 0,3 m ali manj (tu je že vključena tudi napaka zaradi višine vegetacije). Tako izboljšan DMR bi predstavljal tudi veliko boljšo podlago za izdelavo ortofotografij na podlagi cikličnega aerosnemanja. Ko bi se izboljšala natančnost aerofotografij, bi se izboljšala tudi natančnost fotointerpretacije (slika 8.6). S tem bi se izboljšale tudi evidence dejanske rabe prostora.

10.7   Sklep

Zračno lasersko skeniranje se lahko uporablja kot samostojna tehnika zajema ali pa jo kombiniramo z drugimi metodami daljinskega zaznavanja. V tem doktorskem delu smo analitično opredelili minimalne pogoje, ki opredeljujejo, kakšne podatke zračnega laserskega skeniranja potrebujemo, da jih lahko uporabimo kot samostojno tehniko zajema pri izdelavi oz. posodobljanje geodetskih podatkov, ki se uporabljajo v lokalnem prostorskem načrtovanju. S tem omogočimo opredelitev zračnega laserskega skeniranja tudi, ko je kombinirano z drugimi metodami daljinskega zaznavanja.

Najprej smo na osnovi detajlnega pregleda literature določili vire napak zračnega laserskega skeniranja, njihovo obnašanje in tipične velikosti. Nato smo uporabili rigorozni Schenkov model napak kot osnovo za analitično izpeljavo a-priori poenostavljenega modela napak laserskega skeniranja. S pomočjo simulacije napak v Matlabu smo primerjali obnašanje Schenkovega modela in poenostavljenega modela napak. Poenostavljeni model napak ni odvisen od kota skeniranja in kota pozibavanja nosilca laserskega skeniranja ter podrobnih tehničnih specifikacij

posameznega sistema za lasersko skeniranje. Vnaprej moramo predvidevati samo višino leta, velikosti napak INS-kotov in vegetacijski tip, ki ga bomo posneli. Rezultat poenostavljenega modela napak lahko izračunamo brez uporabe linearne algebre. S tem odpremo možnosti za vpeljavo zračnega laserskega skeniranja tudi uslužbencem, ki skrbijo za organizacijo izvedbe prostorskega načrtovanja na različnih nivojih odločanja (lokalni, regionalni in državni deležniki prostorskega načrtovanja). S poenostavljenim a-priori modelom napak lahko sedaj preizkušamo, kateri robni pogoji nam dajo zadovoljivo točnost laserskega skeniranja za naše konkretne namene.

Preučili smo še povezavo med geometrično ločljivostjo določene podatkovne zbirke oz. grafično natančnostjo določene prostorske podlage in zadostno gostoto laserskih točk na enoto površine, ki nam tako geometrično ločljivost omogoča. Z Nyquistovo frekvenco smo povezali geometrično ločljivost in gostoto laserskih točk. Tako dobljeno teoretično vrednost smo nadgradili z upoštevanjem deleža prodiranja laserskega žarka skozi različne tipe vegetacije, ki smo ga izmerili na testnem primeru (mediteranska vegetacija, gost gozd, mešano rastje in poseljeno območje). Izračunali smo optimalno gostoto laserskih točk za posamezni testiran tip vegetacije.

Znani a-priori natančnost zračnega laserskega skeniranja in optimalna gostota laserskih točk omogočita uvajanje zračnega laserskega skeniranja v metodologijo zajema za različne geodetske podatke, ki se uporabljajo v prostorskem načrtovanju.

Osrednji znanstveni prispevek doktorske naloge je analitična izpeljava poenostavljenega modela napak, ki nam omogoči analitično opredelitev robnih pogojev pri naročilu zračnega laserskega skeniranja. Teoretična gostota potrebnih laserskih točk na enoto površine je izpeljana analitično iz geometrijske ločljivosti določene baze geodetskih podatkov ali karte. Teoretična gostota pa je nadgrajena še na osnovi testa na realnem primeru oblaka laserskih točk. S tem smo pridobili optimalno praktično gostoto laserskih točk, potrebno za izdelavo geodetskih podatkov, ki so opredeljeni z določeno geometrično ločljivostjo. Pred naročilom zračnega laserskega skeniranja moramo sedaj določiti samo: natančnost INS-kotov, višino leta, tip vegetacije v katerem bomo snemali in geometrično ločljivost geodetskih podatkov, za katere nameravamo zračno lasersko skeniranje uporabiti.

Opisani robni pogoji so osnova za predlog izboljšave metodologije zajema podatkov za različne geodetske podatke, ki se uporabljajo v lokalnem prostorskem načrtovanju. Zračno lasersko skeniranje lahko uvedemo v vse obravnavane geodetske zbirke. Največ pa bi pridobili, če bi zračno lasersko skeniranje uvedli v izdelavo državnega DMR-ja, saj bi s tem omogočili tudi izdelavo natančnejših ortofotografij in naknadno tudi natančnejše baze dejanske rabe prostora.

Rezultate doktorske naloge lahko apliciramo tudi izven Slovenije, saj sta poenostavljen a-priori model napak, prav tako tudi optimalna gostota točk na enoto površine splošni količini. Izsledki so bili v tej nalogi sicer aplicirani na primer geodetskih podatkov namenjenih lokalnemu prostorskemu načrtovanju v Sloveniji. Vendar s poznavanjem geometrijske ločljivosti drugih geodetskih izdelkov izven našim meja, lahko izračun a-priori model napak, izračun optimalne gostote točk in optimizacijo metodologije zajema apliciramo tudi širše.

11   SUMMARY

Aerial laser scanning, also named LIDAR, is becoming a widely used technique for acquisition of topographic or bathymetric data. It is an active system, where sensor measures the time interval between the laser pulse transmission and the pulse echo return to the receiver. This time interval defines the distance from the transmitter to the target and back to the receiver, which together with the scan angle define the location of the target in physical space. Additional information to the location is the intensity or amplitude of the returning echo. This can give us a lot of information on the material from which the echo reflected.

Aerial laser scanning technique can be used as a stand-alone technique or in combination with the multi- or hyperspectral photogrammetric data. Aerial laser scanning can be effectively implemented in the production of geodetic data used in local spatial planning. Traditionally, photogrammetric and geodetic methods have been applied for local spatial data acquisition, so the existing processing methodology is based upon these methods. To enable an optimization of data processing methodology by applying aerial laser scanning this thesis developed two advantages in the decision-making process: the simplified a-priori error model which can be easily used for aerial laser scanning planning, and a model for aerial laser scanning point density prediction on the basis of requred end-product precision.

Spatial planning is an interdisciplinary science, which defines how the physical space on the national, regional or local level should develop. Spatial planning of Slovenia is mainly regulated by the Spatial planning act (2007). This act defines possible geodetic data used for spatial planning, spatial planning stakeholders, legal procedures how spatial planning has to be conducted, and the intention of spatial planning. Therefore in the first part of this thesis the geodetic data, which can be used for local spatial planning, and their current acquisition methodology are described. The following geodetic data are described: nationwide digital terrain models, ortophotographies in the scale $1:5000$, national topographic maps in the scale $1:5000$ (DTK5), Land cadastre, Building cadastre, Real estate register, Register of spatial units, Register of geographical names, Cadastre of public infrastructure, databases on land use.

In the second part physical background of aerial laser scanning is described: different types of products (stand-alone aerial topographic and bathymetric laser scanning or combinations with multi- and hyperspectral photogrammetric data), the intensity of received laser echo, the principle of laser measurements (range resolution, horizontal resolution, reflectivity and laser equation) and the geometrical characteristics of the flight. To enable aerial laser scanning a-priori error assessment, a detailed study of lasers scanning errors is given in the next chapter.

Different error sources have been identified and evaluated according to error sizes and importance. As a base for the error model development and simplification, the Schenk's geolocation equation was used. The error sources were divided in three groups: basic systematic errors, flight mission related errors and errors caused by the target characteristics (the object from which the laser echo reflects). The basic systematic errors are: scan angle errors, mounting bias errors, errors of INS angles, error of rotation from navigational to local reference frame and errors of rotation from local to global reference frame. The errors resulting from the laser scanning mission are: influence of flying height, synchronization errors, gravity model errors and error of GPS sensor positioning errors. The errors resulting from the characteristic of the target are: error caused by reflectivity and structure of the target, height error resulting from the thickness of vegetation and snow, turbidity of water for bathymetric laser scanners and additional vertical error in steeper terrain.

Analytically a simplified a-priori error model was developed in this thesis, which returns an average and maximal error size for the whole aerial laser scanning point cloud. This simplified error model is independent from the scan and heading angles. To calculate the average and maximal error sizes, we have to decide only on the permitted size of INS errors (roll, pitch and heading error components), GPS sensor positioning errors, vegetation height related error and flying height. Therefore our simplified error model provides an easy tool to define possible error sizes in aerial laser scanning a-priori to laser scanning ordering. Just two simple equations define the average and maximal possible error sizes.

To enable easier decision making, one has to decide in advance also on the level of detail which should be present in the end-product – the geodetic data for local spatial planning. The level of detail, which can be acquired from aerial laser scanning, defines the precision of the end-product. The precision which can be acquired from the laser scanning data is connected to the laser scanning point density by the Nyquist frequency (minimal sampling density). Based on a practical test also a correction factor was introduced which includes the penetration rate in a certain vegetation type. Again a simple equation was given, which can be used to define a-priori an optimal laser scanning point density for a certain end-product.

In the last chapter of the thesis, the proposal for the methodology change from photogrammetric stereo-restitution to stand alone aerial laser scanning for the next geodetic data, used in Slovenia for local spatial planning, was given: the topographic maps in scale 1 : 5000, Real estate register and for above-ground layers of the Cadastre of public infrastructure.

12   POVZETEK

Zračno lasersko skeniranje, imenovano tudi LIDAR, se čedalje več uporablja za zajem topografskih in batimetričnih podatkov. Uporablja aktivni sistem, kjer senzor meri čas med oddajo in sprejemom laserskega pulza. Ta čas določa razdaljo med sprejemnikom in tarčo, od katere se laserski žarek odbije. Iz te razdalje in kot skeniranja izračunamo lego tarče v prostoru. Dodaten podatek o tarči, ki ga dobimo poleg razdalje in kota skeniranja, je še intenziteta odboja. Intenziteta oboja pove veliko o materialu, od katerega se je laserski žarek odbil.

Zračno lasersko skeniranje se lahko uporablja kot samostojna tehnika zajema ali pa jo kombiniramo z drugimi fotogrametričnimi podatki (multi- in hiperspektralni posnetki). Zračno lasersko skeniranje lahko efektivno uvedemo v zajem podatkov za različne geodetske podatke, ki se uporabljajo kot podloge v lokalnem prostorskem načrtovanju. Tradicionalno so za te geodetske podatke v uporabi različne fotogrametrične in geodetske metode izmere, zato trenutna metodološka navodila za izdelavo le-teh izdelkov temeljijo na prej naštetih metodah. Da bi omogočili lažje odločevanje za uporabo zračnega laserskega skeniranja tudi za geodetske podatke, ki se uporabjajo pri lokalnem prostorskem načrtovanju, smo v našem delu razvili dva postopka za pomoč: poenostavljen a-priori model napak zračnega laserskega skeniranja, ki je uporaben za naročanje laserskih podatkov, ter model za napoved optimalne gostote laserskih točk glede na zahtevano geometrično ločljivost končnega izdelka.

Prostorsko načrtovanje je interdisciplinarna znanost, ki se ukvarja s celostnim urejanjem prostora držav, regij in občin. Prostorsko načrtovanje v Sloveniji temelji večinoma na prostorski zakonodaji – Zakon o prostorskem načrtovanju (2007). Ta zakon opredeljuje podatke, ki se lahko uporabljajo za potrebe prostorskega načrtovanja, deležnike prostorskega načrtovanja, zakonsko opredeljene postopke za izvajanje prostorskega načrtovanja in sam namen prostorskega načrtovanja. Zato smo v prvem delu doktorskega dela opisali geodetske podatke, ki jih lahko uporabljamo pri prostorskem načrtovanju, in trenutno prepisano metodologijo njihove izdelave. Opisani so naslednji podatki: digitalni modeli reliefa, ortofotografije v merilu 1 : 5000, državne topografske karte merila 1 : 5000 (tudi geodetski načrt istega merila), Zemljiški kataster, Kataster stavb, Register nepremičnin, Register prostorskih enot, Register zemljepisnih imen, Zbirni kataster gospodarske javne infrastrukture ter različne baze dejanske rabe prostora.

Opisane so fizikalne značilnosti zračnega laserskega skeniranja: različne vrste izdelkov (samostojno zračno topografsko ali batimetrično lasersko skeniranje, ali le-to kombinirano z različnimi fotogrametričnimi snemanji), intenziteta odboja, princip laserskih meritev (ločljivost razdalje, ločljivost po planimetriji, odbojnost in enačba laserja) ter na koncu še geometrične značilnosti

misije snemanja. V naslednjem poglavju smo opisali še podrobno princip laserskega skeniranja in napake laserskega skeniranja.

Opisali in ovrednotili smo, glede na velikost in pomen, različne vire napak. Kot osnovo za izvajanje poenostavljenega modela napak smo vzeli Schenkovo geolokacijsko enačbo laserskega skeniranja. Vire napak smo razdelili v tri skupine: osnovne sistematične napake, napake misije snemanja in napake zaradi lastnosti tarče od katere se odbije laserski žarek. V skupino osnovnih sistematičnih napak sodijo: napaka kotov skeniranja, napaka ujemanja med INS/GPS in laserskim sistemom, napake INS-kotov, napake rotacije iz navigacijskega sistema v lokalni koordinatni sistem, napake rotacije iz lokalnega v globalni koordininatni sistem. Med napake zaradi misije snemanja sodijo: napaka sinhronizacije, napaka izmere lege faznega centra GPS-sistema, vpliv višine na natančnost izmerjene razdalje. Med napake zaradi lastnosti tarče, od katere se odbije laserski žarek, sodijo: napaka zaradi različne odbojnosti tarče, napaka zaradi višine vegetacije, snega ali celo motnosti vode pri batimetričnih laserjih ter dodatna višinska napaka zaradi snemanja v hribovitem svetu.

Analitično smo izpeljali poenostavljen a-priori model napak, ki poda povprečno in maksimalno pričakovano napako laserskega skeniranja za celoten oblak laserskih točk. Ta poenostavljen model napak ni odvisen od kota skeniranja in kota pozibavanja. Za izračun povprečne in maksimalne vrednosti napak potrebujemo samo vrednost INS-napak, napako lege faznega centra GPS-sprejemnika, napako zaradi višine vegetacije in višino leta. Zato naš poenostavljen a-priori model napak omogoča enostavno orodje za določitev velikosti napak zračnega laserskega skeniranja že pred samim snemanjem. Končni rezultat sta dve enostavni enačbi, ki omogočita izračun povprečne in maksimalne napake laserskega skeniranja.

Da omogočimo lažjo odločitev za uporabo zračnega laserskega skeniranja, se moramo vnaprej tudi odločiti kakšno podrobnost bi radi zajeli iz oblaka laserskih točk. To pomeni, kakšna podrobnost mora biti prikazana na končnem izdelku, ki so v našem primeru geodetski podatki kot podlage za lokalno prostorsko načrtovanje. Podrobnost, ki je lahko zajeta iz oblaka laserskih točk, je povezana z geometrično ločljivostjo končnega izdelka, oz. tudi grafično natančnostjo, če govorimo o kartah. Z Nyquistovo frekvenco smo povezali geometrično ločljivost in gostoto laserskih točk. Tako dobljeni teoretični vrednosti smo dodali še delež prodiranja laserskega žarka skozi različno vegetacijo, ki smo ga določili na testnem območju. Končni rezultat je enostavna enačba, ki jo lahko uporabimo pred samim laserskim snemanjem, da definiramo optimalno gostoto laserskih točk za določen končni produkt, ki smo ga iz tega oblaka laserskih točk namenjeni izdelati.

V zadnjem poglavju je podan predlog optimizacije metodologije zajema iz fotogrametrične stereorestitucije v samostojno lasersko skeniranje za naslednje podatke, ki se lahko uporabijo za potrebe lokalnega prostorskega načrtovanja v Sloveniji: državne topografske karte merila 1 : 5000 (ali geodetski načrt istega merila), Register nepremičnin ter nadzemne infrastrukture Zbirnega katastra gospodarske javne infrastrukture.

Bibliography

Abo Akel, N., Filin, S., Doytsher, Y. 2005. From airborne laser data to spatial information: Object reconstruction and accuracy analysis, FIG Working Week 2005 and GSDI-8, "From Pharaohs to Geoinformatics", Cairo, Egipt, April 16-21, 2005.
www.fig.net/pub/cairo/papers/ts_38/ts38_03_aboakel_etal.pdf (20. 11. 2008)

Abshire, J.B., Sun, X., Afzal, R.S. 2000. Mars orbiter laser altimeter: receiver model and performance analysis, Applied optics, Vol. 39, No. 15: pp. 2449–2460.

Ackermann, F. 1999. Airborne laser scanning – present status and future expectations, ISPRS PE&RS 54: pp. 64-67.

Albertella, A., Brovelli, M.A., Migliaccio, F., Sona, G. 1997. Esercizi di trattamento statistico dei dati, Milano, Citta Studi Edizioni: p. 165.

Alharthy, A., Bethel, J., Mikhail, E.M. 2004. Analysis and accuracy assessment of airborne laserscanning system, ISPRS Congress Istanbul 2004, July 12-23, 2004, ISPRS.
www.isprs.org/istanbul2004/comm2/papers/113.pdf (10. 11. 2005)

Ahokas, E., Kaartinen, J., Hyyppä, J. 2003: A quality assessment of airborne laser scanner data, Archives of Photogrammetry and Remote Sensing, Vol. XXXIV, 3/W13.
www.isprs.org/commission3/wg3/workshop_laserscanning/papers/Ahokas_ALSDD2003.pdf (20. 1. 2009)

Ahokas, E., Yu, X., Oksanen, J., Hyyppä, J., Kaartinen, H., Hyyppä, H., 2005a. Optimization of the scanning angle for contrywide laser scanning, ISPRS WG III/3, V/3 Workshop "Laser scanning 2005", Enschede, The Netherlands, 12.-14. September 2005, G. Vosselman and C. Brenner (Eds.).
www.commission3.isprs.org/laserscanning2005/papers/115.pdf (20. 1. 2009)

Ahokas, E., Yu, X., Kaartinen, H., Hyyppä, J., Kaasalainen, S., Matikainen, L., Honkavaara, E., Hyyppä, H., Rönnholm, P., Soininen, A. 2005b. Quality of laser scanning, EARSeL-Workshop on Remote Sensing, 2005.
www.ipi.uni-hannover.de/html/aktivitaeten/EARSeL-workshop2005_Paper/Ahokos.pdf (10. 11. 2006)

Akel, N.A., Kremeike, K., Filin, S., Sester, M., Doytscher, Y. 2005. Dense DTM Generalization aided by roads extracted from LiDAR data, ISPRS WG III/3, III/4, V3 Workshop "Laser scanning 2005", Enschede, the Netherlands, September 12-14 2005, G. Vosselman and C. Brenner (Eds.).
www.commission3.isprs.org/laserscanning2005/papers/054.pdf (20. 1. 2009)

Artuso, R., Bovet, S., Streilein, A. 2003. Practical methods for the verification of contrywide terrain and surface models, ISPRS WG III/3, Workshop "3-D reconstruction from arborne laserscanner and InSar data", Dresden, Germany, October 8-10 2003, International Archives of Photogrammetry and Remote Sensing and Spatial Information Sciences, Vol. XXIV, part 3/WG13.

Baltsavias, E.P. 1999a. Airborne laser scanning: existing systems and firm and other resources, ISPRS Journal of Photogrammetry and Remote Sensing, 54: pp. 164–198.

Baltsavias, E.P. 1999b. Airborne laser scanning: basic relations and formulas, ISPRS Journal of Photogrammetry and Remote Sensing, 54: pp. 199–214.

Barilotti, A., Beinat, A., Fico, B., Sossai, E. 2006. Produzione e verifica di DTM da rilievi LiDAR aerei su aree montane ricoperte da foresta, 51° Convegno Nazionale SIFET, 14-16 June 2006, Castellaneta Marina, Italy.
http://geomatica.uniud.it/pubblicazioni/pdf/2006/Sifet%20Barilotti%2006.pdf (20. 1. 2009)

Bäumker, M., Heimes, F.J. 2002. New calibration and computing method for direct georeferencing of image and scanner data using the position and angular data of an hibrid inertial navigation system, Integrated Sensor Orientation, Test report and workshop proceedings, OEEPE N^0 43.

Behan, A., Maas, H.-G., Vosselman, G. 2000. Steps towards quality improvement of airborne laser scanner data, Proceedings of the 26th Annual Conference of the Remote Sensing Society, Leicester, September 12-14, on CD-ROM, 9 pages.
www.itc.nl/personal/vosselman/papers/behan2000.rss.pdf (20. 1. 2009).

Beinat, A., Crosilla, F. 2002. A generalized stochastic model for the optimal global registration of lidar range images, ISPRS Commission III, "Photogrammetric Computer Vision", September 9 - 13, 2002, Graz, Austria.
www.isprs.org/commission3/proceedings02/papers/paper052.pdf (20. 1. 2009)

Berk, S., Duhovnik, M. 2007. Transformacija podatkov geodetske uprave Republike Slovenije v novi državni koordinatni sistem = Transformation of data of the Surveying and mapping authority of Republic Slovenia into the new national coordinate system, Geodetski vestnik, 51, 4: pp. 803–826.

Brnot, M. 2006. Zajem topografskih podatkov DTK 5, Geodetski vestnik, 50, 2: pp. 312.

Bilc, A. 2002. Ali dobiva klasična fotogrametrija konkurenco? Poročilo o prvem projektu LIDAR v Sloveniji, Geodetski vestnik, 46, 4: pp. 404–411.

Bitenc, M. 2007. Analiza podatkov in izdelkov zračnega laserskega skeniranja na projektu Neusidler See = Analysis of Airborne Laser Scanning data and products in the project Neusidler See. Graduation thesis. Ljubljana, University of Ljubljana, FGG.

Burman, H. 2000. Calibration and orientation of airborne image and laser scanner data using GPS and INS, Royal institute of technology, department of geodesy and photogrametry. Photogrammetric reports no 69, PhD dissertation, Stockholm, Sweden, Royal Institute of Technology.

Burman, H, Soininen, A. 2002. TerraMatch User's Guide, Terrasolid, Finland.

Briese, C. 2004. Breakline modeling from airborne lase scanner data. PhD thesis, Vien, Austria, TU Vien.

Brzank, A., Göpferd, J., Lohmann, P. 2005: Aspects of lidar processing in coastal areas.
www.ipi.uni-hannover.de/html/publikationen/2005/paper/alex_workshop05.pdf (2.7.2007).

Chasmer, L., Hopkinson, C., Smith, B., Treitz, P. 2006: Examining the influence of changing laser pulse repetition frequencies on conifer forest canopy returns. Photogrammetric Engineering & Remote Sensing, Vol. 72, 12: pp. 1359–1367.

Clode, S., Rottensteiner, F., Kootsookos, P., Zelniker, E. 2007. Detection and vectorisation of roads from Lidar data. Photogrammetric Engineering & Remote Sensing, Vol. 73, 5: pp. 517–535.

Coren, F., Sterzai, P. 2006. Radiometric correction in laser scanning, International Journal in Remote Sensing, Vol. 27, No. 15: pp. 3097-3104.

Cramer, M. 1997. GPS/INS Integration, Photogrammetric week 97, D. Fitsch and D. Hobbie (edt.), A Wichmann Verlag, Heidelberg.
www.ipf.uni-stuttgart.de/publications/phowo97/cramer.pdf (3. 3. 2007)

Cramer, M., Stallmann, D., 2002. System calibration for direct georeferencing, International archives of the photogrammetry, remote sensing and spatial information science, Vol 34, Part 3A: pp. 79–84.
www.ifp.uni-stuttgart.de/publications/2002/cramer_graz2002_final.pdf (20. 1. 2009)

Crosilla, F., Beinat, A. 2005. personal comunication.

Crosilla, F., Beinat, A. 2006. Interreg IIIA.
http://geomatica.uniud.it/progetti/laserscan/ (20. 1. 2009)

Crosilla, F., Beinat, A., Visintini, D., Fico, B., Sossai, E. 2005a. Likelihood and Accuracy Analysis of 3D Building Models from Airborne Laser Data, Proceedings of Italy-Canada 2005 Workshop on "3D Digital Imaging & Modeling: Aplication of heritage, industry, medicine & land", May 17-18, 2005, Padova, Italy, 7 pages (on CD).

Crosilla, F., Visintini, D., Sepic, F. 2005b. A segmentation procedure of lidar data by applying mixed parametric and nonparametric models, ISPRS WG III/3, V/3 Workshop "Laser scanning 2005", Enschede, The Netherlands, September 12-14, 2005, G. Vosselman and C. Brenner (Eds.).

Čopič, M. 1995. Elektrooptika, skripta za 4. letnik fizike.

Davis, P.A., Gonzales, F., Brown, K.M., Melis, T.S. 2005. Evaluation of the SHOALS 1000T Bathymetric LIDAR System for monitoring channerl sedimenmts within the Colorado river in Arizona, American Geophysical Union fall meeting 2005.

Deems, J.S., Painter, T.H. 2006. Lidar measuremet of snow depth: accuracy and error sources, International Snow Science Workshop 2006, Telluride, Colorado, USA.
www.warnercnr.colostate.edu/~deems/DeeemsPainter_ISS06.pdf (1. 8. 2007)

Ding, W.D., Wang, J.L., Mumford, P., Li, Y., Rizos, C. 2005. Time synchronization design for integrated positioning and georeferencing systems, Proceedings of SSC 2005 Spatial Intelligence, Innovation and Praxis: The national biennial conference of the Spatial Science Institute, September 2005, Melburne, Australia.
www.gmat.unsw.edu.au/snap/publications/ding_etal2005a.pdf (20. 1. 2009)

Ding, W.D., Wang, J.L., Li, Y., Mumford, P., Rizos, C. 2008. Time synchronisation error and calibration in integrated GPS/INS systems. Journal of ETRI (Electronics & Telecommunications Research Institute, Korea), 30, 1: pp. 59-67.
www.gmat.unsw.edu.au/snap/publications/ding_etal2006d.pdf (20. 1. 2009)

Duhovnik, M. 2005. Zajem topografskih podatkov DTK 5, Geodetski vestnik, 49, 3: pp. 441-443.

Državna kartografija, katalog digitalnih podatkov. 2005. MOP & GU RS.

Državni razvojni program = National development program, 2008. Ljubljana, Služba vlade Republike Slovenije za lokalno samoupravo.
http://www.svlr.gov.si/index.php?id=1182

Filin, S. 2001a. Calibration of spaceborne and airborne laser altimeters using natural surfaces. PhD thesis, Columbus, The Ohio State University, Department of civil and enviromental engineering and geodetic science.

Filin, S. 2001b. Recovery of systematic biases in laser altimeters using natural surfaces, International Archives of Photogrammetry and Remote Sensing 33 (B3/1): pp. 85–91.

Filin, S., Pfeifer, N. 2006. Segmentation of airborne laser scanning data using a slope adaptive neighborhood. ISPRS Journal of Photogrammetry & Remote Sensing, 60, 2: pp. 71-80.

Filin, S., Vosselman, G. 2004. Adjustment of airborne laser altimetry strips, ISPRS Congress Istanbul 2004, July 12-23, 2004, ISPRS.
www.isprs.org/istanbul2004/comm2/papers/filin2004.istanbul.pdf (10. 11. 2005)

Filippovska, Y., Walter, V., Fritch, D. 2008. Quality evaluation of generalization algorithms, Proceedings of XXI congres of ISPRS, July 3-11, 2008, Beijing, China.

Francis, K., Tuell, G. 2005. Rapid environmental assessment: The next advancement in airborne bathymetric lidar, Ocean news & Technology, May/June 2005, pp. 2-4.

Friess, P. 2006. Toward a rigorous methodology for airborne laser mapping, Proceedings of International Calibration and Orientation Workshop EuroCOW 2006, 25-27 January 2006, Castelldefels, Spain. www.isprs.org/commission1/euroCOW06/euroCOW06_files/papers/PeterFriessEuroCOW_2006.pdf (12. 8. 2007)

Geist, T., Lutz, E., Stötter, J. (2003): Airborne laser scanning technology and its potential for applications in glaciology. http://omega.utu.fi/reports/Geist_ALSDD2003.pdf (20.5. 2005)

Geodetske podlage za prikaz in izdelavo prostorskih planskih aktov občine, 2006. GU RS. http://192.168.1.2./gu/projekti/podlage/podlage.asp (24. 2. 2006)

Goodwin, N.R., Coops, N.C., Bater, C., Gergel, S.E. 2007. Assesment od sub-canopy structure in complex coniferous forests, ISPRS Workshop on laser scanning 2007 and SilviLaser 2007, September 12-14, Espoo, Finland, ISPRS: pp. 169-172.

Göpfert, J., Heipke, C. 2006. Assesment of lidar DTM accuracy in coastal vegetated areas. http://www.ipi.uni-hannover.de/html/publikationen/2006/paper/ISPRS_Bohn_Goepfert_Heipke.pdf (1. 10. 2007)

Göpfert, W. Raumbezogene Informationssysteme, Karlsruhe, A Wichmann Verlag.

Gorte, B., Pfeifer, N., Oude Elberink, S. 2005. Height texture of low vegetation in airborne laser scanner data and its potential for DTM correction, ISPRS WG III/3, III/4, V/3 Workshop "Laser scanning 2005", September 12-14, Enschede, the Netherlands, ISPRS.

GU RS, 2008. Survaying and mapping authority home page, www.gu.gov.si (1. 8. 2008).

Gutelius, B. 2002. High performance airborne LIDAR for terrain and bathymetric mapping technologies, "Integrated Remote Sensing at the Global, Regional and Local Scale" ISPRS Comission I Mid-Term Symposium in conjunction with Pecora 15/Land Satellite Information IV Conference, November 10-15, 2002, Denver, CO USA.

Grejner-Brzezinska, D.A., Wang, J. 1998. Gravity modeling for high-accuracy GPS/INS integration, Navigation, Vol. 45, No. 3, pp. 209–220.

Habib, A., Ghanma, M., Morgan, M., Al-Ruzouq, R. 2005. Photogrammetric and lidar data registration using linear features, Photogrammetric Engeneering & Remote Sensing, 71, 6: pp. 699–707.

Hasegava, H. 2006. Evaluation of LIDAR reflectance amplitude sensitivity towards land cover conditions, Bulletin of Geographical survey Institute, Vol. 53, March, 2006. www.gsi.go.jp/ENGLISH/RESEARCH/BULLETIN/vol-53/53-6.pdf (1.2. 2007)

Hašaj, M., Petrovič, D., Brumec, M., Mlinar, J. 2006. Topografski ključ za izdelavo in prikaz vsebine geodetskih načrtov, Ljubljana, Geodetska uprava RS.

Hodgson, M.E., Bresnahan, P. 2004. Accuracy of airborne Lidar-derived elevation: empirical assessment and error budget, Photogrammetric Engeneering & Remote Sensing, Vol. 70, 3: pp. 331–339.

Hodgson, M.E., Jensen, J., Raber, G., Tullis, J., Davis, B.A., Thompson, G., Schuckman, K. 2005: An evaluation of lidar-derived elevations and terrain slope in leaf-off conditions, Photogrammetric Engeneering & Remote Sensing, 71, 7: pp. 817–823.

Hopkinson, C., Sitar, M., Chasmer, L., Gynan, C., Agro, D., Enter, R., Foster, J., Heels, N., Hoffman, C., Nillson, J., St.Pierre, R. 2001: Mapping the spatial distribution of snowpack depth beneath a variable forest canopy using airborne laser altimetry, 58th Eastern Snow Conference, Ottawa, Ontario, Canada.

Hopkinson, C., Chasmer, L.E., Sass, G., Creed, I.F., Sitar, M., Kalbfleisch, W., Treitz, P. 2005: Vegetation class dependent errors in lidar ground elevation and canopy height bestimates in boreal wetland environment, Can. J. Remote Sensing, 31, 2: pp. 191–206.

Hopkinson, C., Chasmer, L., Lim, K., Treitz, P., Creed, I. 2006: Towards a universal lidar canopy height indicator, Can. J. Remote Sensing, 32, 2: pp. 1–14.

Hofmann, A.D., Mass, H.-G., Streilein. A. 2002. Knowledge-based building detection based on laser scanner data and topographic map information, ISPRS Tehnical commission III Symposium 2002 "Photogrammetric computer vision PCV'02" September 9-13, 2002, Graz, Austria, ISPRS. www.isprs.org/commission3/proceedings02/papers/paper025.pdf (15.11.2006)

Hudnik, J. 2008. Ne mečite denarja in časa skozi okno! Cenejši in predvsem hitrejši način izdelave topografskih načrtov načrtov meril 1:500 oz. 1:1000, Flycom novice – interno glasilo podjetja Flycom d.o.o, letnik 3, številka 5, julij 2008.

Hyyppä, H., Yu, X., Hyyppä, J., Kaartinen, H., Kaasalainen, S., Honkavaara, E., Rönnholm, P. 2005: Factors affecting the quality of DTM generation in forested areas, ISPRS WG III/3, III/4, V/3 Workshop "Laser scanning 2005", September 12-14, Enschede, the Netherlands: pp. 85–90.

Iliffe, J.C. 2000. Datums and map projections, for remote sensing, gis and surveying, Whittles Publishing.

Jacobsen, K. 2005. Photogrammetry and geoinformation trends for large scale mapping, Map Middle East 2005, April 23-25, 2005, Dubai. www.ipi.uni-hannover.de/html/publicationen/2005/paper/jac_MapMEOS.pdf. (10.10.2006)

Jutzi, B., Stilla, U. 2003: Laser pulse analysis for reconstruction and classification of urban objects, ISPRS Archives, Vol. XXXIV, Part 3/W8, September 17-19, 2003, Munich, ISPRS.

Jutzi, B., Neulist, J., Stilla, U. 2005. Sub-pixel edge localization based on laser waveform analysis, ISPRS WG III/3, III/4, V3 Workshop "Laser scanning 2005", September 12-14, 2005, Enschede, the Netherlands.

Kager, H. 2005. Quality check and georeferencing of aerial laser scanner strips, University course: Laser scanning – Data Acquisiton and Modeling, October 6-7, 2005, Vienna, Institute of photogrammetry and remote sensing, TU Vienna.

Karničnik, I., Radovan, D., Petrovič, D. 2000. The first Slovenian nautical chart – digital on WGS 84, Int. arch. photogramm. remote sens., 2000, vol. 32, 6W8/1: pp. 82–88.

Karničnik, I., Radovan, D. 2003. GPS survey of Slovenian coastline and its integration with hydrographic data, In: BAČIĆ, Željko (edt.). Geoinformation for practice : proceedings of the ISPRS WG VI/3 workshop, 15th to 18th october 2003, Zagreb, Croatia, (International archives of the photogrammetry, remote sensing and spatial information science, Part 6/W11, commission 6, Vol 34): pp. 113–116.

Karničnik, I. 2006 Povečanje varnosti pomorskega prometa z uporabo elektronskih navigacijskih kart = Increase of safety of maritime traffic with the use of electronic navigational charts, Master thesis, Portorož, 160 f.

Katzenbeisser, R. About the calibration of lidar sensors, ISPRS Workshop "3-D Reconstruction from airborne laser-scanner and InSAR data", Dresden, 8-10 Oktober, International archives of the photogrammetry, remote sensing and spatial information science, Vol. 34, Part 3/W13: pp. 59–64. http://www.isprs.org/commission3/wg3/workshop_laserscanning/papers/Katzenbeisser_ALSDD2003.pdf (10.10.2006)

Koetz, B., Morsdorf, F., Curt, T., van den Linden, S., Borgniet, L., Odermatt, D., Alleaume, S., Lampin, C., Jappiot, M., Allgöwer, B. 2007. Fusion of imaging spectrometer and lidar data using suport vector machines for land cover classification in the context of forest fire management. ftp://ftp.geo.unizh.ch/pub/rsl2/paper/2007/ISPMSRS07_koetz_SVM.pdf (1. 10. 2007)

Kosmatin-Fras, M. 2002. Total quality management in photogrammetric projects – models and applications in Slovenia = Celovito obvladovanje kakovosti v fotogrametričnih projektih – modeli in aplikacije v Sloveniji, PhD thesis, Politecnico di Milano, 254 p.

Kosmatin-Fras, M. 2004. Vpliv kakovosti vhodnih podatkov na kakovost ortofota = Influence of input data quality on the quality of ortophoto, Geodetski vestnik, 48, 2: pp. 167–178.

Kosmatin-Fras, M., Drobne, S., Gregorič, H., Oven, J. 2006. Raziskava uporabe ortofota (DOF5) v praksi = Research on the use of ortophoto (DOF5) in practice, Geodetski vestnik, 50, 2: pp. 258–269.

Kozmus, K., Stopar, B. 2003. Načini določanja položaja s satelitskimi tehnikami = Satellite-based point positioning techniques, Geodetski vestnik, 47, 4: pp. 404–413.

Kuhar, M. 2006. Geofizika, Študijski pripomoček, Ljublana, FGG.

Kröpfl, M., Kruck, E., Gruber, M. 2004. Geometric calibration of the digital large format aerial camera UltraCamD, http://www.vexcel.com/downloads/photogram/ultracam/whitepapers/paper-UCD-ISPRS-2004b.pdf (1. 3. 2007)

Kraus, K., Pfeifer, N. 1998. Determination of terrain models in wooden areas with airborne laser scanner data, ISPRS Journal of Photogrammetry & Remote Sensing, 53: pp. 193–203.

Kraus, K. (edt.) 2005. Physical principles of airborne laser scanning, University course: Laser scanning – Data Acquisiton and Modeling, Vienna, TU Vienna, Institute of photogrammetry and remote sensing, October 6-7, 2005.

Kraus, K. 2004. Photogrammetrie. Band 1. Walter de Gruyter, pp. 467.

Latypov, D. 2005. Effects of laser beam alignment tolerance on lidar accuracy, ISPRS Journal of Photogrammetry & Remote Sensing, 59: pp. 361–368.

Lee, B.K., Yu, K., Pyeon, M. 2003. Effective reduction of horizontal error in laser scanning information by strip-wise least squares adjustments, ETRI Journal, 25, 2: pp. 109–120.

Leberl, F.W., Perko, R., Gruber, M.A., Ponticelli, M. 2002. Novel concepts for aerial digital cameras, ISPRS Arcives, Volume 34, Part 1, Proceedings of the ISPRS Commission I Symposium, November 2002, Denver, Colorado.
www.isprs.org/commission1/proceedings02/paper/00067.pdf (20. 1. 2009)

Legat, K. Skaloud, J. Schaer, P. 2006. Real-time processing of GPS/INS data for on-the-fly quality control in airborne mobile mapping, ENC-GNSS 2006, May 7-10, 2006, Manchester, UK.

Lipej, B. 2005. Nekatera izhodišča pri združevanju nepremičninskih evidenc (zemljiška knjiga, zemljiški kataster) = Some starting points for real estate records merger (land register, cadastre), Geodetski vestnik, 49, 4: pp. 594–598.

Lisec, A., 2002. Relativna gravimetrična izmera in relativni gravimeter Scintrex CG-3m = Relative gravimetrical measurements and relative gravimeter Scientrex CG-3m, Geodetski vestnik, 46, 4: pp. 391–403.

Lockhart, C., Arumugam, D., Millar, D. 2005. Meeting hydrographic charting specifications with the SHOALS-1000T airborne LIDAR bathymeter, U.S. Hydro 2005, March 29-31, 2005, Manchester Grand Hyatt, San Diego, California, The hydrographic Society of America.
www.thsoa.org/hy05/07_3.pdf (20. 1. 2009)

Luethy, J., Ingensad, H. 2004. How to evaluate the quality of airborne laser scanning data, ISPRS proceedings of "Laser-scanners for forest and landscape assessment", October 3-6, 2004, Freiburg, Germany, ISPRS.

Luethy, J., Stengele, R. 2005. 3D mapping of Switzerland – challenges and experiences, ISPRS WG III/3, V/3 Workshop "Laser scanning 2005", September 12-14, 2005, Enschede, the Netherland, ISPRS.

Maas, H.-G., 2002. Methods for measuring height and planimetry discrepancies in airborne laserscanner data, Photogrammetric Engineering & Remote Sensing, 68, 9: pp. 933–940.
www.tu-dresden.de/ipf/photo/publikationen/aeltere/Maas_PERS2002.pdf (20. 1. 2009)

Maas, H.-G., 2003. Planimetric and height accuracy of airborne laserscanner data: User requirements and system performance, Proceedings 49. Photogrammetric Week (Ed. D. Fritsch), Wichmann Verlag.
www.tu-dresden.de/ipf/photo/publikationen/2003/Maas_PhoWo2003.pdf (20. 1. 2009)

Maillet, G., Flamanc, D. 2004. Comparison of aerial images, satelite images and laser scnning DSM in a 3D city models production framework, ISPRS Congress Istanbul 2004, July 12-23, 2004, Istanbul, Turkey, ISPRS.
www.isprs.org/istanbul2004/comm2/papers/filin2004.istanbul.pdf. (10. 11. 2005)

Maling, D.H. 1989. Measurements from maps: principles and methods of cartometry. Oxford, Pergamon press.

McKean, J., Roering, J. 2005. Operational accuracy of lidar in mountainous terrain, unpublished manuscript. http://www.uoregon.edu/ jroering/outgoing/McKean_LidarAccuracy2005.pdf (10. 11. 2005)

Medvedev, E. 2004. Towards the full automation of laser scanning and aerial photography data processing, XXth ISPRS Congress Istanbul, July 12-13, 2004, Istanbul, Turkey, ISPRS.
www.isprs.org/istanbul2004/comm2/papers/119.pdf (10. 11. 2005)

Mikhail, E.M., Ackerman, F. 1976. Observations and least squares, reprint in 1982, University press of America, 497 p.

Millar, D., Gerhard, J., Hilldale, R. 2005. Using airborne LIDAR bathymetry to map shallow river environments, Proceedings of the 14th Biennial Coastal Zone Conference, July 17-21, 2005, New Orleans, Louisiana.

Mlinar, J., Grilc, M., Mesner, A., Puhar, M., Bovha, D. 2006. Vzpostavitev sistema evidentiranja gospodarske javne infrastrukture – ponovni izziv za geodezijo = Setting-up public infrastructure records – a renewed challenge for geodesy, Geodetski vestnik, 50, 2: pp. 238–247.

Moffiet, T., Mengersen, K., Witte, C., King, R., Denham, R. 2005: Airborne laser scanning: Exploratory data analysis indicates potential variables for classification of individual trees of forest stands according to species, ISPRS Journal of Photogrammetry & Remote Sensing, 59: pp. 289–309.

Morin, K., El-Sheimy, N. 2002. Post-mission Adjustment of Airborne Laser Scanning Data, FIG XXII International Congress, April 19-26, 2002, Washington, D.C..

Morsdorf, F., Koetz, B., Meier, E., Itten, K.I., Allgöwer, B. 2005: The potential of discrete return, small footprint airborne laser scanning data for vegetation density estimation, ISPRS WG III/3, III/4, V/3 Workshop "Laser scanning 2005", September 12-14, Enschede, the Netherlands, ISPRS, pp. 198–203.

Naprudnik, M. 2005. Regionalno in prostorsko planiranje ali regionalno – prostorsko planiranje, Dela, 24: pp. 23–35.

Oštir., K. 2006. Daljinsko zaznavanje, Ljubljana, Založba ZRC SAZU.

Pak, M., Rus, A. 2005. Problematika razvoja mest in spreminjanja rabe mestnega prostora, Dela, 24: pp. 159–170.

Petek, T. 2005. Sistem zbirk prostorskih podatkov = System of spatial databases, Geodetski vestnik, 49, 4: pp. 558–566.

Petek, T. 2007. Popis nepremičnin zaključen. Geodetski vestnik, 51, 3: pp. 610–611.

Petrovič, D., Brumec, M., Radovan, D. 2005. Geodetski in topografski sistem v prostorskem načrtovanju – od geodetskih podlag do koordinate = Geodetic and topographic system in spatial planning – from geodetic plans to the coordinate, Geodetski vestnik, 49, 4: pp. 545–557.

Petrovič, D. 2007. Trirazsežne (tematske) karte v prostorskem načrtovanju = Three-dimensional (thematic) maps in spatial planning, Geodetski vestnik, 51, 2: pp. 293–303.

Pfeifer, N., Stadler, P. and Beiese, C., 2001. Derivation of digital terrain models in the SCOP++ environment, In the Proceedings of OEEPE Workshop on airborne laser scanning and interferometric SAR for detailed digital terrain models, Stockholm, Sweden.

Pfeifer, N., Gorte, B., Oude Elberink, S. 2004: Influences of vegetation on laser altimetry – analysis and correction approaches, International archieves of Photogrammetry and Remote Sensing, Vol. XXXVI, 8/W2, ISPRS.

Pfeifer, N., Elberink, S. O., Filin, S. 2005. Automatic tie elements detection for laser scanner strip adjustment, ISPRS WG III/3, III/4, V3 Workshop ”Laser scanning 2005”, September 12-14, 2005, Enschede, the Netherlands, ISPRS.

Podobnikar, T. 1999. Termina natančnost in točnost v geodeziji, Geodetski vestnik, 43, 1: pp. 49–55.

Podobnikar, T. 2003. Kronologija izdelave digitalnega modela reliefa Slovenije = Chronology of digital terrain model production of Slovenia, Geodetski vestnik, 47, 1&2: pp. 47–54.

Podobnikar, T. 2008. Simulation and representation of the positional errors of boundary and interior regions in maps, In: Moore, A. (ed.), Drecki, I. (ed.). Geospatial vision : new dimensions in cartography : selected papers from the 4th National Cartographic Conference Geocart'2008, New Zealand, (Lecture notes in geoinformation and cartography). Berlin, Heidelberg, Springer: str. 141-169.

Podobnikar, T., Mlinar, T. 2006. Izdelava in vzdrževanje digitalnega modela reliefa Slovenije z integracijo obstoječih virov = Production and maintenance of digital elevation model of Slovenia with data integration, Geodetski vestnik, 50, 3: pp. 472–480

Pogačnik, A. 1992. Urejanje prostora in varstvo okolja, Univerzitetni učbenik. Ljubljana, Založba Mladinska knjiga.

Pogačnik, A. 2005. Prispevek k integraciji prostorskega, socialnega, gospodarskega in okoljskega načrtovanja, Dela, 24: pp. 49-59.

Pravilnik o evidenci dejanske rabe kmetijskih in gozdnih zemljišč, UL RS 90/2006.

Pravilnik o podrobnejši vsebini, obliki in načinu priprave Strategije prostorskega razvoja Slovenije ter vrstah njenih strokovnih podlag, 2003. št. 350-01-25/2003.

Pravilnik o vsebini in načinu vodenja zbirke podatkov o dejanski rabi prostora, 2004, UL RS št. 9/2004: pp. 1052–1061.

Pravilnik o geodetskem načrtu = Rules on land survey plan, 2004. UL RS št. 40/2004: pp. 4754–4757.

Pravilnik o vsebini, obliki in načinu priprave prostorskega reda občine ter vrstah njegovih strokovnih podlag, 2004. UL RS št. 91/2003.

Pravilnik o vsebini, obliki in načinu priprave občinskega prostorskega načrta ter pogojih za določitev območij sanacij razpršene gradnje in območij za razvoj in širitev naselij, 2007, UL RS št. 99/2007: pp. 13398–13424.

Pravilnik o vsebini, obliki in načinu priprave občinskega podrobnega prostorskega načrta, 2007, UL RS št. 99/2007: pp. 13425–13427.

Pravilnik o prostorskem informacijskem sistemu, 2007, UL RS št. 119/2007, pp. 17149–17153.

Prešeren, P., 2007. Slovenija po novem celotna v barvah, Geodetski vestnik, 51, 3: pp. 614-615.

Pribičević, B. 2000. Uporaba geološko - geofizičnih in geodetskih baz podatkov za računanje ploskve geoida Republike Slovenije = The use of Geological, Geophysical and Geodetical Databases in Determination of the Shape of Geoid in the Republic of Slovenia, PhD thesis, Ljubljana, FGG.

Priporočila za izdelavo strokovnih podlag pri pripravi prostorskih aktov, 2005. MOP, Direktorat za prostor. www.gov.si/upr/doc/priporocilo_podlage_31.05.pdf (12. 7. 2006).

Raber, G.T., Jensen, J.R., Hodgson, M.E., Tullis, J.A., Davis, B.A., Berglund, J. 2007. Imapct of lidar nominal post-spacing on DEM accuracy and flood zone delineation, Photogrammetric Engineering & Remote Sensing, 73, 7: pp. 793–804.

Radovan, D., Karničnik, I., Petrovič, D. 1999. Prva slovenska pomorska karta. V: 32. Geodetski dnevi, Bled, October 28-30, 1999, Geodetski vestnik, 43, 3: pp. 241–249.

Radovan, D., Karničnik, I., Petrovič, D. 2000. Hidrografski podatki slovenskega morja in elektronska pomorska kartografija, In: Hladnik, D., Krevs, M., Perko, D., Podobnikar, T., Stančič, Z. (edt.). Geografski informacijski sistemi v Sloveniji 1999-2000 : zbornik referatov simpozija, Ljubljana, 26. september 2000. Ljubljana, Znanstvenoraziskovalni center SAZU, Zveza geografskih društev Slovenije, Zveza geodetov Slovenije: pp. 13–19.

Reutebuch, S.E., McGaughey, R.J., Andersen, H-E., Carson, W.W. 2003: Accuracy of a high-resolution lidar terrain model under a conifer forest canopy, Can. J. Remote Sensing, 29, 5: pp. 527–535.

Režek, J., Kupic, A. 2003. Geodetski podatki za pripravo in prikaz občinskih planov, Geodetski vestnik, 47, 1&2: pp. 125–128.

Režek, J. 2007. Inventarizacija prostora in načrtovanje na podlagi dejstev = Spatial data inventory and evidence-based planning, Geodetski vestnik, 51, 2: pp. 255–263.

Režek, J. 2008. Sistem kazalcev za spremljanje prostorskega razvoja v Evropski uniji in stanje v Sloveniji=System of Indicators for Monitoring Spatial Development in the European Union and Situation in Slovenia, M.Sc. thesis, Ljubljana, University of Ljubljana, FGG.

Rönnholm, P. 2004. The elevation of the internal quality of the laser scanning strips using the interactive orientation method and point clouds, XXth ISPRS Congress, Istanbul, Turčija, International arhiveres of photogrammetry and remote sensing XXXY: pp. 55–261.

Rönnholm, P., Hyyppä, H., Pöntinen, P., Haggren, H., Hyyppä, J. 2003: A method for interactive orientation of digital images using backprojection of 3D data, The photogrammetric journal of Finland, 18, 2: pp. 16–31.

Rotar, M. 2008. Vzpostavitev registra nepremičnin (REN), Geodetski vestnik, 52, 2: pp. 372–373.

Schenk, T. 1999. Photogrammetry and laser altimetry, International archives of photogrammetry and remote sensing, 32 (3W14).

Schenk, T. 2001. Modeling and analyzing systematic errors in airborne laser scanners, Technical Notes in Photogrametry No 19, Columbus, The Ohio State University, Department of Civil and Environmental Engineering and Geodetic Science.

Schenk, T., Seo, S., Csatho, B. 2001. Accuracy strudy of airborne laser scanning data with photogrammetry, Proceedings of the ISPRS Workshop "Land surface mapping and characterization using laser altimetry", XXXIV-3/W4, October 22-24, 2001, Annapolis, Maryland, ISPRS. www.isprs.org/commission3/annapolis/pdf/Schenk.pdf (20. 1. 2009)

Schnurr, D, Pettersson, M., Grierson, H. 2004. Investigation, assessment and correction of systematic errors in large LiDAR datasets, RSPSoc/BGS two day meeting Keyworth, November 11-12, 2004, Keyworth, UK.

Sithole, G., Vosselman, G. 2004. Experimental comparison of filter algorithms for bare-Earth extraction from airborne laser scanning point clouds, ISPRS journal of photogrammetry and remote sensing, 59, 1-2: pp. 85-101.

Sithole, G., Vosselman, G. 2005. Filtering of airborne laser scanner data based on segmented point clouds, ISPRS WG III/3, III/4, V3 Workshop "Laser scanning 2005", September 12-14, 2005, Enschede, the Netherlands.

Skaloud, J., Schaer, P. 2003. Towards a more rigorous boresight calibration, Proceedings ISPRS International Workshop "Theory, technology and realities if Inertial/GPS/Sensor orientation", September 22-23, 2003, Castelldefels, Spain, ISPRS.
www.isprs.org/commission1/theory_tech_realities/pdf/p01_s2.pdf (20. 1. 2009)

Skaloud, J., Lichti, D. 2006. Rigorous approach to bore-sight self-calibration in airborne laser scanning, ISPRS Journal of Photogrammetry & Remote Sensing, 61: pp. 47–59.

Soininen, A. 2004. TerraScan User's Guide, Terrasolid, Finland.

Stopar, B., Kuhar, M. 2001. Moderni geodetski koordinatni sistemi in astrogedetska mreža Slovenije = Modern geodetic coordinate systems and astrogeodetic network of Slovenia, Geodetski vestnik, 45, 1&2: pp. 11–26.

Odlok o strategiji prostorskega razvoja Slovenije, 2004. UL RS št. 76/2004.

Strategija regionalnega razvoja Slovenije = Strategy of regional development of Slovenia, 2001. Ljubljana, Ministrstvo za Gospodarstvo, Agencija RS za regionalni razvoj.

Šušteršič, J., Rojec, M., Korenika, K. (edt.). 2005. Strategija razvoja Slovenije = Development strategy of Slovenia, Ljubljana, Urad RS za makroekonomske analize in razvoj.

Strnad, J. (translation and redaction) 1993. Atlas klasične in moderne fizike, Ljubljana, DZS.

Terrasolid spletna stran, 2005. Short descriptions of Terrasolid programes.
terrasolid.fi/ftp/brochure/Eng/*.pdf (20. 1. 2009)

Teunissen, P.J.G., Kleusberg, A., 1998. GPS for Geodesy, Berlin, Springer.

Tiede, D., Blaschke, T. 2004. An integrated workflow for Lidar / optical data mapping for security applications, Workshop on "Processing and visualization using high-resolution images", November 18-20, 2004, Pitsanulok, Tailand.
www.photogrammetry.ethz.ch/pitsanulok_workshop/papers/06.pdf (20. 1. 2009)

Thiel, K.-H., Wehr, A. 2004. Performance capabilities of laser scanners – an overview and measurement principle analysis, Proceedings of the ISPRS working group VIII/2 "Laser-scanners for forest and landscape assessment", October 3-6, 2004, Freiburg, Germany, ISPRS.
www.isprs.org/commission8/workshop_laser_forest/THIEL.pdf (20. 1. 2009)

Tóváári, D., Pfeifer, N. 2005. Segmentation bassed robust interpolation – A new approach to laser data filtering, ISPRS WG III/3, III/4, V3 Workshop "Laser scanning 2005", September 12-14, 2005, Enschede, the Netherlands, ISPRS.

Toth, C.K. 2002. Calibrating Airborne Lidar Systems, Internationa Archives of Photogrammetry Remote Sensing and Spatial Information Sciences, 34, 2: pp. 475-480.

TopoSys, 2008. TopoSys Presents Advantages of Simultaneous Aerial LIDAR/Ortho Image Acquisition at ILMF.
www10.giscafe.com/goto.php?http://www.lidarcomm.com/id31.html (10. 3. 2008)

Thoma, D.P., Gupta, S.C., Bauer, M.E., Kirchoff, C.E. 2005. Airborne laser scanning for riverbank erosion assessment, Remote Sensing of Environment, 95: pp. 493–501.

Triglav, M., Pegan-Žvokelj, B., Pogorelčnik, E., Grilc, M. 2003. The setup of building cadastre in Slovenia, Proceedings of the ISPRS WG VI/3 workshop "Geoinformation for practice", October 15-18, 2003, Zagreb, Croatia, ISPRS.

Triglav Čekada, M. 2004. Lasersko skeniranje: osnove, analitični model in obnašanje napak pri aerolaserskih sistemih, Seminarska naloga na podiplomskem študiju geodezije, Ljubljana.

Tuell, G., Park, J.Y., Aitken, J., Ramnath, V., Feygels, V. 2005. Adding hyperspectral to CHARTS: Early results, U.S. Hydro 2005, March 29-31, 2005, Manchester Grand Hyatt, San Diego, California, The hydrographic Society of America.
www.thsoa.org/hy05/07_1.pdf (20. 1. 2009)

Turton, D.A. 2006. Factors influencin ALS Accuracy, AAMHatch,
www.aamhatch.com.au/resources/pdf/publications/documents/FactorswhichinfluenceALSaccuracy2.pdf (20. 1. 2009)

Uredba o prostorskem redu Slovenije, 2004. UL RS št. 122/2004.

Uredba o vrstah prostorskih ureditev državnega pomena = Decree on the types of spatial planning of national significance, 2007. UL RS 95/2007.

Vaniček, P. Krakiwski, E. 1996: Geodesy, the consepts (secon edition), Elsevier.

Viitanen, K., Hyyppä, H., Hyyppä, J., Rönnholm, P. 2005. The use of laser scanning data in real estate analyses, FIG Commission 9, CIREA and HKISW Symposium – Property valuers fronting the tripple bottom lines of economics, Enviroment and social conflicts, October 16-20, 2005, Xian, China.
www.fig.net/news/news_2005/xian_2005/viitanen_etal.pdf, (20. 1. 2009).

Vosselman, G., Mass, H.-G. 2001. Adjustment and filtering of raw laser altimeter data, OEEPE Workshop on Airborne Laserscanning and Interferometric SAR for Detailed Digital Elevation Models, March 1-3 2001, Stockholm, Sweden, OEEPE.

Vosselman, G. 2002. Fusion of laser scanning data, maps, and aerial photographs for building reconstruction, IEEE International Geoscience and Remote Sensing Symposium and the 24th Canadian Symposium on Remote Sensing, IGARSS'02, June 24-28, Toronto, Canada, IEEE.
www.itc.nl/personal/vosselman/papers/vosselman2002.igarss.pdf (20. 1. 2009)

Vosselman, G., Gorte, B.G.H., Sithole, G. 2004. Change detection for updating medium scale maps using laser altimetry, XXth ISPRS Congress "Geo-images bridging continents", July 12-13, 2004, Istanbul, Turky, ISPRS.
www.isprs.org/istanbul2004/comm3/papers/268.pdf (20. 1. 2009)

Vosselman, G., Gorte, B.G.H., Sithole, G., Rabbani, T. 2004. Recognising structure in laser scanner point cloud, Internationa Archives of Photogrammetry Remote Sensing and Spatial Information Sciences, 36, 8/W2: pp. 33-38.

Vosselman, G. 2005. Sensing geo-information. www.itc.nl/library/papers_2005/book_rev/vosselman_sen.pdf (1. 6. 2006).

Vozikis, G. 2005. Automated generation and updating of digital city models using high-resolution line scanning systems, PhD thesis, Vienna, Austria, TU Vienna.
www.ipf.tuwien.ac.at/phdtheses/diss_liste.html (20. 5. 2006)

Wack, R., Stelzl, H. 2005. Laser DTM generation for South-Tyrol and 3D-visualisation, ISPRS WG III/3, V/3 Workshop "Laser scanning 2005", September 12-14, 2005, Enschede, The Netherland, ISPRS.

Wagner, W. 2005a. Physical principles of airborne laser scanning, University course: Laser scanning – Data Acquisiton and Modeling, K. Kraus (ed.), October 6-7, 2005, Vienna, TU Vienna, Institute of photogrammetry and remote sensing.

Wagner, W. 2005b. Full wave laser scanning, University course: Laser scanning – Data Acquisiton and Modeling, K. Kraus (ed.), October 6-7, 2005, Vienna, TU Vienna, Institute of photogrammetry and remote sensing.

Wehr, A., Lohn, U. 1999: Airborne laser scanning – an introduction and overview, Photogrammetrical Engeneering & Remote Sensing, 54: pp. 68–82.

Welch, G., Bishop, G. 2006. An introduction to the Kalman filter, UNC-Chapel Hill, TR95-041. www.cs.unc.edu/w̃elch/media/pdf/kalman_intro.pdf (20. 3. 2006)

Wotruba, L., Morsdorf, F., Meier, E., Nüesch, D. 2005. Assessment of sensor characteristics of an airborne laser scanner using geometric reference targets, ISPRS WG III/3, III/4, V3 Workshop "Laser scanning 2005", September 12-14, 2005, Enschede, the Netherlands, ISPRS.

Zakon o javnih naročilih, 2000. UL RS 39/2000.

Zakon o spodbujanju skladnega regionalnega razvoja = Promotion of balanced regional development act, 2005. UL RS 93/2005.

Zakon o lokalni samoupravi = Local self-government act, 1993. UL RS 72/1993.

brazložitev finančnega načrta sprejetega proračuna Službe vlade za lokalno samoupravo SPU 151, 2008. www.mf.gov.si/slov/proracun/sprejet_proracun/2008/spremembe/OBR08_151.pdf (28. 10. 2008)

Zakon o vodah (ZV-1) – Water act, 2002. UL RS 67/2002: pp. 7648-7680.

Zakon o urejanju prostora (ZureP-1) = Spatial planning act, 2002. UL RS 110/2002: pp. 13057-13083, amandment 8/03.

Zakon o prostorskem načrtovanju (ZPNačrt) = Spatial planning act, 2007. UL RS 33/2007: pp. 4585-4602.

Zakon o evidentiranju nepremičnin = Real-Estate recording act, 2006. UL RS 47/2007, pp. 5029–5056.

APPENDICES

Appendix A

Spatial planning in Slovenia

A.1   The history of spatial planning in Slovenia

Spatial planning is an interdisciplinary science, which defines how the physical space on national, regional and local level should develop. It provides guidelines and acts which direct the development of urban and rural areas (Pogačnik, 1992). Spatial planning must include also social and economical planning (Naprudnik, 2005). Nowadays the spatial planning emphasizes the sustainable development and the necessity of physical space preservation, therefore various European and word-wide directives (Pogačnik, 2005) has to be implemented in spatial planning acts: Kyoto protocol, EU INSPIRE directive (Režek, 2007). The new interdisciplinary spatial planning has a tendency towards evidence-based planning (Režek, 2007), therefore a detailed presentation of the current state of physical space is needed. Today there is a trend of increasing role of spatial data (geodetic data). Spatial data is not used just for studying the current state of space on which spatial planning is conducted, but also to monitor the realization of spatial plans (Režek, 2007).

The first act including also spatial planing on the area of Slovenia was enacted in 1875 as Building order for the Dukedom of Kranjska[1]. The Building act of Kingdom of Jugoslavia[2] followed in 1931. After WWII the first Act on spatial planning[3] in 1958 was enacted in Yugoslavia. In the year 1967 the basic acts defining regional and spatial planning were enacted: Urbanistic planning act and Regional planning act (see the timetable in Figure A.1[4]). This acts enroled social spatial planning with (Naprudnik, 2005):

- short-term spatial plans – mainly used on local level

- medium-term spatial plans for the state and regional level

- long-term spatial plan for the whole country

The long- and medium-term plans remained valid even after the social spatial planing was abolished by the fall of planned economy (socialism) in Slovenia in 1990. The new country

---

[1]Stavbni red za Vojvodino Kranjsko
[2]Gradbeni zakon Kraljevine Jugoslavije
[3]Zakon o urbanističnem planiranju
[4]The diagram in Slovene is in Appendix A.2 on page 167.
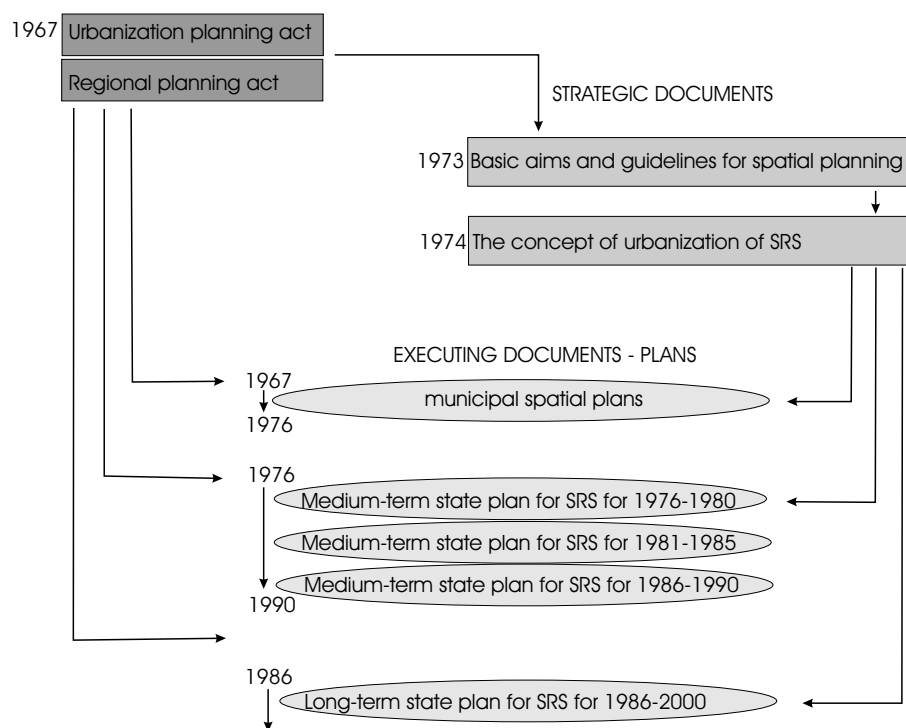
Figure A.1: The timetable of spatial planning in Slovenia before the spatial planning act of 2002 (Naprudnik, 2005). SRS – Socialist Republic of Slovenia.

Slika A.1: Časovnica prostorskega načrtovanja pred zakonom sprejetim v letu 2002.

needed a relatively long time to enact the new Spatial planing and management act in 2002. After it the Strategy of spatial development of Slovenia was adopted in 2004. Apart from the Strategy of spatial development of Slovenia, Slovenia adopted the National development programme 2001–2006, concerning economic development (Državni razvojni program, 2008), and Strategy of regional development in 2001, concerning regional policy, which also influences spatial planning. As late as in 2005 the Development strategy of Slovenia was adopted, which should be a base for all the strategic and program documents of Slovenia (Naprudnik, 2005; Strategija razvoja Slovenije, 2005). The influencing strategies and acts on spatial planning are presented in Figure 2.1[5]. Apart of Promotion of balanced regional development act (UL RS 60/1999 and 93/2005) and Public finance act (UL RS 79/1999) the local spatial planing depends also on Local self-government act (UL RS 72/1993), which defines the competences of municipalities.

Because the Spatial planning and management act from 2002 had some weak points (e.g. not totaly considering EU regulation for spatial planning and environment preservation) the new Spatial planing act was enacted in 2007 (UL RS 33/2007). Unfortunately until now all the regulations of Spatial planning act from 2007 are not enacted jet, therefore at this moment both acts are relevant and presented in Chapter 2.3 on page 8.

---

[5]this diagram in Slovene is on Figure A.3 on page 167

A.2 Diagrams of spatial planning in Slovene
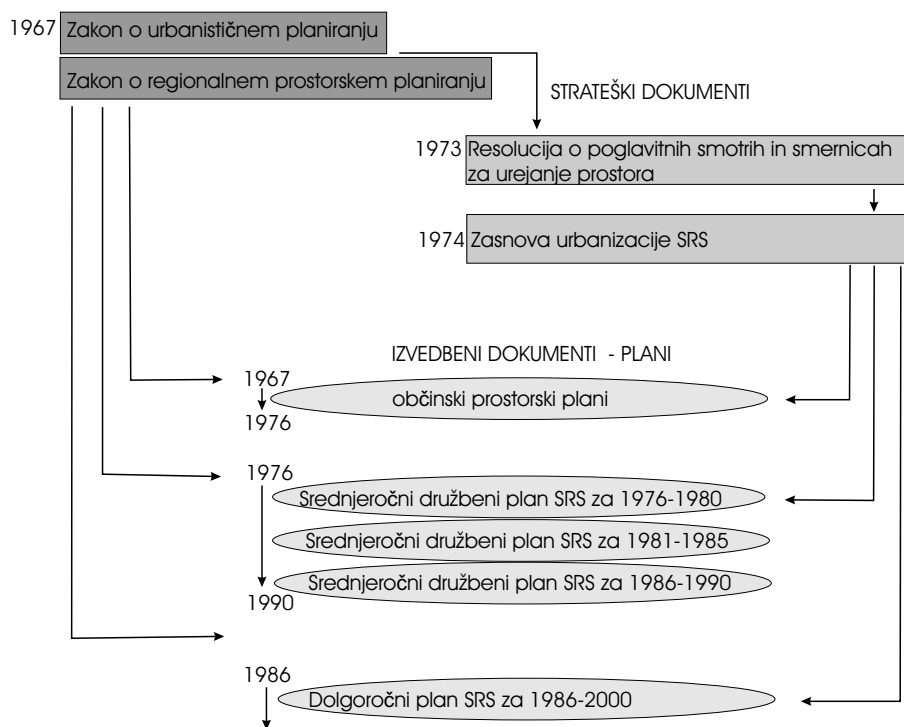
Figure A.2: The timetable of spatial planning in Slovenia before the spatial planning act of 2002 in Slovene (Naprudnik, 2005).
Slika A.2: Časovnica prostorskega načrtovanja pred zakonom sprejetim v letu 2002. (v slovenščini)
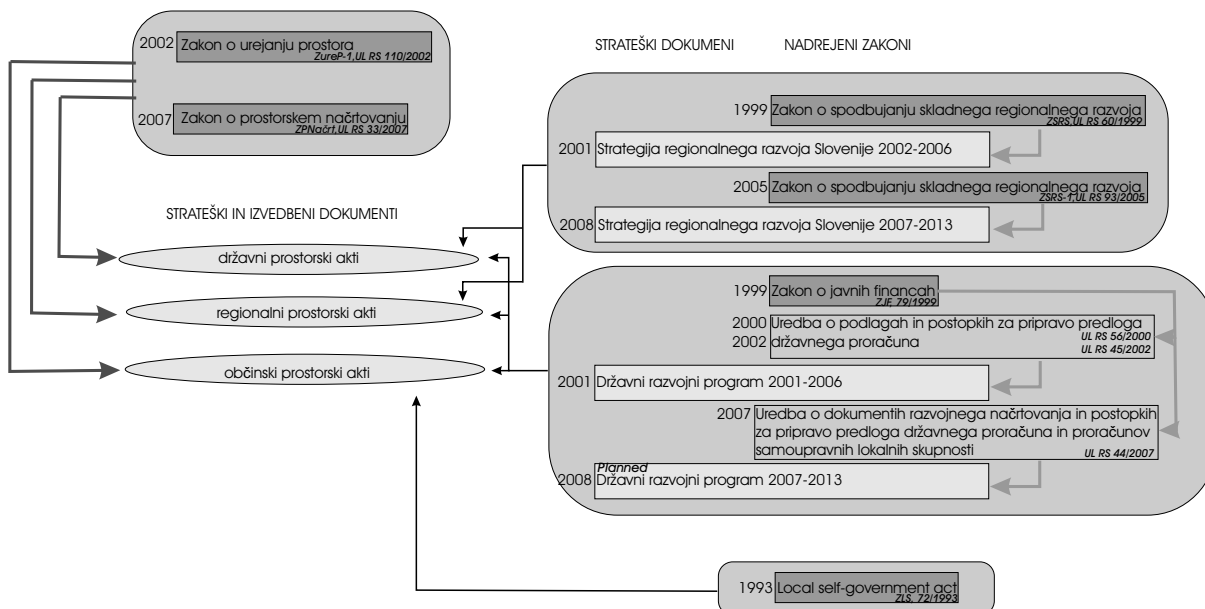
Figure A.3: The influencing acts on Slovenian spatial planning after 1991 (in Slovene).
Slika A.3: Vplivajoči zakoni in strategije na prostorsko planiranje v Sloveniji po 1991.

Figure A.4: Spatial planning documents in Slovenia as proposed by current legislation (in Slovene).

Slika A.4: Dokumenti, ki opredeljujejo prostorsko planiranje.

PODZAKONSKI AKTI

2002 Zakon o urejanju prostora
      ZureP-1,UL RS 110/2002

2007 Zakon o prostorskem načrtovanju
      ZPNačrt,UL RS 33/2007

Pravilnik o podrobnejši vsebini, obliki in načinu priprave strategije prostorskega razvoja Slovenije in vrstah njenih strokovnih podlag
      UL RS 38/2003

Program priprave strategije prostorskega razvoja Slovenije
      UL RS 50/2003

Odlok o strategiji prostorskega razvoja Slovenije
      OdSPRS, UL RS 76/2004

Pravilnik o podrobnejši vsebini, obliki in načinu priprave prostorskega reda Slovenije ter vrstah njegovih strokovnih podlag   *UL RS 42/2004*

Program priprave prostorskega reda Slovenije
      UL RS 60/2004

Uredba o prostorskem redu Slovenije
      UL RS 122/2004

DOKUMENTI

državni prostorski akti

2004 Strategija prostorskega razvoja Slovenije

2004 Prostorski red Slovenije

Državni prostorski načrt

Uredba o vrstah prostorskih ureditev državnega pomena
      UL RS 95/2007
      UL RS 54/2003

regionalni prostorski akti

regionalni prostorski načrt

Pravilnik o vsebini, obliki in načinu priprave državnih in občinskih lokacijskih načrtov
      UL RS 86/2004

Pravilnik o vsebini, obliki in načinu priprave državnega prostorskega načrta ter o načinu priprave variantnih rešitev prostorskih ureditev, njihovega vrednotenja in primerjave   *UL RS 99/2007*

občinski prostorski akti

občinski prostorski načrt

občinski strateški prostorski načrt kot samostojen akt

občinski podrobni prostorski načrt

Program priprave državnega prostorskega načrta

Sklep o javni razgrnitvi predloga državnega prostorskega načrta

Uredba o državnem prostorskem načrtu

Program priprave sprememb in dopolnitev državnega prostorskega načrta

Uredba o spremembah in dopolnitvah državnega prostorskega načrta

Figure A.5: Subacts regulating national spatial planning (in Slovene).
Slika A.5: Podzakonski akti, ki definirajo državno prostorsko planiranje.

Figure A.6: Subacts regulating regional spatial planning (in Slovene).
Slika A.6: Podzakonski akti, ki definirajo regionalno prostorsko planiranje.

Figure A.7: Subacts regulating local spatial planning (in Slovene).
Slika A.7: Podzakonski akti, ki definirajo lokalno prostorsko planiranje.

Appendix B

Basic equations for rotation between different coordinate systems

B.1 Rotation matrices

We can write the rotation from one spatial coordinate system (system 1) to another (system 2) by three rotations:

$$\mathbf{r}_2 = \mathbf{R}_z(\gamma) \cdot \mathbf{R}_y(\beta) \cdot \mathbf{R}_x(\alpha) \cdot \mathbf{r}_1 \tag{B.1}$$

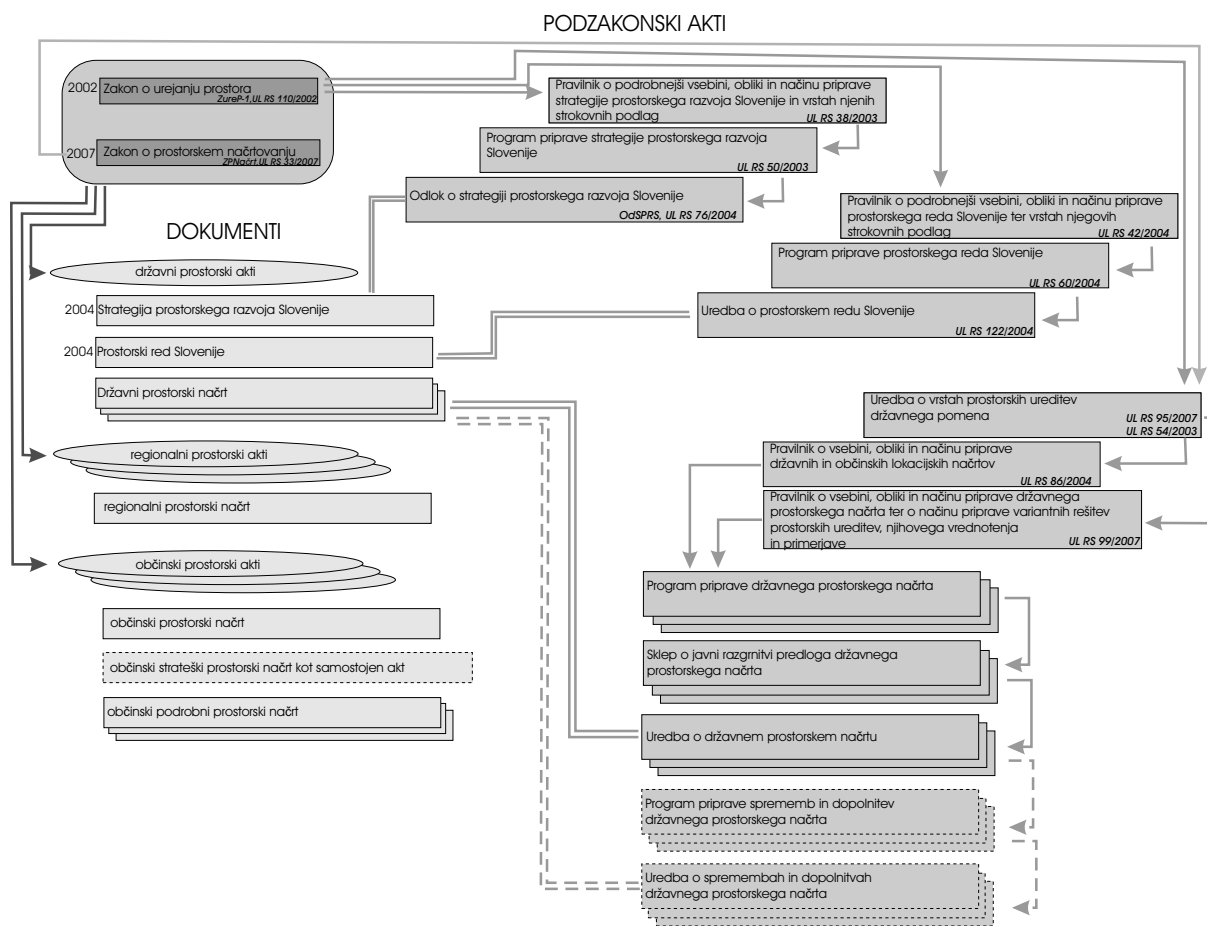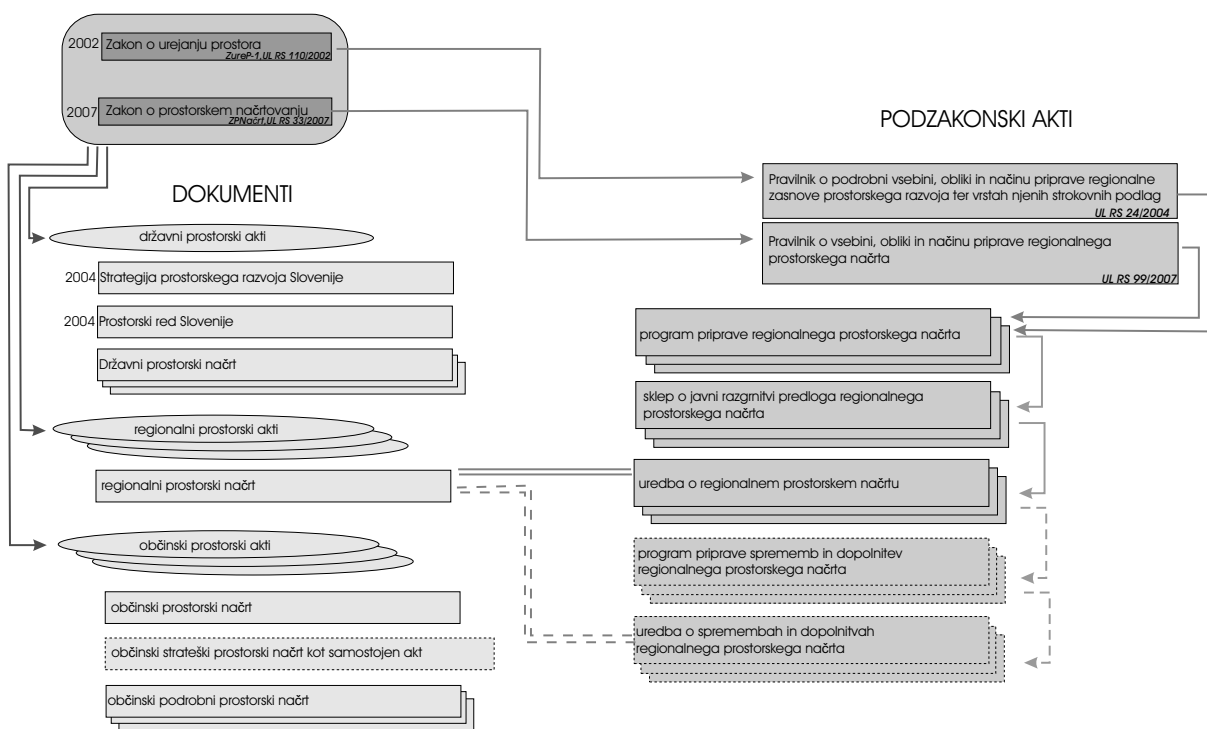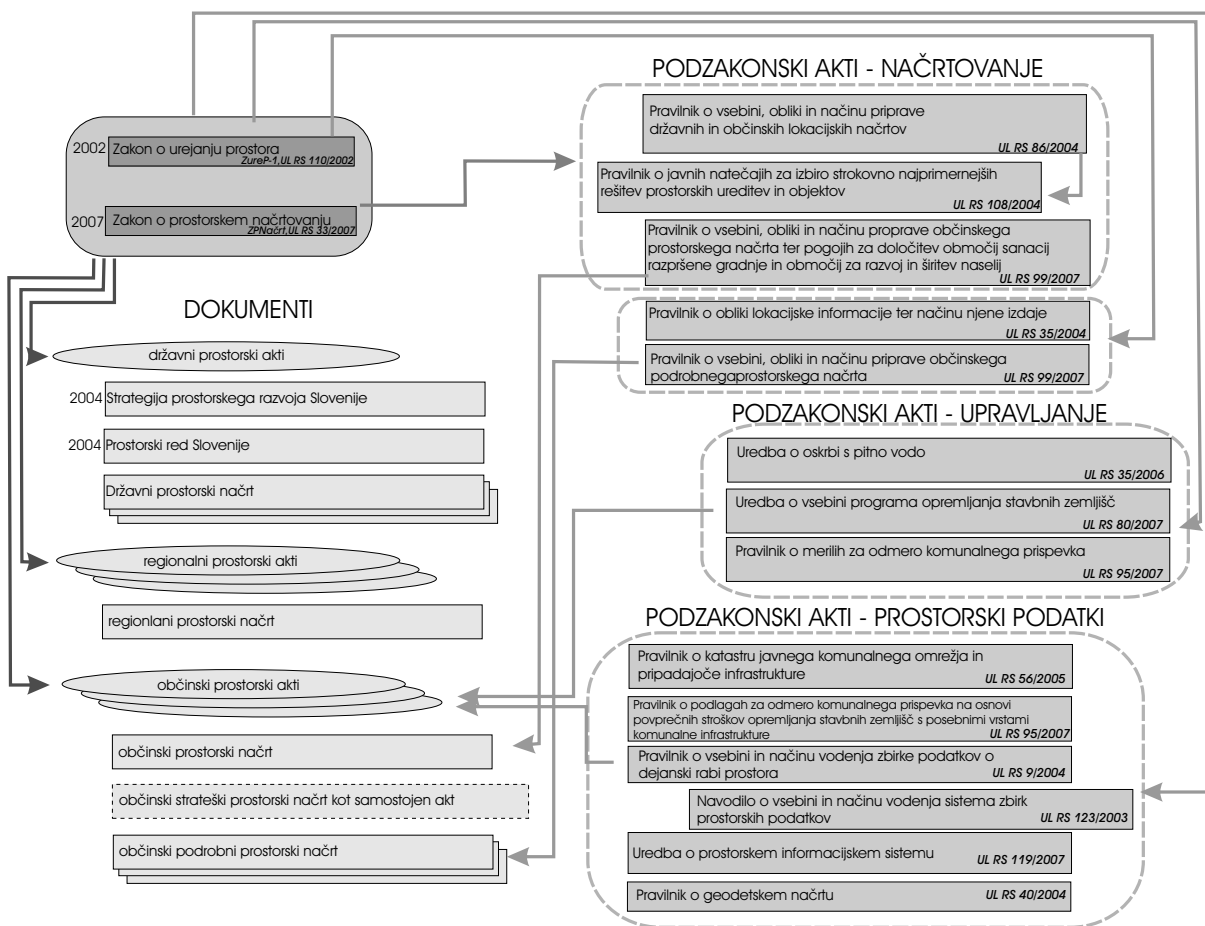If we have a right-handed coordinate system and the angles of transformation are directed in the clockwise direction (**geodetical coordinate systems**) we can write the rotation matrices as:

$$\mathbf{R}_z(\gamma) = \begin{bmatrix} \cos\gamma & \sin\gamma & 0 \\ -\sin\gamma & \cos\gamma & 0 \\ 0 & 0 & 1 \end{bmatrix} \quad \mathbf{R}_y(\beta) = \begin{bmatrix} \cos\beta & 0 & -\sin\beta \\ 0 & 1 & 0 \\ \sin\beta & 0 & \cos\beta \end{bmatrix} \quad \mathbf{R}_x(\alpha) = \begin{bmatrix} 1 & 0 & 0 \\ 0 & \cos\alpha & \sin\alpha \\ 0 & -\sin\alpha & \cos\alpha \end{bmatrix} \tag{B.2}$$
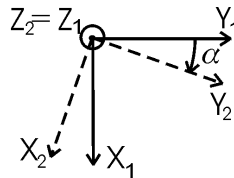
Figure B.1: Righthanded coordinate system and the clockwise direction of transformation from system 1 to system 2 around the Z axis.
Slika B.1: Desnosučni koortdinatni sistem in transformacija iz sistema 1 v sistem 2 okrog Z osi v smeri vrtenja urinega kazalca.

If we have right-handed coordinate system and the rotations from one to another are in counter clockwise direction (**mathematical coordinate systems** — they are used in most cases) we can say that we have negative angles. By comparing them to the upper case, we replace in Equation B.2 matrices the $\cos(-\alpha) = \cos\alpha$, $\sin(-\alpha) = -\sin\alpha$:

$$\mathbf{R}_z(\gamma) = \begin{bmatrix} \cos\gamma & -\sin\gamma & 0 \\ \sin\gamma & \cos\gamma & 0 \\ 0 & 0 & 1 \end{bmatrix} \quad \mathbf{R}_y(\beta) = \begin{bmatrix} \cos\beta & 0 & \sin\beta \\ 0 & 1 & 0 \\ -\sin\beta & 0 & \cos\beta \end{bmatrix} \quad \mathbf{R}_x(\alpha) = \begin{bmatrix} 1 & 0 & 0 \\ 0 & \cos\alpha & -\sin\alpha \\ 0 & \sin\alpha & \cos\alpha \end{bmatrix} \tag{B.3}$$

When dealing with rotations we have to take care on the order of rotations. By changing the order of rotations we get different rotations.

Rotation matrices for small angles

Rotation matrices for small angles can be written in the **mathematical coordinate system** (Equation B.3) as:

$$
\mathbf{R}_z(\gamma) = \begin{bmatrix} 1 & -\gamma & 0 \\ \gamma & 1 & 0 \\ 0 & 0 & 1 \end{bmatrix} \quad
\mathbf{R}_y(\beta) = \begin{bmatrix} 1 & 0 & \beta \\ 0 & 1 & 0 \\ -\beta & 0 & 1 \end{bmatrix} \quad
\mathbf{R}_x(\alpha) = \begin{bmatrix} 1 & 0 & 0 \\ 0 & 1 & -\alpha \\ 0 & \alpha & 1 \end{bmatrix} \tag{B.4}
$$

B.2 Transformation from ellipsoidal to cartesian coordinates

In our measurements, location of the phase center of GPS receiver is known in the ellipsoidal coordinates (ϕ, λ, h). Where h is height on the ellipsoid. We can compute the cartesian coordinates (X, Y, Z) by the knowledge of the ellipsoid parameters (e, a) (Iliffe, 2000):

$$
\begin{bmatrix} X \\ Y \\ Z \end{bmatrix} = \begin{bmatrix} (N + h) \cdot \cos\phi \cdot \cos\lambda \\ (N + h) \cdot \cos\phi \cdot \sin\lambda \\ (N \cdot (1 - e^2) + h) \cdot \sin\phi \end{bmatrix} \tag{B.5}
$$

where N is

$$
N = \frac{a}{\sqrt{1 - e^2 \cdot \sin^2\phi}} \tag{B.6}
$$

The parameters of WGS84 are defined as:

$$
a = 6378137 \quad \text{and} \quad f = 1/298.257223563 \tag{B.7}
$$

The relations of the ellipsoid give the eccentricity (e) from flattening f:

$$
e = \sqrt{f^2 - 2 \cdot f} \tag{B.8}
$$

The inverse rotation from ellipsoidal to cartesian coordinates of is written with:

$$
\lambda = \arctan\frac{Y}{X} \tag{B.9}
$$

$$\phi = \arctan \frac{Z + e'^2 \cdot b \cdot \sin^3 u}{p - e^2 \cdot a \cdot \cos^3 u}$$

$$h = \frac{p}{\cos \phi} - N$$

where

$$p = \sqrt{X^2 + Y^2} \qquad u = \frac{Z}{p} \cdot \frac{a}{b} \tag{B.10}$$

$$e^2 = \frac{a^2 - b^2}{a^2} \qquad e'^2 = \frac{a^2 - b^2}{b^2}$$

Appendix C

Behaviour of the laser scanning error model when applying different geometrical parameters

C.1   Components and derivatives

C.1.1   Components of $\Delta \mathbf{x}_s$

The error components of vector $\Delta \mathbf{x}_s = [\Delta X_s, \Delta Y_s, \Delta Z_s]^T$:

$\Delta X_s = (\cos\psi\cos\theta - \Delta\psi\sin\psi\cos\theta - \Delta\theta\sin\theta)x_1(1,1) +$
$(\cos\psi\sin\theta\sin\phi - \sin\psi\cos\phi - \Delta\psi(\sin\psi\sin\theta\sin\phi + \cos\psi\cos\phi) + \Delta\theta\cos\theta\sin\varphi)x_1(2,1) +$
$(\cos\psi\sin\theta\cos\phi + \sin\psi\sin\phi - \Delta\psi(\sin\psi\sin\theta\cos\phi - \cos\psi\sin\phi) + \Delta\theta\cos\theta\cos\phi)x_1(3,1) -$
$[\cos\psi\cos\theta x_1^*(1,1) + (\cos\psi\sin\theta\sin\phi - \sin\psi\cos\phi)x_1^*(2,1) + (\cos\psi\sin\theta\cos\phi + \sin\psi\sin\phi)x_1^*(3,1)]$

$\Delta Y_s = (\Delta\psi\cos\psi\cos\theta + \sin\psi\cos\theta - \Delta\phi\sin\theta)x_1(1,1) +$
$(\Delta\psi(\cos\psi\sin\theta\sin\phi - \sin\psi\cos\phi) + \sin\psi\sin\theta\sin\phi + \cos\psi\cos\phi - \Delta\phi\cos\theta\sin\phi)x_1(2,1) +$
$(\Delta\psi(\cos\psi\sin\theta\cos\phi + \sin\psi\sin\phi) + \sin\psi\sin\theta\cos\phi - \cos\psi\sin\phi - \Delta\psi\cos\theta\cos\phi)x_1(3,1) -$
$[\sin\psi\cos\theta x_1^*(1,1) + (\sin\psi\sin\theta\sin\phi + \cos\psi\cos\phi)x_1^*(2,1) + (\sin\psi\sin\theta\cos\phi - \cos\psi\sin\phi)x_1^*(3,1)]$

$\Delta Z_s = (-\Delta\theta\cos\psi\cos\theta + \Delta\phi\sin\psi\cos\theta - \sin\theta)x_1(1,1) +$
$(-\Delta\theta(\cos\psi\sin\theta\sin\phi - \sin\psi\cos\phi) + \Delta\phi(\sin\psi\sin\theta\sin\phi + \cos\psi\cos\phi) + \cos\theta\sin\phi)x_1(2,1) +$
$(-\Delta\theta(\cos\psi\sin\theta\cos\phi + \sin\psi\sin\phi) + \Delta\phi(\sin\psi\sin\theta\cos\phi - \cos\psi\sin\phi) + \cos\theta\cos\phi)x_1(3,1) -$
$[-\sin\theta x_1^*(1,1) + \cos\theta\sin\phi x_1^*(2,1) + \cos\theta\cos\phi x_1^*(3,1)]$

For easier calculation of integrals, first and second derivatives, equations can be written as:

$$\Delta \mathbf{x}_s = \mathbf{A}_s \cos\psi + \mathbf{B}_s \sin\psi + \mathbf{C}_s$$

and:
$$\mathbf{A}_s = \begin{bmatrix} A_{sx} \\ A_{sy} \\ A_{sz} \end{bmatrix}, \qquad \mathbf{B}_s = \begin{bmatrix} B_{sx} \\ B_{sy} \\ B_{sz} \end{bmatrix}, \qquad \mathbf{C}_s = \begin{bmatrix} C_{sx} \\ C_{sy} \\ C_{sz} \end{bmatrix}$$

The rearranged upper equation by putting out scan angle β is written as:

$$\Delta\mathbf{x}_s = (\mathbf{D}_s \cos\beta + \mathbf{E}_s \sin\beta)\cos\psi + (\mathbf{F}_s \cos\beta + \mathbf{G}_s \sin\beta)\sin\psi + (\mathbf{H}_s \cos\beta + \mathbf{J}_s \sin\beta)$$

the coeficients are:
$$\mathbf{A}_s = \mathbf{D}_s \cos\beta + \mathbf{E}_s \sin\beta$$
$$\mathbf{B}_s = \mathbf{F}_s \cos\beta + \mathbf{G}_s \sin\beta$$
$$\mathbf{C}_s = \mathbf{H}_s \cos\beta + \mathbf{J}_s \sin\beta$$

again:
$$\mathbf{D}_s = \begin{bmatrix} D_{sx} \\ D_{sy} \\ D_{sz} \end{bmatrix}, \mathbf{E}_s = \begin{bmatrix} E_{sx} \\ E_{sy} \\ E_{sz} \end{bmatrix}, \mathbf{F}_s = \begin{bmatrix} F_{sx} \\ F_{sy} \\ F_{sz} \end{bmatrix}, \mathbf{G}_s = \begin{bmatrix} G_{sx} \\ G_{sy} \\ G_{sz} \end{bmatrix}, \mathbf{H}_s = \begin{bmatrix} H_{sx} \\ H_{sy} \\ H_{sz} \end{bmatrix}, \mathbf{J}_s = \begin{bmatrix} J_{sx} \\ J_{sy} \\ J_{sz} \end{bmatrix}$$

For each component (X_s, Y_x, Z_s) separately this brings:

$A_{sx} = \cos\theta x_1(1,1) + (\sin\theta\sin\phi - \Delta\psi\cos\phi)x_1(2,1) + (\sin\theta\cos\phi + \Delta\psi\sin\phi)x_1(3,1)$
$- \cos\theta x_1^*(1,1) - \sin\theta\sin\phi x_1^*(2,1) - \sin\theta\cos\phi x_1^*(3,1)$
$B_{sx} = -\Delta\psi\cos\theta x_1(1,1) - (\cos\phi + \Delta\psi\sin\theta\sin\phi)x_1(2,1) + (\sin\phi - \Delta\psi\sin\theta\cos\phi)x_1(3,1)$
$+ \cos\phi x_1^*(2,1) - \sin\phi x_1^*(3,1)$
$C_{sx} = -\Delta\theta\sin\theta x_1(1,1) + \Delta\theta\cos\theta\sin\phi x_1(2,1) + \Delta\theta\cos\theta\cos\phi x_1(3,1)$
$\qquad H_{sx} = -\Delta\theta\sin\theta k_{13} + \Delta\theta\cos\theta\sin\phi k_{23} + \Delta\theta\cos\theta\cos\phi k_{33}$

$A_{sy} = \Delta\psi\cos\theta x_1(1,1) + (\Delta\psi\sin\theta\sin\phi + \cos\phi)x_1(2,1) + (\Delta\psi\sin\theta\cos\phi - \sin\phi)x_1(3,1) - \cos\phi x_1^*(2,1) + \sin\phi x_1^*(3,1)$
$B_{sy} = \cos\theta x_1(1,1) + (-\Delta\psi\cos\phi + \sin\theta\sin\phi)x_1(2,1) + (\Delta\psi\sin\phi + \sin\theta\cos\phi)x_1(3,1)$
$- \cos\theta x_1^*(1,1) - \sin\theta\sin\phi x_1^*(2,1) - \sin\theta\cos\phi x_1^*(3,1)$
$C_{sy} = \Delta\phi\sin\theta x_1(1,1) - \Delta\phi\cos\theta\sin\phi x_1(2,1) - \Delta\phi\cos\theta\cos\phi x_1(3,1)$
$\qquad H_{sy} = \Delta\phi\sin\theta k_{13} - \Delta\phi\cos\theta\sin\phi k_{23} - \Delta\phi\cos\theta\cos\phi k_{33}$

$A_{sz} = -\Delta\theta\cos\theta x_1(1,1) + (-\Delta\theta\sin\theta\sin\phi + \Delta\phi\cos\phi)x_1(2,1) - (\Delta\theta\sin\theta\cos\phi + \Delta\phi\sin\phi)x_1(3,1)$
$B_{sz} = \Delta\phi\cos\theta x_1(1,1) + (\Delta\theta\cos\phi + \Delta\phi\sin\theta\sin\phi)x_1(2,1) + (-\Delta\theta\sin\phi + \Delta\phi\sin\theta\cos\phi)x_1(3,1)$
$C_{sz} = -\sin\theta x_1(1,1) + \cos\theta\sin\phi x_1(2,1) + \cos\theta\cos\phi x_1(3,1) +$
$\sin\theta x_1^*(1,1) - \cos\theta\sin\phi x_1^*(2,1) - \cos\theta\cos\phi x_1^*(3,1)$
$\qquad H_{sz} = -\sin\theta k_{13} + \cos\theta\sin\phi k_{23} + \cos\theta\cos\phi k_{33} + \sin\theta R_m(1,3) - \cos\theta\sin\phi R_m(2,3) - \cos\theta\cos\phi R_m(3,3)$

C.1.2 Average value for different scan angles

The average value for a changing scan angle for each component can be written as (only the ΔX_s is written):

$$< \Delta X_s > = \frac{1}{2\pi}\int_0^{2\pi}(A_{sx}\cos\psi + B_{sx}\sin\psi + C_{sx})d\psi = \frac{1}{2\pi}C_{sx}|_0^{2\pi} = C_{sx}$$

Therefore:

$$< \Delta \mathbf{x}_s > = \begin{bmatrix} < \Delta X_s > \\ < \Delta Y_s > \\ < \Delta Z_s > \end{bmatrix} = \begin{bmatrix} C_{sx} \\ C_{sy} \\ C_{sz} \end{bmatrix} =$$

$$\begin{bmatrix} -\Delta\theta \sin\theta x_1(1,1) + \Delta\theta \cos\theta \sin\phi x_1(2,1) + \Delta\theta \cos\theta \cos\phi x_1(3,1) \\ \Delta\phi \sin\theta x_1(1,1) - \Delta\phi \cos\theta \sin\phi x_1(2,1) - \Delta\phi \cos\theta \cos\phi x_1(3,1) \\ -\sin\theta x_1(1,1) + \cos\theta \sin\phi x_1(2,1) + \cos\theta \cos\phi x_1(3,1) + \sin\theta x_1^*(1,1) - \cos\theta \sin\phi x_1^*(2,1) - \cos\theta \cos\phi x_1^*(3,1) \end{bmatrix}$$

C.1.3   Average value independent from scan angle

The average value independent from scan angle and heading for each component can be written as (only the ΔX_s component is written):

$$<< \Delta X_s >> = \frac{1}{2\pi} \int_0^{2\pi} d\psi \int_{-\beta_0}^{\beta} d\beta [(D_{sx} \cos\beta + E_{sx} \sin\beta) \cos\psi + (F_{sx} \cos\beta + G_{sx} \sin\beta) \sin\psi +$$

$$+ (H_{sx} \cos\beta + J_{sx} \sin\beta)] =$$

$$= \frac{1}{4\pi\beta_0} \left[\left(D_{sx} \int_{-\beta_0}^{\beta} \cos\beta d\beta + E_{sx} \int_{-\beta_0}^{\beta} \sin\beta d\beta \right) \int_0^{2\pi} \cos\psi d\psi + \right.$$
$$\left. \left(F_{sx} \int_{-\beta_0}^{\beta} \cos\beta d\beta + G_{sx} \int_{-\beta_0}^{\beta} \sin\beta d\beta \right) \int_0^{2\pi} \sin\psi d\psi + \left(H_{sx} \int_{-\beta_0}^{\beta} \cos\beta d\beta + J_{sx} \int_{-\beta_0}^{\beta} \sin\beta d\beta \right) \right] =$$

$$= \frac{1}{4\pi\beta_0} \left[0 + 0 + \left(H_{sx} \sin\beta |_{-\beta_0}^{\beta} - J_{sx} \cos\beta |_{-\beta_0}^{\beta} \right) \psi |_0^{2\pi} \right] =$$

$$= \frac{1}{4\pi\beta_0} [H_{sx}(\sin\beta_0 - \sin(-\beta_0)) - J_{sx}(\cos\beta_0 - \cos(-\beta_0))](2\pi - 0) =$$

$$= \frac{1}{2\beta_0}(H_{sx} 2\sin\beta_0 - J_{sx} \cdot 0) =$$

$$= \frac{\sin\beta_0}{\beta_0} H_{sx}$$

Therefore:

$$<< \Delta \mathbf{x}_s >> = \begin{bmatrix} << \Delta X_s >> \\ << \Delta Y_s >> \\ << \Delta Z_s >> \end{bmatrix} = \begin{bmatrix} \frac{\sin\beta_0}{\beta_0} H_{sx} \\ \frac{\sin\beta_0}{\beta_0} H_{sy} \\ \frac{\sin\beta_0}{\beta_0} H_{sz} \end{bmatrix} =$$

$$\begin{bmatrix} \frac{h \cdot \sin\beta_0}{\beta_0}(-\Delta\theta \sin\theta k_{13} + \Delta\theta \cos\theta \sin\phi k_{23} + \Delta\theta \cos\theta \cos\phi k_{33}) \\ \frac{h \cdot \sin\beta_0}{\beta_0}(\Delta\phi \sin\theta k_{13} - \Delta\phi \cos\theta \sin\phi k_{23} - \Delta\phi \cos\theta \cos\phi k_{33}) \\ \frac{h \cdot \sin\beta_0}{\beta_0}(-\sin\theta k_{13} + \cos\theta \sin\phi k_{23} + \cos\theta \cos\phi k_{33} + \sin\theta R_m(1,3) - \cos\theta \sin\phi R_m(2,3) - \cos\theta \cos\phi R_m(3,3)) \end{bmatrix}$$

C.1.4 First and second derivatives – searching for maximum

If the first derivative of a component $\frac{\partial \Delta \mathbf{x}_s}{\partial \psi}$ is 0, it represents an extreme of the this component (ΔX_s, ΔY_s and ΔZ_s):

$\frac{\partial \Delta X_s}{\partial \psi} = -A_{sx} \sin \psi + B_{sx} \cos \psi = 0$

$\psi_{\Delta X_s} = \arctan \frac{B_{sx}}{A_{sx}}$

$\frac{\partial \Delta Y_s}{\partial \psi} = -A_{sy} \sin \psi + B_{sy} \cos \psi = 0$

$\psi_{\Delta Y_s} = \arctan \frac{B_{sy}}{A_{sy}}$

$\frac{\partial \Delta Z_s}{\partial \psi} = -A_{sz} \sin \psi + B_{sz} \cos \psi = 0$

$\psi_{Z_s} = \arctan \frac{B_{sz}}{A_{sz}}$

To find out, which extreme represents the maximum of each component, the second derivative should be negative $\frac{\partial^2 \Delta X_s}{\partial^2 \psi} < 0$. In this case calculated $\psi_{\Delta X_s}$ represents the maximum of the function ΔX_s (similar for ΔY_s and ΔZ_s).

$\frac{\partial^2 \Delta X_s}{\partial^2 \psi} = -A_{sx} \cos \psi_{\Delta X_s} - B_{sx} \sin \psi_{\Delta X_s} < 0 \longrightarrow \psi_{\Delta X_{s\_max}} = \psi_{\Delta X_s}$

$\frac{\partial^2 \Delta Y_s}{\partial^2 \psi} = -A_{sy} \cos \psi_{\Delta Y_s} - B_{sy} \sin \psi_{\Delta Y_s} < 0 \longrightarrow \psi_{\Delta Y_{s\_max}} = \psi_{\Delta Y_s}$

$\frac{\partial^2 \Delta Z_s}{\partial^2 \psi} = -A_{sz} \cos \psi_{\Delta Z_s} - B_{sz} \sin \psi_{\Delta Z_s} < 0 \longrightarrow \psi_{\Delta Z_{s\_max}} = \psi_{\Delta Z_s}$

C.2   Behaviour of the Schenk's and the simplified error model in graphs

C.2.1   Influence of $\Delta\mathbf{R}_s$ and $\Delta\mathbf{R}_m$

Figure C.1: Basic systematic errors by Schenk's $\Delta\mathbf{x}_s$ and simplified average $\Delta\mathbf{x}_{ave}$ ($= \Delta\mathbf{x}_{s\_ave}$) error model for **different combinations of $\Delta\mathbf{R}_s$ and $\Delta\mathbf{R}_m$ (Table 6.1) and scan angle $0°$** with variable heading angle. The simulation is done for roll and pitch errors of $\Delta\phi = \Delta\theta = 0.005°$, and heading error $\Delta\psi = 0.007°$, and average magnitude of roll and pitch angles of $3°$ and flying height of 1000 m. Error components: A) ΔX, B) ΔY and C) ΔZ.

Slika C.1: Osnovne sistematične napake po Schenkovem $\Delta\mathbf{x}_s$ in poenostavljenem povprečnemu modelu napak $\Delta\mathbf{x}_{s\_ave}$ za različne kombinacije $\Delta\mathbf{R}_s$ and $\Delta\mathbf{R}_m$ (kot so označene v Tabeli 6.1) in kot skeniranja $0°$.

Figure C.2: Basic systematic errors by Schenk's $\Delta\mathbf{x}_s$ and simplified average $\Delta\mathbf{x}_{ave}$ $(= \Delta\mathbf{x}_{s\_ave})$ error model for **different combinations of $\Delta\mathbf{R}_s$ and $\Delta\mathbf{R}_m$ (Table 6.1) and scan angle 10°** with variable heading angle. The simulation is done for roll and pitch errors of $\Delta\phi = \Delta\theta = 0.005°$, and heading error $\Delta\psi = 0.007°$, and average magnitude of roll and pitch angles of 3° and flying height of 1000 m. Error components: A) ΔX, B) ΔY and C) ΔZ.

Slika C.2: Osnovne sistematične napake po Schenkovem $\Delta\mathbf{x}_s$ in poenostavljenem povprečnemu modelu napak $\Delta\mathbf{x}_{s\_ave}$ za različne kombinacije $\Delta\mathbf{R}_s$ in $\Delta\mathbf{R}_m$ (kot so označene v Tabeli 6.1) in kot skeniranja 10°.
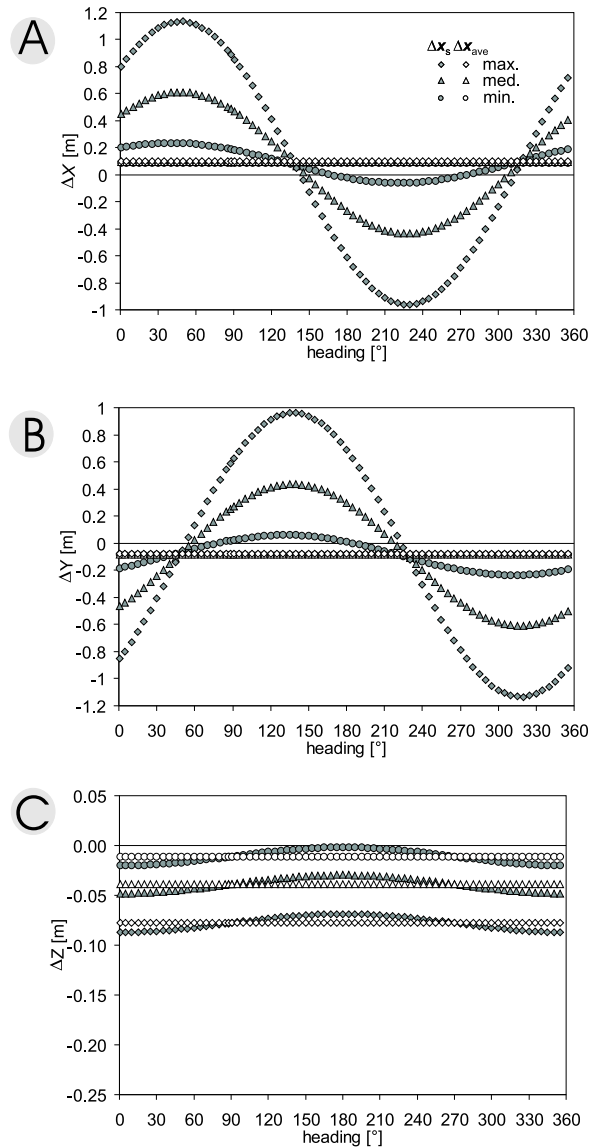
C.2.2 Influence of $\mathbf{R}_m$
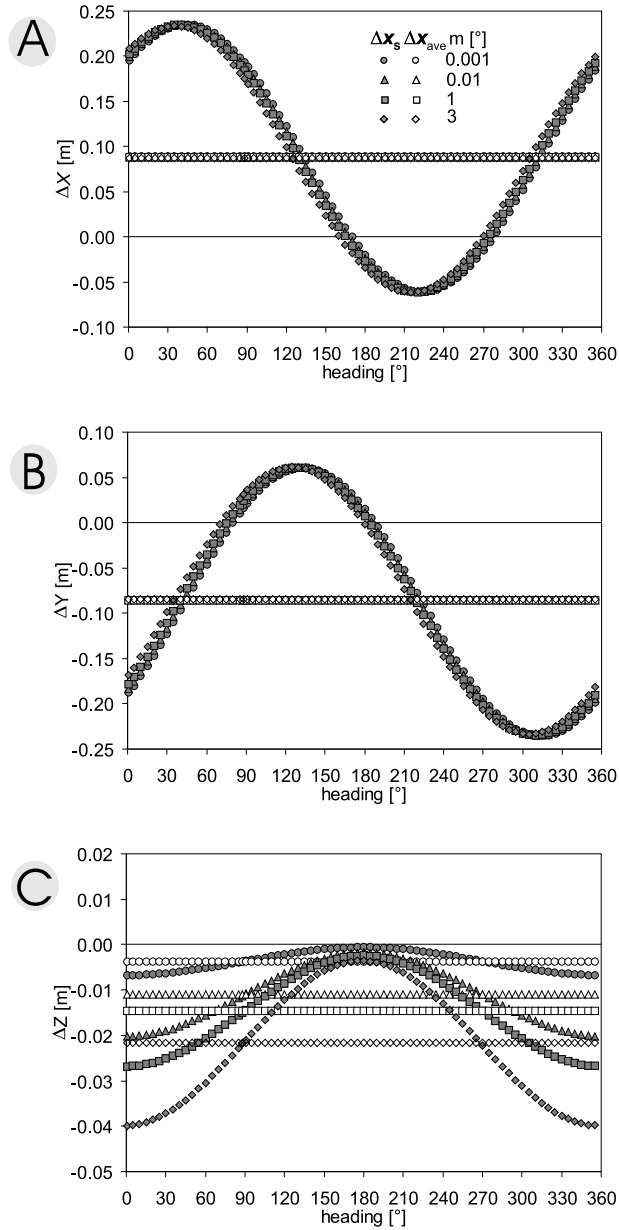
Figure C.3: Basic systematic errors by Schenk's $\Delta\mathbf{x}_s$ and simplified average $\Delta\mathbf{x}_{ave}$ error model for **different $\mathbf{R}_m$ values ($m = m_z = m_y = m_x$) and scan angle $\mathbf{0}°$** with variable heading angle. The simulation is done for flying height of 1000 m and $\Delta\mathbf{R}_{\mathrm{INS}}$ values of $\Delta\phi = \Delta\theta = 0.005°$ and $\Delta\psi = 0.007°$, and average magnitude of roll and pitch angles $1°$. Error components: A) ΔX, B) ΔY and C) ΔZ.

Slika C.3: Osnovne sistematične napake po Schenkovem $\Delta\mathbf{x}_s$ in poenostavljenem povprečnemu modelu napak $\Delta\mathbf{x}_{ave}$ pri različni vrednostih kotov $\mathbf{R}_m$, kotu skeniranja $0°$, višini leta 1000 m ter spremenljivem kotu pozibavanja ψ.

C.2.3   Influence of $\mathbf{R}_{\mathrm{GEO}}$
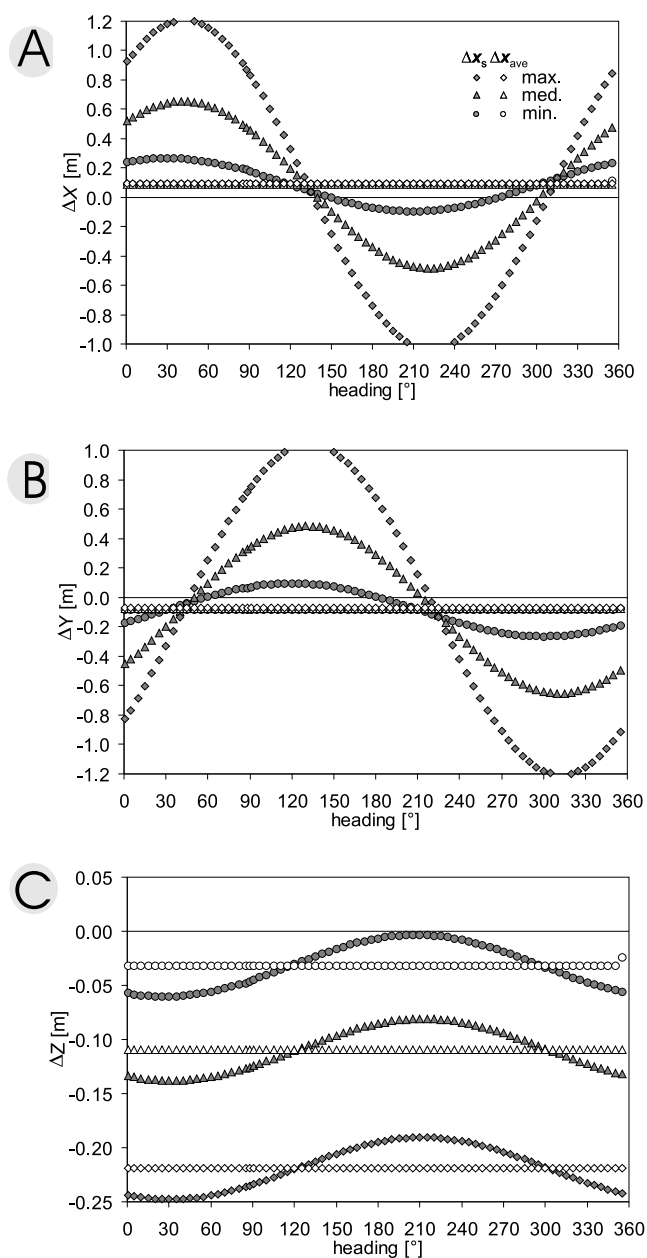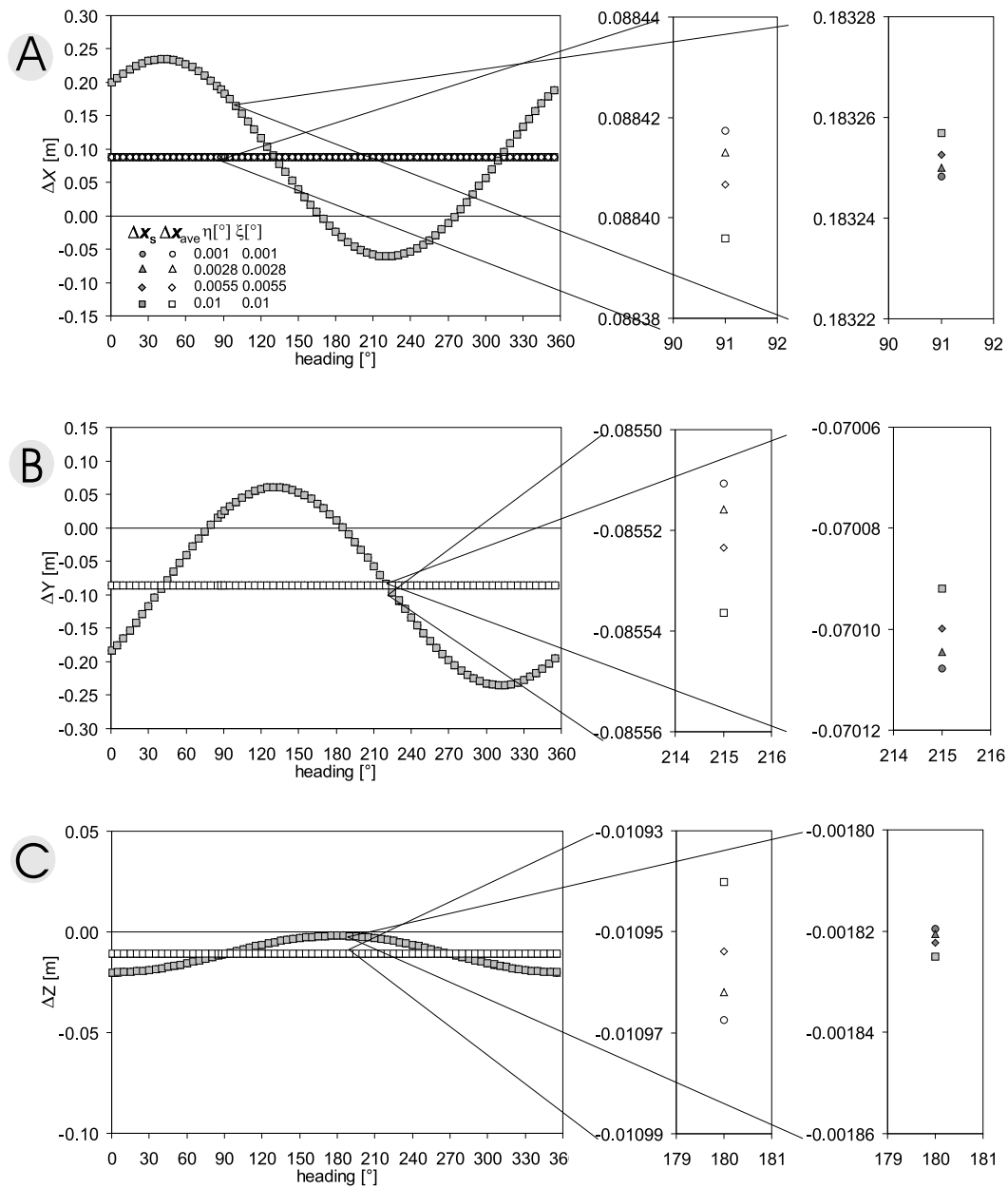

Figure C.4: Basic systematic errors by Schenk's $\Delta\mathbf{x}_s$ and simplified average $\Delta\mathbf{x}_{ave}$ error model for **different $\mathbf{R}_{\mathrm{GEO}}$ values, scan angle $0°$**, with variable heading angle. The simulation is done $\Delta\mathbf{R}_{\mathrm{INS}}$ values of $\Delta\phi = \Delta\theta = 0.005°$ and $\Delta\psi = 0.007°$, and average magnitude of roll and pitch angles of $1°$. Error components A) ΔX , B) ΔY and C) ΔZ.

Slika C.4: Osnovne sistematične napake po Schenkovem $\Delta\mathbf{x}_s$ in poenostavljenem povprečnemu modelu napak $\Delta\mathbf{x}_{ave}$ za različne vrednosti $\mathbf{R}_{\mathrm{GEO}}$ in kot skeniranja $0°$.
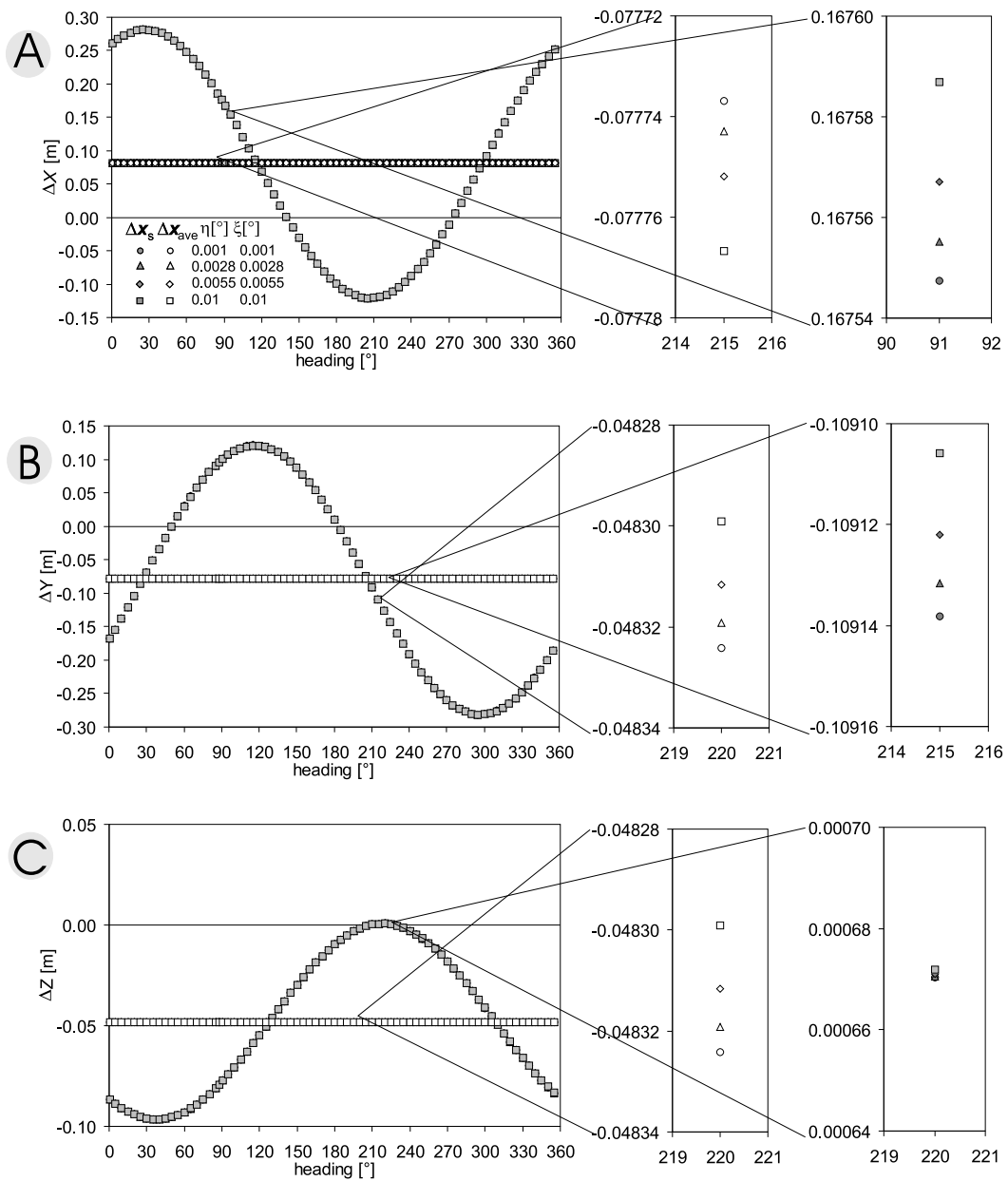
Figure C.5: Basic systematic errors by Schenk's $\Delta \mathbf{x}_s$ and simplified average $\Delta \mathbf{x}_{ave}$ error model for **different $\mathbf{R}_{GEO}$ values, scan angle 20°**, with variable heading angle. The simulation is done $\Delta \mathbf{R}_{INS}$ values of $\Delta \phi = \Delta \theta = 0.005°$ and $\Delta \psi = 0.007°$, and average magnitude of roll and pitch angles of $1°$. Error components A) ΔX , B) ΔY and C) ΔZ.

Slika C.5: Osnovne sistematične napake po Schenkovem $\Delta \mathbf{x}_s$ in poenostavljenem povprečnemu modelu napak $\Delta \mathbf{x}_{ave}$ za različne vrednosti $\mathbf{R}_{GEO}$, kot skeniranja $20°$ ter spremenljivem kotu pozibavanja ψ.

C.2.4   Influence of $\mathbf{R}_{\mathrm{INS}}$
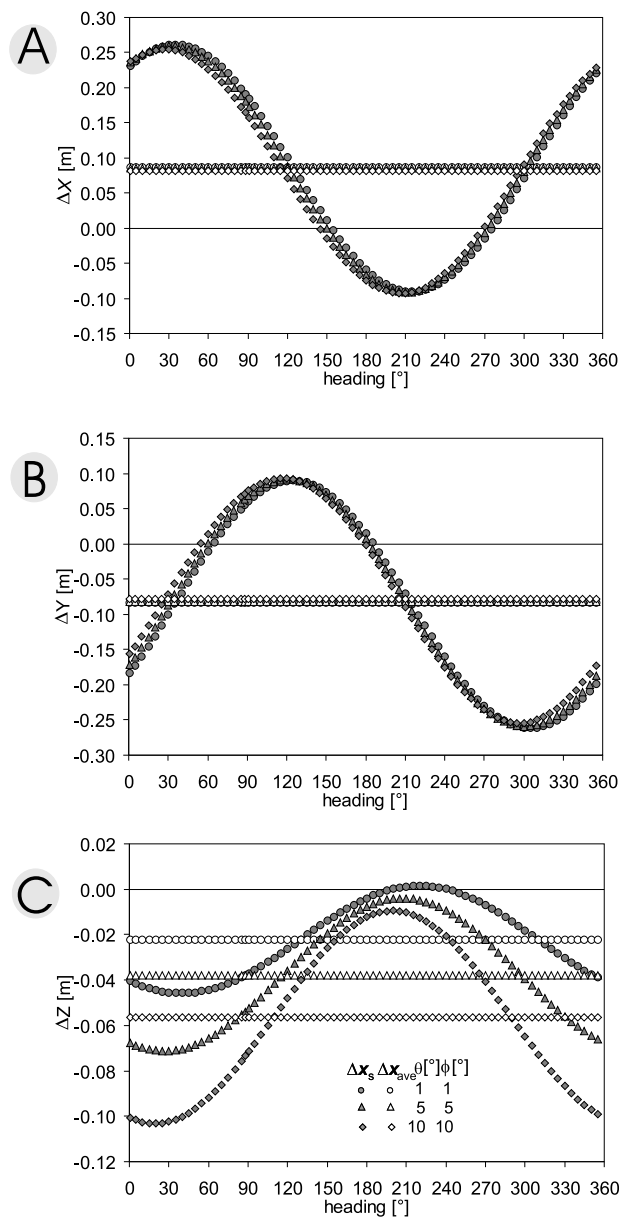
Figure C.6: Basic systematic errors by Schenk's $\Delta\mathbf{x}_s$ and simplified average $\Delta\mathbf{x}_{ave}$ error model for **different average magnitudes of roll and pitch values ($\mathbf{R}_{\mathrm{INS}}$ values)** and variable heading angle. The simulation is done for flying height of 1000 m and scan angle $0°$ and $\Delta\mathbf{R}_{\mathrm{INS}}$ values of $\Delta\phi = \Delta\theta = 0.005°$ and $\Delta\psi = 0.007°$. Error components: A) ΔX , B) ΔY and C) ΔZ.

Slika C.6: Osnovne sistematične napake po Schenkovem $\Delta\mathbf{x}_s$ in poenostavljenem povprečnemu modelu napak $\Delta\mathbf{x}_{ave}$ pri različni srednjih velikostih kotov zibanja ϕ in guganja θ ($\mathbf{R}_{\mathrm{INS}}$) ter spremenljivem kotu pozibavanja ψ. Za višino leta 1000 m in kot skeniranja $10°$.
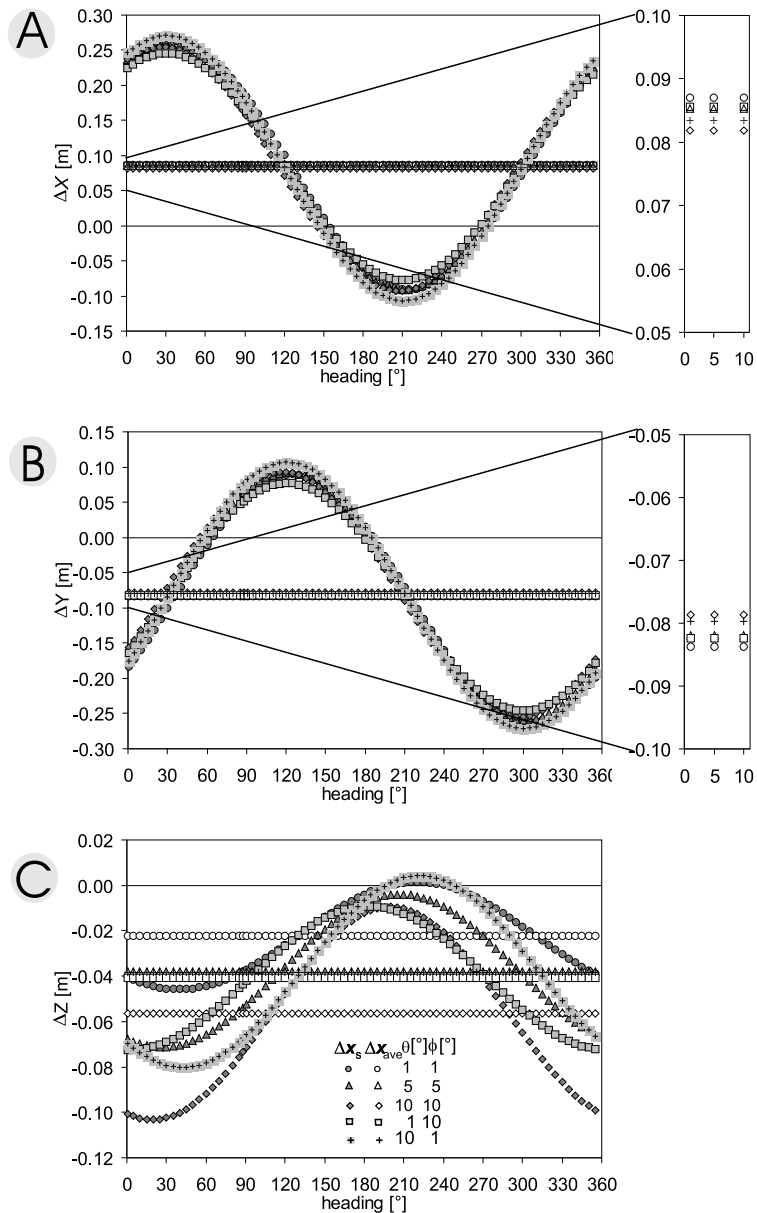
Figure C.7: Basic systematic errors by Schenk's $\Delta\mathbf{x}_s$ and simplified average $\Delta\mathbf{x}_{ave}$ error model for **different average magnitudes of roll and pitch values ($\mathbf{R}_{INS}$ values)** and variable heading angle for two more combinations of average magnitudes of roll and pitch angles than on Figure C.6. Error components: A) ΔX, B) ΔY and C) ΔZ.

Slika C.7: Osnovne sistematične napake po Schenkovem $\Delta\mathbf{x}_s$ in poenostavljenem povprečnemu modelu napak $\Delta\mathbf{x}_{ave}$ pri različni srednjih velikostih kotov zibanja ϕ in guganja θ ($\mathbf{R}_{INS}$) ter spremenljivem kotu pozibavanja ψ. Še dve kombinaciji več kot na sliki C.6.

C.2.5 Maxima
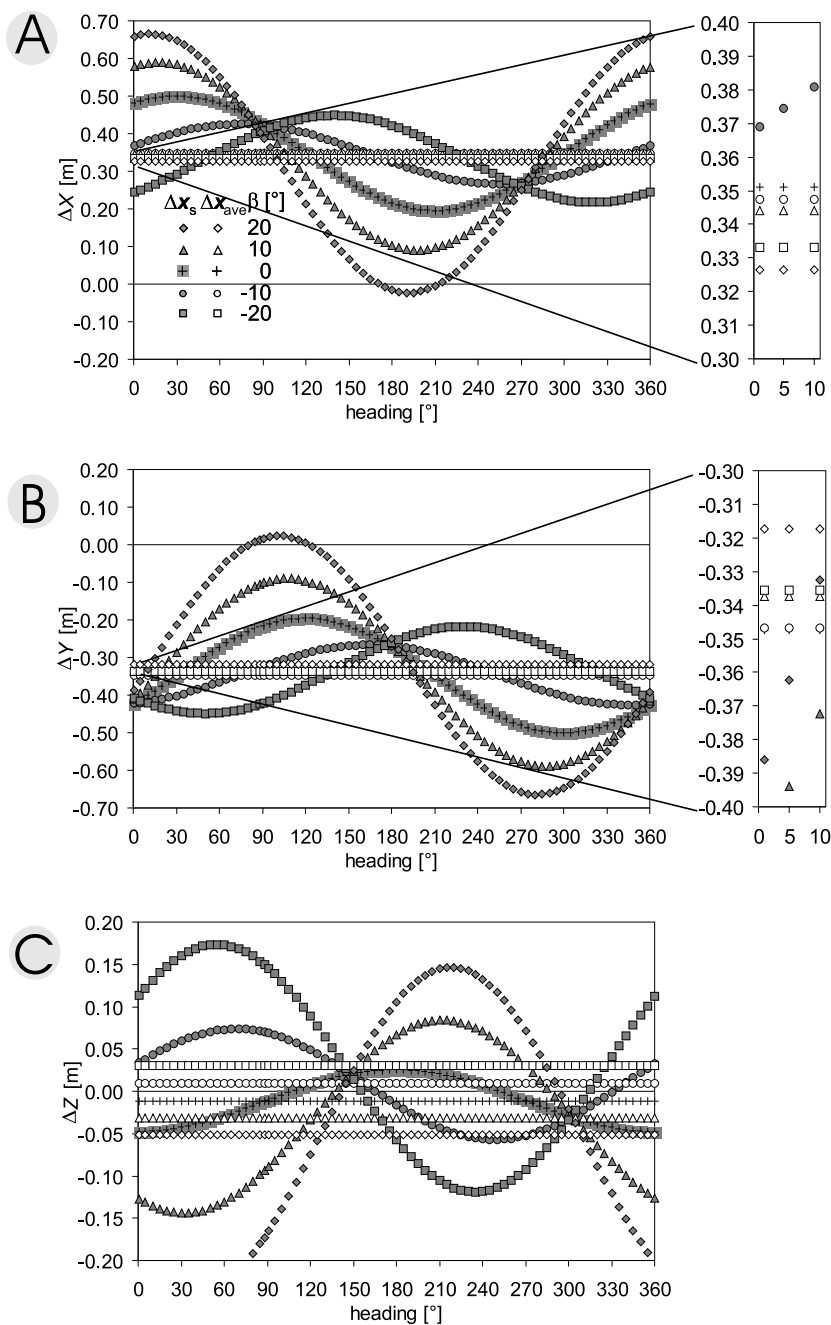
Figure C.8: Basic systematic errors by Schenk's $\Delta\mathbf{x}_s$ and simplified average $\Delta\mathbf{x}_{ave}$ error model for different scan angle β, at flying height 1000 m. The simulation is done for $\Delta\mathbf{R}_{\mathrm{INS}}$ **values of** $\boldsymbol{\Delta\phi = \Delta\theta = 0.02°}$ **and** $\boldsymbol{\Delta\psi = 0.03°}$, and average magnitude of roll and pitch angles of 1°. Error components: A) ΔX , B) ΔY and C) ΔZ.

Slika C.8: Osnovne sistematične napake po Schenkovem $\Delta\mathbf{x}_s$ in poenostavljenem povprečnemu modelu napak $\Delta\mathbf{x}_{ave}$ pri različni kotih skeniranja za vrednosti $\Delta\mathbf{R}_{\mathrm{INS}}$ $\Delta\phi = \Delta\theta = 0.02°$ in $\Delta\psi = 0.03°$.
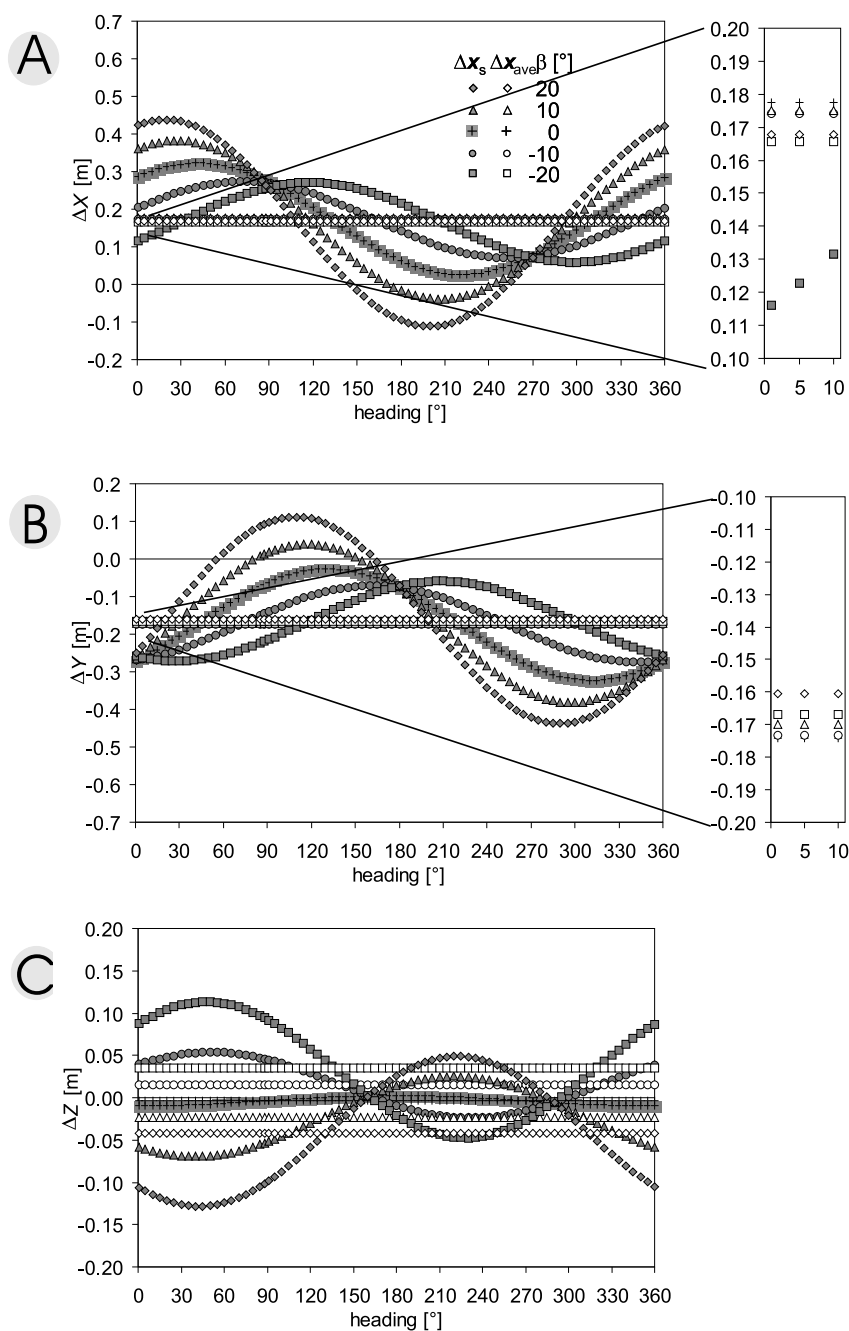
Figure C.9: Basic systematic errors by Schenk's $\Delta \mathbf{x}_s$ and simplified average $\Delta \mathbf{x}_{ave}$ error model for different scan angle β, at flying height 1000 m. The simulation is done for $\Delta \mathbf{R}_{\mathrm{INS}}$ **values of** $\boldsymbol{\Delta \phi = \Delta \theta = 0.01°}$ **and** $\boldsymbol{\Delta \psi = 0.02°}$, and average magnitude of roll and pitch angles of 1°. Error components: A) ΔX , B) ΔY and C) ΔZ.

Slika C.9: Osnovne sistematične napake po Schenkovem $\Delta \mathbf{x}_s$ in poenostavljenem povprečnemu modelu napak $\Delta \mathbf{x}_{ave}$ pri različni kotih skeniranja za vrednosti $\Delta \mathbf{R}_{\mathrm{INS}}$ $\Delta \phi = \Delta \theta = 0.01°$ in $\Delta \psi = 0.02°$.
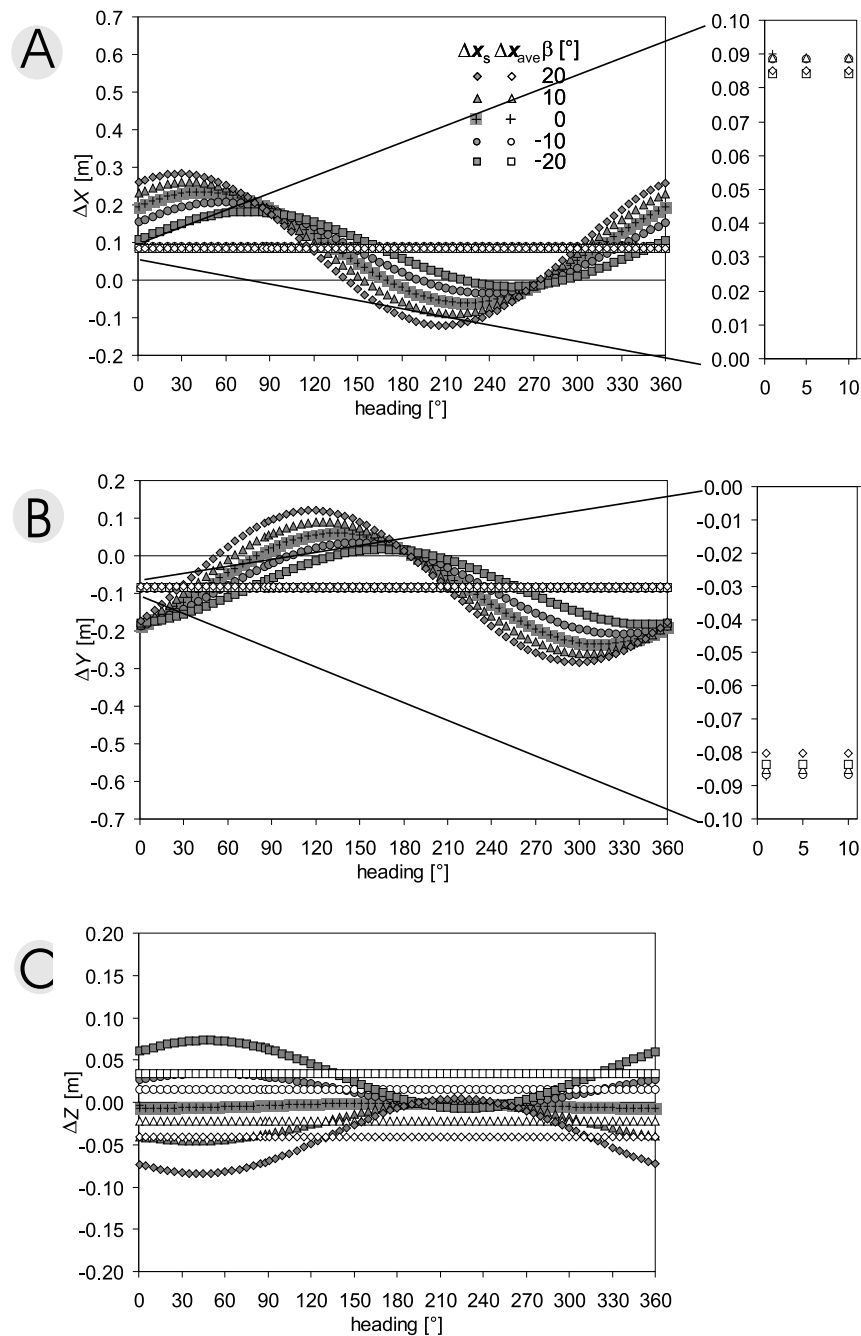
Figure C.10: Basic systematic errors by Schenk's $\Delta\mathbf{x}_s$ and simplified average $\Delta\mathbf{x}_{ave}$ error model for different scan angle β, at flying height 1000 m. The simulation is done for $\Delta\mathbf{R}_{\mathrm{INS}}$ **values of** $\boldsymbol{\Delta\phi = \Delta\theta = 0.005°}$ **and** $\boldsymbol{\Delta\psi = 0.007°}$, and average magnitude of roll and pitch angles of $1°$. Error components: A) ΔX , B) ΔY and C) ΔZ.

Slika C.10: Osnovne sistematične napake po Schenkovem $\Delta\mathbf{x}_s$ in poenostavljenem povprečnemu modelu napak $\Delta\mathbf{x}_{ave}$ pri različni kotih skeniranja za vrednosti $\Delta\mathbf{R}_{\mathrm{INS}}$ $\Delta\phi = \Delta\theta = 0.005°$ in $\Delta\psi = 0.007°$.
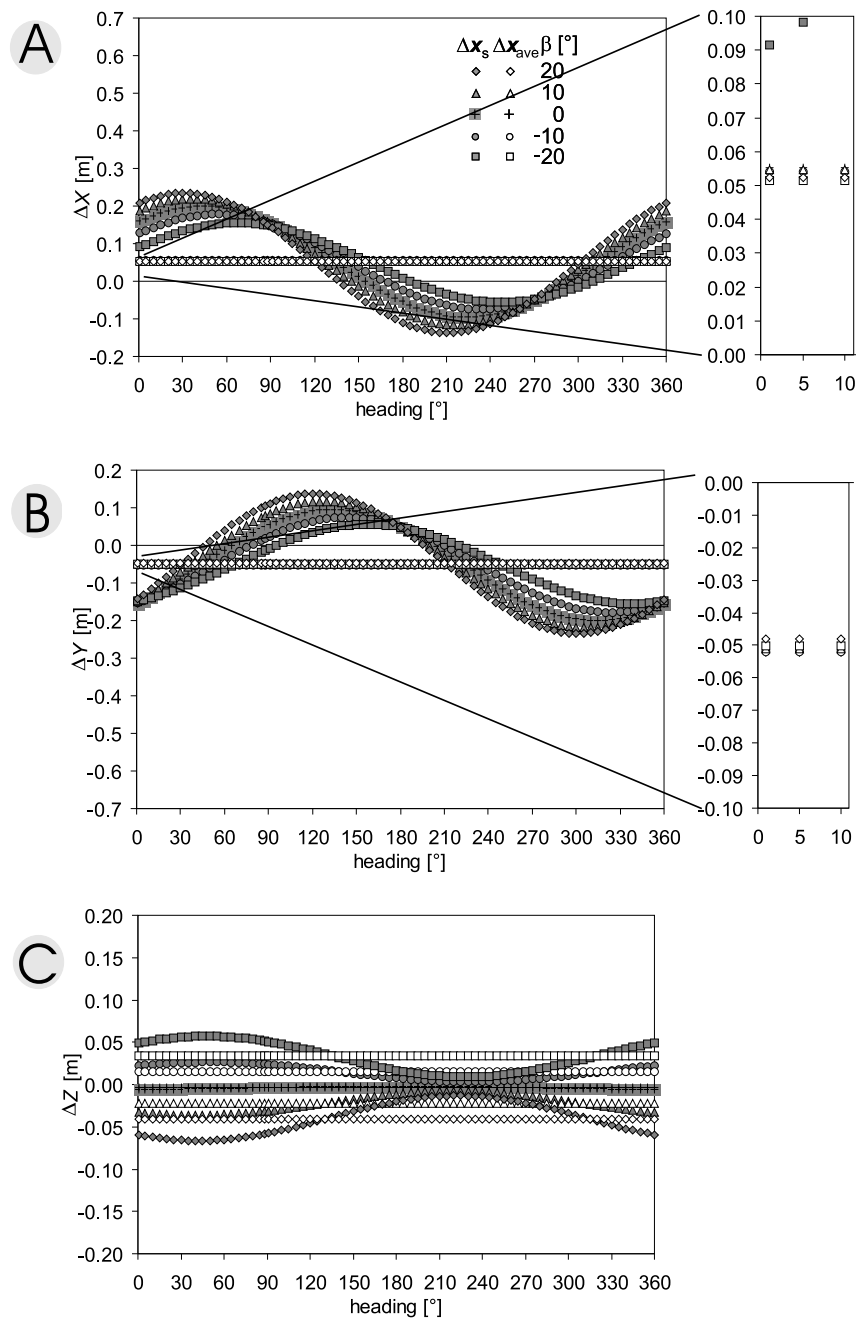
Figure C.11: Basic systematic errors by Schenk's $\Delta\mathbf{x}_s$ and simplified average $\Delta\mathbf{x}_{ave}$ error model for different scan angle β, at flying height 1000 m. The simulation is done for $\Delta\mathbf{R}_{\mathrm{INS}}$ **values of** $\boldsymbol{\Delta\phi = \Delta\theta = 0.003°}$ **and** $\boldsymbol{\Delta\psi = 0.004°}$, and average magnitude of roll and pitch angles of 1°. Error components: A) ΔX , B) ΔY and C) ΔZ.

Slika C.11: Osnovne sistematične napake po Schenkovem $\Delta\mathbf{x}_s$ in poenostavljenem povprečnemu modelu napak $\Delta\mathbf{x}_{ave}$ pri različni kotih skeniranja za vrednosti $\Delta\mathbf{R}_{\mathrm{INS}}$ $\Delta\phi = \Delta\theta = 0.003°$ in $\Delta\psi = 0.004°$.

Appendix D

Least square curve fitting

D.1   Derivation

Least square curve fitting can be performed by using different variations of the least square method. Two possibilities of least square adjustment will be presented here on the example from the page 96 (linear regression fitting between average $\Delta\mathbf{x}_{s\_ave}$ and maximal values $\Delta\mathbf{x}_{s\_max}$ of basic systematic errors):

- general case with conditions

- adjustment of indirect observations

For the computations performed in Matlab the most straithforward method was used: **adjustment of indirect observations**. More details on least square fitting can be found in Mikhail and Ackerman (1976) and Albertella et al. (1997).

D.1.1   General case with conditions

A special example of least square method is a least square curve fitting which is applied for each components separately (X, Y and Z) from page 96. We have calculated 32 values of ΔX_{s_ave} and 32 values of ΔX_{s_max} which we would like to connect in linear way.

First we write down the **general case of least square adjustment with conditions** (observations and parameters):

$$\mathbf{A}\mathbf{v} + \mathbf{B}\boldsymbol{\Delta} = \mathbf{f} \tag{D.1}$$

where: $\mathbf{v}$ are residuals of observations (original observations are $\mathbf{l}$ and corrected observations $\hat{\mathbf{l}}$, therefore $\hat{\mathbf{l}} = \mathbf{l} + \mathbf{v}$), $\mathbf{A}$ is the cofactor matrix of residuals, $\boldsymbol{\Delta}$ are unknown or searched parameters which describe our searched line ($\hat{\boldsymbol{\Delta}} = \boldsymbol{\Delta}_0 + \boldsymbol{\Delta}$: where $\boldsymbol{\Delta}_0$ is the first approximation of unknown parameters and $\hat{\boldsymbol{\Delta}}$ are the final unknown parameters), $\mathbf{B}$ is the cofactor matrix of unknowns and $\mathbf{f}$ the vector of constants.

Conditional equation

To solve the least square problem, a conditional equation C which describes the connection between the observations and unknown parameters, has to be written. In the case of linear fitting between $\Delta X_{\text{s\_ave}}$ and $\Delta X_{\text{s\_max}}$ the connection is:

$$C: \qquad \Delta X_{\text{s\_max}} - k_{\Delta X_{\text{s\_ave}}} \cdot \Delta X_{\text{s\_ave}} - k_{\Delta \psi} \cdot \Delta \psi - k_{\Delta \phi} \cdot \Delta \phi - k_h \cdot h - k_0 = 0 \qquad \text{(D.2)}$$

where $k_{\Delta X_{\text{s\_ave}}}$, $k_{\Delta \psi}$, $k_{\Delta \phi}$, k_h and k_0 are 5 unknowns which describe the linear fit.

The vector of constants $\mathbf{f}$ is in the case of nonlinear condition equation C for least square solution (the least square fitting counts under the nonlinear conditions) $\mathbf{f} = -C(\mathbf{l}_0, \mathbf{\Delta}_0)$, when $\mathbf{l}_0$ and $\mathbf{\Delta}_0$ are first approximations of the observations and the unknowns. Matrix $\mathbf{A}$ is $\frac{\partial C}{\partial \mathbf{l}}$ and matrix $\mathbf{B}$ is $\frac{\partial C}{\partial \mathbf{\Delta}}$.

Dimensions

c is the number of conditional equations or the smallest number of equations allowing the solution of the system. n is the number of the given observations (estimates). u is the number of (unknown) parameters and r is the redundancy or (statistical) degrees of freedom ($r = n - u$):

dimension($\mathbf{A}$) $= c \times n$ matrix (rank($\mathbf{A}$)$=$ c) $= 5 \times (32 \times 5)$ in our case
dimension($\mathbf{v}$) $= n \times 1$ vector $= (32 \times 5) \times 1$ in our case
dimension($\mathbf{B}$) $= c \times u$ matrix $= 5 \times 5$ in our case
dimension($\mathbf{\Delta}$) $= u \times 1$ vector $= 5 \times 1$ in our case
dimension($\mathbf{f}$) $= n \times 1$ vector $= (32 \times 5) \times 1$ in our case

The vector of the observations is:

$$\mathbf{l}^T = [\Delta X_{\text{s\_max\_1}}, \Delta X_{\text{s\_ave\_1}}, \Delta \psi_1, \Delta \phi_1, h_1, ..., \Delta X_{\text{s\_max\_n}}, \Delta X_{\text{s\_ave\_n}}, \Delta \psi_n, \Delta \phi_n, h_n] \qquad \text{(D.3)}$$

The vector of the unknown parameters is:

$$\mathbf{\Delta}^T = [k_{\Delta X_{\text{s\_ave}}}, k_{\Delta \psi}, k_{\Delta \phi}, k_h, k_0] \qquad \text{(D.4)}$$

Weight matrix $\mathbf{W}$ of observations $\mathbf{l}$ has a dimension of $n \times n$ (in our case 160×160) with diagonal term σ_0^2 / σ_1^2:

$$\mathbf{W} = \begin{bmatrix} \sigma_0^2/\sigma_1^2 & 0 & \cdots & 0 \\ 0 & \sigma_0^2/\sigma_2^2 & \cdots & 0 \\ \vdots & \vdots & \ddots & \vdots \\ 0 & 0 & 0 & \sigma_0^2/\sigma_n^2 \end{bmatrix} \qquad \text{(D.5)}$$

The matrix $\mathbf{W}$ with just one conditional equation C is written:

$$
\begin{bmatrix}
\frac{\sigma_0^2}{\sigma_{\Delta X_{s\_max1}}^2} & 0 & 0 & 0 & 0 & \cdots \\
0 & \frac{\sigma_0^2}{\sigma_{\Delta X_{s\_ava1}}^2} & 0 & 0 & 0 & \cdots \\
0 & 0 & \frac{\sigma_0^2}{\sigma_{\Delta\psi1}^2} & 0 & 0 & \cdots \\
0 & 0 & 0 & \frac{\sigma_0^2}{\sigma_{\Delta\phi1}^2} & 0 & \cdots \\
0 & 0 & 0 & 0 & \frac{\sigma_0^2}{\sigma_{h_1}^2} & \cdots \\
\vdots & \vdots & \vdots & \vdots & \vdots & \ddots
\end{bmatrix}
\tag{D.6}
$$

If the observations are not correlated between each other, the cofactor matrix $\mathbf{Q}$ is:

$$
\mathbf{Q}_{ll} = \mathbf{W}^{-1}
\tag{D.7}
$$

The minimum condition by general least square method is:

$$
\mathbf{\Phi}' = \mathbf{v}^T\mathbf{W}\mathbf{v} - 2\mathbf{k}^T(\mathbf{A}\mathbf{v} + \mathbf{B}\mathbf{\Delta} - \mathbf{f}) \longrightarrow \min
\tag{D.8}
$$

The derivatives of the minimum condition by residuals ($\mathbf{v}$) and unknown parameters ($\mathbf{\Delta}$) are:

$$
\frac{\partial\mathbf{\Phi}'}{\partial\mathbf{v}} = 2\mathbf{v}^T\mathbf{W} - 2\mathbf{k}^T\mathbf{A} = 0 \qquad \Longrightarrow \qquad \mathbf{W}\mathbf{v} = \mathbf{A}^T\mathbf{k}
\tag{D.9}
$$

$$
\frac{\partial\mathbf{\Phi}'}{\partial\mathbf{\Delta}} = 2 - 2\mathbf{k}^T\mathbf{B} = 0 \qquad \Longrightarrow \qquad \mathbf{B}^T\mathbf{k} = 0
\tag{D.10}
$$

From equation D.9 we express the residuals $\mathbf{v}$:

$$
\mathbf{v} = \mathbf{W}^{-1}\mathbf{A}\mathbf{k}
\tag{D.11}
$$

Now we put equation D.11 in equation D.1, from there we can express the matrix $\mathbf{k}$:

$$
\mathbf{A}\mathbf{Q}\mathbf{A}^T\mathbf{k} + \mathbf{B}\mathbf{\Delta} = \mathbf{f} \quad \Longrightarrow \quad \mathbf{Q}_e\mathbf{k} = \mathbf{f} - \mathbf{B}\mathbf{\Delta} \quad \Longrightarrow \quad \mathbf{k} = \mathbf{Q}_e^{-1}(\mathbf{f} - \mathbf{B}\mathbf{\Delta})
\tag{D.12}
$$

while $\mathbf{Q}_e = \mathbf{A}\mathbf{Q}\mathbf{A}^T$ and $\mathbf{W}_e = \mathbf{Q}_e^{-1}$. Knowing that, the residuals of observations in the matrix $\mathbf{k}$ can be calculated as follows:

$$
\mathbf{v} = \mathbf{Q}\mathbf{A}\mathbf{W}_e(\mathbf{f} - \mathbf{B}\mathbf{\Delta})
\tag{D.13}
$$

The unknown parameters $\mathbf{\Delta}$ can be calculated by inserting $\mathbf{k}$ in the Equation D.12 and in the Equation D.10 of $\frac{\partial\mathbf{\Phi}'}{\partial\mathbf{\Delta}}$:

$$
\mathbf{B}^T\mathbf{P}_e\mathbf{B}\mathbf{\Delta} = \mathbf{B}\mathbf{P}_e\mathbf{f} \quad \Longrightarrow \quad \mathbf{N}\mathbf{\Delta} = \mathbf{t} \quad \Longrightarrow \quad \mathbf{\Delta} = \mathbf{N}^{-1}\mathbf{t}
\tag{D.14}
$$

D.1.2   Adjustment of indirect observations

Adjustment of indirect observations is one of two classical cases of least square adjustment (the second one is adjustment of observations only). The adjustment is performed with both observations and parameters but with a restriction that each conditional equation (C) contains only one observation. Therefore the number of conditional equations is the same as the number of observations ($c = n$).

The general equations are of the form:

$$\mathbf{v} + \mathbf{B\Delta} = \mathbf{f} \tag{D.15}$$

where $\mathbf{v}$ are residuals of observations, $\mathbf{\Delta}$ are unknown or searched parameters which describe our searched line, $\mathbf{B}$ is the cofactor matrix of unknowns and $\mathbf{f}$ the vector of constants.

Conditional equation

In the case of linear fitting between $\Delta X_{\text{s\_ave}}$ and $\Delta X_{\text{s\_max}}$ a conditional equation C which connects them is:

$$C: \qquad \Delta X_{\text{s\_max}} - k_{\Delta X_{\text{s\_ave}}} \cdot \Delta X_{\text{s\_ave}} - k_{\Delta\psi} \cdot \Delta\psi - k_{\Delta\phi} \cdot \Delta\phi - k_h \cdot h - k_0 = 0 \tag{D.16}$$

The conditional equations for the general and the indirect observation case are the same, therefore equation D.2 is identical to the equation D.16. The main difference is how the parameters which are described in conditional equation are treated.

In the case of indirect observations, $\Delta X_{\text{s\_ave}}$ are treated as observations and $\Delta X_{\text{s\_max}}$ are treated as constant values.

The vector of observations is:

$$\mathbf{l}^T = [\Delta X_{\text{s\_ave\_1}}, \Delta X_{\text{s\_ave\_2}}, \Delta X_{\text{s\_ave\_3}}, ..., \Delta X_{\text{s\_ave\_n}}] \tag{D.17}$$

The vector of unknown parameters is the same as in the general case (equation D.4):

$$\mathbf{\Delta}^T = [k_{\Delta X_{\text{s\_ave}}}, k_{\Delta\psi}, k_{\Delta\phi}, k_h, k_0] \tag{D.18}$$

The vector of constant values is:

$$\mathbf{f}^T = [\Delta X_{\text{s\_max\_1}}, \Delta X_{\text{s\_max\_2}}, \Delta X_{\text{s\_max\_3}}, ..., \Delta X_{\text{s\_max\_n}}] \tag{D.19}$$

The cofactor matrix of unknowns is:

$$\mathbf{B} = \begin{bmatrix} \Delta X_{\text{s\_ave\_1}} & \Delta\psi_1 & \Delta\phi_1 & h_1 & 1 \\ \vdots & \vdots & \vdots & \vdots & \vdots \\ \Delta X_{\text{s\_ave\_n}} & \Delta\psi_n & \Delta\phi_n & h_n & 1 \end{bmatrix} \tag{D.20}$$

Dimensions

The dimensions of upper terms are:

dimension($\mathbf{v}$) = $n \times 1$ vector = 32×1 in our case
dimension($\mathbf{B}$) = $n \times u$ matrix = 32×5 in our case
dimension($\mathbf{\Delta}$) = $u \times 1$ vector = 5×1 in our case
dimension($\mathbf{f}$) = $n \times 1$ vector = 32×1 in our case

The minimum condition by indirect observations least square method is:

$$\mathbf{\Phi}' = \mathbf{v}^T \mathbf{W} \mathbf{v} = (\mathbf{f} - \mathbf{B}\mathbf{\Delta})^T \mathbf{W}(\mathbf{f} - \mathbf{B}\mathbf{\Delta}) \longrightarrow \min \tag{D.21}$$

$$\mathbf{\Phi}' = \mathbf{\Delta}^T \mathbf{B}^T \mathbf{W} \mathbf{B} \mathbf{\Delta} - 2\mathbf{f}^T \mathbf{W} \mathbf{B} \mathbf{\Delta} + \mathbf{f}^T \mathbf{W} \mathbf{f} \tag{D.22}$$

The derivative of the minimum condition should be 0:

$$\frac{\partial \mathbf{\Phi}'}{\partial \mathbf{\Delta}} = 2\mathbf{\Delta}^T \mathbf{B}^T \mathbf{W} \mathbf{B} - 2\mathbf{f}^T \mathbf{W} \mathbf{B} = 0 \tag{D.23}$$

From the Equation D.23 we can extract $\mathbf{\Delta}$:

$$(\mathbf{B}^T \mathbf{W} \mathbf{B})\mathbf{\Delta} = \mathbf{W} \mathbf{B} \mathbf{f} \quad \Longrightarrow \quad \mathbf{N}\mathbf{\Delta} = \mathbf{t} \quad \Longrightarrow \quad \mathbf{\Delta} = \mathbf{N}^{-1}\mathbf{t} \tag{D.24}$$

D.2   Statistical testing

D.2.1   Estimation of a-posteriori standard variance $\hat{\sigma}_0^2$

As we do not have a reliable a-priori common standard variance σ_0^2 of all observations, we have to use a-posteriori calculation $\hat{\sigma}_0^2$. This can be done using the results of least square fitting:

$$\hat{\sigma}_0^2 = \frac{\mathbf{v}^T \mathbf{W} \mathbf{v}}{c - u} = \frac{\mathbf{v}^T \mathbf{W} \mathbf{v}}{r} \tag{D.25}$$

D.2.2   Statistical testing whether a-priori and a-posteriori variances are equal

This statistical testing can be done, if the sample of observations is distributed by Gauss distribution — normal distribution. We presume that this is true in our example.

As we do not have a reliable a-priori common standard variance σ_0^2 of all observations ($\Delta X_{\text{s\_max}}$, $\Delta X_{\text{s\_ave}}$, $\Delta \psi$, $\Delta \phi$, h), we will take that its value is 1. Because the a-priori standard variation is not precisely known (is given by presumption) we have first to check if its value is reliable. This

is done by testing a-priori and a-posteriori variances as two variances of independent samples. The null hypothesis is:

$$H_0: \qquad \frac{\hat{\sigma}_0^2}{\sigma_0^2} = 1 \qquad \text{vs.} \qquad H_1: \qquad \frac{\hat{\sigma}_0^2}{\sigma_0^2} \neq 1 \tag{D.26}$$

The null hypothesis H_0 is tested by test F test. If a-priori variance would be known for certain, the χ test would be applied.

The test is written as $F(m_1, m_2)_{\alpha/2} = \frac{\hat{\sigma}_0^2}{\sigma_0^2}$, when $m_1 = n_1 - 1$ and $m_2 = n_2 - 1$. In our case m_1 describes the a-posteriori and m_2 a-priori data sample size. Both are the same in our case $(32 \times 5 - 1)$. We use $\alpha = 10\%$ as the hypothesis describes the two sided data sample, meaning that the test is made with 10% significance level. We find the nearest value from F table for $F(30, 30)_{0.5}$. The null hypothesis is rejected when $F_{\text{calcualated}} < F(30, 30)_{0.5}$.

If the null hypothesis is rejected, the first possibility is to change σ_0^2 and perform the whole least square fitting again, and at the end to test the new a-priori and new a-posteriori variances by equation D.26 once again. (We will not take into consideration the reason that the null hypothesis is rejected because of: the conditional equation F does not describe the reality correctly or the sampling is not done by normal distribution.)

When the null hypothesis, that a-priori and a-posteriori variances are the same, can be accepted, we proceed with elimination of unknown parameters.

D.2.3   Statistical testing on the unknown parameters significance

First the precise estimation of residuals of observations and unknown parameters has to be calculated, starting from equation D.14 or equation D.24 on.

The cofactor matrix of observations is:

$$\mathbf{Q}_{ll} = \mathbf{Q} \tag{D.27}$$

The cofactor matrix of estimated (final fitted) observations is:

$$\mathbf{Q}_{\hat{l}\hat{l}} = \mathbf{Q} - \mathbf{Q}_{vv} \tag{D.28}$$

while for general least square fitting is:

$$\mathbf{Q}_{vv} = \mathbf{Q}\mathbf{A}^T(\mathbf{W}_e - \mathbf{W}_e\mathbf{B}\mathbf{N}^{-1}\mathbf{B}^T\mathbf{W}_e)\mathbf{A}\mathbf{Q} \tag{D.29}$$

The cofactor matrix of unknown (estimated) parameters is:

$$\mathbf{Q}_{\Delta\Delta} = \mathbf{N}^{-1} \tag{D.30}$$

Covariance for $\mathbf{Q}_{\Delta\Delta}$ parameters are gained by multiplying $\mathbf{Q}_{\Delta\Delta}$ with a-posteriori variance (or a-priori — they should be the same) $\hat{\sigma}_0^2$:

$$\mathbf{\Sigma}_{\Delta\Delta} = \hat{\sigma}_0^2 \mathbf{Q}_{\Delta\Delta} = \begin{bmatrix} \hat{\sigma}_{k_{\Delta X_{\mathrm{ave}}}}^2 & 0 & 0 & 0 & 0 \\ 0 & \hat{\sigma}_{k_{\Delta\psi}}^2 & 0 & 0 & 0 \\ 0 & 0 & \hat{\sigma}_{k_{\Delta\psi}}^2 & 0 & 0 \\ 0 & 0 & 0 & \hat{\sigma}_{k_h}^2 & 0 \\ 0 & 0 & 0 & 0 & \hat{\sigma}_{k_0}^2 \end{bmatrix} \tag{D.31}$$

The statistical test on insignificance of coefficients is based upon the null hypothesis that insignificant coefficient has a value 0. After proving this, such coefficient can be neglected. The least square fitting with $(u-1)$ unknown parameters should now be performed once again.

For statistical testing we are using a large sample (more than 30 observations by Sincich (1996) is a large sample) therefore the t test statistic will be used.

To reject one parameter, e.g. we would like to test if $k_0 = 0$, the null hypothesis is written as:

$$H_0 : k_0 = 0 \tag{D.32}$$

$$z = \frac{k_0 - 0}{\hat{\sigma}_{k_0}}$$

Now we test the null hypothesis $t_{1-\alpha/2}(n-1) = z$. We use $\alpha = 10\%$ and $n = 32$ and read the $t_{1-\alpha/2}(n-1)$ from the t table. The null hypothesis is rejected when $t(30)_{0.5} > t_{\mathrm{calcualated}}$ (in our case t(from table)=1.684).

After finding unknown parameters which can be rejected, we get rid of them in equation D.2 and calculate the whole least square fitting once again. After this, we test the null hypothesis of a-posteriori variance from the conditional equation $C(r)$ written for all parameters with a-posteriori variance $\hat{\sigma}_{0(r)}^2$ and for the conditional equation $C(r-1)$ with reduced number of parameters $\hat{\sigma}_{0(r-1)}^2$ being the same:

$$H_0 : \frac{(n-r)\hat{\sigma}_{0(r-1)}^2 - (n-r-1)\hat{\sigma}_{0(r)}^2}{r \cdot \hat{\sigma}_{0(r)}^2} \leq F(1, n-r-1)_{1-\alpha} \tag{D.33}$$

The null hypothesis is tested by F distribution, as we are testing two independent variances. The limit in our example was $F(1.25)_{0.05} = 4.23$.

Appendix E

Case study area – the Nova Gorica test sample

The laser scanning point cloud, used for measurement of penetration rate in different vegetation classes, was acquired in the scope of European Union co-funded Interreg IIIA Slovenia-Italy 2000-2006 project "HarmoGeo: The production of common methodology for renovation and harmonization of geodetic groundwork charts for local spatial planning needs on the cross-border area of Slovenia and Italy". The lead partner of this project was Municipality of Nova Gorica in Slovenia, other partners were: Geodetic institute of Slovenia, University of Udine, Municipality of Gorizia (Italy), Municipality of Šempeter-Vrtojba (Slovenia), RRA Koper, Icra d.o.o.

The main outcomes of this project are:

- harmonization of cadastral maps in test areas on the cross-border area of Nova Gorica (Slovenia) and Gorizia (Italy)
- Nova Gorica aerial laser scanning data for for acquisition of detailed 3D model, which was used for detailed visualization of Nova Gorica
- knowledge dissemination in the cross-border area

The aerial laser scanning point cloud of Nova Gorica used in our test was acquired in early April of 2006 with the average total point density of 15–20 pt/m^2 and average flying height of 1000 m, covering 200 ha of Nova Gorica. The acquisition was made in early leaf-on season, meaning that there was a lot of new vegetation present. The laser scanning point cloud was acquired by the company OGS from Trieste (Italy). For laser scanning the ALTM3100 laser scanner was used, with the frequency of laser pulses of 100 kHz. The applied INS system a had frequency of 200 Hz, an accuracy of INS angles of 0.02° in roll and pitch and in 0.04° in heading. The aerial laser scanning acquisition was performed in ETRS89 coordinate system. In addition to the laser scanning point cloud, color stereo-photographing was performed, used for production of digital ortophotographies with a resolution of 0.5 m.

In the process of detailed 3D model production from laser scanning point cloud of Nova Gorica, in the scope of HarmoGeo project, also the independent ortophotographies in scale 1:1000 were used. These were ordered separately by Municipality of Nova Gorica as a classical photogram-metric aero-photographing in spring 2006.

These two types of aerophotographies were also used in our test to enable easier identification of the vegetation classes presented by the laser scanning point cloud.